



THE HONG KONG  
POLYTECHNIC UNIVERSITY

香港理工大學

Pao Yue-kong Library

包玉剛圖書館

---

## Copyright Undertaking

This thesis is protected by copyright, with all rights reserved.

**By reading and using the thesis, the reader understands and agrees to the following terms:**

1. The reader will abide by the rules and legal ordinances governing copyright regarding the use of the thesis.
2. The reader will use the thesis for the purpose of research or private study only and not for distribution or further reproduction or any other purpose.
3. The reader agrees to indemnify and hold the University harmless from and against any loss, damage, cost, liability or expenses arising from copyright infringement or unauthorized usage.

### IMPORTANT

If you have reasons to believe that any materials in this thesis are deemed not suitable to be distributed in this form, or a copyright owner having difficulty with the material being included in our database, please contact [lbsys@polyu.edu.hk](mailto:lbsys@polyu.edu.hk) providing details. The Library will look into your claim and consider taking remedial action upon receipt of the written requests.

Pao Yue-kong Library, The Hong Kong Polytechnic University, Hung Hom, Kowloon, Hong Kong

<http://www.lib.polyu.edu.hk>

**MULTILAYER PVDF ELECTRET  
NANOFIBER FILTERS FOR ENHANCED  
AEROSOL FILTRATION**

**QIANGQIANG SUN**

**PhD**

**The Hong Kong Polytechnic University**

**2020**

**The Hong Kong Polytechnic University**

**Department of Mechanical Engineering**

**Multilayer PVDF Electret Nanofiber Filters for  
Enhanced Aerosol Filtration**

**Qiangqiang SUN**

A thesis submitted in partial fulfillment of the requirements for the degree  
of Doctor of Philosophy

December 2019

## CERTIFICATE OF ORIGINALITY

I hereby declare that this thesis is my own work and that, to the best of my knowledge and belief, it reproduces no material previously published or written, nor material that has been accepted for the award of any other degree or diploma, except where due acknowledgement has been made in the text.

\_\_\_\_\_  
(Signed)

Qidngqiang SUN (Name of Student)

## **Abstract**

The pervasive existence of submicron and nano- aerosols emitted from human activities have created serious air pollution problems and raised a major health concern. Filtration using fibrous filters is one main method used for removing particles from gas streams. However, traditional mechanical filters are either ineffective due to large fiber diameters or inefficient because of high pressure drop.

Electret fibrous filters, being able to improve aerosol removal without increasing pressure drop to the filters through electrostatic filtration mechanisms compared to mechanical nanofiber filters, have been of increasing interest for researchers. Specially, more attention is paid to dielectrophoretic filtration effect between charged polymeric fibers and neutral particles. To date, several polymers have been used to make fibrous filters and investigated for their chargeability and filtration performance. However, the studied materials for electret fibrous filters are still limited, and charge instability and nondurability remain problems for their long-term storage and use.

Polyvinylidene fluoride (PVDF), contributed by its outstanding physicochemical properties, is a promising material of great chargeability and charge stability. Nonetheless, few studies focused on the electrostatic charging properties of PVDF fibrous filters and their filtration performance for aerosol particles.

The objective of this study was to investigate both the short-term and long-term aerosol filtration properties of multilayer nanofiber PVDF electret fibrous filters as a potential candidate for face masks. In this study, defect-free PVDF nanofiber filters were fabricated by electrospinning. It was confirmed that PVDF filters had superior chargeability. The concept of “multilayering” was then first applied for electret filters

in this study based on the potential benefits of lowering pressure drop and enhancing filtration efficiency. Through comparative tests with 1-layer counterparts, the excellent filtration performance of multilayer PVDF electret filters was then verified. Without changing the filter basis weight, by redistributing the charged fibers all packed in a 1-layer filter into a multilayer filter, the filtration efficiency was improved attributed to the weakened electrical interference among randomly oriented charged nanofibers. Meanwhile, the air flow resistance was significantly alleviated due to the much more porous structure compared with the 1-layer filters. Moreover, via the analyses of single fiber efficiency, it was proved that dielectrophoretic filtration effect played the main role in aerosol capture enhancement using PVDF electret filters and multilayering could help maintain the single fiber efficiency of multilayer electret filters at higher levels than the 1-layer counterparts. In addition, based on the filter tests during a three-month period, the charge stability on the multilayer PVDF electret filters was proved. In conclusion, by combining the advantages of PVDF and “multilayering”, we managed to fabricate electret filters with high filtration efficiency, low pressure drop and long-term storage stability.

After confirming the merits of multilayer PVDF electret filters, it is essential to optimize the filtration performance by modifying the physical properties of the filters. Several modified charging methods have been adopted in literature to facilitate electrostatic filtration effects of electret filters. However, these methods either have the risk of damaging filters and charging devices or need complicated apparatus to carry out, which makes the preparation of electret filters less feasible.

Compared to the enhancement in electrostatic effects, a more realistic method to boost aerosol capture while maintaining a low fiber amount is using thinner fibers

through improving the mechanical filtration effects of Brownian diffusion and interception. Nonetheless, there exists a limit on fiber size reduction because air resistance is more sensitive to a filter with finer fibers. Besides, the contribution of electrostatic effect can be insignificant because of the already remarkable mechanical filtration efficiency.

To obtain the ideal filtration performance, an approach was taken based on first optimizing the 1-layer electret filters and then using multiple of the optimized filter (module layer) to construct multilayer electret filters. It was confirmed that an optimal basis weight existed for a 1-layer PVDF electret filter to ensure sufficient deposited charges and to prevent electrical interference so that they could obtain the highest quality factors. And as long as the quality factors of the module 1-layer filter were high enough with moderate filtration efficiency, excellent filtration performance of multilayer electret filters could also be assured. Thus, comparative filtration tests were first conducted using varied filter basis weights and fiber diameters of 1-layer PVDF electret filters. From the tests, it was demonstrated that high dielectrophoretic filtration efficiency did not guarantee high filtration performance of the 1-layer PVDF electret filters. The relative importance of dielectrophoretic filtration effect over mechanical filtration effect was found to be the key factor for filter performance improvement. Therefore, a proper basis weight was needed for 1-layer filters to not only ensure enough electrostatic effect but also to avoid excessive mechanical effect. In this study, the filter 525-S-0.765-C with the highest quality factors was chosen as the module layer to compose multilayer PVDF electret filters. The 4-layer PVDF electret filter with a mean fiber diameter of 525 nm and a basis weight of 3.060 gsm was determined as the optimized filter. It had a filtration efficiency value of 95.1% and a quality factor of

0.164 Pa<sup>-1</sup> for aerosols of 300 nm. Moreover, the pressure drop of the optimized filter was only 18.4 Pa, indicating the high potential for further improvement in filtration performance.

The merits of multilayer PVDF electret filters have been clearly verified in the lab filtration tests. Yet, what is more important is the effectiveness of the filters in real applications. In most of the researches on nano-aerosol filtration, experiments were carried out in labs, where monodisperse aerosols with a single component and a specific charge state were applied. However, real environmental nano-aerosols consist of varied components with irregular shapes, a wide range of sizes and an unstable charge distribution. Therefore, the test results were too preliminary to directly equate with filter performance in real applications. The complexities of airborne nano-aerosols render filter tests under real environments necessary. Given the importance and wide availability of vehicles, traffic environment located near a road with busy traffic was chosen as an example of real conditions for filter field tests.

Through the field filtration tests, high filtration efficiency and quality factors of the multilayer PVDF electret filters could still be achieved, although the oily aerosols and the humid air are normally detrimental to the electret filters. The efficiency of aerosols of 36.87-433.7 nm followed the same trend as that of the lab tests, where the efficiency increased with aerosol size attributed to the stronger dielectrophoretic filtration effect on large particles. Aerosols with lower sizes were largely removed due to the dominant diffusion effect which was independent of electrostatic effects.

While the merits of multilayer electret PVDF filters have been well-proved through short-term filtration tests, it is the long-term performance of the filters that is more valued when health impact, financial cost or energy consumption is considered. There

have been some researches on variations of aerosol penetration and air resistance with aerosol deposition amount on electret filters. As commonly reported, efficiency of electret filters initially decreased to a certain point before increasing with loading due to shielding of electrostatic effect and enhanced mechanical effect. And aerosol holding capacity could be apparently improved because of more uniform distribution of deposited aerosols. Nevertheless, without investigating the real morphology of particle deposition, previous researches merely drew conclusions based on the difference in pressure drop evolutions between electret and mechanical filters. Moreover, the electret filters in these researches usually had a large thickness within just one single layer, where “skin effect” was easily initiated on filter surface and downstream charged fibers were insufficiently used.

Since pressure drop has been confirmed to reduce by redistributing fibers from a single layer to multiple layers, it was intuitively hypothesized that a multilayer filter with an identical basis weight to a 1-layer filter but a much lower packing fraction has a higher resistance to clogging and a larger aerosol holding capacity. Furthermore, for a multilayer electret filter, the charges on the fibers in deep layers are hopeful to be more effectively used, and on the level of individual fibers, the distribution of captured particles is expected to be more even.

Through the filtration efficiency variations of uncharged/electret, single-/multi-layer filters with aerosol loading, it was observed that mechanical PVDF filters had continuously increasing filtration efficiency, while PVDF electret filters had initially decreasing and subsequently increasing filtration efficiency until reaching 100%.

By combining the pressure drop evolution of different filters during aerosol loading and detailed SEM images of the loaded filters, it was demonstrated that multilayer

PVDF filters, especially the electret ones, could significantly slow down the pace of filter clogging (skin effect) and elevate the aerosol holding capacity during depth filtration. Generally, the multilayer filters received the most aerosol deposit during depth filtration, whereas the 1-layer filters received the most deposit during cake filtration. The multilayer nanofiber filters had approximately 70% of aerosol deposit in the filter during depth filtration fully utilizing the full filter thickness, especially for the electret filters that had charged fibers, and only 30% of deposit in the cake. In contrary, the 1-layer uncharged/electret nanofiber filters were exactly the reverse due to persistency of the skin effect with only 30% of deposit in the filter, yet 70% of deposit in the cake. During depth filtration, the pressure drop per added mass deposit for the multilayer electret filter was very low at  $11 \text{ Pa gsm}^{-1}$ , which was at least twice below any other nanofiber filters. This was all attributed to the uniform capture of aerosols by electrostatic effect across the entire filter depth from the upstream to downstream layers of the multilayer electret filter, as confirmed by the detailed SEM taken across the different filter layers for the multilayer filter configuration. Based on highest efficiency and capacity standpoint with maximum pressure drop imposed on the filtration operation, the multilayer electret filter was the best among all 4 filters, it had 52% more aerosol holding capacity than the 1-layer uncharged filter and 38% more capacity than the 1-layer electret and multilayer uncharged filters.

To conclude, the multilayer PVDF electret filters possess excellent filtration performance for both short-term and long-term aerosol filtration, as well as high stability during storage. They have a great potential of applications in the fields of personal health care and environmental protection.

## **Publications Arising from the Thesis**

- [1] Q. Sun, W.W.-F. Leung, Charged PVDF multi-layer filters with enhanced filtration performance for filtering nano-aerosols, *Sep. Purif. Technol.* 212 (2019) 854-876.
- [2] Q. Sun, W.W.-F. Leung, Enhanced nano-aerosol loading performance of multilayer PVDF nanofiber electret filters, *Sep. Purif. Technol.* 240 (2020) 116606.
- [3] W.W.-F. Leung, Q. Sun, Electrostatic charged nanofiber filter for filtering airborne novel coronavirus (COVID-19) and nano-aerosols, *Sep. Purif. Technol.* (2020) 116886.
- [4] W.W.-F. Leung, Q. Sun, Charged PVDF multilayer nanofiber filter in filtering simulated airborne novel coronavirus (COVID-19) using ambient nano-aerosols, *Sep. Purif. Technol.* 245 (2020) 116887.
- [5] Q. Sun, W.W.-F. Leung, Optimization of multilayer PVDF nanofiber electret filters for aerosol filtration by adjusting fiber diameter and filter basis weight. (Ready for submission)
- [6] Q. Sun, W.W.-F. Leung, High-efficiency and low-resistance multilayer PVDF nanofiber electret filters for filtration of traffic-induced sub-micron aerosols. (Ready for submission)

## Acknowledgements

Over the last three years and eight months many people helped me with my academic research, but none could compare to my supervisor, Prof. Wallace Leung. His profound knowledge and deep understanding of fibrous filtration theories were a great assistance, and his philosophy of conducting research was a valuable treasure to me. I wish to express my sincere gratitude to him for the time and energy he contributed to my study.

Further thanks are due to my groupmates. They all left marks, more or less, in my life in Hong Kong. I would like to thank Ms. Yun Li for share her experience with me. Specially, I want to thank her to share her rice to me when I first came to Hong Kong and did not know how to ask the canteen staff for more food. I want to thank Ms. Xuan Cao for accompanying me to go around the city during my early stay here and for leaving me a good memory. I would like to give my thankfulness to Mr. Kenneth Lo, Mr. Kent Choy, Ms. Curie Hau and Ms. Eva Mak for their detailed guidance and suggestions on my experiments. Last but not least, I want to thank Ms. Rachel Chau, Mr. Austin Jimeno and Ms. Marie Bouyx for their contribution to the project.

A great deal of thanks also goes to the technical staff in the Department of Mechanical Engineering and Materials Research Centre, especially to Mr. Chris Tsang and Dr. Pai Wong. for their instruction in using the filtration test rig and the filter characterization device.

I would also like to thank the Department of Mechanical Engineering for part of my research studentship, without which I would not survive the high cost of living in Hong Kong.

I want to pay my deep respect to my beloved motherland China who is not yet perfect but never stops improving for the happiness of her people.

None of my life would be possible without the endless and selfless love of my family. I owe everything to my kind and hard-working parents for raising me up and supporting me with patience and encouragement throughout my seemingly endless education. I also owe a big thanks to my older sisters who gave up their chance of higher education so I could get mine and who offered to support me financially even when they were far from well off.

Finally, I want to say “thank you” to my girlfriend, hopefully my future wife, Dr. Yu Wang. I owe her the deepest gratitude for accompanying me through ups and downs with understanding and tolerance in the last eight years. My love for her is beyond words.

# Table of Contents

<b>Abstract</b> .....	I
<b>Publications Arising from the Thesis</b> .....	VII
<b>Acknowledgements</b> .....	VIII
<b>List of Figures</b> .....	I
<b>List of Tables</b> .....	X
<b>Symbols &amp; Abbreviations</b> .....	XI
<b>Symbols</b> .....	XI
<b>Abbreviations</b> .....	XV
<b>Chapter 1: Introduction</b> .....	1
<b>1.1. Background</b> .....	1
<b>1.2. Objectives of study</b> .....	4
<b>1.3. Scope of thesis</b> .....	5
<b>Chapter 2: Literature Review</b> .....	7
<b>2.1. Definition of electret fibrous filters</b> .....	7
<b>2.2. Types of electret fibrous filters</b> .....	8
<b>2.2.1. Corona-charged electret fibrous filters</b> .....	9
<b>2.2.2. Tribo-charged electret fibrous filters</b> .....	10
<b>2.2.3. Electrospun electret fibrous filters</b> .....	12
<b>2.3. Performance characterization of electret fibrous filters</b> .....	13
<b>2.3.1. Filtration efficiency</b> .....	13
<b>2.3.2. Pressure drop</b> .....	16

2.3.3.	Quality factor .....	17
2.4.	Filtration mechanisms of electret fibrous filters .....	18
2.4.1.	Mechanical capture mechanisms .....	19
2.4.1.1.	Brownian diffusion .....	19
2.4.1.2.	Interception .....	21
2.4.1.3.	Inertial impaction .....	21
2.4.2.	Electrostatic capture mechanisms .....	23
2.4.2.1.	Coulombic force .....	23
2.4.2.2.	Dielectrophoretic force .....	25
2.5.	Loading behaviors of electret fibrous filters .....	27
2.5.1.	Filtration efficiency of electret fibrous filters with loaded aerosol mass .....	29
2.5.2.	Pressure drop across electret fibrous filters with loaded aerosol mass .....	31
2.6.	Studies on filtration performance of electret fibrous filters .....	32
2.6.1.	Single-component electret fibrous filters .....	33
2.6.2.	Multi-component electret fibrous filters .....	34
2.6.3.	Commercialized electret fibrous filters .....	37
<b>Chapter 3: Preliminary Filtration Tests of Multilayer PVDF Electret Filters ....</b>		<b>39</b>
3.1.	Overview .....	39
3.2.	Experimental .....	39

3.2.1.	<b>Materials</b> .....	39
3.2.2.	<b>Fabrication of filters</b> .....	40
3.2.3.	<b>Corona discharge of filters</b> .....	42
3.2.4.	<b>Characterization of filters</b> .....	44
3.2.5.	<b>Filtration performance evaluation of filters</b> .....	45
3.3.	<b>Theoretical analysis of single fiber efficiency from dielectrophoretic filtration effect</b> .....	50
3.4.	<b>Results and discussion</b> .....	53
3.4.1.	<b>Morphology of PVDF filters</b> .....	53
3.4.2.	<b>Optimization of charging condition on filtration performance of 1-layer PVDF electret filters</b> .....	56
3.4.3.	<b>Filtration performance evaluation of 1-layer PVDF electret filters</b>	63
3.4.4.	<b>Influence of PVDF basis weight on filtration performance of 1-layer PVDF electret filters</b> .....	69
3.4.5.	<b>Filtration performance evaluation of multilayer PVDF electret filters</b> .....	73
3.4.6.	<b>Analysis of dielectrophoretic filtration effect on Single fiber efficiency</b> .....	82
3.4.7.	<b>Stability test</b> .....	89
3.5.	<b>Summary</b> .....	91
<b>Chapter 4: Performance Optimization of Multilayer PVDF Electret Filters</b> .....		93
4.1.	<b>Overview</b> .....	93

<b>4.2. Experimental.....</b>	<b>96</b>
<b>4.2.1. Fabrication of filters .....</b>	<b>96</b>
<b>4.2.2. Filter performance evaluation .....</b>	<b>100</b>
<b>4.3. Results and discussion.....</b>	<b>100</b>
<b>4.3.1. Influence of filter properties on filtration performance.....</b>	<b>101</b>
<b>4.3.1.1. Influence of filter basis weight.....</b>	<b>103</b>
<b>4.3.1.2. Influence of fiber diameter .....</b>	<b>104</b>
<b>4.3.2. MPPS variations with filter basis weight and fiber size.....</b>	<b>106</b>
<b>4.3.2.1. MPPS variations with filter basis weight .....</b>	<b>107</b>
<b>4.3.2.2. MPPS variations with fiber diameter .....</b>	<b>108</b>
<b>4.3.3. Determination of optimized module single PVDF layer.....</b>	<b>109</b>
<b>4.3.4. Filtration performance of multilayer electret PVDF filters     composed of optimized single layers .....</b>	<b>115</b>
<b>4.3.5. Comparison of filtration performance of optimized multilayer     PVDF electret filter with commercial face masks .....</b>	<b>118</b>
<b>4.4. Summary .....</b>	<b>121</b>
<b>Chapter 5: Filtration Performance of Multilayer PVDF Electret Filters in Real Aerosol-Laden Environment.....</b>	<b>123</b>
<b>5.1. Overview .....</b>	<b>123</b>
<b>5.2. Experimental.....</b>	<b>125</b>
<b>5.2.1. Fabrication of filters .....</b>	<b>125</b>

5.2.2.	<b>Description of micro-environment for field tests .....</b>	125
5.2.3.	<b>Filtration performance evaluation of filters .....</b>	126
5.3.	<b>Results and discussions .....</b>	127
5.4.	<b>Summary .....</b>	134
<b>Chapter 6: Aerosol Loading Behaviors of Multilayer PVDF Electret Filters....</b>		136
6.1.	<b>Overview .....</b>	136
6.2.	<b>Experimental.....</b>	139
6.2.1.	<b>Fabrication of filters .....</b>	139
6.2.2.	<b>Filtration performance evaluation of filters .....</b>	140
6.2.3.	<b>Aerosol loading behavior evaluation of filters.....</b>	141
6.3.	<b>Results and discussions .....</b>	146
6.3.1.	<b>Comparison of loading behaviors between 1-layer and multilayer uncharged PVDF filters—merits of multilayering .....</b>	147
6.3.1.1.	<b>Variation of filtration efficiency and pressure drop of uncharged PVDF filters with loaded mass .....</b>	147
6.3.1.2.	<b>Deposition of aerosols on uncharged PVDF filters.....</b>	150
6.3.2.	<b>Loading behaviors of 1-layer PVDF electret filters—effects of charging .....</b>	155
6.3.2.1.	<b>Variation of filtration efficiency and pressure drop of 1-layer PVDF electret filters with loaded mass .....</b>	155
6.3.2.2.	<b>Deposition of aerosols on 1-layer PVDF electret filters .....</b>	164

6.3.3. Enhanced loading performance of multilayer PVDF electret filters due to both multilayering and charging .....	165
6.3.3.1. Variation of filtration efficiency and pressure drop of multilayer PVDF electret filters with loaded mass .....	165
6.3.3.2. Deposition of aerosols on multilayer PVDF electret filters.....	170
6.3.4. Theoretical analyses of filter efficiency, loading capacity and pressure drop .....	174
6.3.4.1. Efficiency .....	174
6.3.4.2. Loading capacity and pressure drop .....	174
6.4. Summary .....	180
Chapter 7: Conclusions and Suggestions for Future Research .....	183
7.1. Conclusions .....	183
7.2. Suggestions for future research .....	187
Appendices .....	191
Appendix 1. – Figures .....	191
Appendix 2. – Tables .....	203
Appendix 3. – Calculation method of $M_{dep}$ .....	213
References.....	215

## List of Figures

**Fig. 2.1.** Particle collection by mechanical mechanisms including Brownian diffusion, interception, inertial impaction and gravitational settling [36].

**Fig. 2.2.** Particle collection by electrostatic mechanisms including Coulombic and dielectrophoretic forces [36].

**Fig. 2.3.** Efficiency compositions of mechanical filters and electret filters for neutralized aerosol capture.

**Fig. 2.4.** Schematics for aerosol deposition distribution in varied filters a certain time after complete formation of aerosol cake.

**Fig. 3.1.** Schematic diagram of the electrospinning apparatus.

**Fig. 3.2.** Schematic diagrams of (a) the corona discharge set-up, (b) the apparatus for surface potential (*SP*) tests and (c) a filter sample used for charging and *SP* tests.

**Fig. 3.3.** Schematic diagram of set-up for aerosol filtration tests of filters.

**Fig. 3.4.** Filtration efficiency ( $\eta$ ) a typical 1-layer PVDF electret filter.

**Fig. 3.5.** SEM images of (a) 450-S-0.87, (b) 450-S-1.75, (c) 450-S-3.46, (d) 450-S-5.10 and (e) 450-S-6.98.

**Fig. 3.6.** Fiber diameter distribution of 450-nm PVDF filters.

**Fig. 3.7.** (a) Filtration efficiency ( $\eta$ ) and (b) quality factors (*QF*) of pristine and electret 1-layer PVDF filters with varied charging voltages. (PVDF layer basis weight: 2.43 gsm.)

**Fig. 3.8.** (a) Filtration efficiency ( $\eta$ ) and (b) quality factors (*QF*) of pristine and electret 1-layer PVDF filters with varied charging distances. (PVDF layer basis weight: 2.43

gsm.)

**Fig. 3.9.** Surface potential ( $SP$ ) distribution on 1-layer PVDF electret filters with charging voltages of (a) 10 kV, (b) 15 kV and (c) 20 kV. (PVDF layer basis weight: 2.43 gsm.)

**Fig. 3.10.** Surface potential ( $SP$ ) distribution on 1-layer PVDF electret filters with charging voltages of (a) 35 mm, (b) 30 mm and (c) 25 mm. (PVDF layer basis weight: 2.43 gsm.)

**Fig. 3.11.** (a) Filtration efficiency ( $\eta$ ) and (b) quality factors ( $QF$ ) of pristine, uncharged and electret 1-layer PVDF filters. (PVDF layer basis weight: 1.75 gsm.)

**Fig. 3.12.** Surface potential ( $SP$ ) distribution on (a) pristine, (b) uncharged and (c) electret 1-layer PVDF filters. (PVDF layer basis weight: 1.75 gsm.)

**Fig. 3.13.** Filtration efficiency ( $\eta$ ) of pristine, uncharged and electret 2-layer PP substrate.

**Fig. 3.14.** Surface potential ( $SP$ ) distribution on (a) pristine, (b) uncharged and (c) electret PP substrate.

**Fig. 3.15.** (a) Filtration efficiency ( $\eta$ ) and (b) quality factors ( $QF$ ) of pristine and electret 1-layer PVDF filters with varied layer basis weights.

**Fig. 3.16.** Average surface potential ( $SP_{Avg.}$ ) of 1-layer PVDF filters with varied layer basis weights.

**Fig. 3.17.** Comparisons of (a) filtration efficiency ( $\eta$ ) and (b) quality factors ( $QF$ ) between 1-layer and multilayer pristine PVDF filters. (Basis weight of PVDF layer in multilayer filter: 1.75 gsm. Note 450-S-1.75 and 450-M1-1.75 denote the same filter.)

**Fig. 3.18.** Comparisons of (a) filtration efficiency ( $\eta$ ) and (b) quality factors ( $QF$ ) between 1-layer and multilayer electret PVDF filters. (Basis weight of PVDF layer in multilayer filter: 1.75 gsm. Note 450-S-1.75 and 450-M1-1.75 denote the same filter.)

**Fig. 3.19.** Comparison of filtration efficiency ( $\eta$ ) between multilayer PVDF filters with layer basis weights of 0.87 gsm and 1.75 gsm: (a) pristine ones and (b) electret ones.

**Fig. 3.20.** Comparison of quality factors ( $QF$ ) between pristine multilayer PVDF filters with layer basis weights of 0.87 gsm and 1.75 gsm: (a) pristine ones and (b) electret ones.

**Fig. 3.21.** Filtration efficiency due to dielectrophoretic filtration effect of varied PVDF electret filters for 200-nm aerosols.

**Fig. 3.22.** Evolution of (a) filtration efficiency ( $\eta$ ) and (b) quality factor ( $QF$ ) of pristine and electret 1-layer and multilayer PVDF filters for 200-nm aerosols with corresponding pressure drop ( $\Delta p$ ).

**Fig. 3.23.** Single fiber efficiency of different electret filters due to dielectrophoretic filtration effect ( $\eta_{s,o}$ ) versus reduced parameter ( $Cd_p^2/U$ ).

**Fig. 3.24.** Comparison of single fiber efficiency due to dielectrophoretic filtration effect ( $\eta_{s,o}$ ) versus reduced parameter ( $Cd_p^2/U$ ) between 1-layer and 6-layer electret filters both at 5.10 gsm and 5.3 cm s<sup>-1</sup>.

**Fig. 3.25.** Comparison of single fiber efficiency due to dielectrophoretic filtration effect ( $\eta_{s,o}$ ) versus reduced parameter ( $Cd_p^2/U$ ) between 1-layer and 4-layer (0.87 gsm per layer) electret filters both at 3.5 gsm and 5.3 cm s<sup>-1</sup>, and also 4-layer (0.87 gsm per layer) electret filters at 2.5 and 7.5 cm s<sup>-1</sup>, respectively.

**Fig. 3.26.** Comparison of single fiber efficiency due to dielectrophoretic filtration

effect ( $\eta_{s,o}$ ) versus reduced parameter ( $Cd_p^2/U$ ) between 1-layer and 8-layer (0.87 gsm per layer) electret filters both at 7.0 gsm and 5.3 cm s<sup>-1</sup>.

**Fig. 3.27.** Ratios of single fiber efficiency ( $\eta_{s,o,n}/\eta_{s,o,1}$ ) due to dielectrophoretic force of multilayer electret filters to that of corresponding 1-layer electret filters.

**Fig. 3.28.** Filtration efficiency of M4-1.75-C with storage time.

**Fig. 3.29.** Surface potential decay of S-1.75-C with time.

**Fig. 4.1.** SEM images of PVDF filters with mean diameters of (a) 84, (b) 191, (c) 349 and (d) 525 nm.

**Fig. 4.2.** Fiber diameter distribution of (a) 84-nm, (b) 191-nm, (c) 349-nm and (d) 525-nm PVDF filters.

**Fig. 4.3.** (a) Filtration efficiency ( $\eta$ ) and (b) quality factors ( $QF$ ) of 1-layer PVDF filters with varied filter basis weights and fiber sizes for 200-nm aerosols. (Filters were in uncharged or charged state.)

**Fig. 4.4.** Pressure drop ( $\Delta p$ ) of 1-layer PVDF filters with varied filter basis weights and fiber sizes. (Each filter had the same pressure drop in uncharged and charged states.)

**Fig. 4.5.** MPPS of (a) uncharged and (b) electret 1-layer PVDF filters with varied filter basis weights and fiber sizes.

**Fig. 4.6.** (a) Dielectrophoretic filtration efficiency ( $\eta_o$ ) of PVDF electret filters with varied filter basis weights and fiber sizes for 200-nm aerosols; (b) Proportions of dielectrophoretic filtration efficiency ( $\eta_o$ ) in combined dielectrophoretic and mechanical filtration efficiency ( $\eta_o + \eta_M$ ) for 200-nm aerosols.

**Fig. 4.7.** Filtration efficiency ( $\eta$ ) versus quality factors ( $QF$ ) of 1-layer PVDF electret

filters with varied filter basis weights and fiber sizes for 200-nm aerosols.

**Fig. 4.8.** (a) Filtration efficiency ( $\eta$ ) and quality factors ( $QF$ ) for 200-nm aerosols and (b) pressure drop ( $\Delta p$ ) of 1-layer 525-nm PVDF electret filters with the lowest filter basis weight being 0.765 gsm.

**Fig. 4.9.** Filtration efficiency ( $\eta$ ) versus quality factors ( $QF$ ) of 1-layer 525-nm PVDF electret filters with varied filter basis weights for 200-nm aerosols.

**Fig. 4.10.** (a) Filtration efficiency ( $\eta$ ) and (b) quality factors ( $QF$ ) of multilayer 525-nm PVDF electret filters with the layer basis weight being 0.765 gsm.

**Fig. 4.11.** Pressure drop ( $\Delta p$ ) of multilayer 525-nm electret filters with the layer basis weight being 0.765 gsm.

**Fig. 4.12.** Comparison of filtration efficiency ( $\eta$ ) versus quality factors ( $QF$ ) for 200-nm aerosols between 525-S-C, 525-M-0.191-C and 525-M-0.765-C with varied filter basis weights.

**Fig. 4.13.** Comparisons of (a) filtration efficiency ( $\eta$ ), (b) pressure drop ( $\Delta p$ ) and (c) quality factors ( $QF$ ) between 450-M8-0.87-C and commercial face masks.

**Fig. 5.1.** Schematic diagram of set-up for aerosol filtration field tests of filters.

**Fig. 5.2.** Typical diameter distribution of aerosols detected by inner CPC of PAMS at the field test site.

**Fig. 5.3.** Pressure drop of 525-nm 1-layer and multilayer PVDF filters with varied filter basis weights at the outdoor experimental site. (Each filter had the same pressure drop in uncharged and charged states.)

**Fig. 5.4.** Filtration efficiency ( $\eta$ ) and fit curves of 525-nm (a) 1-layer uncharged, (b) 1-

layer electret, (c) multilayer uncharged and (d) multilayer electret PVDF filters with varied filter basis weights in field tests. (Note 525-S-0.765 and 525-M1-0.765 denote the same filter.)

**Fig. 5.5.** Quality factors ( $QF$ ) and fit curves of 525-nm (a) 1-layer uncharged, (b) 1-layer electret, (c) multilayer uncharged and (d) multilayer electret PVDF filters with varied filter basis weights in field tests. (Note 525-S-0.765 and 525-M1-0.765 denote the same filter.)

**Fig. 5.6.** Comparison of filtration efficiency ( $\eta$ ) of 525-M6-0.765-C in field test (polydisperse ambient aerosols) and lab test (monodisperse NaCl aerosols).

**Fig. 6.1.** Schematic diagram of set-up for aerosol loading of filters.

**Fig. 6.2.** Typical diameter distribution of particles for (a) filtration efficiency tests and (b) aerosol loading.

**Fig. 6.3.** SEM images of (a) S-3.060 and (b) one layer of M4-0.765 in clean state.

**Fig. 6.4.** Evolution of filtration efficiency ( $\eta$ ) of (a) 525-S-3.060-U and (b) 525-M4-0.765-U with loading time.

**Fig. 6.5.** Evolution of pressure drop ( $\Delta p$ ) of 525-S-3.060-U and 525-M4-0.765-U with loaded aerosol mass.

**Fig. 6.6.** SEM images of (a) and (b) the front side, and (c) and (d) the back side of loaded 525-S-3.060-U.

**Fig. 6.7.** SEM images of (a) and (b) the first, (c) and (d) the second, (e) and (f) the third and (g) and (h) the fourth layers of loaded 525-M4-0.765-U seen from the front side.

**Fig. 6.8.** SEM images of (a) and (b) the first, (c) and (d) the second, (e) and (f) the third

and (g) and (h) the fourth layers of loaded 525-M4-0.765-U seen from the back side.

**Fig. 6.9.** Evolution of filtration efficiency ( $\eta$ ) of (a) 525-S-3.060-C-1, (b) 525-S-3.060-C-2 and (c) 525-S-3.060-C-3 with loading time.

**Fig. 6.10.** Typical diameter distribution of particles for aerosol loading of 525-S-3.060-C-3.

**Fig. 6.11.** SEM images of the back side of loaded (a) 525-S-3.060-C-1 and (b) 525-S-3.060-C-3.

**Fig. 6.12.** Evolution of pressure drop ( $\Delta p$ ) of 525-S-3.060-U and 525-S-3.060-C-1 with loaded aerosol mass.

**Fig. 6.13.** Evolution of pressure drop ( $\Delta p$ ) of 525-S-3.060-C-1 and 525-S-3.060-C-2 with loaded aerosol mass.

**Fig. 6.14.** SEM images of (a) and (b) the front side, and (c) and (d) the back side of loaded 525-S-3.060-C-1.

**Fig. 6.15.** Evolution of filtration efficiency ( $\eta$ ) of (a) 525-M4-0.765-C-1 and (b) 525-M4-0.765-C-2 with loading time.

**Fig. 6.16.** Evolution of pressure drop ( $\Delta p$ ) of 525-S-3.060-C-1, 525-M4-0.765-U and 525-M4-0.765-C-1 with loaded aerosol mass.

**Fig. 6.17.** Evolution of pressure drop ( $\Delta p$ ) of 525-M4-0.765-C-1 and 525-M4-0.765-C-2 with loaded aerosol mass.

**Fig. 6.18.** SEM images of (a) and (b) the first, (c) and (d) the second, (e) and (f) the third and (g) and (h) the fourth layers of loaded 525-M4-0.765-C-1 seen from the front side.

**Fig. 6.19.** SEM images of (a) and (b) the first, (c) and (d) the second, (e) and (f) the third and (g) and (h) the fourth layers of loaded 525-M4-0.765-C-1 seen from the back side.

**Fig. 6.20.** Schematic of pressure drop versus aerosol deposit.

**Fig. A3.1.** Electrospinning apparatus used for spinning PVDF fibrous filters in this study.

**Fig. A3.2.** Corona discharge set-up used for charging PVDF filters in this study.

**Fig. A3.3.** Apparatus for surface potential (SP) tests in this study.

**Fig. A3.4.** SMAG system used for aerosol filtration tests and loading of filters in this study.

**Fig. A4.1.** Filtration efficiency ( $\eta$ ) of 84-nm (a) 1-layer and (b) multilayer PVDF filters; quality factors ( $QF$ ) of 84-nm (c) 1-layer and (d) multilayer PVDF filters. (Filters were in uncharged or charged state with varied layer filter weights. Note 84-S-0.191 and 84-M1-0.191 denote the same filter.)

**Fig. A4.2.** Filtration efficiency ( $\eta$ ) of 191-nm (a) 1-layer and (b) multilayer PVDF filters; quality factors ( $QF$ ) of 191-nm (c) 1-layer and (d) multilayer PVDF filters. (Filters were in uncharged or charged state with varied filter basis weights. Note 191-S-0.191 and 191-M1-0.191 denote the same filter.)

**Fig. A4.3.** Filtration efficiency ( $\eta$ ) of 349-nm (a) 1-layer and (b) multilayer PVDF filters; quality factors ( $QF$ ) of 349-nm (c) 1-layer and (d) multilayer PVDF filters. (Filters were in uncharged or charged state with varied filter basis weights. Note 349-S-0.191 and 349-M1-0.191 denote the same filter.)

**Fig. A4.4.** Filtration efficiency ( $\eta$ ) of 525-nm (a) 1-layer and (b) multilayer PVDF

filters; quality factors ( $QF$ ) of 525-nm (c) 1-layer and (d) multilayer PVDF filters. (Filters were in uncharged or charged state with varied filter basis weights. Note 525-S-0.191 and 525-M1-0.191 denote the same filter.)

**Fig. A4.5.** Pressure drop ( $\Delta p$ ) of 1-layer and multilayer PVDF filters with varied filter basis weights and fiber sizes. (Each filter had the same pressure drop in uncharged and charged states.)

**Fig. A4.6.** MPPS of (a) 1-layer uncharged, (b) multilayer uncharged, (c) 1-layer electret and (d) multilayer electret PVDF filters with varied filter basis weights and fiber sizes.

**Fig. A4.7.** Filtration efficiency ( $\eta$ ) of the optimized 525-nm (a) 1-layer and (b) multilayer PVDF filters; quality factors ( $QF$ ) of the optimized 525-nm (c) 1-layer and (d) multilayer PVDF filters. (Filters were in uncharged or charged state with varied layer basis weights. Note 525-S-0.765 and 525-M1-0.765 denote the same filter.)

**Fig. A6.1.** Variation of most penetrating particle size (MPPS) of different filters with loaded aerosol mass ( $M_{\text{dep}}$ ).

## List of Tables

**Table 3.1.**Physical parameters of 450-nm PVDF filters and PP substrate.

**Table 3.2.**Average surface potential ( $SP_{Avg.}$ ) of 450-nm PVDF filters.

**Table 6.1.**Pressure drop and deposit mass during depth and cake filtration.

**Table 6.2.**Ranking of 4 filters based on maximum pressure, efficiency and capacity.

**Table A1.**Physical properties of 450-nm PVDF filters and PP substrate.

**Table A2.**Loading data of 525-M4-0.765-C-1.

## Symbols & Abbreviations

### Symbols

$B$	Cake thickness	m
$c_{\text{down}}$	Aerosol number concentrations downstream of filter	$\text{cm}^{-3}$
$c_{\text{up}} / c_{\text{p}}$	Aerosol number concentrations upstream of filter	$\text{cm}^{-3}$
$c(d_{\text{p}}, \tau)$	Number concentration of upstream particles in the size bin with a geometric mean diameter $d_{\text{p}}$ at loading time $\tau$	$\text{cm}^{-3}$
$C$	Cunningham slip correction factor	~
$C'$	Constant	~
$d_{\text{a}}$	Aerodynamic diameter of particles	nm
$d_{\text{f}}$	Fiber diameter	nm
$d_{\text{p}}$	Particle diameter	nm
$D$	Coefficient of particle diffusion	~
$E$	Electrostatic field strength	$\text{N C}^{-1}$
$F_{\text{D}}$	Dielectrophoretic force acting on a particle	N
$G$	Constant	~
$k_{\text{B}}$	Boltzmann constant	~
$K_1$	Kozeny constant (= 5)	~
$Ku$	Kuwabara hydrodynamic factor	~
$M_{\text{dep}}$	Aerosol loaded mass	$\text{g m}^{-2}$

$M_{\text{dep}}(\tau)$	Aerosol loaded mass at loading time $\tau$	$\text{g m}^{-2}$
$M_{\text{dep}}(\Delta\tau)$	Aerosol loaded mass within loading time period $\Delta\tau$	$\text{g m}^{-2}$
$n$	Number of layers in a composite filter	$\sim$
$N_{Q0}$	Induction parameter	$\sim$
$N_{Qq}$	Columbic parameter	$\sim$
$N_R$	Interception parameter	$\sim$
$p$	Pressure	Pa
$p_{\text{down}}$	Pressure downstream of filter	Pa
$p_{\text{up}}$	Pressures upstream of filter	Pa
$P$	Aerosol penetration through filter	$\sim$
$P_M$	Aerosol penetration through filter with loaded mass	$\sim$
$Pe$	Peclet number	$\sim$
$q$	Charge held by an aerosol particle	C
$Q$	Charge per unit length of fiber	$\text{C m}^{-1}$
$QF$	Quality factor of filter	$\text{Pa}^{-1}$
$r$	Distance from fiber center	m
$SP$	Surface potential	V
$Stk$	Stokes number	$\sim$
$T$	Absolute temperature	K
$U$	Face velocity	$\text{m s}^{-1}$

$U_{d,C}$	Particle drift velocity towards a fiber under Coulombic force	$m s^{-1}$
$U_{d,C}$	Particle drift velocity towards a fiber under dielectrophoretic force	$m s^{-1}$
$W$	Filter basis weight	gsm
$W_L$	Basis weight of each individual layer in a multilayer filter	gsm
$Z$	Filter thickness	m
$\Delta p$	Pressure drop across filter	Pa
$\alpha$	Filter solidity	~
$\epsilon_0$	Permittivity of free space	$F m^{-1}$
$\epsilon_p$	Dielectric constant of particle	~
$\eta$	Filtration efficiency of filter	~
$\eta(d_p, \tau)$	Filtration efficiency of particles with a diameter $d_p$ at loading time $\tau$	~
$\eta_M$	Filtration efficiency of filter due to mechanical effects	~
$\eta_o$	Filtration efficiency of filter due to dielectrophoretic force	~
$\eta_l$	Filtration efficiency of one layer in composite filter with $n$ identical layers	~
$\eta_n$	Filtration efficiency of composite filter with $n$ identical layers	~
$\eta_s$	Single fiber efficiency of filter	~
$\eta_{s,D}$	Single fiber efficiency of filter due to Brownian diffusion	~

$\eta_{s,I}$	Single fiber efficiency of filter due to inertial impaction	~
$\eta_{s,o}$	Single fiber efficiency of filter due to dielectrophoretic force	~
$\eta_{s,o,1}$	Single fiber efficiency of 1-layer filter due to dielectrophoretic force	~
$\eta_{s,o,n}$	Single fiber efficiency of n-layer filter due to dielectrophoretic force	~
$\eta_{s,C}$	Single fiber efficiency of filter due to Columbic force	~
$\eta_{s,R}$	Single fiber efficiency of filter due to interception	~
$(\eta_s)_E$	Single fiber efficiency of filter due to electrostatic effects	~
$(\eta_s)_M$	Single fiber efficiency of filter due to mechanical effects	~
$(\eta_s)_{M+o}$	Single fiber efficiency of filter due to mechanical effects and dielectrophoretic force	~
$\lambda$	Mean free pass of air molecules	m
$\mu$	Particle mobility	m s <sup>-1</sup>
$\rho_p$	Particle material weight density	kg m <sup>-3</sup>
$\rho_f$	Fiber material weight density	kg m <sup>-3</sup>
$\sigma$	Fiber surface charge density	C m <sup>-2</sup>
$\nu$	Viscosity of air	Pa s
$\varphi$	Filter surface aerosol cake porosity	~
$\omega_e$	Particle electrical mobility	m s <sup>-1</sup>

## Abbreviations

CPC	Condensation particle counter
CMD	Count median diameter
DOP	Diocetyl phthalate
DMA	Differential mobility analyzer
DMF	N,N-dimethylformamide
EMD	Electrical mobility diameter
IPA	Isopropyl alcohol
MPPS	Most penetrating particle size
MW	Molecular weight
PAMS	Portable Aerosol Mobility Spectrometer
PET	Polyethylene terephthalate
PFTS	Portable filter test system
PM	Particulate matter
PP	Polypropylene
PS	Polystyrene
PPE	Polyphenylene ether
PTFE	Polytetrafluoroethylene
PU	Polyurethane
PVDF	Polyvinylidene fluoride

RH	Relative humidity
SEM	Scanning electron microscope
SMAG	Sub-micrometer aerosol generation system
STP	Standard temperature and pressure
VOC	Volatile organic compound

# Chapter 1: Introduction

## 1.1. Background

The large amount of fine suspended particulate matter (PM), PM<sub>2.5</sub> (PM with aerodynamic diameter  $d_a \leq 2.5 \mu\text{m}$ ) especially, emitted from human activities, e.g., traffic and industry, has created serious air pollution problems and raised a major health concern [1-6]. Submicron and nano- aerosols are airborne aerosols smaller than 1000 nanometers. They are present in pollutants to viruses (with high concentrations in polluted places such as industrial areas and traffic environment), both of which can seriously damage our health as we can inhale them readily. Once entering our body, they can diffuse readily by virtue of their small sizes into various tracks, including our vascular track, and can cause serious chronic diseases. Effective protective measures are urgently required to protect people from PM but remain a great challenge due to the small sizes of fine particles. Filtration is one of the main methods used for removing particles from gas streams. Of the available filters, fibrous filters are proved relatively efficient and economically applicable in removing micro-, submicron aerosols and nano-aerosols (less than 100nm). They have been widely applied in the areas of respirators, indoor air purification, vehicle air filtration and industrial gas cleaning [7-9]. To improve filtration efficiency, two main approaches, including increasing fiber amount and reducing fiber diameter while maintaining basis weight, have been applied to the fabrication of fibrous filters. However, because of the highly compact structure, the high efficiency is often achieved at the expense of high pressure drop, leading to high energy consumption. Besides, the fibers are typically made of microfibers 2 to 20  $\mu\text{m}$  from melt-blown method. Because of their large fiber diameters, they are not so

effective in filtering nano-aerosols [10-13].

Attributed to the electrical attraction between charged fibers and particles with net or induced charges, electret fibrous filters have been of increasing interest for researchers in recent decades. Specially, since coulomb force only acts on particles with net charges, researchers began to pay more attention to the dielectrophoretic filtration effect, where dipoles are induced on particles when in close proximity with charged fibers in a filter. The subsequent electrical interaction between the dipole of the particle and the charged fiber results in particle capture by the filter. Because of the imparted electrostatic force from the surface/volume charges or dipoles, filters can be fabricated with less compacted fibers, thus reducing air flow resistance while keeping high filtration efficiency [7, 11, 13, 14]. Moreover, compared with pure mechanical filters, electret filters were reported to have higher aerosol holding capacities due to the more uniform distribution of aerosols and slower formation of dendrites and aerosol cake on fibers when applied for long-term use [11, 15-18]. Apparently, electret filters exhibit certain advantages than traditional mechanical filters.

Generally, to exhibit electret properties, the filter material (usually polymers) should have sufficient charge traps or be easily polarized [13, 19]. To date, several polymers, e.g. polypropylene (PP), polyurethane (PU) and Nylon-6, have been used to make fibrous filters and studied for their chargeability and filtration performance [20-24]. Sim et al. found that the polyurethane fiber filter treated by corona discharge had about 30% improvement in filtration efficiency up to 80.9% for KCl particles ranging from 20 to 660 nm compared with the uncharged filter [23]. Yeom et al. observed that after charging the filtration efficiency of their nanofiber filter increased to 96.8% for 300-nm DOP (dioctyl phthalate) aerosols, with an absolute surface potential of 89 V

and pressure drop of 48.0 Pa at a 5.3 cm s<sup>-1</sup> face velocity [24]. Based on the available researches, electret fibrous filters are believed to be promising for aerosol removal without increasing pressure drop to the filters. However, the studied materials for air filtration are still limited, and the problems of charge instability and charge screening by deposited aerosols which prevent filters from long-term storage and use are yet to be solved [13, 19, 25-27].

Because of its outstanding properties: superior electrical insulation, ferroelectricity, chemical resistance, thermal properties, and biocompatibility, polyvinylidene fluoride (PVDF) has been extensively investigated for its applications in the fields of sensors, water treatment, membrane distillation and acid gases absorption, mostly in the form of membrane [28-30]. While some researchers have investigated the preparation of PVDF fibers by electrospinning, only a few studied the electrostatic charging property of fibrous filters and their filtration performance [31-42]. Of several approaches to making electret filters, corona discharge was most applied due to the simplicity and effectiveness of this technology. With the high electric field during charging, a large portion of space charges might reside in deep traps [13, 19, 43]. Moreover, benefiting from the strong electronegativity of fluorine atoms, polarized dipoles could be generated under the electric field of embedded charges [40, 44]. In addition, the properties of high hydrophobicity and extremely low conductivity may endow PVDF filters with superior charge stability and stable filtration performance [30, 38, 39].

Other than materials, filter configurations also play an important part in filtration performance. The merit of “multilayering”, i.e. redistributing fibers from a 1-layer filter into multiple layers, has been confirmed for reducing pressure drop owing to the decreased fiber packing density while keeping relatively high efficiency in our previous

research [45-47]. After separating fibers into 12 layers, Leung et al. obtained a pressure drop saving of 93.12 Pa from the original 161.2 Pa of the 1-layer filter, while the filtration efficiency only dropped by 8.77% from 91.37% [46]. Based on the existing knowledge, it is intuitively to think that this outstanding property applies to electret filters as well. Considering that a high density of charges in a 1-layer filter may actually lead to interference of electrostatic effect between adjacent charges, filtration efficiency is also expected to improve after fiber redistribution, apart from pressure drop alleviation [7, 48, 49]. In addition, when a 1-layer electret filter is meant for long-term use in a heavily aerosol-laden environment, aerosols can quickly aggregate on the filter surface and form a packed particle layer (“skin layer”), leaving the downstream charged fibers insufficiently used and the pressure drop dramatically rising [16, 17, 50]. Through increasing filter porosity, the formation rate of “skin layer” is highly possible to be lower as more aerosols can penetrate the filter surface and the downstream charged fibers are more accessible.

Despite the merits of PVDF, relatively few studies focused on the filtration performance of PVDF electret filters. And to the best of our knowledge, multilayer electret filters was not reported in the literature. Therefore, more effort is needed to investigate the filtration properties of multilayer PVDF electret filters.

## **1.2.Objectives of study**

Based on the outstanding physiochemical characteristics of PVDF and the merits of filter multilayering, both the short-term and long-term aerosol filtration properties of multilayer PVDF electret nanofiber filters were systematically investigated in this study as a potential candidate for face masks.

The detailed objectives of this study are as follows:

- 1) Fabricate PVDF nanofiber filters with good morphology using electrospinning.
- 2) Investigate the electrostatic chargeability and the charge stability of PVDF filters and optimize the charging condition of corona discharge.
- 3) Examine the short-term filtration performance and find the work mechanism of multilayer PVDF electret filters.
- 4) Optimize filter short-term performance by adjusting filter structure and configuration.
- 5) Testify the applicability of multilayer PVDF electret filters in real aerosol-laden environment.
- 6) Study the aerosol loading behaviors, i.e. long-term filtration performance, of multilayer PVDF electret filters.

### **1.3.Scope of thesis**

This thesis consists of seven chapters and is structured as follows:

Chapter 1 briefly covers the background, the objectives of this research and the scope of this thesis.

Chapter 2 presents a review of relevant literature on the evolution, the fabrication methods and the work mechanisms of electret filters.

Chapter 3 reports the preliminary test results and discusses the work mechanism of multilayer PVDF electret filters which showed great advantages over other filters.

Chapter 4 describes the optimization of filter performance by adjusting the structure and configuration of multilayer PVDF electret filters.

Chapter 5 testifies the applicability of multilayer PVDF electret filters for aerosol removal in a real traffic environment.

Chapter 6 presents the excellent aerosol loading behaviors of multilayer PVDF electret filters compared with other filters and proposed the main reasons for the improvement in aerosol holding capacity.

Chapter 7 summarizes the main conclusions, discusses the limitations of this study and suggests future investigations.

Specially, to make it convenient to be referred to, the experimental details related to specific chapters were respectively presented in Chapter 3 to Chapter 6, instead of in just a single chapter.

## Chapter 2: Literature Review

### 2.1. Definition of electret fibrous filters

Electret fibrous filters (or electrically active fibrous filters) are a kind of filter that consists of charged fibers (often made of dielectric polymers) and within which electrostatic field exists. Filters of this type have similar structures to the conventional mechanical filters. When an electric field or triboelectrification is applied to the dielectric materials used for fabricating filters, quasi-permanent electrical charges (net or dipole charges) are developed on the fibers and thus turn the mechanical filters into electret ones [13, 19]. Therefore, besides the mechanical filtration mechanisms (including mainly Brownian diffusion, interception and inertial impaction), aerosols in air stream can be captured via additional electrostatic filtration mechanisms by Columbic or dielectrophoretic force [7]. Benefitting from the electrostatic mechanisms, electret filters with more porous structures can be manufactured for which high clean filter filtration efficiency can be achieved with much lower pressure drop [13]. Moreover, it is widely believed that aerosols deposit more uniformly on charged fibers, hence the pressure drop can increase at a lower rate with aerosol loading and the electret filter has a higher aerosol holding capacity than a purely mechanical filter [15-17]. Nevertheless, for electret filters, there is also the unavoidable shortcoming that filtration efficiency decreases with loaded aerosol mass in initial stage, due to the screening of charges or the chemical erosion of fibers by the deposited aerosols [15-17, 50-52].

For an electret filter to exhibit excellent electrostatic filtration performance, the composition material(s) should have two characteristics: superior chargeability and high charge stability, with the former one affecting charge density and the latter one long-term performance. Charge density is concerned with injected charges or

polarization, while charge stability is related to charge transport and recombination processes. In general, traps for electrons, ions and dipoles exist at structurally defective sites in polymeric materials in molecular, conformational and morphological levels [13, 19]. To have better chargeability, the materials should have sufficiently deep traps (mostly from chemical impurities) because of the extremely fast dissipation of charges in shallow traps [43, 53, 54]. And to achieve a long charge retention time, the electrical conductivities of the materials should be low (i.e. high electrical resistivities) and not exceed  $10^{-8}$ - $10^{-10} \Omega \text{ cm}^{-1}$ . Also, the moisture regain of the materials should be low as water is much more conductive than most polymers and may enhance the discharging process of charged fibers [19].

According to the required properties, several polymers (e.g. PP, PTFE and PVDF) have been used to fabricate electret filters for their potential application in aerosol filtration. Based on the manufacturing methods, the existing electret air filters can be generally categorized as (i) corona-charged, (ii) triboelectrically-charged and (iii) electrospun-charged electret filters, which will be reviewed in detail later on.

## **2.2. Types of electret fibrous filters**

Since the invention of the Hansen filter in the 1930s, various kinds of electret filters were fabricated to make use of the electrostatic effects for aerosol capture [13, 15]. Based on the manufacturing methods, electret filters can be classified as corona-charged, tribo-charged and electrospun electret filters, though oftentimes more than one method are involved in the preparation of an electret filter to improve filtration performance.

### **2.2.1. Corona-charged electret fibrous filters**

Mechanical fibrous filters can be converted to electret filters using the technique of corona discharge [13, 55]. The charging device normally involves two asymmetric electrodes, with the emitting electrode being a fine point or wire and the receiving electrode being a plate or cylinder. When a sufficiently high potential difference exists between them, ions are generated from ionization of the air molecules near the emitting electrode by the high electric field and are driven towards the receiving electrode on which the insulating filter is placed. As a result, some charges are injected to the fibers and exist as space charges whose polarity are the same as that of the emitting electrode. Positive and negative corona discharges can both cause charge deposition on filters but have different generation approaches, species, densities and energy of ions.

Many factors, including device settings (e.g. charging distance, voltage and time), ambient environment (e.g. gas medium, and relative humidity (RH)) and filter property (e.g. temperature), affect charge density or stability on corona-charged filters [56-62]. On the premise that ions have enough momentum, a long distance between corona electrode and filter facilitates uniform distribution of charges over the filter. Higher charging voltage is expected to increase the charge density in filters. However, it is suggested that there exists a critical voltage beyond which surface potential decreases due to the local discharge (back corona) inside the filter. For charging time, a longer duration of corona discharge does not necessarily bring a higher charge density because a sheath layer of deposited charges will form close to the filter surface and will repulse the ions coming later. Therefore, there is a threshold of charging time because of charge saturation in the filter. To a less extent, the influence of gas medium on corona discharge was also studied. It was found that electronegative gases, such as oxygen,

could weak the resultant corona, whereas non-electronegative gases, like inert gases, could lead to more intense and more uniform corona discharge. Humidity mainly affect corona discharge by increasing hydrated ion species, as well as by causing shorter charge retentions on filter due to higher electrical conductivities. Compared with device settings and ambient environment, a more influential factor is the temperature of the filter during corona discharge. It was reported that by first heating up (sometimes in molten state) and then cooling off the filter under the continuous electric field, the injected space charges had a higher density and better stability. Moreover, more dipoles were formed due to the higher molecular mobility of polymer and were “frozen” permanently in the filter.

Corona discharge method can prepare filters with high charge densities by adjusting various parameters. However, electrical arcing through filter is prone to happen at high charging voltages [58, 63]. Another drawback of corona discharge is the generation of functional groups from the injection of high-energy charges, which can increase charge mobility and raise charge decay rate on the filter [61, 64]. More importantly, uniform distribution of charges is difficult to realize using the classical dual-type electrode system [65]. To tackle these problems, the triode-type electrode system was developed by placing a metallic grid between the corona tip and the filter holder. Via this modification, the voltage acting on the filter was lowered and charge uniformity was better, though no distinct improvement of charge density was observed [27, 59, 66].

### **2.2.2. Tribo-charged electret fibrous filters**

Tribo-charged electret filters are manufactured based on the phenomenon of frictional electrification where there is charge transfer after frictional contact between

two dissimilar materials with at least one being insulator [19, 55]. These electret filters are comprised of fibers or fibers and particles with opposite charge polarities. Many filters have been fabricated by mixing two kinds of fibers, such as PTFE/steel and PP/acrylic, and showed great performance for aerosol filtration [52, 67-69]. The famous Hansen resin-wool filter, which binds colophony powder and wool fibers together during carding process, belongs to the latter category [7]. Generally, both positive and negative charges exist on each material surface, but oftentimes one polarity is dominant and decides the net charges. As commonly seen, simple contact and separation can be sufficient to get the filters charged. And filter composition, fiber surface properties, contact area and acting forces are the key factors for the effect of triboelectrification [19].

Basically, there are two mechanisms for triboelectrification, with the main difference being that whether the charge transfer takes place via electrons or ions [19]. In the first mechanism, kinetic and equilibrium components are believed to be involved during frictional contact, which results in electron transfer due to the different electron affinities of the two materials [70, 71]. Based on the tendency of donating/accepting electrons, a variety of commonly-used materials are ranked to form the triboelectric series. Higher charge intensity is expected to be produced by blending two materials from the two sides farther away from each other. In general, polar polymers occupy the more positive side while nonpolar polymers the more negative side [72, 73]. The mechanism of electron transfer has been proved valid for many cases. However, some researchers argued that the thermal energy generated from contact/friction would be far from enough for electron transfer between nonionic polymers, though sufficient for metals or semiconductors. They proposed the second mechanism in which charge

transfers indirectly through a water interface between the surfaces of the two contacting materials [19, 74]. Based on their affinities to anionic/cationic ions, the two polymers get oppositely charged ions from the splitting of the water layer where hydroxide and hydronium ions are originally in equilibration. This theory has been proved in several studies where less or even no electrification was observed at 0% relative humidity [74, 75]. According to this mechanism, water is necessary in facilitating ion transfer. Nevertheless, there is an upper limit of relative humidity for tribo-electrification because of the increased surface electrical conductivity at high humidity.

Manufacturing electret filters by tribo-electrification methods can avoid the increase of fiber surface hydrophilicity (thus higher electrical conductivity) which occurs during corona discharge process. Nonetheless, the parameters of triboelectric charging are difficult to control and the charging effect cannot be easily predicted. Therefore, corona discharge may be a better option when a controlled charging process is needed.

### **2.2.3. Electrospun electret fibrous filters**

Electrospinning is mainly applied as a technique to fabricate fibrous filters with submicron and nano-sized fibers from polymer solutions, in which process charges reside on the filters. The spinning device normally consists of a metallic nozzle/needle and a grounded collector. During a typical process, a high voltage is applied to the nozzle/needle where charges are introduced to the polymer solution and charged jets are ejected towards the collector. Fibers are formed during the flight of jets under the electric field and eventually deposit on the collector, with some net charges residing on the newly formed filter [76-79].

Compared to electret filters prepared by corona discharge or tribo-electrification, fewer studies were concerned with the electrical properties of electrospun electret filters, especially of those made of pure fibers, which is mainly because of lower charge densities [80]. Among the various polymers used for electrospinning, only several materials, such as Nylon-6 and PVDF, were co-spun with additives (to improve chargeability) as electret filters for aerosol removal and different results were achieved [24, 40-42]. Although high surface potential can be achieved with large filter basis weights, the filters usually have enormously high pressure drop which makes aerosol filtration inefficient. Besides, attributed to the instability of electrospinning and nonuniformity of fibers, it is hard to establish the dependency of the distribution of electrostatic charges on electrical polymer properties and filter structures. Therefore, other kinds of charging processes are often applied to electrospun filters before being used as electret filters.

### **2.3. Performance characterization of electret fibrous filters**

The criteria for evaluating the performance of electret air filters have no difference from that of conventional mechanical ones, i.e. “what percentage of target aerosols are removed at what cost?”. Specifically, the commonly-used indexes include filtration efficiency, pressure drop and quality factor.

#### **2.3.1. Filtration efficiency**

As air filters are widely used in areas concerning human health (e.g. respirator and indoor air purifiers) and at places where low aerosol concentration is required (e.g. cleanrooms and precision instrument manufacturing plants), it is the effectiveness of the filters that is most valued. The filtration efficiency is defined as the fraction of the entering particles that are collected by the filter, i.e., by the ratio of the difference

between the number concentrations of particles upstream and downstream of the filter to that upstream of the filter [1, 7, 13]. This is shown below:

$$\eta = \frac{c_{\text{up}} - c_{\text{down}}}{c_{\text{up}}} \quad (2.1)$$

where  $\eta$  represents the filtration efficiency of the filter, and  $c_{\text{up}}$  and  $c_{\text{down}}$  are, respectively, the number concentrations upstream and downstream of the filter. Alternatively, mass concentration of particles can be used to define the efficiency. Clearly, the filter performance is better when the filtration efficiency is higher.

Sometimes the filtration performance of electret air filters is characterized using the term “penetration”. For a high-efficiency filter, the penetration is a clearer indicator because it is a smaller number and therefore shows a larger relative change than the collection efficiency. The penetration is determined by the ratio of the number concentration of particles downstream of the filter to that upstream of the filter. This is expressed as follows:

$$P = \frac{c_{\text{down}}}{c_{\text{up}}} \quad (2.2)$$

where  $P$  represents aerosol penetration. Evidently, the better performance of the filter is indicated by the lower penetration. The relationship between penetration and filtration efficiency is shown below:

$$P = 1 - \eta \quad (2.3)$$

Apart from getting filtration efficiency of filters experimentally, a lot of theoretical work has been done to determine aerosol capture based on single fiber efficiency [7, 11, 13, 15]. Because of the highly porous structure of fibrous filters and the random distribution of fibers, it is intuitive to think that an individual particle has a high

possibility to interact with just one fiber. By applying the single fiber microscopic approach and accounting for the macroscopic properties (e.g. fiber diameter ( $d_f$ ), filter solidity ( $\alpha$ ) and flow pattern) at the same time, the overall filtration efficiency of a filter can be achieved and this approach has been proved effective in efficiency prediction by much modelling work. One of the most popular equations that relate filter efficiency to single fiber efficiency is as follows:

$$\eta = 1 - \exp \left[ -\frac{4\alpha\eta_s Z}{\pi(1-\alpha)d_f} \right] \quad (2.4)$$

where  $\alpha$  denotes filter solidity,  $\eta_s$  represents single fiber efficiency,  $Z$  stands for filter thickness and  $d_f$  refers to fiber diameter. This equation simplifies the properties of filters that all fibers (1) are straight with identical diameter, (2) are perpendicular to the aerosol flow direction, (3) distribute uniformly in the filter, and (4) have the same single fiber efficiency across the filter [11]. Although real filters are far more complex, the equation has been proved useful throughout years' application.

For a single fiber in an electret filter, it captures aerosols via both mechanical and electrostatic filtration mechanisms. Assuming the two kinds of mechanisms act independently, single fiber efficiency can be expressed as follows:

$$\eta_s = \eta_{s,M} + \eta_{s,E} \quad (2.5)$$

where  $\eta_{s,M}$  and  $\eta_{s,E}$  indicate the mechanical and the electrostatic efficiency of a single electret fiber, respectively.

Generally, for submicron and nano- aerosols, mechanical filtration mechanisms mainly include Brownian diffusion, interception and inertial impaction, and electrostatic filtration mechanisms primarily consist of Columbic force capture and electrophoretic force capture [13]. Again, to simplify theoretical studies, these

mechanisms are normally assumed mutually independent to each other, which gives the following equations:

$$\eta_{s,M} = \eta_{s,D} + \eta_{s,R} + \eta_{s,I} \quad (2.6)$$

$$\eta_{s,E} = \eta_{s,Qq} + \eta_{s,Q0} \quad (2.7)$$

where  $\eta_{s,D}$ ,  $\eta_{s,R}$  and  $\eta_{s,I}$  stand for diffusional, interceptional and impactional capture efficiency, and  $\eta_{s,Qq}$  and  $\eta_{s,Q0}$  refer to Columbic and dielectrophoretic capture efficiency of a single electret fiber, respectively.

### 2.3.2. Pressure drop

Pressure drop is another important characterization to evaluate the performance of filters [1, 7, 13]. It occurs primarily because there exists drag forces from individual fibers when air fluid flows across a filter. Since air resistance is concerned with energy consumption, low pressure drop is preferred on the premise that filtration efficiency meets the requirement of application. Pressure drop is defined by the difference of flow pressures between the upstream and the downstream sides of a filter, which is expressed as:

$$\Delta p = p_{up} - p_{down} \quad (2.8)$$

where  $\Delta p$  is the pressure drop, and  $p_{up}$  and  $p_{down}$  are the flow pressures upstream and downstream of the filter, respectively.

Alternatively, the pressure drop ( $\Delta p$ ) of a filter can be predicted using theoretically derived equations. By combining Darcy's law and a large amount of experimental data, a classical expression was introduced by Davies as shown below:

$$\Delta p = \frac{64\nu UZ}{d_f^2} \alpha^{3/2} (1 + 56\alpha^3) \quad (2.9)$$

where  $\nu$  is the viscosity of air,  $U$  is the face velocity,  $Z$  is the filter thickness,  $d_f$  is the fiber diameter, and  $\alpha$  is the filter solidity.

According to Davies, this equation is valid for  $1.6 \mu\text{m} < d_f < 80 \mu\text{m}$  and  $0.006 < \alpha < 0.3$ . And the scattering of experimental pressure drop should be within  $\pm 30\%$  of the estimated values. Later, Werner and Clarenburg further extended the application range of fiber diameter to  $0.098 \mu\text{m} < d_f < 1.54 \mu\text{m}$  with  $\alpha$  between 0.039 and 0.084 using glass fiber filters [11]. Davies' equation has been frequently used in practice and found to agree well with measured data, though it is highly empirical.

Besides Davies, based on Darcy's law, several other researchers, including Happel, Kuwabara and Pich, also proposed varied expressions considering different interactions between fluid flow and single fibers [1, 7, 13]. These expressions have as well found their application in many scenarios concerning fibrous air filters.

### 2.3.3. Quality factor

The performance of fibrous air filters is evaluated accounting for both filtration efficiency and pressure drop. However, it is often impractical and difficult to compare filters manufactured with different materials, filter structures or techniques using these two indexes. Properly designed filters are expected to first remove a high proportion of aerosols while simultaneously maintaining the pressure drop as low as possible. To couple filtration efficiency and pressure drop together, another characteristic parameter "quality factor ( $QF$ )" of filter is introduced, which is defined as the ratio of negative natural log of penetration to pressure drop as follows [1, 7, 13]:

$$QF = -\frac{\ln P}{\Delta p} = -\frac{\ln(1-\eta)}{\Delta p} \quad (2.10)$$

where  $P$  is the aerosol penetration through filter,  $\Delta p$  is the pressure drop across filter, and  $\eta$  is the filtration efficiency of filter.

For a given aerosol size and a given face velocity, a higher value of quality factor means more efficient removal of aerosols by the filter.

#### 2.4. Filtration mechanisms of electret fibrous filters

When an aerosol flow moves near a fiber, particles may be captured by the fiber through the concurrent effects of mechanical capture mechanisms (mainly Brownian diffusion, interception and inertial impaction) and electrostatic capture mechanisms (mainly Coulombic force and dielectrophoretic force) [1, 7, 11, 13, 15]. Fig. 2.1 and Fig. 2.2 depict the primary mechanical and electrostatic capture mechanisms, respectively.

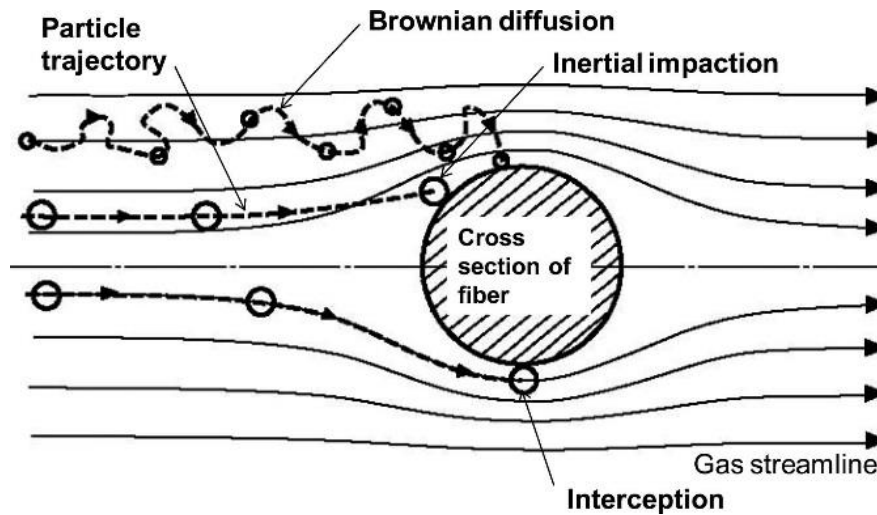


**Fig. 2.1.** Particle collection by mechanical mechanisms including Brownian diffusion, interception, inertial impaction and gravitational settling [11].

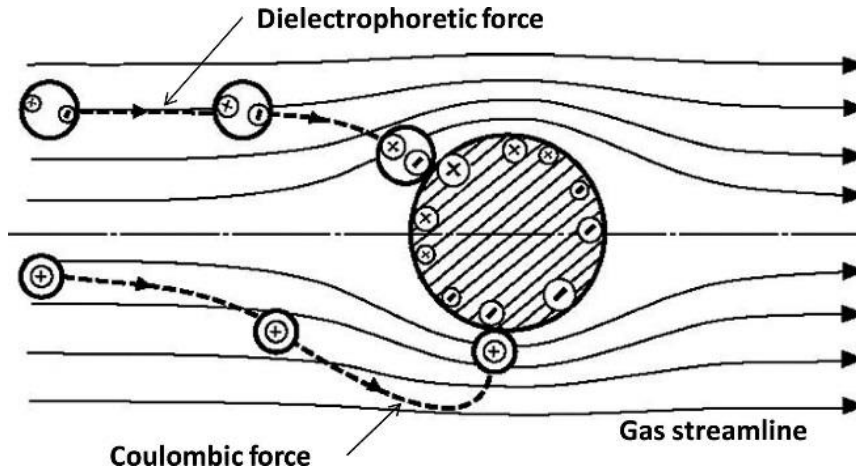


**Fig. 2.2.** Particle collection by electrostatic mechanisms including Coulombic and dielectrophoretic forces [11].

## 2.4.1. Mechanical capture mechanisms

### 2.4.1.1. Brownian diffusion

Small aerosol particles have a random Brownian motion due to their collisions with gas molecules surrounding them and instant thermal energy equilibrium. In an air stream approaching a fiber, these particles roughly do not flow along the original streamlines because of the strong Brownian motion. Instead, they continuously deviate from the streamlines and may contact the fiber under the combined action of airflow and Brownian motion and attach to it by the van der Waals attraction force. This process is diffusional capture and is the dominant mechanism for particles smaller than  $0.1 \mu\text{m}$ . The diffusional capture of particles is found to increase with smaller particle size attributed to higher randomness of motion and with lower face velocity contributed by longer retention time at the vicinity of fiber surface [1, 7, 11, 13, 15].

The coefficient of particle diffusion,  $D$ , in specific air stream conditions is expressed by the Einstein equation:

$$D = \mu k_B T \quad (2.11)$$

where  $\mu$  is the particle mobility,  $k_B$  is the Boltzmann constant and  $T$  is the absolute temperature.

The particle mobility,  $\mu$ , is given by:

$$\mu = \frac{C}{3\pi\eta d_p} \quad (2.12)$$

where  $\eta$  is the air viscosity,  $d_p$  is the particle diameter, and  $C$  is the Cunningham slip correction factor accounting for the aerodynamic slip at particle surface which is normally defined by:

$$C = 1 + 2.492 \frac{\lambda}{d_p} + 0.84 \frac{\lambda}{d_p} \exp\left(-0.435 \frac{d_p}{\lambda}\right) \quad (2.13)$$

where  $\lambda$  is the mean free path of air molecules, and  $d_p$  is the particle diameter.

Diffusional capture depends on the relative magnitude of convection and diffusion of air past the fiber, which is well explained by the dimensionless parameter Peclet number,  $Pe$ :

$$Pe = \frac{d_f U}{D} \quad (2.14)$$

where  $d_f$  is the fiber diameter,  $U$  is the face velocity, and  $D$  is the coefficient of particle diffusion.

Based on the Kuwabara flow field and a multiple cylinder model that considers the flow interference of the neighboring fibers, the equation for single fiber efficiency by Brownian diffusion,  $\eta_{s,D}$ , was proposed as follows:

$$\eta_{s,D} = 2.58 \left(\frac{1-\alpha}{Ku}\right)^{1/3} Pe^{-2/3} \quad (2.15)$$

where  $\alpha$  is the filter solidity,  $Pe$  is the Peclet number, and  $Ku$  is the Kuwabara hydrodynamic factor:

$$Ku = -\frac{1}{2}\ln\alpha - \frac{3}{4} + \alpha - \frac{\alpha^2}{4} \quad (2.16)$$

where  $\alpha$  is the filter solidity.

#### 2.4.1.2. Interception

A particle with a negligible mass but a finite size may be captured by a fiber when it comes within one particle radius from the fiber surface moving along its streamline. Such mechanism of particle collection is described as interception. For a given fiber, aerosol capture is solely related to particle size and independent of flow velocity during interception [1, 7, 11, 13, 15].

The aerosol capture by interception is described by a dimensionless interception parameter,  $N_R$ , as shown below:

$$N_R = \frac{d_p}{d_f} \quad (2.17)$$

where  $d_p$  is the particle diameter, and  $d_f$  is the fiber diameter.

For the most popular single fiber model, Kuwabara model, single fiber efficiency by interception,  $\eta_{s,R}$ , is expressed as:

$$\eta_{s,R} = \frac{1+N_R}{2Ku} \left[ 2 \ln(1 + N_R) - (1 - \alpha) + (1 + N_R)^{-2} \left( 1 - \frac{\alpha}{2} \right) - \frac{\alpha}{2} (1 + N_R)^2 \right] \quad (2.18)$$

where  $N_R$  is the dimensionless interception parameter,  $Ku$  is the Kuwabara hydrodynamic factor, and  $\alpha$  is the filter solidity.

#### 2.4.1.3. Inertial impaction

When an aerosol particle has sufficiently high momentum, it can deviate from the diverged streamlines of the fluid flow as it approaches a fiber and keep moving towards the fiber, thus causing the particle to impact on the fiber. The likelihood of impaction is affected by the particle aerodynamic size and the velocity difference between the

particle and the fiber. This kind of capture due to the inertia of particles is described as inertial impaction. The inertial impaction is significant for particles with high masses (dominant for particles larger than 0.5  $\mu\text{m}$ ) or on highly-curved streamlines due to their higher inertia [1, 7, 11, 13, 15].

The degree to which the capture of a particle is influenced by inertial impaction is related to the relative magnitude of the inertia of the particle and the fluid drag acting upon it, which is quantified by the dimensionless Stokes number,  $Stk$ , as below:

$$Stk = \frac{Cd_p \rho_p U}{18\mu d_f} \quad (2.19)$$

where  $C$  is the Cunningham slip correction factor,  $d_p$  is the particle diameter,  $\rho_p$  is the particle density,  $U$  is the face velocity,  $\mu$  is the particle mobility, and  $d_f$  is the fiber diameter.

For small Stokes number, the single fiber efficiency by inertial impaction,  $\eta_{s,I}$ , was shown below:

$$\eta_{s,I} = \frac{Stk}{2Ku^2} [(29.6 - 28\alpha^{0.62})N_R^2 - 27.5N_R^{2.8}] \quad (2.20)$$

where  $Stk$  is the Stokes number,  $Ku$  is the Kuwabara hydrodynamic factor,  $\alpha$  is the filter solidity, and  $N_R$  is the dimensionless interception parameter.

As each mechanical filtration mechanism dominates a specific particle diameter range and the mechanisms response differently to the variation in particle size, for a mechanical filter, there exists a particle size range where filtration efficiency is apparently low. The least captured particle size is named “most penetrating particle size (MPPS)”. To improve the capture of particles in this region, electrostatic filtration by electret filters is particularly essential.

## 2.4.2. Electrostatic capture mechanisms

### 2.4.2.1. Coulombic force

For a charged particle approaching an oppositely charged fiber in an electret filter, it can deviate from the fluid streamline and be pulled toward the fiber surface by the simple principle of “opposite charges attract” under Coulombic force. The extent of this mechanism depends on the relative strength of the Coulombic attractive force to the fluid drag acting on the aerosol particle [1, 7, 11, 13, 15, 81].

The complex configuration of electric charges on charged fibers makes approximations necessary in developing theories for particle capture by electric forces. The primary approximation assumes that a charged filter fiber carries a uniform charge amount  $Q$  per unit length and acts purely in the radial direction from the fiber center. Based on this assumption, the electrostatic field strength,  $E$ , at a distance  $r$  from the fiber center can be expressed as:

$$E = \frac{Q}{2\pi\epsilon_0 r} \quad (2.21)$$

where  $Q$  is the charge amount per unit length of fiber,  $\epsilon_0$  is the permittivity of free space, and  $r$  is the distance from fiber center.

For a charged particle with a charge  $q$ , its electrical mobility  $\omega_e$  is:

$$\omega_e = \frac{q}{3\pi\mu d_p} \quad (2.22)$$

where  $q$  is the charge amount held by an aerosol particle,  $\mu$  is the particle mobility, and  $d_p$  is the particle diameter.

By multiplying the magnitude of electric field ( $E$ ) and the electrical mobility ( $\omega_e$ ), the drift velocity of the particle,  $U_{d,C}$ , towards the fiber can be obtained:

$$U_{d,C} = \frac{Qq}{6\pi^2 \varepsilon_0 \mu d_p r} \quad (2.23)$$

where  $Q$  is the charge amount per unit length of fiber,  $q$  is the charge amount held by an aerosol particle,  $\varepsilon_0$  is the permittivity of free space,  $\mu$  is the particle mobility,  $d_p$  is the particle diameter, and  $r$  is the distance from fiber center.

Then, a dimensionless number,  $N_{Qq}$ , characterizing the Coulombic effect, can be achieved by dividing  $U_{d,C}$  by the convective velocity as shown below:

$$N_{Qq} = \frac{Qq}{3\pi^2 \varepsilon_0 \mu d_p d_f U} \quad (2.24)$$

where  $N_{Qq}$  is the Columbic parameter,  $d_f$  is the fiber diameter, and  $U$  is the face velocity.

Assuming the acting forces are solenoidal, the single fiber efficiency by Coulombic force,  $\eta_{s,C}$ , can be given by:

$$\eta_{s,C} = \pi N_{Qq} \quad (2.25)$$

where  $N_{Qq}$  is the Columbic parameter.

### 2.4.2.2. Dielectrophoretic force

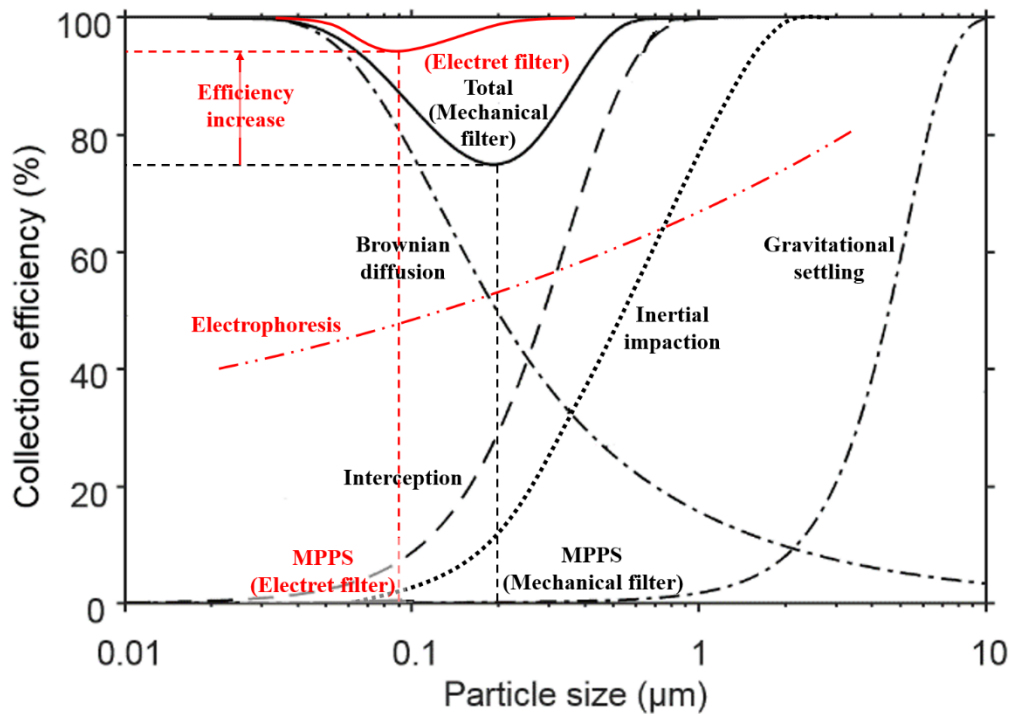


**Fig. 2.3.** Efficiency compositions of mechanical filters and electret filters for neutralized aerosol capture.

When a neutral aerosol particle moves close to a charged fiber, the uniformly distributed charges in the particle are affected by the electric field around the surface of the charged fiber. The charges with the same polarity to that of the fiber are repelled away from while those with the opposite polarity are drawn near to the fiber, resulting in the generation of macroscopic dipole. The strength of this induced dipole is related to the particle size and its dielectric constant ( $\epsilon_p$ ). Within the uneven electric field around the charged fiber, a dielectrophoretic force is then formed between the charged fiber and the polarized particle, thus attracting the particle to the fiber surface. The capture efficiency of a single charged fiber for neutral particles is not as high as for charged particles. It should also be mentioned that polarized charges can also be

induced on charged particles, though the dielectrophoretic force is relatively insignificant compared with the Coulombic force [1, 7, 11, 13, 15, 81].

The dielectrophoretic force,  $F_D$ , is expressed as follows:

$$F_D = \frac{Q^2 d_p^3}{8\pi\epsilon_0 r^3} \left( \frac{\epsilon_p - 1}{\epsilon_p + 2} \right) \quad (2.26)$$

where  $Q$  is the charge amount per unit length of fiber,  $d_p$  is the particle diameter,  $\epsilon_0$  is the permittivity of free space,  $r$  is the distance from fiber center, and  $\epsilon_p$  is the dielectric constant of particles.

The drift velocity of the particle  $U_{d,D}$  under  $F_D$  towards the fiber can be given by:

$$U_{d,D} = \frac{Q^2 d_p^2}{3\pi^2 \epsilon_0 \nu r^3} \left( \frac{\epsilon_p - 1}{\epsilon_p + 2} \right) \quad (2.27)$$

Then, a dimensionless number,  $N_{Q0}$ , characterizing the dielectrophoretic effect, can be achieved by dividing  $U_{d,D}$  by the convective velocity as shown below:

$$N_{Q0} = \frac{Q^2 d_p^2}{3\pi^2 \epsilon_0 \nu r^3 U} \left( \frac{\epsilon_p - 1}{\epsilon_p + 2} \right) \quad (2.28)$$

where  $N_{Q0}$  is the induction parameter,  $\nu$  is the air viscosity, and  $U$  is the face velocity.

Similar to the Coulombic force, the single fiber efficiency by the dielectrophoretic force,  $\eta_{s,0}$ , using the simplest approximation can be expressed as:

$$\eta_{s,0} = \pi N_{Q0} \quad (2.29)$$

where  $N_{Q0}$  is the induction parameter.

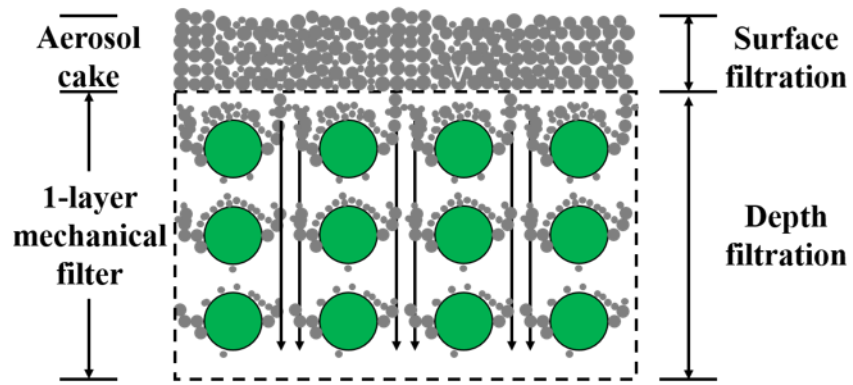
The efficiency compositions of mechanical filters and electret filters for neutralized aerosol capture are shown in Fig. 2.3. It can be seen that filtration efficiency of mechanical filters is greatly improved due to the dielectrophoretic effect. Meanwhile,

the MPPS decreases to a much lower value attributed to the more significant influence on larger particles.

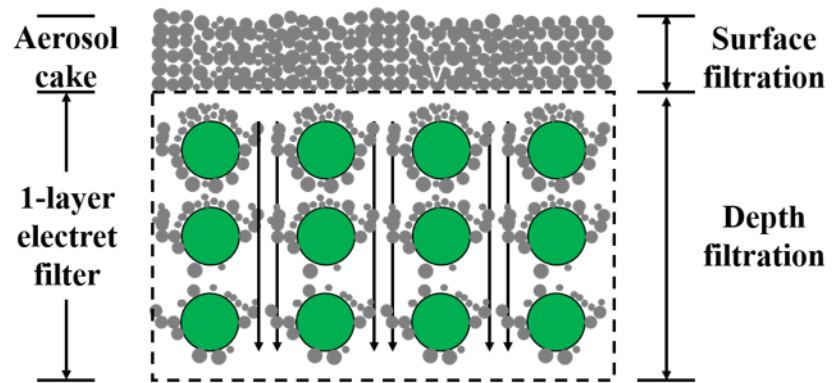
## **2.5. Loading behaviors of electret fibrous filters**

The single fiber theories have been proved helpful in studying the filtration properties of electret filters. However, these theories are only applicable in the early stage of filter life, i.e. clean filters. As an electret filter is continually challenged with aerosols, the captured particles occupy certain space and alter the structure of the filter. The schematics for aerosol deposition distribution in varied filters a certain time after complete formation of aerosol cake are shown in Figs. 2.3a-d. From the figures, it is clearly seen that aerosol particles deposit on different spots with different dendrites/cake structures based on the charging state and configuration of the filters. As a result, both the filtration efficiency and the pressure drop change gradually, while the filter becomes increasingly loaded [1, 7, 11, 15]. Though normally dust cake will not be formed in general application for face masks, in certain harsh environments, e.g. mining sites, cake may be formed on mask surface after long-time use. More importantly, apart from the short-term performance, our study also focuses on the long-term filtration performance of filters. Loading filters with high concentrations of aerosols until cake formation can represent a worst-case scenario. In this section, the experimental results and the theoretical findings are summarized for the filtration behaviors of electret filters during loading process.

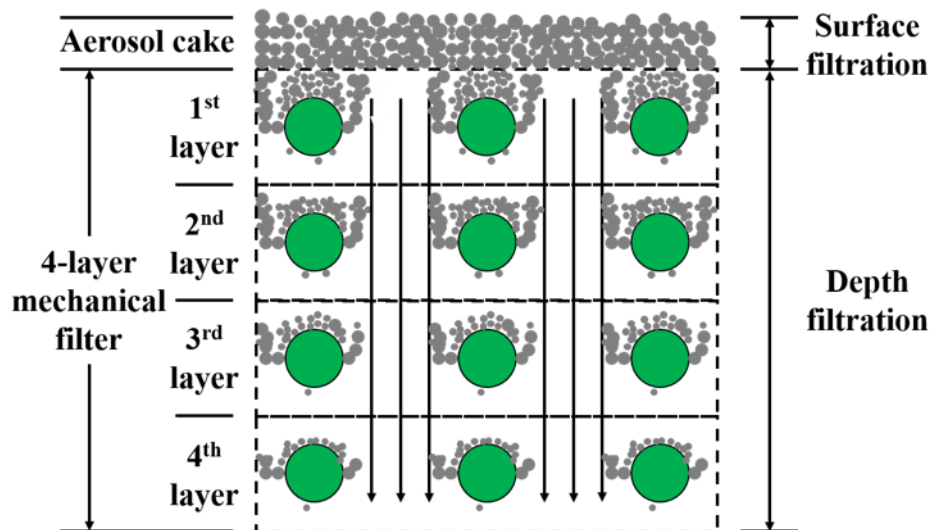
(a)



(b)



(c)



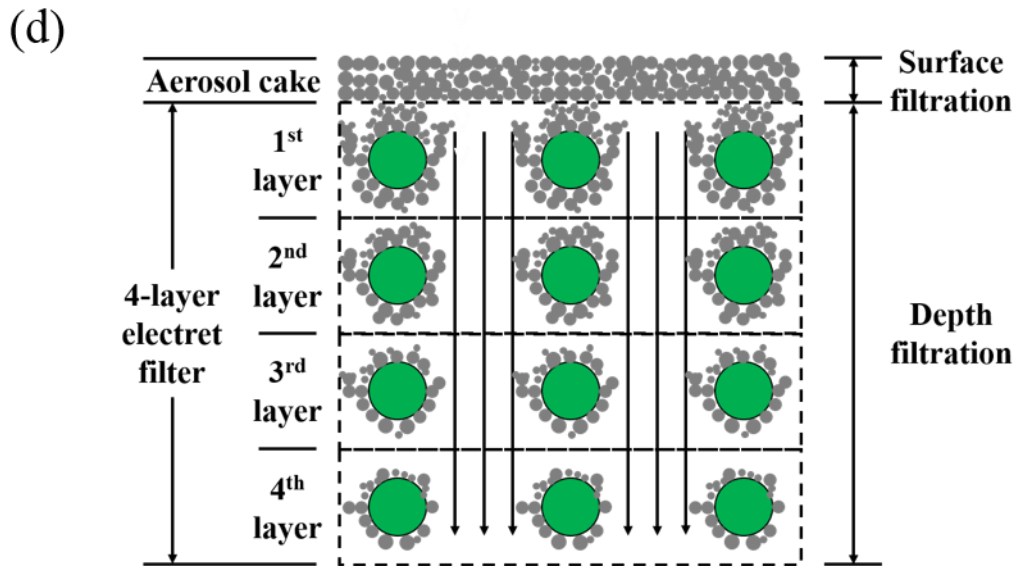


**Fig. 2.4.** Schematics for aerosol deposition distribution in varied filters a certain time after complete formation of aerosol cake.

### 2.5.1. Filtration efficiency of electret fibrous filters with loaded aerosol mass

In terms of filtration efficiency, different from mechanical filters which show increasing values throughout the loading process, the efficiency of electret filters initially decreases to a certain point before increasing with loading, as commonly reported [1, 7, 15]. This phenomenon is due to the shielding of electrostatic effect and the enhanced mechanical effect during aerosol loading. With filtration proceeding, the initially captured particles may act as collection sites for the latter particles and gradually form dendritic structures. The adjacent dendrites gradually join together, which initiates the formation of a “cake” on the front side of the filter. During the dendrites/cake growth stage, the electrostatic effect diminishes because of the screening effect on fiber charges by deposited particles, while the mechanical collection enhances contributed by the dendrites/cake. The filtration efficiency keeps decreasing until the reduction in electrostatic efficiency is equally compensated by the improvement in

mechanical efficiency, at which point the filtration efficiency falls to its minimum values before increasing thereafter. On forming a complete cake layer, particle penetration falls to zero, where electrostatic effect is fully shielded and the following challenging particles are solely collected via the mechanical effect of the cake layer, i.e., the aerosol capture has totally transferred from depth filtration to surface filtration.

Over the years, some theoretical and modelling work has been carried out in developing expressions to predict single fiber efficiency of mechanical filters with loading based on different assumptions [1, 7, 15]. On the contrary, few researches were reported on the numerical relationship between aerosol deposition mass and filtration efficiency for electret filters. One of the known studies was done by Brown et al., where a theoretical expression of aerosol penetration with loaded mass ( $P_M$ ) was derived from the experimental values [7]. In the experiments, several kinds of electret filters were loaded with various types of industrial aerosols. The expression obtained is shown below:

$$\ln \frac{P_M}{P} = \beta M_{\text{dep}} \quad (2.30)$$

where  $P_M$  is the aerosol penetration with loaded mass,  $P$  is the aerosol penetration,  $\beta$  is the degradation factor, which is related to the type of loading aerosol, and  $M_{\text{dep}}$  is the aerosol loaded mass.

The influence of particle properties on electret filter efficiency variation were often investigated [1, 7, 14, 16-18, 22, 51, 82-86]. Particularly, compared to uncharged particles, charged particles were found to delay the decrease rate of filtration efficiency in the initial loading stage, which proved that the inhibition of electrostatic effect was attributed to charge screening instead of charge neutralization. In addition, it was reported that the maximum penetration was reached more quickly when smaller

particles were used to load the electret filter, perhaps due to the stronger screening effect on fiber charges.

### **2.5.2. Pressure drop across electret fibrous filters with loaded aerosol mass**

As for pressure drop, electret filters have generally similar increasing trend to conventional filters [1, 7, 15]. In the early stage, particles deposit on the surface of individual fibers across the porous filter depth. Due to the intensely limited space occupied by the captured particles, the fluid flow is only slightly affected and the pressure drop increases at fairly low rates. With dendrites/cake forming and the filter more and more clogged, the pressure drop keeps rising with the rate of increase accelerating. When the cake is completely formed, the increase rate of pressure drop reaches its peak value, after which the pressure drop increases linearly at this rate with the loading mass.

Despite the similarity in the general trend of pressure drop evolution, due to the great role played by electrostatic mechanism in the early stage of loading, the deposition properties of particles on an electret filter, including the capture position, dendrite/cake formation rates and cake structures, are different from a purely mechanical filter. As observed in several studies, the captured particles deposited more uniformly on fibers of electret filters than mechanical filters due to electrostatic forces. This uniform aerosol deposition then led to lower growth rates of dendrites and postponed formation of surface cake. In addition, surface cake formed on electret filters were claimed to be more porous. As a result, larger clogging points and higher aerosol holding capacities were eventually achieved for the electret filters [1, 7, 15].

A lot of work has been conducted to theoretically relate pressure drop to aerosol deposited mass [1, 7, 15]. However, few satisfactory theories were obtained resulting

from the complex nature of dendrite structure and the large number of influencing factors, such as particle size and fiber packing density. To make theoretical approaches practicable, the loading models were often overly-simplified. For instance, loaded aerosols were assumed to deposit evenly on every charged fiber, while in fact dendrites may form unevenly around individual fibers and the fibers downstream of the filter surface may be shadowed by the dendrites formed in the upstream layers.

While it is impractical to establish a definite relationship between pressure drop and loaded mass before full cake formation, predicting the pressure drop of a fully clogged filter is relatively easy. One expression of pressure drop with loading was given by:

$$\frac{1}{\Delta p} = \frac{1}{K_1} \left( \frac{\phi^3}{(1-\phi)^2} \right) \left( \frac{d_p^2}{36\nu} \right) \left( \frac{1}{UB} \right) \quad (2.31)$$

where  $\Delta p$  is the pressure drop,  $K_1$  is the Kozeny constant (= 5),  $\phi$  is the cake porosity,  $d_p$  is the particle diameter,  $\nu$  is the air viscosity,  $U$  is the face velocity, and  $B$  is the cake thickness.

The influences of particle properties on pressure drop variation of electret filters were also studied [1, 7, 15-18, 50, 51, 85, 87]. It was widely believed that small particles were more clogging than large particles, due to the denser structures of dendrites and cake formed during aerosol loading. Besides, electret filters had higher loading capability towards charged particles because of the more uniform distribution of deposited particles on fibers.

## **2.6. Studies on filtration performance of electret fibrous filters**

Since the invention of the first known electret filter—Hansen resin-wool filter, many researches have been conducted to prepare electrically active air filters for aerosol

removal using various materials and configurations [1, 7, 15]. In this section, different kinds of electret filters reported in literature are reviewed separately according to their compositions.

### **2.6.1. Single-component electret fibrous filters**

One earlier kind of electret filters which have been studied intensively are those composed of a single polymeric material [20, 88-90]. Due to the widely applied melt-blow technology, micro-fiber filters were usually used for manufacturing electret filters. And because of the simple device setup, corona discharge was mostly used as the charging technique. Studies were carried out to compare the filtration performance of electret filters made using varied polymers, charging methods and filter configurations, as well as the influence of different particle properties and environmental conditions. Makowski found that filtration process in electrostatic filters designed for respiratory protective devices depended mainly on the filter material type, the material electrostatic field strength, and the aerosol charge density, while less on the aerosol charge sign and the air relative humidity [88]. Tian et al. developed a compact electrostatically assisted air coarse filter and observed that the single pass filtration efficiency for 0.3- $\mu\text{m}$  particles increased with increasing charging voltage and decreasing polarizing distance used for charging the filters. Also, they found that filter material with larger relative dielectric constant or larger tortuosity yielded higher filtration efficiency [20]. Though high filtration efficiency could be obtained using microfibers, it often came at the cost of high air resistance which made the filters less applicable for respirator use. Nifuku et al. aimed to find the optimal corona method for filter (made from PP or PTFE) efficiency improvement using high voltage DC corona, pulse corona and pulse with DC corona. They found that pulse with slower pulse rise time with DC superimposition was

more effective for providing a larger surface charge density. And their optimized electret filter could remove 99.32% of 0.1-0.15  $\mu\text{m}$  DOP particles. However, the pressure drop was as high as 171.6 Pa at an air velocity of 5.3  $\text{cm s}^{-1}$  [89]. Since the development of electrospinning, nanofiber electret filters have gained more and more popularity. Nevertheless, to make full use of electrostatic effect, oftentimes more than one material was used instead of just a single material. Lolla et al. electrospun PVDF fiber mats with an average fiber diameter of 200 nm and claimed the polarized fiber mats had higher capture efficiencies, lower pressure drops and higher filtration indexes (quality factors) than the non-polarized mats over time using 150-nm NaCl particles. However, seen from the given data, the non-polarized mats already had high filtration efficiency of about 95%, probably due to the high filter basis weight of 20 gsm. Therefore, the improvement by electrostatic effect was indeed minimal. And because of the high pressure drop (around 580 Pa at 10  $\text{L min}^{-1}$  for the clean polarized filter), the quality factor was only about  $6.8 \times 10^{-3} \text{ Pa}^{-1}$ , which was extremely low and thus not suitable to be applied as air filters [90].

### **2.6.2. Multi-component electret fibrous filters**

Compared with the single-component electret filters, there are more types of multi-component electret filters prepared by corona discharge, polarization or triboelectrification [23, 24, 40-42, 51, 52, 68, 91-95]. One popular kind of electret filters consists of supporting fibers and dielectric materials which were added to increase the electrostatic effect. These additional materials, including PTFE,  $\text{SiO}_2$ ,  $\text{TiO}_2$  particles and graphite platelets, were always added in the polymer solution, then co-spun during the electrospinning process and eventually anchored on the surface of fibers. Wang et al. fabricated electret nanofibrous membranes using PVDF as the matrix polymer for

fibers and PTFE nanoparticles as an inspiring charge enhancer through the in situ charging of electrospinning. By combining the two materials, charge density and stability were greatly enhanced by more polarized intra- and inter-molecular dipoles and deepened energy level depth. As a result, the fibrous membrane exhibited a high filtration efficiency of 99.972%, a low pressure drop of 57 Pa at  $5.3 \text{ cm s}^{-1}$ , a satisfactory quality factor of  $0.14 \text{ Pa}^{-1}$  and superior long-term service performance [40]. Particle-on-fiber structure of nanofiber filters was proved useful to improve filter performance. Nonetheless, attributed to the small fiber diameter, these filters tended to have high mechanical filtration efficiency, which shadowed the electrostatic effect. Huang et al. electrospun PVDF filters with dispersed nanoscale graphite platelets and obtained the highest filtration efficiency of 98.989% for aerosols with an average size of 100 nm. However, the pressure drop reached 1279.1 Pa under face velocity of  $1.26 \text{ m s}^{-1}$  and the highest quality factor was merely  $3.591 \times 10^{-3} \text{ Pa}^{-1}$ . More importantly, the filtration efficiency of pure PVDF filter without graphite platelets was already 93.803%, which means the added “charge enhancer” actually improved little of the filter performance [41]. Another method to improve the electrostatic field of electret filters is by incorporating another ingredient within fibers. These ingredients, including inorganic salts and organic nucleating agents, were pre-mixed with the polymer melt or solution before being incorporated within fibers during the process of melt-blow or electrospinning. Then, the resultant filters underwent corona discharge treatment to become electret filters. Kilic et al. studied the effects of  $\text{BaTiO}_3$  addition on electrostatic charging and particle capture performance of PP melt-blown webs. They found that cold charging (under room temperature) and thermal charging (first heating and then cooling the filter) could both enhance the charging ability of the PP filter. But thermally charging around Curie temperature of  $\text{BaTiO}_3$  ( $\sim 130^\circ\text{C}$ ) provided higher-density and

more stable charges for the aerosol filtration of fibrous webs and HEPA-level efficiency (99.97% for 0.3- $\mu\text{m}$  particles) was reached at 95 Pa [92]. Similar phenomenon was observed by the same group where nucleating agents DMDBS and NA11 were used as the electret additives to PP filters. Upon thermal charging, surface potential and filtration performance of the webs were significantly improved, both in magnitude and stability [91].

Another kind of electret filter is mixed-fiber filters, i.e. fibers made from different kinds of materials co-present in one filter. Based on filter structure, this kind of filter can be categorized as multilayer filters (each layer consists one kind of material) and blended-fiber filters (fibers are blended in the same layer). For a multilayer filter, each layer is normally sandwiched by two layers made of another material. Bai et al. fabricated a triboelectric air filter consisting of five layers of PTFE fabrics and nylon fabrics, which was charged by rubbing the two kinds of fabrics against each other. They achieved removal efficiency values of 84.7% for PM<sub>0.5</sub> and 96.0% for PM<sub>2.5</sub> respectively for the electret filter, which were 3.22 and 1.39 times larger than the uncharged one. Nevertheless, it can be seen from the paper that the electret filter had a fairly high pressure drop of about 180 Pa at 4 cm s<sup>-1</sup> and the quality factor barely reached 0.018 Pa<sup>-1</sup>, which indicates that the filter was inefficient as a candidate for face masks [95]. For a blended-fiber filter, oftentimes different fibers are mixed by mechanical force, usually through felting process, using the pre-manufactured fibers. A less common kind is the filters co-spun from multi-component melt or solution. Schutz and Church investigated the filtration performance of fiber blends combining PP or wool with one of several other polymers, which were found to generate significant electrostatic enhancements in nonwoven felts that are stable over time. They found that

PP was an essential component for most of the blended-fiber needle felts, and the triboelectric effect were significant and stable over time [52]. Though mixing fibers of different materials was proved an outstanding method to get fibers charged a long time ago, this type of filter is less common compared to others. The reason might be the lack of proper technology to mix different fibers in good fibrous structures without distortion [96].

### **2.6.3. Commercialized electret fibrous filters**

Nanofiber filters have been the major focus of research these years. Yet, because nanofibers cannot be produced in large quantities, commercialized electret filters are almost all made of microfibers. Due to the superior chargeability and wide availability, PP is often used as the polymeric material for large-quantity production of electret filters. Researches involving commercialized products mainly focus on the influences of aerosol properties and environmental conditions on the filtration efficiency and loading behavior of the electret filters [50, 69, 86, 87, 97-100]. Sanchez et al. quantified the effects of electrostatic fiber charges and particle charges by measuring the collection efficiency for uncharged/charged aerosols by neutralized/original 3M Filtrete™ electrostatic filter. The results showed varied contribution of Coulombic, induction and polarization effects under different face velocities [86]. Barrett and Rousseau compared the loading behaviors of several electret filters made by different approaches. They observed significant differences among electrostatic filters [69]. Generally, electrostatically charged filter media with large diameter fibers, such as tribo-charged or fibrillated electret film media, exhibited excellent initial filtration performance. However, the penetration increased dramatically when these media were loaded with certain aerosol particles, especially oily mist aerosols such as DOP. In comparison,

electrostatic media of newer technology exhibited higher electrostatic charge level and oily mist resistance, which could be promising in keeping high filter efficiency while eliminating efficiency loss due to aerosol loading.

## **Chapter 3: Preliminary Filtration Tests of Multilayer PVDF**

### **Electret Filters**

#### **3.1. Overview**

In this study, PVDF was used to fabricate nanofiber filters and their electrostatic chargeability was investigated. Subsequently, the filtration performance of multilayer PVDF electret filters were investigated and compared with 1-layer configuration. Other than maintaining the flow path with least resistance as with previous investigation [45-47], the separation of charged fibers by insulated porous substrate media into multiple layers also reduced negative electrostatic interference among randomly oriented charged nanofibers all packed in 1-layer configuration [48, 49]. In any event, these different filter configurations were further analyzed and compared based on the dielectrophoretic filtration effect on single-fiber efficiency, which was independent of the filter thickness, filter solidity, face velocity and fiber diameter to obtain a fair comparison and deeper insight. Further, these nanofiber electrets were compared with microfiber electret filters based also on single fiber efficiency to determine the effect attributed to fiber diameter. In addition, charge stability on the multilayer PVDF electret filters was tested during a three-month period. By combining the advantages of PVDF and “multilayering”, we managed to fabricate electret filters with high filtration efficiency, low pressure drop and long-term performance stability.

#### **3.2. Experimental**

##### **3.2.1. Materials**

PVDF with a molecular weight (MW) of 530,000 and sodium chloride (NaCl) were purchased from Sigma-Aldrich (USA). Isopropyl alcohol (IPA) and acetone were

acquired from Anaqua Chemicals Supply (USA). N,N-Dimethylformamide (DMF) was obtained from Duk San Pure Chemicals Incorporated (South Korea). All reagents were analytical grade and used as received.

### **3.2.2. Fabrication of filters**

In a typical preparation, the PVDF solution was prepared by dissolving 20 w/v% PVDF pellets into a mixture solvent of DMF/acetone (v/v 8/2) blended at 70 °C for 24 h. The needle-based electrospinning machine (Model TL-Pro, Shenzhen Tong Li Tech Co. Ltd.) was employed to prepare PVDF nanofiber mats. As shown in Fig. 3.1, the electrospinning apparatus consists of a micro syringe pump, a grounded drum collector and a high voltage supply set. The syringe pump was used to feed the polymer solution into a 20-gauge steel needle tip (ID = 0.6 mm) at the rates of 0.9 mL h<sup>-1</sup>. The electrospinning process was carried out with a voltage of 20 kV, a tip-to-collector distance (traveling distance) of 15 cm and a drum rotating speed of 10 r min<sup>-1</sup>. The temperature was kept at 25 ± 1 °C and the relative humidity was 40 ± 2%. As solution oozed out of the syringe tip, under the high electrical field, the liquid formed a Taylor cone. When the electrical force overcame the interfacial tension of the liquid, a thin jet was ejected toward the ground electrode. The diameter of the jet reduced due to repulsion of the positive charges deposited along the entire jet together with evaporation of the solvent. The jet diameter became smaller during free flight until it became the size of a nanofiber with diameter less than 1 μm and deposited as a mat on the collector. The nanofiber mat was collected on the surface of a grounded steel drum covered with anti-static nonwoven polypropylene (PP) cloth which acted as the support of nanofiber layer. After spinning, the PVDF nanofiber filters (coated on PP substrate) were then dried in a vacuum oven at 40 °C overnight to remove the residual solvent, and the

resultant filters were referred to as “pristine filters”. To evaluate the contribution from pure mechanical filtration effect, filters were pre-treated with IPA to remove the residual charges before further use, resulting in “uncharged filters”. And the filters treated with corona discharge were referred to as “electret filters”.

To get 1-layer nanofiber mats with different basis weights ( $W$ ), different time durations were used as the amount of fiber deposition is proportional to the electro-spinning (hereafter simply referred as spinning) time. In this case, it was reasonable to speculate that the filter thickness ( $Z$ ) increased with spinning time of the single nanofiber layer. To a lesser extent the fiber packing density ( $\alpha$ ) may also increase slightly with spinning time when  $W$  is large, otherwise for smaller  $W$  it can be assumed to be reasonably constant. The other configuration of filters applied in our study was made by stacking up a certain number of nanofiber filters with the same spinning duration to form a multilayer filter. In this way, filters with the same  $\alpha$  and the same individual-layer basis weight ( $W_L$ ) but different total  $W$  and  $Z$  of nanofiber layers were fabricated, with the latter two values being in proportion to each other [46]. Each filter was denoted based on its fiber diameter ( $d_f$ ), configuration (S for single layer and M for multiple layers),  $W_L$  and charging state (P for pristine, U for uncharged and C for charged), e.g., 450-S-1.75-P represents a 1-layer pristine filter with the fiber diameter of 450 nm and the  $W_L$  (for a 1-layer filter,  $W_L = W$ ) of 1.75 gsm, while 450-M2-0.87-C refers to a 450-nm 2-layer electret filter with the  $W_L$  of 0.87 gsm for each individual layer, but the total basis weight for both 2 layers added up to 1.75 gsm. Specially, filters whose names start with M1 are equivalent to those of S as they were the building module for multilayer filters.

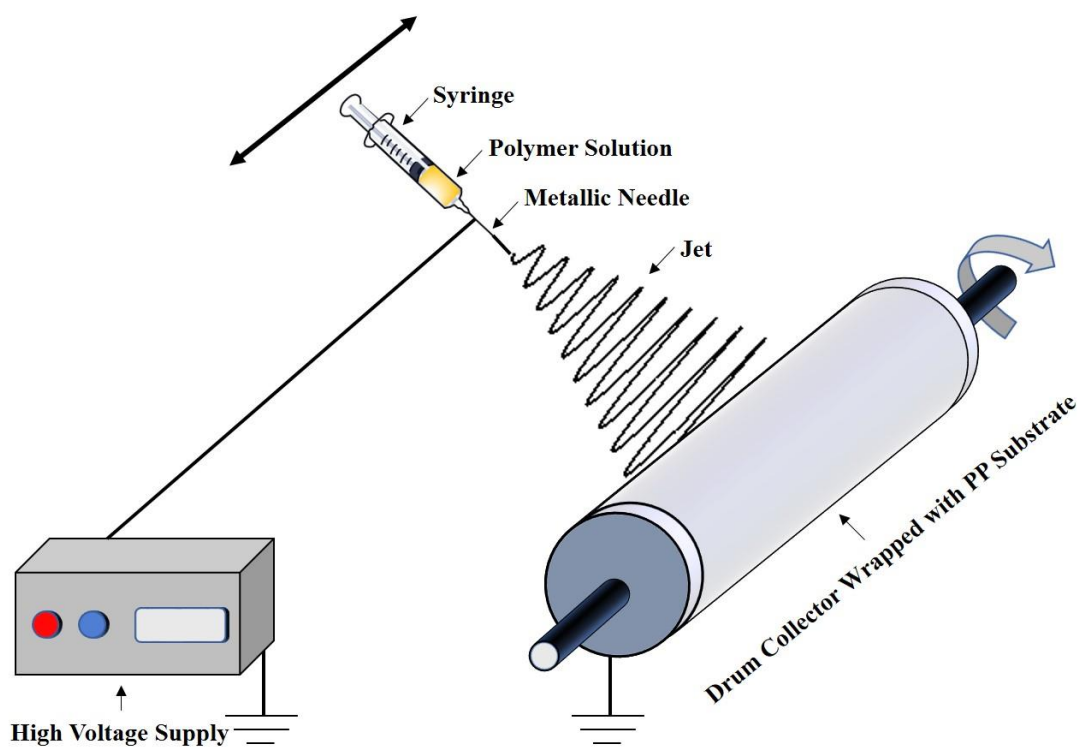
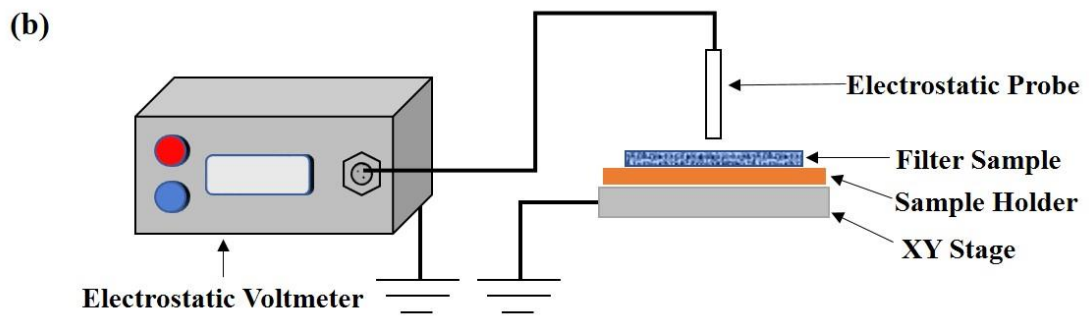
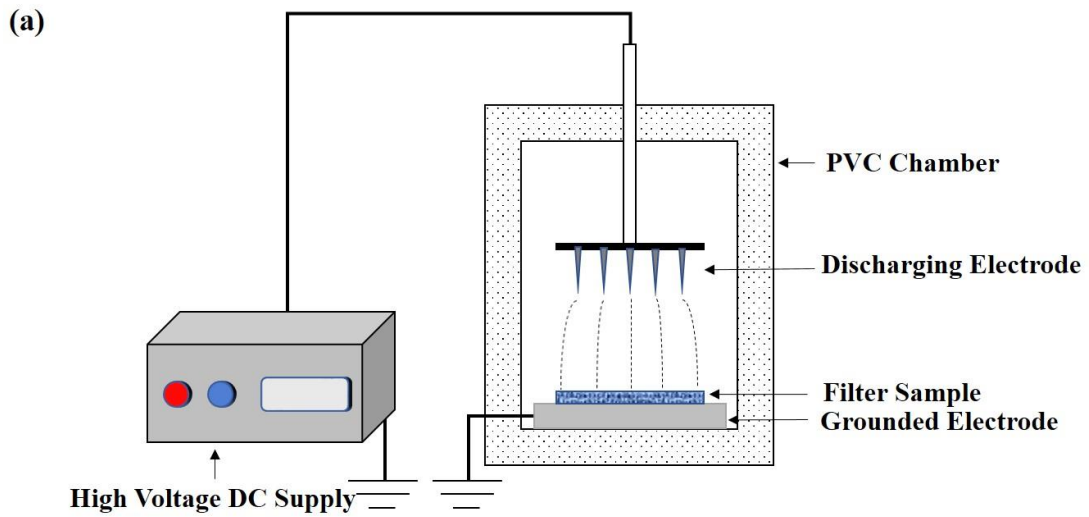


**Fig. 3.1.** Schematic diagram of the electrospinning apparatus.

### 3.2.3. Corona discharge of filters

The corona discharge, which is a commonly applied method to make fibrous filters charged as described in Section 2.2.1, was performed on a homemade wire-type dual electrode device as shown in Fig. 3.2a. A high positive voltage was applied to the five-wire emitting electrode made of tungsten, facing a 10 cm × 10 cm filter mat attached on a grounded plate electrode. Charges were emitted around the energized wire electrode and deposited on the filter under the influence of electric field. The distance between the wire and the plate electrode surface was adjustable in a certain range. The charging was carried out in ambient air at temperature of  $20 \pm 2$  °C and relative humidity of  $50 \pm 5\%$ . Based on our preliminary experiment, prolonged charging time over 60 s did not bring apparent differences in surface potential. Thus, 60 s was used for the preparation of all our electret filters. In the entire investigation, charging voltage of 15

kV, charging distance of 30 mm and charging time of 60 s were used as the corona discharge condition unless otherwise stated. These parameters were optimized to provide the maximum corona discharge to the nanofiber mat without locally burning the fibers from over-intensified electrical field.



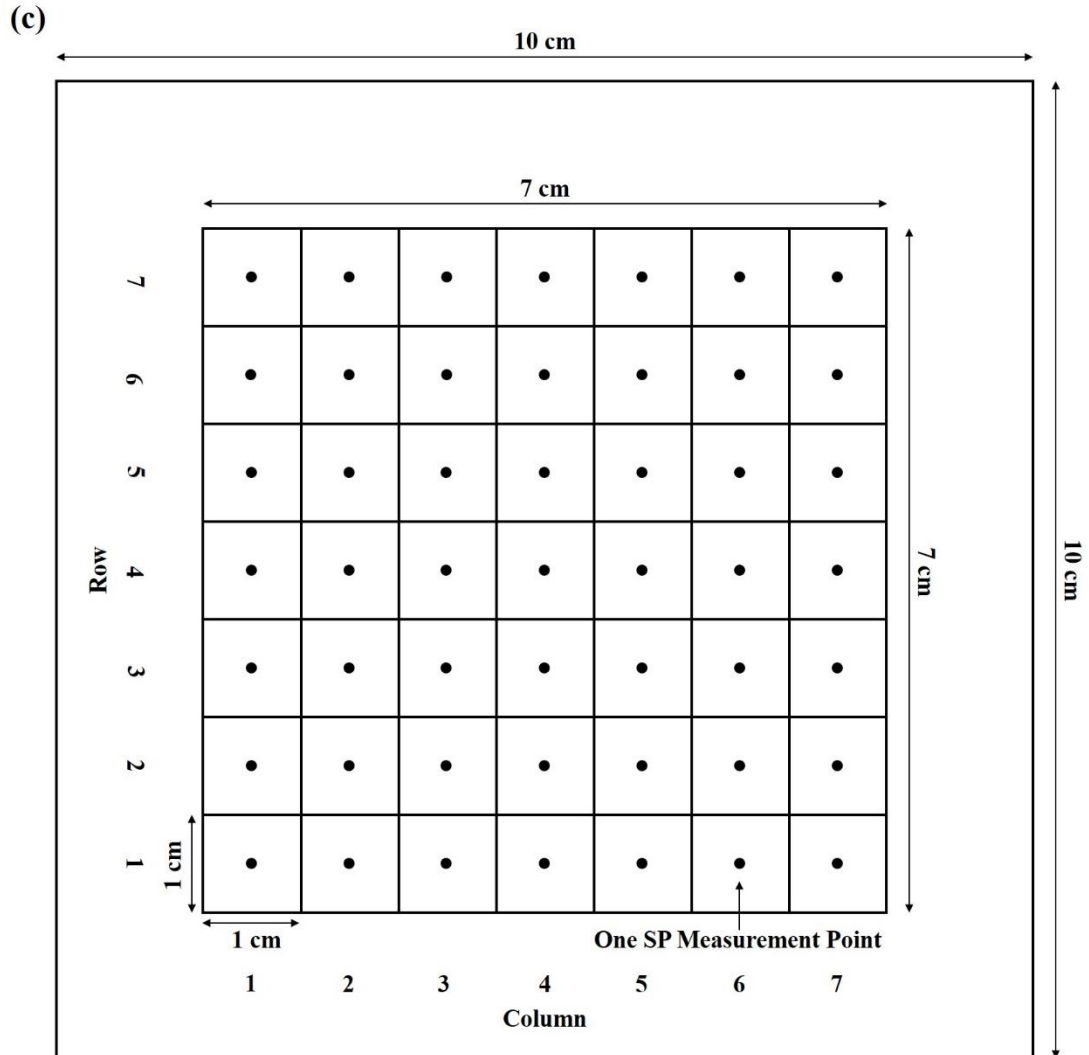


**Fig. 3.2.** Schematic diagrams of (a) the corona discharge set-up, (b) the apparatus for surface potential (*SP*) tests and (c) a filter sample used for charging and *SP* tests.

### 3.2.4. Characterization of filters

Surface morphology of nanofiber filters was analyzed using scanning electron microscopy (Model JSM-6490, JEOL, USA). The fiber mean diameters were measured by the software ImageJ (NIH, USA). The thickness of PP substrate was measured by a micrometer, while that of nanofiber layer was obtained using a surface profile device (Model DektakXT, Bruker, Germany). The weight of substrate and each whole filter (nanofibers and substrate) were measured on an electronic balance, with the difference

between the two values being the weight of the nanofiber layer. The surface potential ( $SP$ ) of the filtration media was measured by an electrostatic voltmeter (Model 244A, Monroe, USA) as depicted in Fig. 3.2b. In a typical measurement, surface potential of 49  $1\text{ cm} \times 1\text{ cm}$  grids on the evenly divided central  $7\text{ cm} \times 7\text{ cm}$  part of a filter (the details of filter surface can be seen in Fig. 3.2c) was obtained (corresponding to the filter area challenged by aerosols in the cylindrical filtration chamber). The aperture of the electrostatic probe was placed 1 mm right above the central point of each subdivided grid during the tests. The distance of 1 mm was set to both ensure the accuracy (high resolution) of  $SP$  values and avoid probe-to-surface arc-over, as suggested by the manufacture. An XY stage was used to support and move the tested sample to get precise positioning. Both front-and-back sides of the filter were tested, and the absolute difference was taken as the surface potential of a certain grid as the electric field over particles would be close to that value [92]. The fiber packing density (i.e. filter solidity)  $\alpha$  of the nanofiber layer as well as the substrate was calculated by the following mass balance equation:

$$W = \rho_f Z \alpha \quad (3.1)$$

where  $W$  is the filter basis weight,  $\rho_f$  is the density of the polymer raw material, and  $Z$  is the filter thickness.

### 3.2.5. Filtration performance evaluation of filters

Fig. 3.3 shows the schematic diagram of the set-up for aerosol filtration test. The aerosol filtration performance of filters was evaluated with a monodisperse sub-micrometer aerosol generation system (SMAG System, A&P, HK) and a homemade filtration testing unit. Note that for electret filters, the filtration tests were conducted 24 h after the corona discharge treatment to get relatively stable amount of charges and

filter performance. The test aerosols were sodium chloride particles (NaCl, 50-500 nm) generated from atomizing NaCl solution with a constant output atomizer (7388SJA, JV Technology). In a typical run, a clean and dry compressed air flow from a filtered air supply system was fed to the atomizer containing a certain concentration of NaCl solution, where liquid droplets containing salt aerosol were generated. The stream was then passed through a Nafion membrane air dryer for moisture removal, resulting in dry aerosols ranging between 10-1000 nm (count median diameter (CMD), hereafter denoted as aerosol/particle diameter/size). After drying, the aerosol stream flowed through an impactor with a nozzle diameter of 0.65 mm where particles larger than the cut size were removed. The resultant polydisperse aerosols subsequently flowed through a neutralizer, a differential mobility analyzer (DMA, Model 3081, TSI) and a second neutralizer to get particles with a certain monodisperse size controlled by DMA voltage and in electrostatic charge equilibrium (Generation Mode of SMAG). The function of the first neutralizer was to bring the highly and unevenly charged particles generated from the atomizer to a Boltzmann charge distribution. In this way, most particles passing through the DMA would be the required size with just one unit of charge, instead of those with larger sizes and higher charge amounts. The function of the second neutralizer was to bring the charged aerosols exiting the DMA to neutralized state, where most particles were zero-charged. This approach followed the NIOSH mask testing standard because neutralized particles are hard to be filtered out than charged particles. Alternately, polydisperse aerosols could be used to challenge the filter and filtration efficiency could be determined by rearranging the sequence of the two neutralizers and DMA (Scanning Mode of SMAG). Nevertheless, the latter set-up was not applied due to the difficulty in tuning the equipment response time for detecting polydisperse aerosols, which could bring inaccurate and misleading results. Therefore,

Generation Mode was used instead of Scanning Mode, although it normally took about 1 h to get a filtration curve applying the former method while only less than 10 min for the latter one. The neutralized monodisperse NaCl aerosols were fed into a cylindrical filtration chamber with a diameter of 7 cm and an effective area of 38.5 cm<sup>2</sup> and down through the filter which was covered by a PP substrate to protect the PVDF layer from abrasion. The filter samples were tested at the flow rate of 12.24 L min<sup>-1</sup>, representing the face velocity of 5.3 cm s<sup>-1</sup> (this velocity follows ASTM F2299 method for PFE testing of surgical masks and is commonly used in literature as the challenging face velocity for fibrous filter tests used as face masks). The system flow rate was measured with a mass flow meter (Model 4100, TSI Inc., Shoreview, MN, USA) at the inlet of the filter test system and a make-up air source was used to meet the required flow rate. Aerosols were extracted isokinetically with sampling probes upstream and downstream of the filter to a condensation particle counter (CPC, Model 3010, TSI Inc., Shoreview, MN, USA) to measure aerosol concentrations. To realize isokinetic sampling, a make-up air stream was supplied to CPC and the flow rate was finely tuned so that the aerosol flow velocity at the entrance of either sampling probe was 5.3 cm s<sup>-1</sup>, the same as the face velocity challenging the filter. The pressure drop ( $\Delta p$ ) across the filters was measured using a digital pressure manometer (Model 2080P, Digitron, Elektron Technology, UK) at two points located immediately upstream and downstream of the filter. The following two equations (same as those in Chapter 2) were applied to calculate filtration efficiency ( $\eta$ ) and quality factor ( $QF$ , benefit-to-cost ratio), respectively:

$$\eta = \frac{c_{\text{up}} - c_{\text{down}}}{c_{\text{up}}} \quad (3.2)$$

$$QF = -\frac{\ln(1-\eta)}{\Delta p} \quad (3.3)$$

where  $c_{up}$  and  $c_{down}$  denote the aerosol number concentrations of the upstream and the downstream flows, respectively.

For the capture of neutralized aerosols by PVDF electret filters, mechanical filtration and dielectrophoretic filtration were the two major mechanisms. Therefore, the filtration efficiency of a filter,  $\eta$ , could also be given by the following equation:

$$\eta = 1 - (1 - \eta_M)(1 - \eta_o) \quad (3.4)$$

where  $\eta_M$  and  $\eta_o$  represents filtration efficiency contributed from mechanical and dielectrophoretic filtration effects of the filter, respectively.

The pure mechanical filtration efficiency of the electret filter,  $\eta_M$ , was obtained directly from the filtration tests for the uncharged filter, whereas the dielectrophoretic filtration efficiency,  $\eta_o$ , could be calculated from Eq. 3.4.

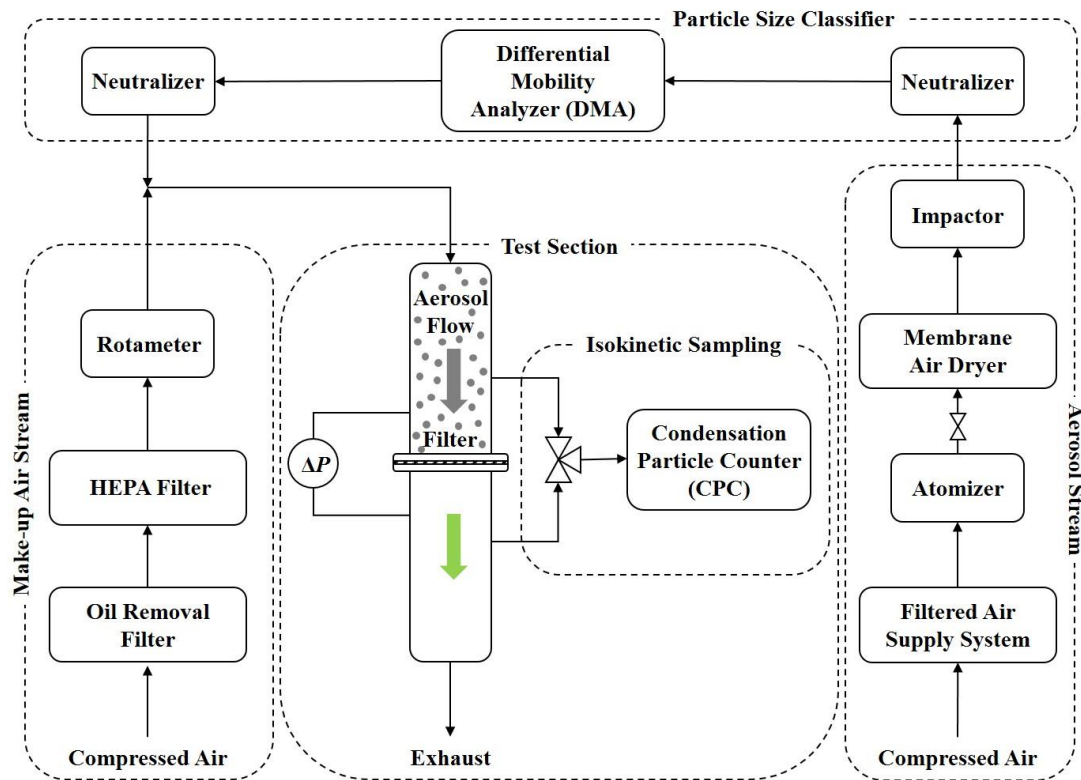


**Fig. 3.3.** Schematic diagram of set-up for aerosol filtration tests of filters.

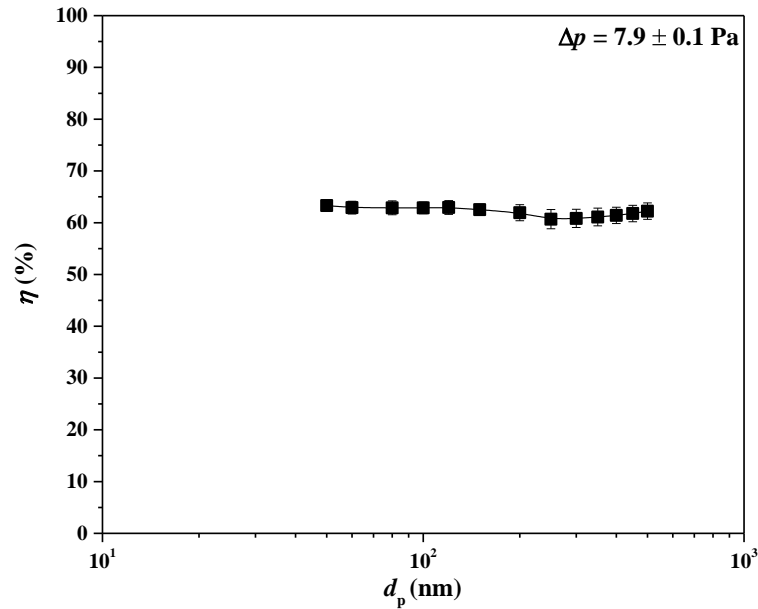


**Fig. 3.4.** Filtration efficiency ( $\eta$ ) a typical 1-layer PVDF electret filter.

Normally, to get convincing conclusions, a filter should be tested repetitively to ensure the filtration performance is repeatable. Nevertheless, in our case, due to the highly constant challenging aerosol size distribution and strictly controlled work parameters of SMAG, the variation of repeated test results was insignificant. Besides, to get a full filtration efficiency curve for a filter, at least 1 h was needed, which was very time-consuming. Therefore, in most cases, a filter was only tested once. Fig. 3.4 shows the filtration efficiency of a randomly selected filter tested consecutively three times. The relative variations for the efficiency of aerosols with varied sizes were around 2.3%. The data of large aerosols are a little more scattered than that of small aerosols, which is attributed to the gradually lower concentrations of large aerosols generated by SMAG. For pressure drop, the values were very stable (relative variation was only 1.3%) due to the finely tuned air flow rate.

### 3.3. Theoretical analysis of single fiber efficiency from dielectrophoretic filtration effect

The pressure drop,  $\Delta p$ , across a fibrous filter is given by the Davis equation [7],

$$\frac{\Delta p d_f^2}{4\nu U Z} = 16\alpha^{3/2}(1 + 56\alpha^3) \approx 16\alpha^{3/2} \quad (3.5)$$

where  $d_f$  is the fiber diameter,  $\nu$  is the air viscosity,  $U$  is the face velocity,  $Z$  is the filter thickness, and  $\alpha$  is the filter solidity.

The approximation made in Eq. 3.5 can be justified provided  $\alpha \ll (1/56)^{1/3}$ , or  $\alpha \ll 0.26$ . Otherwise, we have to solve Eq. 3.5 numerically, which can still be done relatively easily.

Combining Eqs. 3.1 and 3.5, we can express  $\alpha$  independently of the filter thickness  $Z$  as follows,

$$\alpha = \left( \frac{\Delta p d_f^2 \rho_f}{64\nu U W} \right)^2 \quad (3.6)$$

where  $\Delta p$  is the pressure drop across filter,  $d_f$  is the fiber diameter,  $\rho_f$  is the fiber material weight density,  $\nu$  is the air viscosity,  $U$  is the face velocity, and  $W$  is the filter basis weight.

If the approximation  $\alpha \ll 0.26$  is not used, then the numerical solution on  $\alpha$  is required, which replaces Eq. 3.6. The filter filtration efficiency  $\eta$  is related to the single fiber efficiency  $\eta_s$  by,

$$\eta = 1 - \exp\left[-\frac{4\alpha\eta_s Z}{\pi(1-\alpha)d_f}\right] \quad (3.7)$$

where  $\alpha$  is the filter solidity,  $Z$  is the filter thickness, and  $d_f$  is the fiber diameter.

Based on this, we can express the single fiber efficiency  $\eta_s$  in terms of the filter

efficiency, thus

$$\eta_s = \frac{\pi(1-\alpha)d_f\rho_f}{4W} \ln \left[ \frac{1}{1-\eta} \right] \quad (3.8)$$

If  $n$  similar modular filters, each with efficiency of  $\eta_1$ , are stacked to produce a composite filter with overall efficiency of  $\eta_n$ , thus

$$\eta_n = 1 - (1 - \eta_1)^n \quad (3.9)$$

where  $\eta_n$  is the filtration efficiency of a composite filter with  $n$  identical layers,  $\eta_1$  is the filtration efficiency of one layer in the composite filter, and  $n$  is the number of layers.

The filter efficiency of the basic module,  $\eta_1$ , can be determined if we know  $\eta_n$ ,

$$\eta_1 = 1 - (1 - \eta_n)^{1/n} \quad (3.10)$$

Using Eq. 3.10, we can thus determine the efficiency of the modular filter in composite filter with  $n$  modules, such as 2, 4, 6, and 8 in our experiments. Further from the modular filter,  $\eta_1$ , the single fiber efficiency  $\eta_s$  can be determined via Eq. 3.8 with known values of  $\alpha$  (as determined from Eq. 3.6),  $d_f$  (average fiber diameter as determined from measurements of SEM),  $W$  (basis weight of nanofibers per square meter of filter). We can subsequently determine the single fiber efficiency corresponding to both the mechanical filter  $(\eta_s)_M$  and the single fiber efficiency of both the electret media filter  $(\eta_s)_{M+o}$  consisting of both mechanical and dielectrophoretic capture mechanisms. Given the mechanical and dielectrophoretic capture mechanisms are independent and additive, the efficiency due to dielectrophoretic capture mechanism alone,  $\eta_{s,o}$ , is simply,

$$\eta_{s,o} = (\eta_s)_{M+o} - (\eta_s)_M \quad (3.11)$$

where  $(\eta_s)_{M+o}$  is the single fiber efficiency due to mechanical effects and

dielectrophoretic force, and  $(\eta_s)_M$  is the single fiber efficiency due to mechanical effects.

From the foregoing, in order to determine the dielectrophoretic filtration efficiency for a single fiber in the filter, we need to carry out two sets of experiments under similar operating condition, one for which the aerosol capture is purely mechanical (diffusion and interception), while the other being mechanical plus dielectrophoretic filtration effect. In the experiment, the former corresponds to our test filter dipped in alcohol for a certain period to remove any residual charges from electrospinning, while the latter corresponds to our test filter after being charged by corona discharge and left under equilibrium for a day. Further, it has been demonstrated [7, 81-83] that

$$\eta_{s,o} = C' N_{Q0}^{0.4} \quad (3.12)$$

where  $C'$  is a constant, and  $N_{Q0}$  is the induction parameter which is given by

$$N_{Q0} = \frac{2 \varepsilon_p - 1}{3 \varepsilon_p + 2 \varepsilon_0} \frac{C(\sigma d_p)^2}{(1 + K_f)^2 d_f \nu U} \quad (3.13)$$

where  $\varepsilon_p$  is the dielectric constant of particle,  $\sigma$  is the fiber surface charge density,  $d_p$  is the particle diameter,  $\varepsilon_0$  is the permittivity of free space,  $K_f$  is a constant,  $d_f$  is the fiber diameter,  $\nu$  is the air viscosity,  $U$  is the face velocity, and  $C$  is the Cunningham slip correction factor which is calculated from

$$C(d_p) = 1 + 2.49(65/d_p) + 0.84(65/d_p) \exp\left[\frac{-0.43}{(65/d_p)}\right] \quad (3.14)$$

Assuming the fiber surface charge density  $\sigma$ , the particle dielectric constant  $\varepsilon_p$ , the fiber dielectric constant  $\varepsilon_f$  are all constants.  $C$  is dependent on the aerosol size  $d_p$  and is required when  $d_p$  is nearly 65 nm, the mean free path of air molecules at standard temperature and pressure (STP). Thus, for a filter with given  $d_f$  filtering gas at a fixed temperature,

$$N_{Q0} \propto \frac{c(d_p)^2}{U} \quad (3.15)$$

Substituting Eq. 3.15 into Eq. 3.12, we have

$$\eta_{s,o} = G \left[ \frac{c(d_p)^2}{U} \right]^{0.4} \quad (3.16)$$

where  $G$  is another constant.

## 3.4. Results and discussion

### 3.4.1. Morphology of PVDF filters

For fibrous filters, their aerosol capture performance is greatly affected by physical structure, particularly fiber diameters and their distribution, packing density and thickness, due to the varied influences on mechanical mechanisms of diffusion, interception and inertia impaction. Fig. 3.5 depicts the reticular structure of pristine 1-layer PVDF nanofiber filters with increasing basis weight ( $W$ ) from 0.87 to 6.98 gsm. All the filters showed randomly oriented fibers with polydisperse diameters. Since fiber diameter is mainly determined by solution property, voltage and distance used for electrospinning, filters varying in spinning duration will barely have identical fiber size [47]. The fiber mean diameter of PVDF filters is 450 nm as listed in Table 3.1 and the diameter distribution is shown in Fig. 3.6. As expected, PVDF fiber packing density increased with  $W$ , which can also be intuitively seen from the SEM images. The packing density is only 0.105 at the lowest  $W$  and increases to 0.276 at 3.46 gsm, after which the increment rate remarkably decreases and reach 0.326 at 6.98 gsm. In contrast, the thickness of nanofiber layer does not significantly change for filters with  $W$  from 0.87 to 3.46 gsm due to the relatively high porosity of these filters to accommodate more fibers without a drastic thickness increase. Another possible explanation is the

electrostatic interaction (attraction) among the fibers. At higher filter basis weights, filter thickness begins to increase with increasing fiber amount.

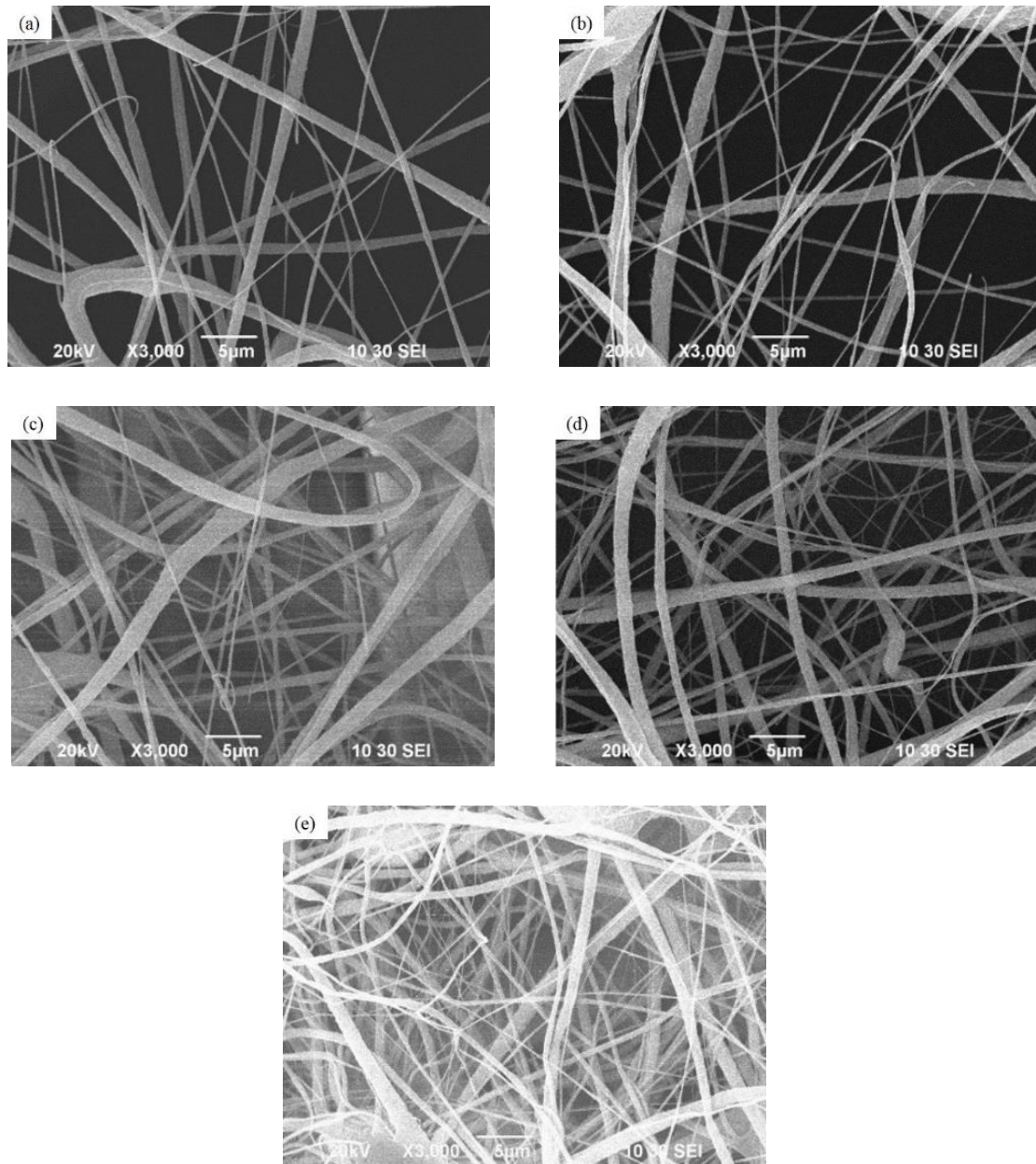


**Fig. 3.5.** SEM images of (a) 450-S-0.87, (b) 450-S-1.75, (c) 450-S-3.46, (d) 450-S-5.10 and (e) 450-S-6.98.

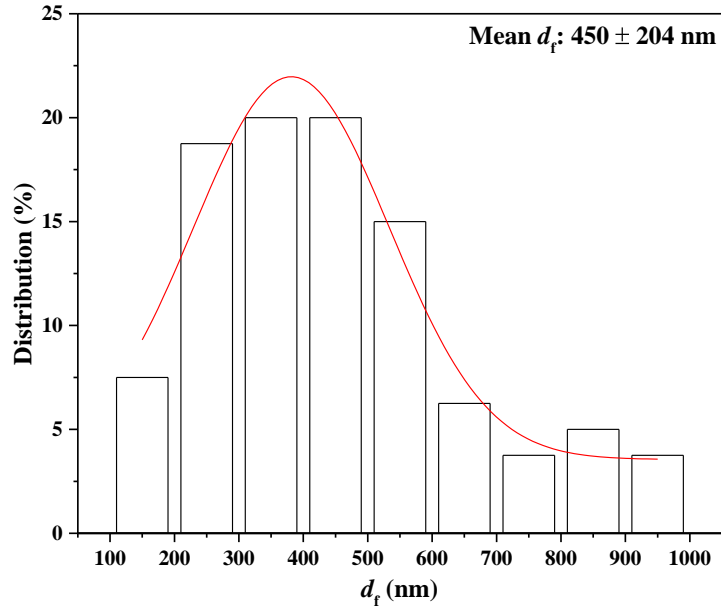


**Fig. 3.6.** Fiber diameter distribution of 450-nm PVDF filters.

**Table 3.1.** Physical properties of 450-nm PVDF filters and PP substrate

Medium	$d_f$ (nm)	$W$ (gsm)	$\alpha$ ( $\times 10^{-2}$ )	$Z$ ( $\mu\text{m}$ )	$\Delta p$ at $5.3 \text{ cm s}^{-1}$ (Pa)		
					P	C	U
450-S-0.87	450	0.87	10.5	5.7	4.4	4.3	n/a
450-S-1.75	450	1.75	16.2	7.1	6.1	5.6	5.6
450-S-3.46	450	3.46	27.6	8.4	13.8	13.2	n/a
450-S-5.10	450	5.10	30.7	10.4	20	19.3	n/a
450-S-6.98	450	6.98	32.6	14.1	37.7	35.9	n/a
450-M2-1.75	450	$1.75 \times 2$	16.2	$7.1 \times 2$	12.4	11.8	n/a
450-M3-1.75	450	$1.75 \times 3$	16.2	$7.1 \times 3$	17.8	17.2	n/a
450-M4-1.75	450	$1.75 \times 4$	16.2	$7.1 \times 4$	24.1	23.3	n/a
450-M2-0.87	450	$0.87 \times 2$	10.5	$5.7 \times 2$	7.1	7.0	n/a
450-M4-0.87	450	$0.87 \times 4$	10.5	$5.7 \times 4$	14.9	14.1	n/a
450-M6-0.87	450	$0.87 \times 6$	10.5	$5.7 \times 6$	21.3	19.8	n/a
450-M8-0.87	450	$0.87 \times 8$	10.5	$5.7 \times 8$	26.2	25.2	n/a
M2-PP	19324	$30.86 \times 2$	34.3	$100 \times 2$	3.6	3.6	3.6

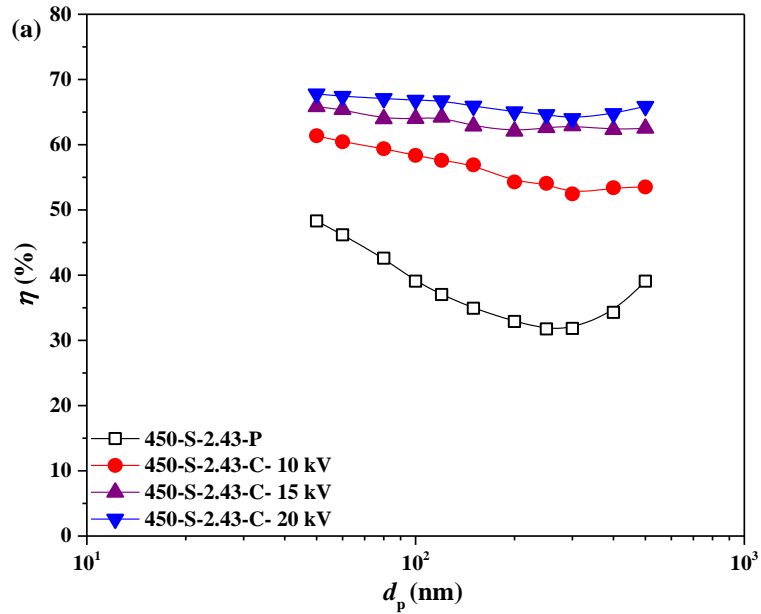
### **3.4.2. Optimization of charging condition on filtration performance of 1-layer PVDF electret filters**

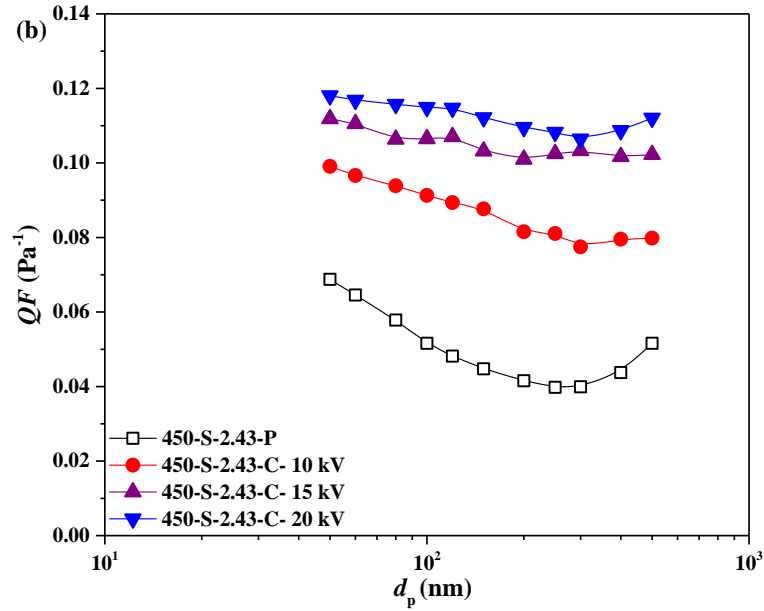
The filtration performance of electret filters has been widely confirmed to improve with charge density indicated by  $SP$ , though particle capture by electrical mechanism is intensely complex when taking charge polarity and distribution into account [7]. To increase charge density, a proper electric field intensity for the corona discharge system has been proven critical for PP nonwoven electret, for which either too low or too high could lead to low initial  $SP$  [56, 58, 60]. In our study, varied charging voltages and distances were applied to study their influences on  $SP$  and more importantly on filtration performance of PVDF filters. In order to get a clearer pattern, filters with a high  $W$  of 2.43 gsm were used in these experiments.

Table 3.2 shows the average surface potential ( $SP_{Avg.}$ ) of PVDF filter with different charging voltages, which was shown to increase with charging voltage from 81.9 V at 10 kV to 115.2 V at 20 kV. This could be explained by that a higher voltage caused greater ionization of air molecules during corona discharge and subsequently deposition of more ions onto the surface of the filters [56, 58, 60]. Correspondingly, as shown in Fig. 3.7, both filtration efficiency and quality factors of PVDF filters were higher at higher charging voltage. Even at the lowest voltage of 10 kV, the filtration performance of the filter was greatly improved.

**Table 3.2.** Average surface potential ( $SP_{Avg.}$ ) of 450-nm PVDF filters

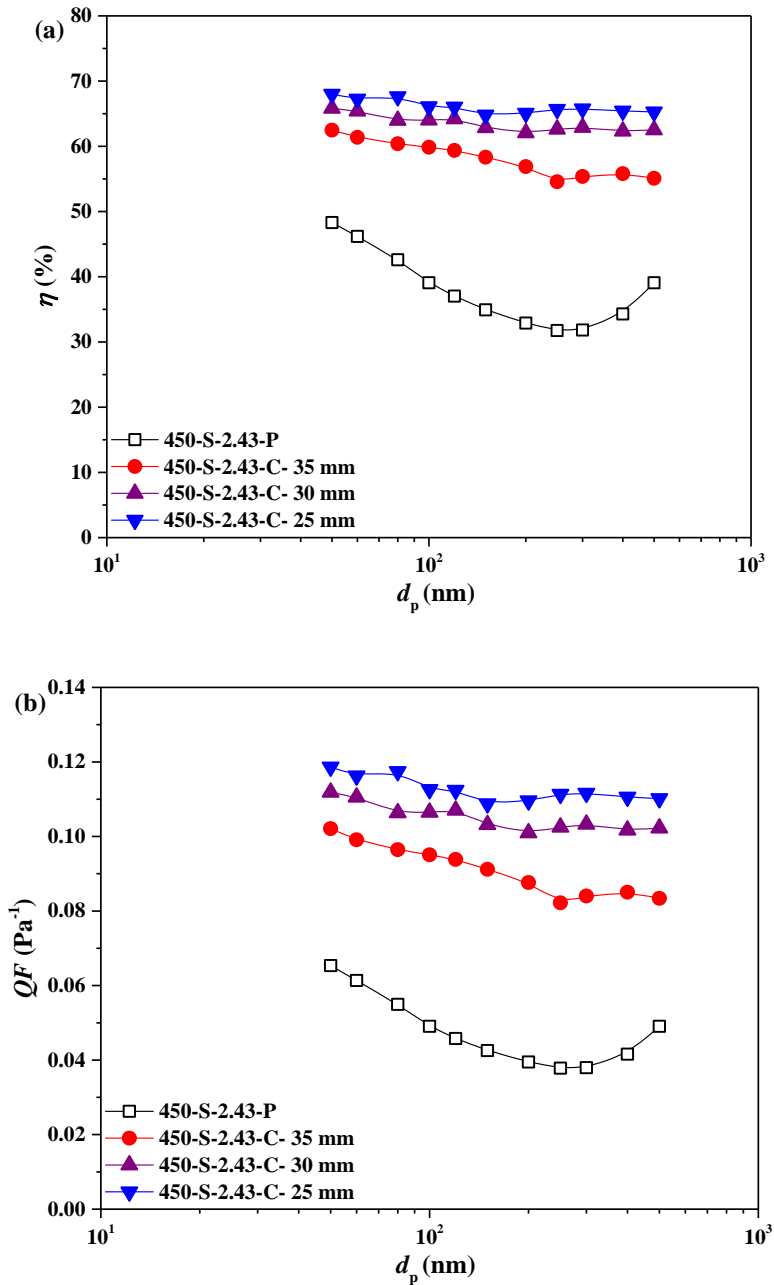
Medium	Charging condition			$SP_{Avg.}$ (V)	
	Voltage (kV)	Distance (mm)	Duration (s)	Pristine	Electret
450-S-0.87	15	30	60	4.6	43.7
450-S-1.75	15	30	60	5.8	80.8
450-S-2.43	10	30	60	6.0	81.9
450-S-2.43	15	30	60	6.0	100.8
450-S-2.43	20	30	60	6.0	115.2
450-S-2.43	15	35	60	6.0	86.7
450-S-2.43	15	25	60	6.0	115.8
450-S-3.46	15	30	60	6.6	138.1
450-S-5.10	15	30	60	8.1	188.1
450-S-6.98	15	30	60	11.5	228.6





**Fig. 3.7.** (a) Filtration efficiency ( $\eta$ ) and (b) quality factors ( $QF$ ) of pristine and electret 1-layer PVDF filters with varied charging voltages. (PVDF layer basis weight: 2.43 gsm.)

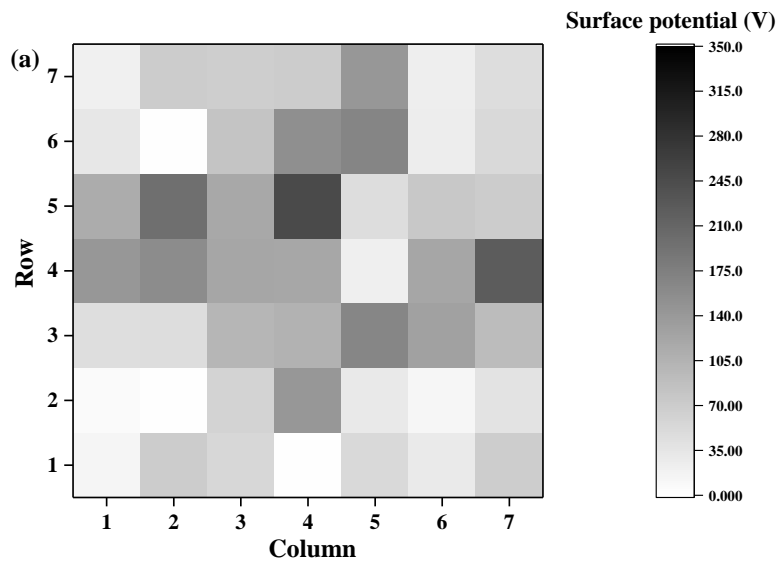
Similar to the effect of charging voltage, the higher  $SP_{Avg.}$  was also reached by reducing charging distance. As shown in Table 3.2, the values varied from 115.8 V at 25 mm to 86.7 V at 35 mm. The reason could be that a shorter distance between the two electrodes led to a higher charge intensity as well as a lower charge loss in air [56, 58, 60]. In conformity to the  $SP_{Avg.}$ , a shorter distance favored the filter filtration performance as seen in Fig. 3.8. At the largest distance of 35 mm, the quality factors of the filter increased by a factor of 1.5 to 2.1 as compared to the pristine filter.

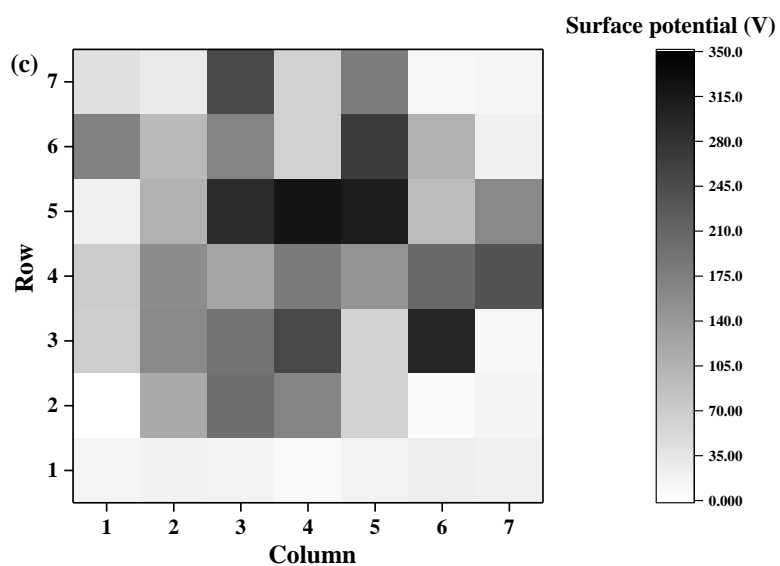
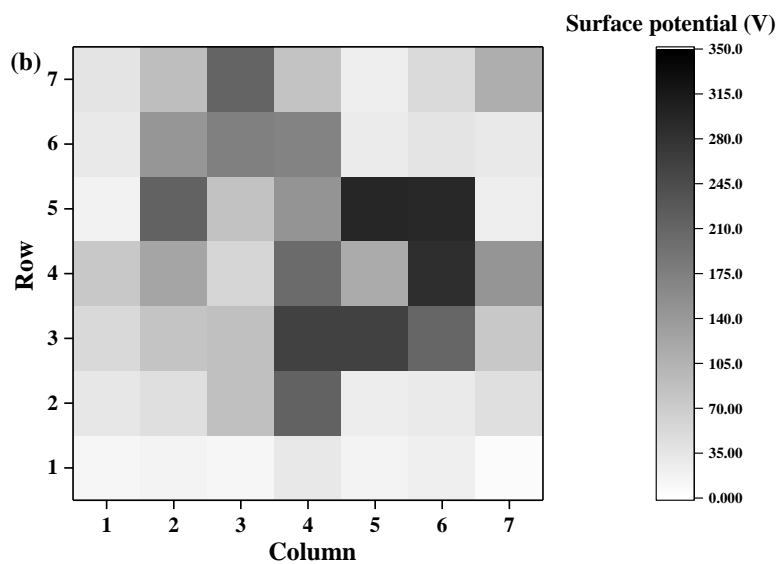


**Fig. 3.8.** (a) Filtration efficiency ( $\eta$ ) and (b) quality factors ( $QF$ ) of pristine and electret 1-layer PVDF filters with varied charging distances. (PVDF layer basis weight: 2.43 gsm.)

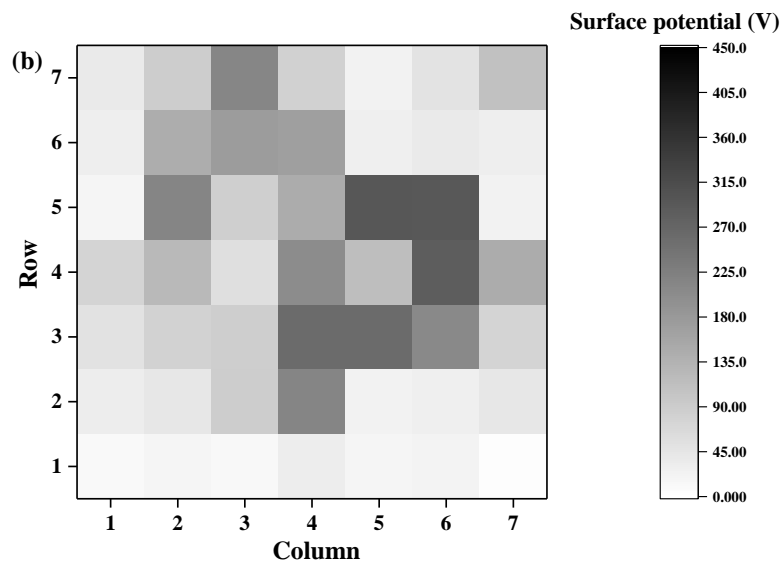
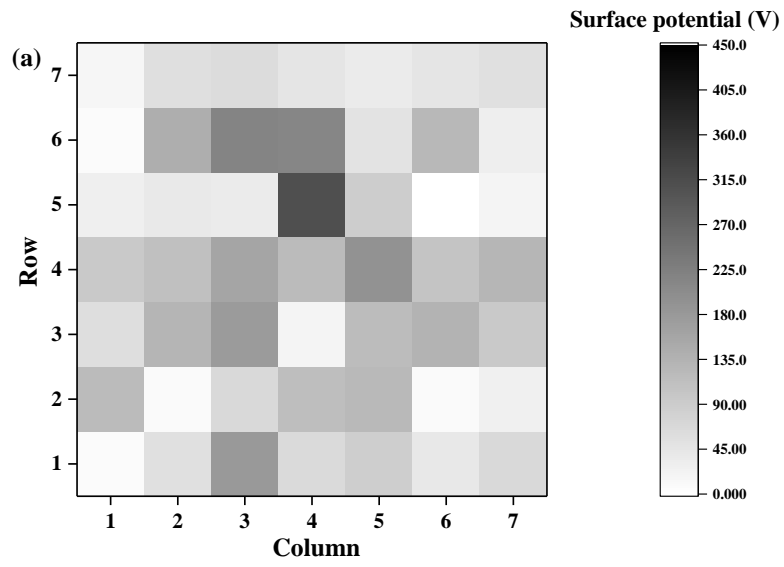
Better filtration performance could be obtained by using stronger electric field. Nevertheless, further increasing the voltage or reducing the distance did not bring distinct enhancement, which might be due to charge saturation resulting from the

limited charge traps for the PVDF filter with low solidity [19]. In addition, the charge distribution was found more uniform when using low voltage or long distance. as depicted in Fig. 3.9 and Fig. 3.10, respectively. The uniformity of charges could avoid high local penetration from insufficient electrical force [7]. Moreover, sparks were observed to generate at 20 kV or 25 mm, which confined the field intensity that could be applied. On the basis of the above result, filters charged optimally at voltage of 15 kV and distance of 30 mm would be used in the following study.





**Fig. 3.9.** Surface potential (*SP*) distribution on 1-layer PVDF electret filters with charging voltages of (a) 10 kV, (b) 15 kV and (c) 20 kV. (PVDF layer basis weight: 2.43 gsm.)



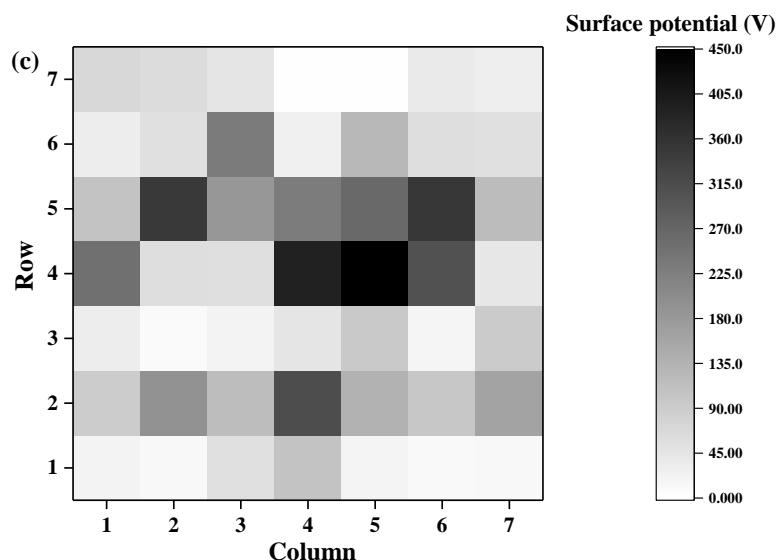
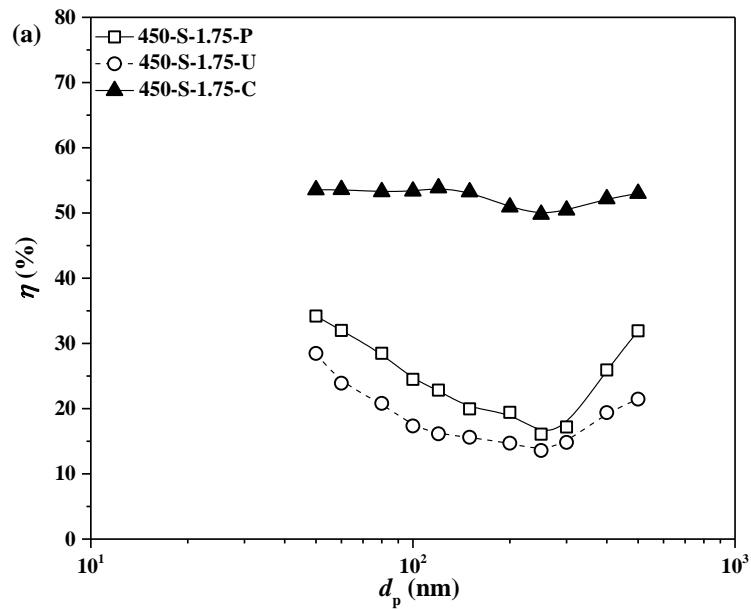


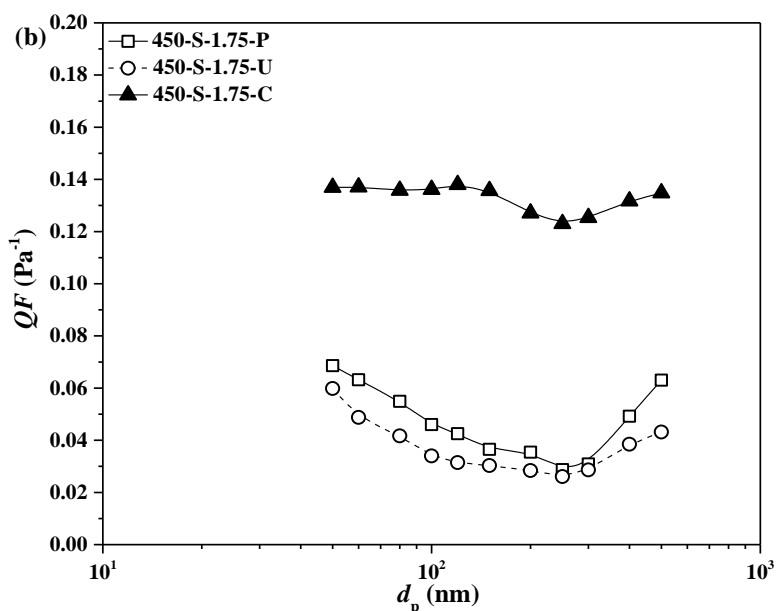
**Fig. 3.10.** Surface potential (*SP*) distribution on 1-layer PVDF electret filters with charging voltages of (a) 35 mm, (b) 30 mm and (c) 25 mm. (PVDF layer basis weight: 2.43 gsm.)

### 3.4.3. Filtration performance evaluation of 1-layer PVDF electret filters

Fig. 3.11 shows the filtration efficiency of PVDF filter in different charging states for particles ranging from 50 nm to 500 nm. For the pristine (i.e., as-spun) PVDF filter, a typical “V”-shape filtration curve was observed in Fig. 3.11a with the most penetrating particle size (MPPS) at around 250 nm. This indicates that mechanical mechanism, mainly interception and diffusion, played a major role in aerosol filtration, which was further confirmed by the insignificant drop in filtration efficiency after eliminating the intrinsic charges on the pristine filter using IPA soaking method [101]. As expected, the filtration efficiency of corona charged filter for aerosols of all sizes was greatly increased from 16.1-34.2% to about 51.5% and the filtration curve became much more flattened due to the enhanced electrical attraction between charged fibers and polarized particles. The larger particles got more benefit from the induced charges

and dipoles [7, 86, 102]. This in turn effected higher efficiency, which became more apparent as we analyzed the single fiber efficiency from dielectrophoretic filtration effect. The “residual” MPPS at 250 nm was attributed to the mixed effects of electrical and mechanical mechanisms. Corresponding to filtration efficiency, as shown in Fig. 3.11b, there was a 1.0-3.3 fold increase in quality factor from 0.026-0.069 Pa<sup>-1</sup> (pristine filter) to 0.123-0.138 Pa<sup>-1</sup> (electret filter), which resulted from the higher filtration efficiency and relatively low pressure drop of 5.6 Pa as listed in Table 3.1. Benefiting from the notable electrical force, the PVDF electret filter was shown to obtain superior filtration performance without incurring high air resistance.

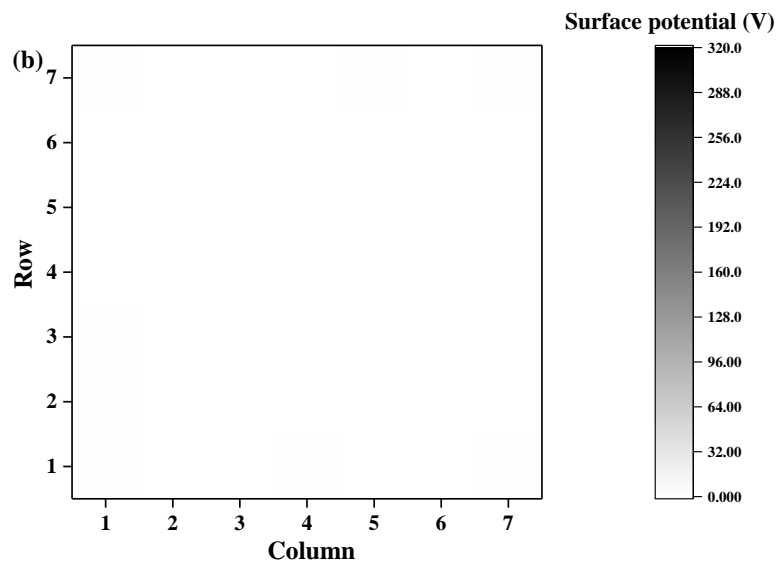
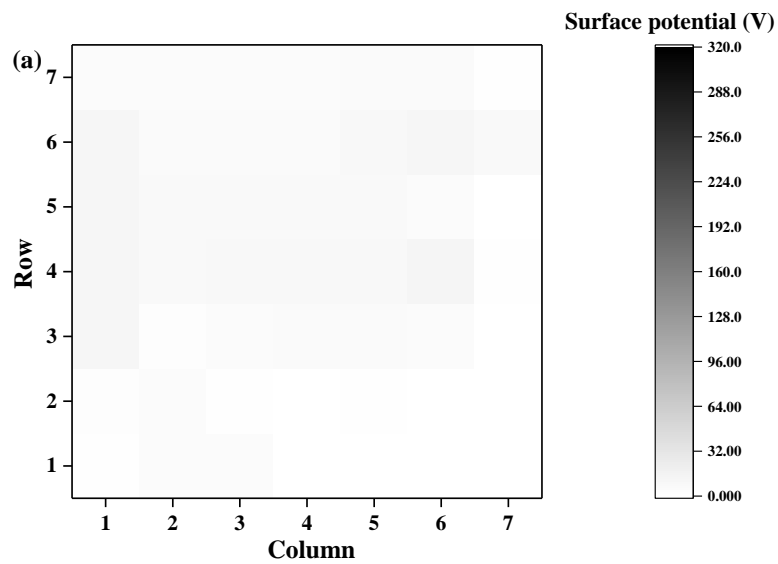


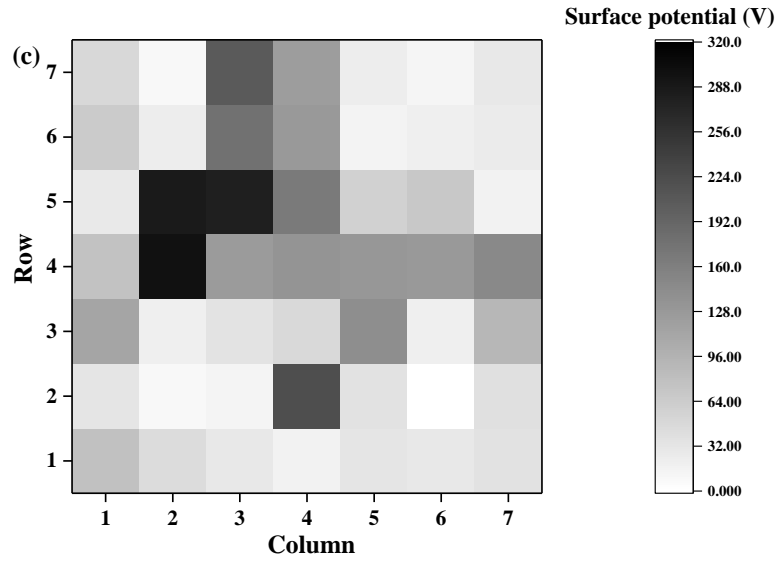


**Fig. 3.11.** (a) Filtration efficiency ( $\eta$ ) and (b) quality factors ( $QF$ ) of pristine, uncharged and electret 1-layer PVDF filters. (PVDF layer basis weight: 1.75 gsm.)

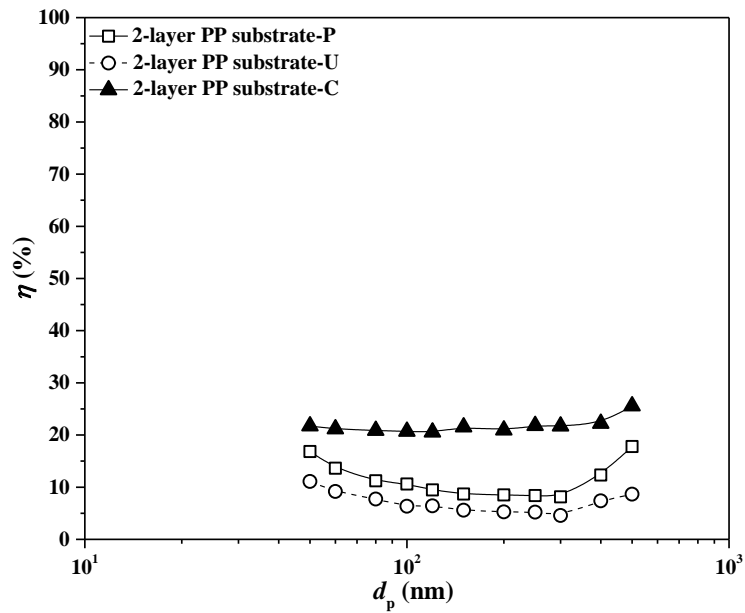
To confirm the role of charges in filtration performance improvement of the PVDF filter, its surface potential ( $SP$ ) distribution in different forms was measured as illustrated in Fig. 3.12. The pristine PVDF filter (Fig. 3.12a) showed low  $SP$ s with an average value ( $SP_{Avg.}$ ) of 6.0 V, while the uncharged filter (Fig. 3.12b) of 0.8 V due to charge removal by IPA [101]. However, after charging (Fig. 3.12c), the  $SP_{Avg.}$  was significantly increased up to 80.8 V, which indicates PVDF filter had a superior chargeability. It should be mentioned that the two PP substrate layers, including one layer as the support of PVDF layer and the other as a proof upstream of PVDF layer, could only contribute an insignificant part to the performance of PVDF filter due to the large diameter, high porosity and antistatic property of the selected substrate material [45]. As shown in Fig. 13, the filtration efficiency of the 2-layer PP substrate filter as a control group in pristine, uncharged and charged states were around 10, 8 and 20%, respectively, which indicates that the PVDF fiber layer was the key component in the

composite filter. The *SP* distribution of PP substrate was also depicted in Fig. 3.14, which indicates insignificant increase after charging due to the antistatic property of the PP material used. It is worth mentioning that *SP* tests as well as filtration tests of pristine and electret filters were taken 24 h after their preparation to ensure the charges remained and filter performance were relatively stable [40].

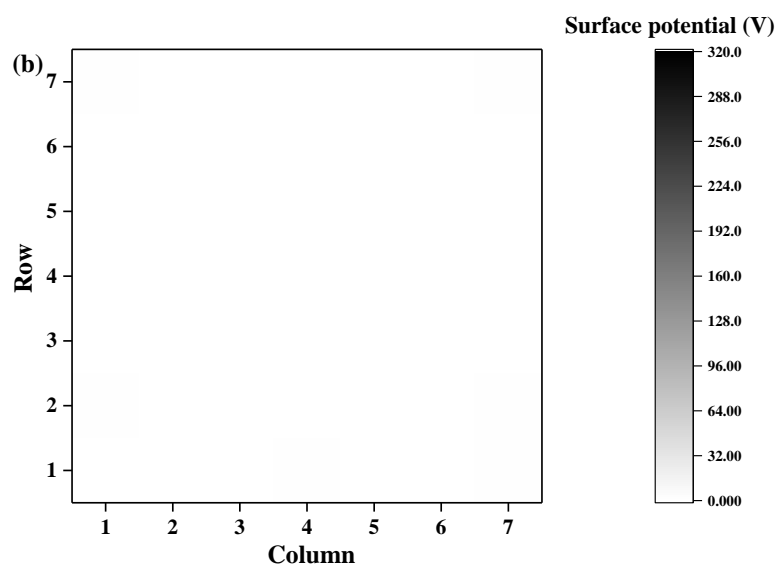
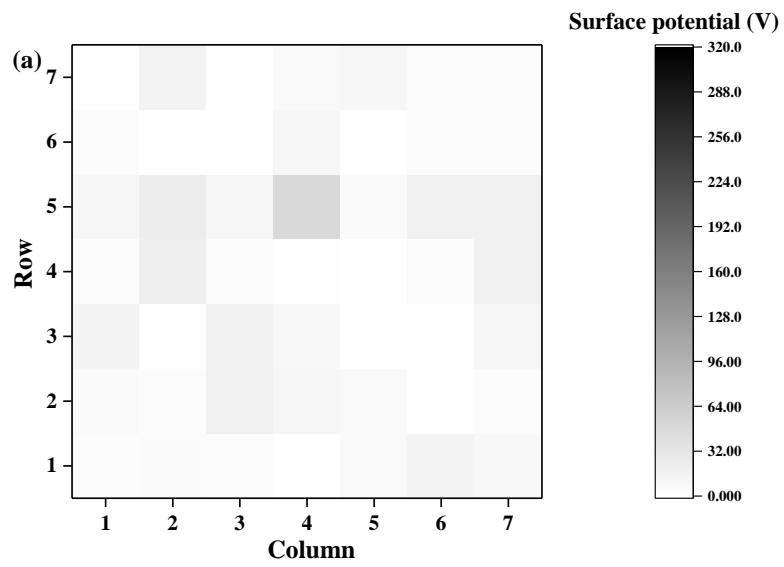




**Fig. 3.12.** Surface potential ( $SP$ ) distribution on (a) pristine, (b) uncharged and (c) electret 1-layer PVDF filters. (PVDF layer basis weight: 1.75 gsm.)



**Fig. 3.13.** Filtration efficiency ( $\eta$ ) of pristine, uncharged and electret 2-layer PP substrate.



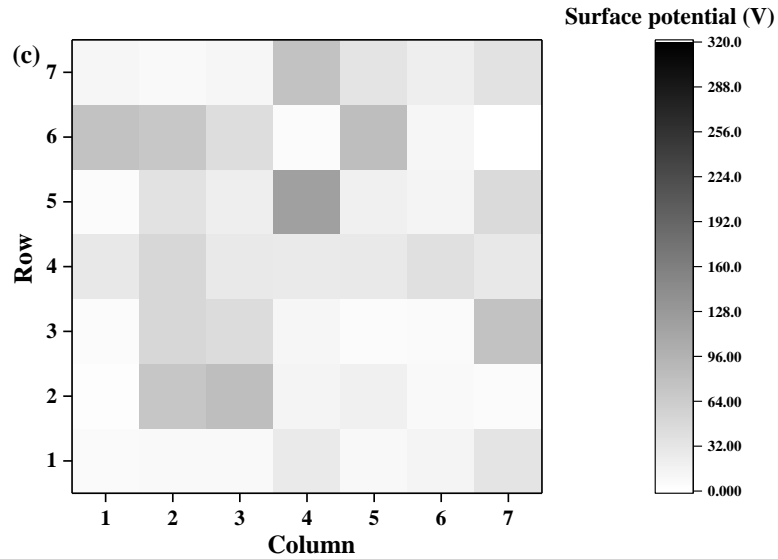


**Fig. 3.14.** Surface potential ( $SP$ ) distribution on (a) pristine, (b) uncharged and (c) electret PP substrate.

#### **3.4.4. Influence of PVDF basis weight on filtration performance of 1-layer PVDF electret filters**

For the mechanical fibrous filter, filtration efficiency can be improved with filter basis weight ( $W$ ) when keeping fiber diameter unchanged [1, 7, 13]. As shown in Fig. 3.15a, the filtration efficiency of pristine PVDF filters, which was mainly governed by mechanical filtration mechanism as their low charge densities (Table 3.2), increased with the  $W$  of PVDF layer. Meanwhile, due to decreasing porosity and increasing thickness of filters as shown in Table 3.1, pressure drop dramatically increased, resulting in lower quality factors (Fig. 3.15b) of the filter with higher  $W$ .

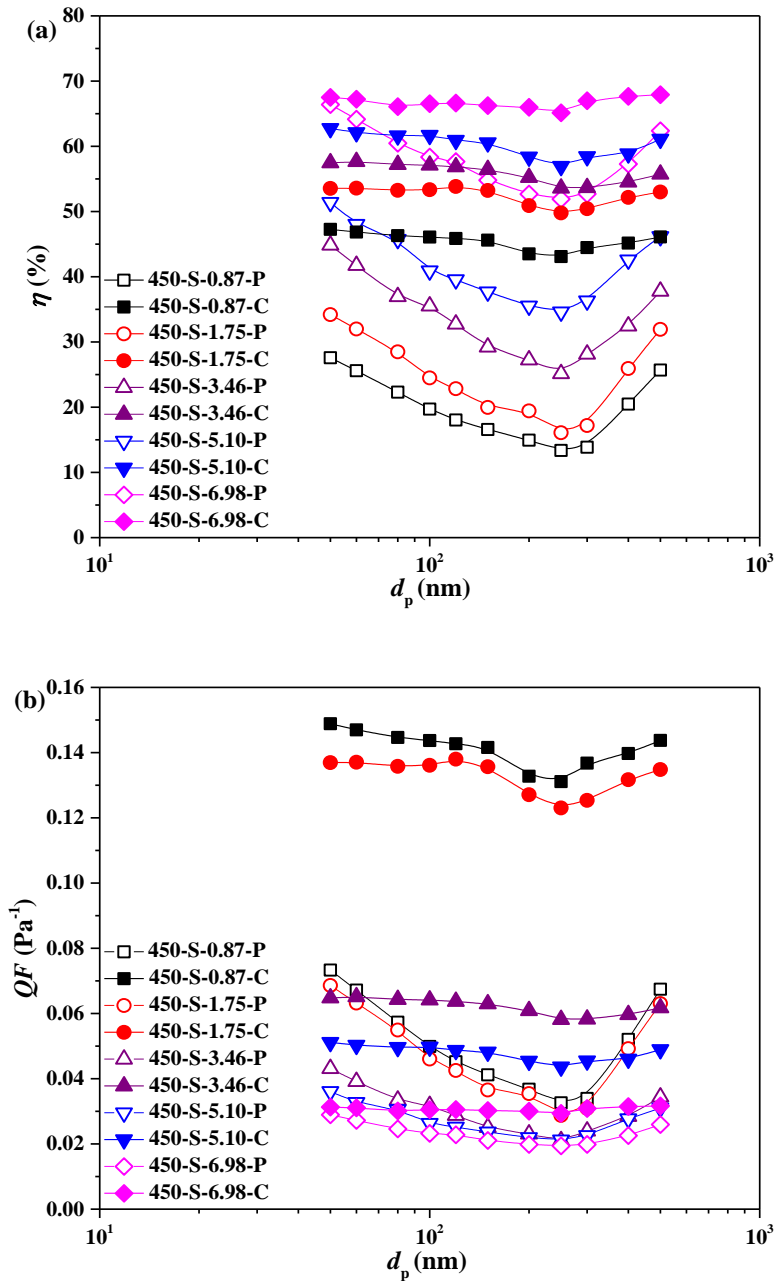


**Fig. 3.15.** (a) Filtration efficiency ( $\eta$ ) and (b) quality factors ( $QF$ ) of pristine and electret 1-layer PVDF filters with varied layer basis weights.

After being charged, single fiber efficiency for particle capture will be improved by the electrical attraction force. Theoretically, if each charged fiber acts independently in aerosol filtration, the filtration efficiency can be markedly augmented with more fibers, i.e., higher  $W$  [1, 7, 13].

The  $SP$  distributions of 1-layer PVDF electret filters with different  $W$  are also shown in Fig. 3.16. It is clearly seen that the  $SP_{Avg}$  increased with  $W$ , from 80.8 V at 1.75 gsm to 228.6 V at 6.98 gsm resulting from more charge traps with higher amount of fibers. It was observed that the increment of  $SP_{Avg}$  was not proportional to that of  $W$  and increased at a decreasing rate. This might be accounted for by two reasons. Firstly, during corona discharge, a sheath layer of charges with the same polarity as the emitting electrode might be formed close to the filter surface and inhibited further deposition of newly generated charge carries. Secondly, fibers might act as a physical barrier and prevent a certain portion of charges from migrating to the deeper filter section, which was more significant with higher packing density, i.e., higher  $W$  [13, 19, 103]. Corresponding to  $SP$ s, electret filter with a higher  $W$  had higher filtration efficiency as well as a flatter filtration curve (Fig. 3.15a). Moreover, although pressure drop (Table 3.1) increased with  $W$  due to the increase in both filter thickness and solidity, the electret filters all showed relatively high quality factors (Fig. 3.15b) above  $0.1 \text{ Pa}^{-1}$ , indicating the important role played by charging. Nevertheless, considering the limited increment in filtration efficiency of electret filters with varied  $W$  and the distinct improvement in  $SP$ , the higher filtration efficiency at a higher  $W$  was more due to the enhanced mechanical mechanism instead of the electrostatic one. The discrepancy might be attributed to the interference between electric fields generated by individual fibers and the decreasing impact of charged fibers with filter thickness and packing density [49]. Firstly, for a single charged fiber, a dipole can be induced in the approaching neutral particles which subsequently are attracted to the fiber surface by the attraction force of this specific fiber. However, in a real electret filter, each fiber is surrounded by many other fibers and various electric fields overlap, which may reduce the field strength in certain areas. For instance, the field between two fibers carrying charges of the same

sign and amount may be quite low and even zero at points of symmetry, though outside the filter the fields which do not contribute to the filtration may be exceedingly strong [7, 15, 48, 49, 103]. Therefore, with lower packing density, the interference among fibers could be mitigated and larger increment in filtration performance could be obtained. Secondly, although most of the aerosols used to challenge the filters were free of net charges, a small portion of them hold certain amount of charges whose distribution followed Boltzmann's law [1, 7]. As a result, it was more likely that particles with higher electrical mobility were collected by the upstream layers of the PVDF filter, and the downstream layers were less efficient in trapping the remaining particles due to their weaker mobility [81]. Furthermore, for relatively large particles, the densely packed fibers in high- $W$  filters might accelerate their velocity within the filter, thus leading to shorter retention time for electrical attraction [1, 7].

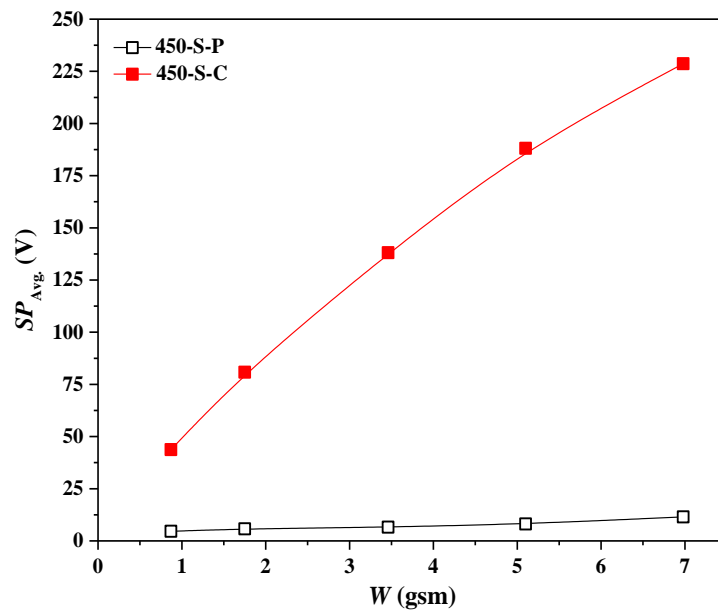


**Fig. 3.16.** Average surface potential ( $SP_{Avg.}$ ) of 1-layer PVDF filters with varied layer basis weights.

### 3.4.5. Filtration performance evaluation of multilayer PVDF electret filters

Given the unsatisfactory filtration performance of high- $W$  PVDF electret filters, it was speculated that the electrical mechanism might be enhanced by dividing the 1-layer filter with high packing density into a multilayer one with fewer fibers in each layer to reduce interference/overlapping electrical fields [48, 49]. To prove this hypothesis, different numbers of pristine or electret PVDF filters of 1.75 gsm were stacked up to form filters with different layers (e.g., a 2-layer filter was formed by stacking two individual filters of 1.75 gsm to produce a filter of 3.5 gsm). Aerosol filtration test was then carried out for each multilayer filter in both their pristine and electret forms and the result was compared with their 1-layer filter counterpart with a similar  $W$ .

For the pristine multilayer filters, like 1-layer ones, the filtration efficiency increased in a decreasing rate with  $W$  as depicted in Fig. 3.17a. However, all the multilayer filters showed an evidently higher filtration efficiency compared with their 1-layer counterparts. As mentioned earlier, the aerosol flow might be speeded up within the packed fibers, especially for the high- $W$  filters, which was disadvantageous to particle capture by diffusion. Also, for a 1-layer filter, the downstream section might be less efficiently used than the upstream one. By using a multilayer filter with the same total amount of fibers, aerosol flow rate within the filter was lowered. Due to the loosely packed layers, extra space was given to aerosol flow to resume its initial face velocity upstream of each layer, hence increasing the utilization rate of fibers. Apart from the increased filtration efficiency, stacking up multiple layers with high porosity also resulted in lower pressure drop, i.e., pressure drop saving was realized. After redistributing fibers in a single-layer filter to multilayer filter, the fiber packing density in each layer of the multilayer filter was much lower and this effect on pressure drop

was far more significant than the increase in filter thickness. Therefore, the flow resistance was lower for the multilayer filter compared to the single-layer filter with the same filter basis weight. As shown in Table 3.1, pressure drop measured across 450-M2-1.75-P, 450-M3-1.75-P and 450-M4-1.75-P were 12.4, 17.8 and 24.1 Pa, respectively, which were approximately two, three and four times of that across 450-S-1.75-P. Note that the filter basis weights of 450-M2-1.75-P, 450-M3-1.75-P and 450-M4-1.75-P were two, three and four times of that of 450-S-1.75-P. The pressure drop saving was more notable with higher  $W$ , with a decrease of 1.4 Pa for 450-M2-1.75-P in comparison with 450-S-3.46-P while 13.6 Pa for 450-M4-1.75-P compared with 450-S-6.98-P. Similar merit of “multilayering” in pressure drop saving was observed and well elaborated in our previous work [36]. With higher filtration efficiency and lower pressure drop, higher quality factors were reached for the multilayer filters (Fig. 3.17b). As a departure from the 1-layer filters, whose increase in filtration efficiency was overshadowed by that of pressure drop leading to decreasing quality factors with  $W$ , quality factors of multilayer filters were little affected by the layer number and remained at relatively high values. This experimental result conformed to the equation of quality factor which shows that composites formed by stacking up different numbers of identical layers have the same quality factor of the single layer [46]. Contrarily, the quality factors dropped with increasing  $W$  for the single layer filters (Fig. 3.17b).

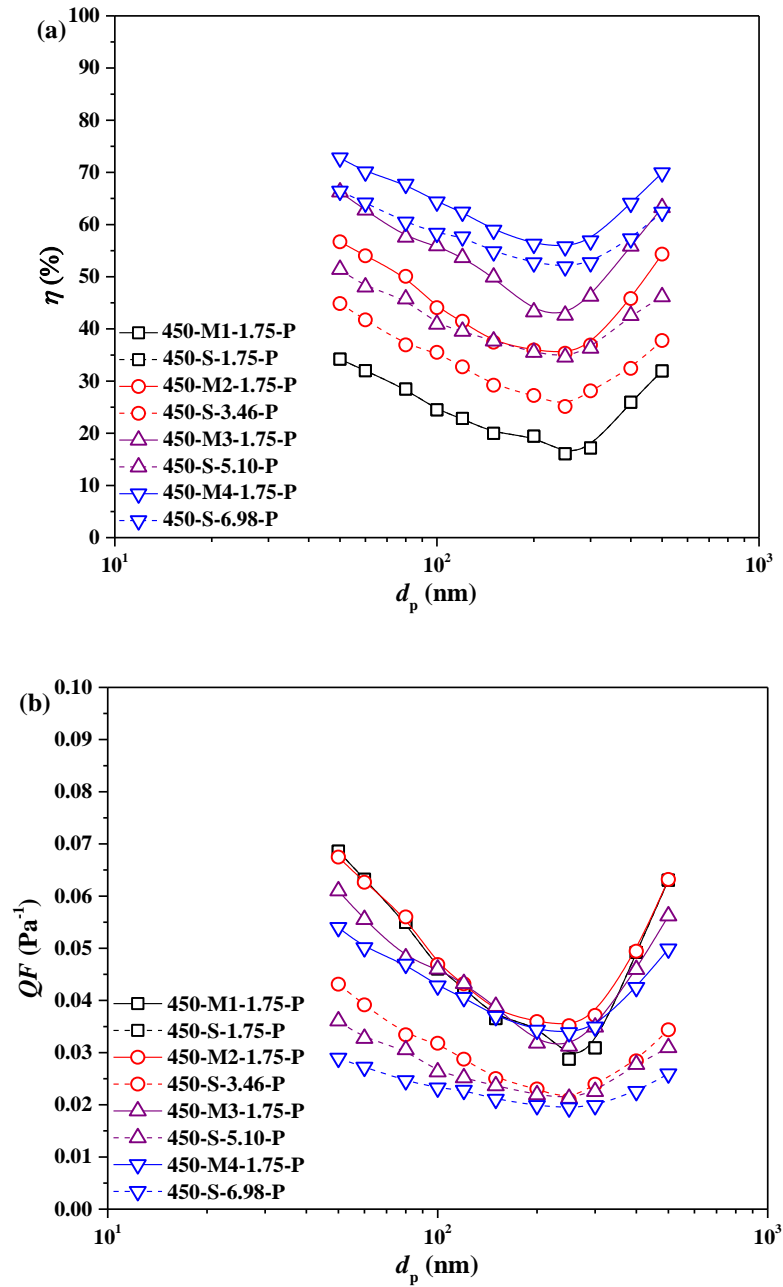


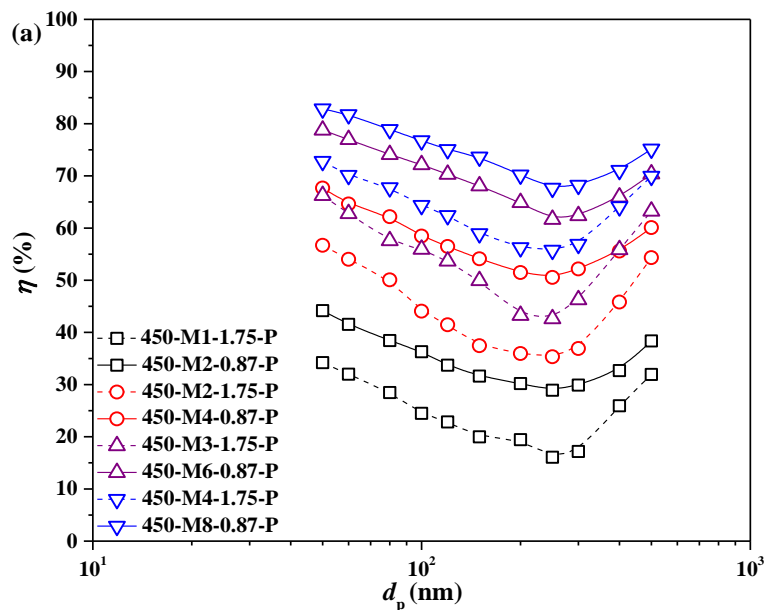
**Fig. 3.17.** Comparisons of (a) filtration efficiency ( $\eta$ ) and (b) quality factors ( $QF$ ) between 1-layer and multilayer pristine PVDF filters. (Basis weight of PVDF layer in multilayer filter: 1.75 gsm. Note 450-S-1.75 and 450-M1-1.75 denote the same filter.)

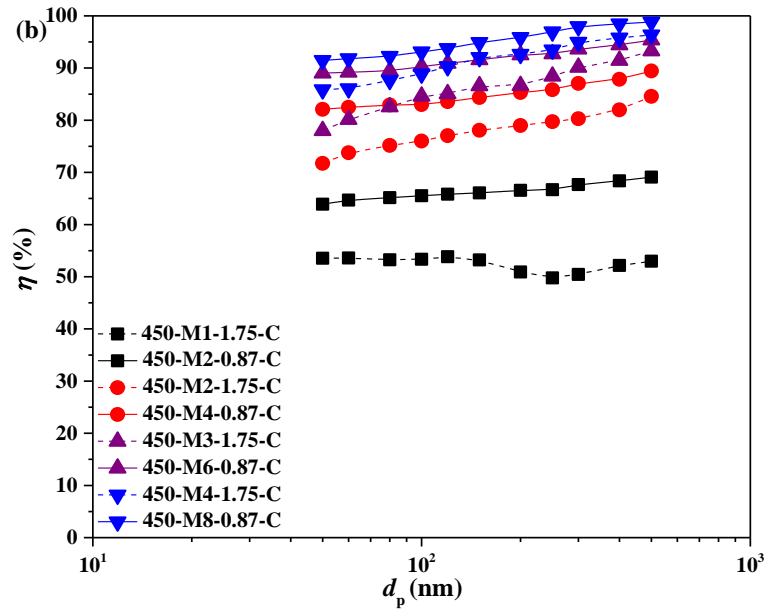
For the multilayer electret filters, filtration efficiency was raised by 15.3-32.2% compared with the corresponding 1-layer electret ones (Fig. 3.18a). All the curves of the three filters show ascending trend with particle diameter, which reveals that the

electrical mechanism took a dominant role and was more favorable to large particles due to higher dielectrophoretic forces [1, 7, 86]. The dipole strength, which is charge multiplied by charge separation distance, are stronger as larger particles can afford to have further charge separation distance. The significantly higher filtration efficiency of the multilayer electret filters than the single ones could be attributed to less interference between electrical fields of adjacent fibers, more efficient utilization of downstream fibers and lower face velocities of aerosols within filters, as well as higher amount of total charges [1, 7, 48, 49, 81, 104]. Since adding charges to filters exerted little change on the physical morphology of filters, pressure drop saving using multilayer filters also applied to their electret form [7, 13]. As shown in Table 3.1, the multilayer electret filters had lower pressure drop than the 1-layer electret filters, with the difference increasing with increasing  $W$ . Similar to filtration efficiency, quality factors of multilayer filters were much higher than 1-layer ones and increased with particle size (Fig. 3.18b). Yet, due to the 2-layer electret filter already had high filtration efficiency ranging from 73.2 to 85.9%, the increment of filtration efficiency with layer number was less remarkable than pressure drop, leading to decreasing quality factors. Nevertheless, the advantage of multilayering was still demonstrated with outstanding quality factors in the range of 0.107-0.158, 0.088-0.157 and 0.084-0.142 Pa<sup>-1</sup>, respectively, although the  $SP_{Avg}$  of a single layer was much lower than those of other researchers' due to the limitation of our corona discharge device [40].

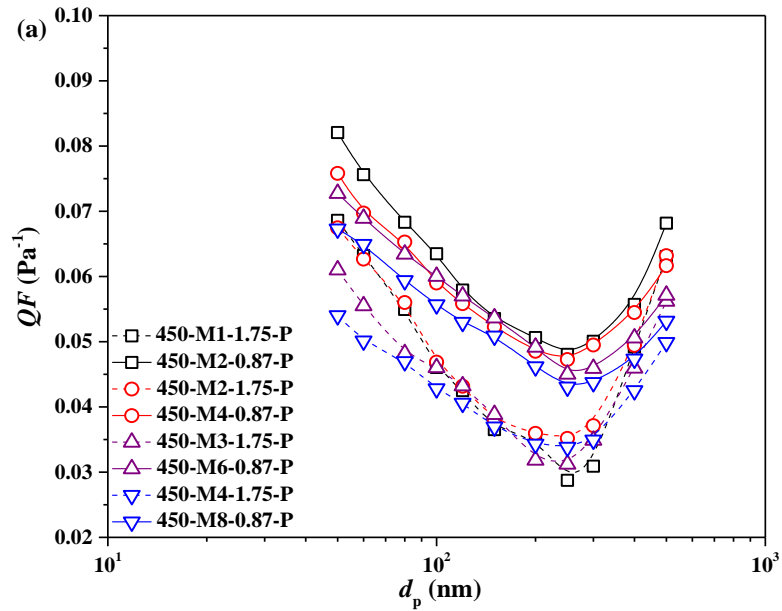


up in accordance to 450-M1-1.75, 450-M2-1.75, 450-M3-1.75 and 450-M4-1.75, respectively, and tested for filtration property. As depicted in Fig. 3.19, the filtration efficiency of 0.87 gsm multilayer filters was all higher than that of those with double gsm and halved layer number, regardless of pristine or electret ones. However, the gsm-halved filters all showed slightly higher pressure drop than their counterparts (Table 3.1), which seems contradictory to the assertion of pressure drop saving. The discrepancy should be contributed by the additional PP substrate layers with 1.3-2 Pa for each. Despite the increase in pressure drop, higher quality factors were still achieved for both pristine and electret filters. Compared with the pristine filters with  $W_L$  of 1.75 gsm, the quality factor curves of the four filters with  $W_L$  of 0.87 gsm were relatively scattered because of the existence of more PP layers which lowered the quality factors (Fig. 3.20a). For electret filters, the highest quality factors achieved ranged from 0.122 to 0.160  $\text{Pa}^{-1}$  (Fig. 3.20b), confirming the superior performance of multilayer PVDF electret filters.





**Fig. 3.19.** Comparison of filtration efficiency ( $\eta$ ) between multilayer PVDF filters with layer basis weights of 0.87 gsm and 1.75 gsm: (a) pristine ones and (b) electret ones.



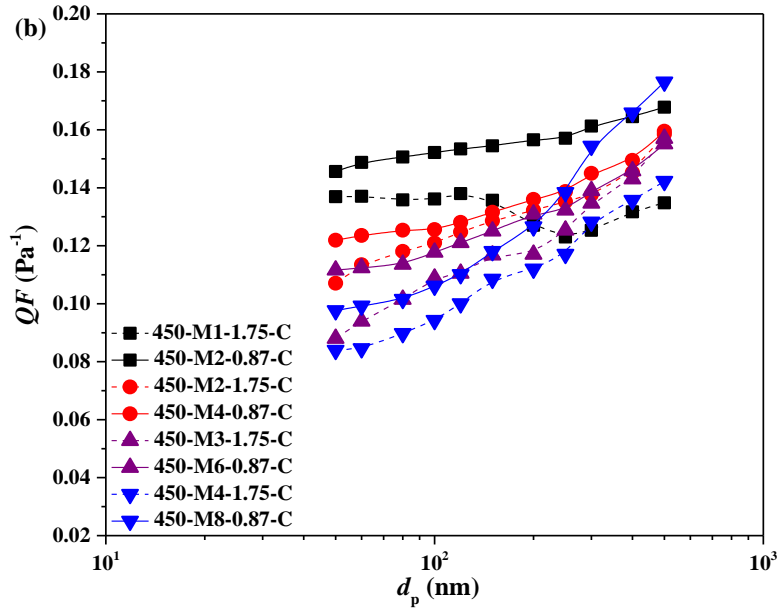


**Fig. 3.20.** Comparison of quality factors ( $QF$ ) between multilayer PVDF filters with layer basis weights of 0.87 gsm and 1.75 gsm: (a) pristine ones and (b) electret ones.

To get a more direct perspective on the enhancement of electrostatic capture after multilayering, the filtration efficiency of varied electret filters for 200-nm aerosols contributed from dielectrophoretic filtration effect was calculated using Eq. 3.4. As shown in Fig. 3.21, for the 1-layer electret PVDF filters (450-S-C), dielectrophoretic filtration efficiency first increased and then decreased with filter basis weight, which indicates that an optimal amount of fibers is essential to achieve the best electrostatic capture effect of a single layer. When the fiber amount was too small, filters could only be deposited with charges of low density through corona discharge. On the other hand, when the fiber amount was too large, the charge density was overwhelmingly high that electrical interference among adjacent charges was incurred [49]. Both the above two cases led to weak dielectrophoretic capture effect towards neutralized aerosols. After redistributing fibers into multiple layers, the dielectrophoretic filtration efficiency of 450-M-1.75-C was greatly improved due to the much alleviated charge interference.

Further redistributing fibers from 450-M-1.75-C into 450-M-0.87-C brought additional enhancement in dielectrophoretic capture effect. Nevertheless, the improvement was less significant because insufficient fibers existed in each layer to support enough charges and sustain high single-layer dielectrophoretic filtration efficiency.

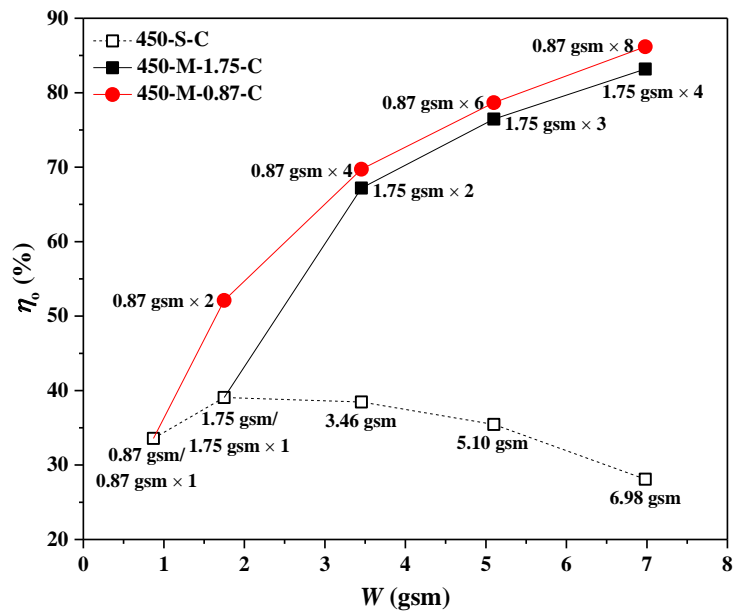


**Fig. 3.21.** Filtration efficiency due to dielectrophoretic filtration effect of varied PVDF electret filters for 200-nm aerosols.

To show a clearer pattern of the effect of multilayering, filtration efficiency and quality factors of 200-nm particles were plotted against the corresponding pressure drop, respectively (Fig. 3.22a and Fig. 3.22b). From the figures, it is further proved that filters with both high filtration efficiency and low pressure drop can be fabricated benefiting from redistributing fibers into more layers.

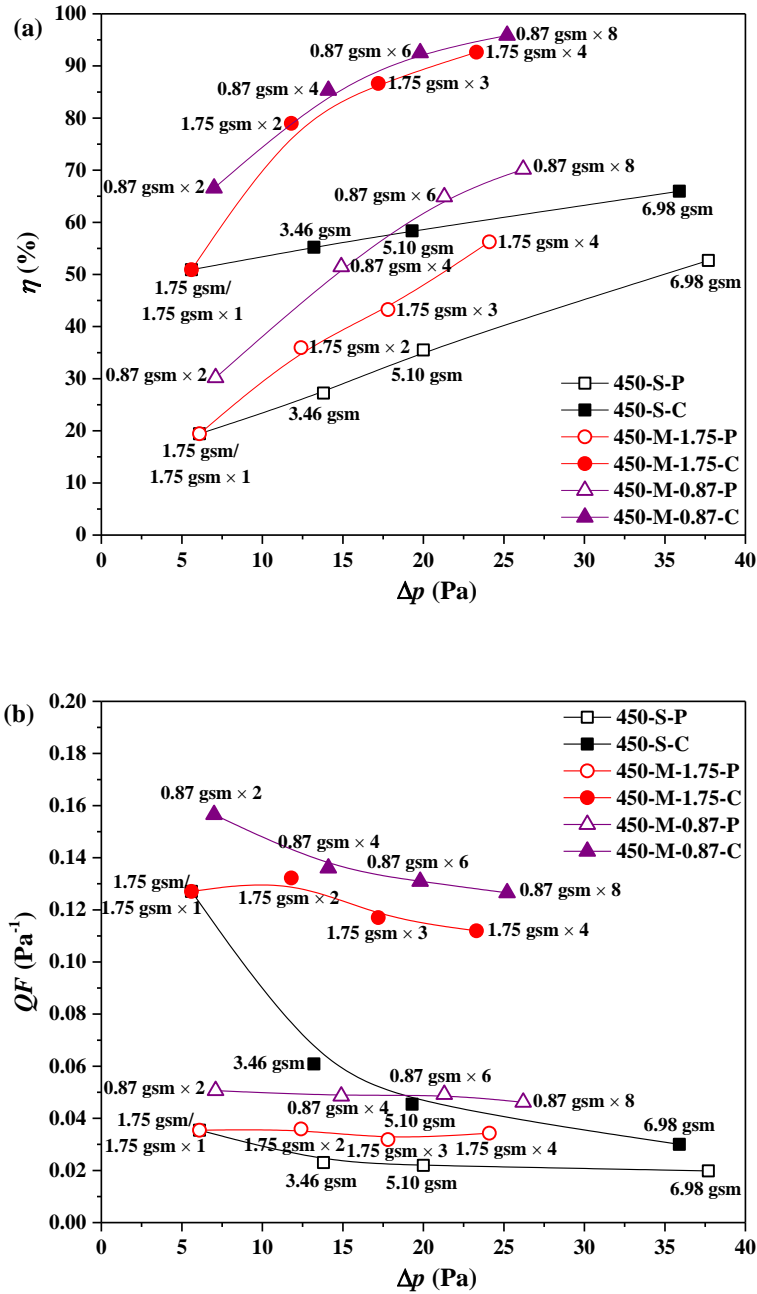


**Fig. 3.22.** Evolution of (a) filtration efficiency ( $\eta$ ) and (b) quality factor ( $QF$ ) of pristine and electret 1-layer and multilayer PVDF filters for 200-nm aerosols with corresponding pressure drop ( $\Delta p$ ).

### 3.4.6. Analysis of dielectrophoretic filtration effect on Single fiber efficiency

There are two sets of test data acquired from testing of multilayer with modular filter with  $W_L$  of 1.75 gsm and 0.875 gsm, respectively under constant face velocity at

5.3 cm s<sup>-1</sup>. There is a further data set with limited testing at a fixed  $W$  but with different face velocities of 2.5, 5.3 and 7.5 cm s<sup>-1</sup>, respectively. We can use the dielectrophoretic filtration effect of single fiber efficiency analysis to obtain better insight to all these data sets.

Fig. 3.23 shows a log-log plot of single fiber efficiency corresponding to dielectrophoretic filtration effect versus  $Cd_p^2/U$  per Eq. 3.14. There are two sets of data. The lower set corresponds to the correlation on three different microfiber-based filters respectively, filter A with 85-300 gsm and electrostatically charged by corona discharge, filter B with 100-290 gsm fibers and charged by triboelectric effect, and filter C with 20-60 gsm and charged by corona discharge [81]. The correlations were based on a large group of data set carried out earlier on commercially available filters, made of melt-blown PP material. The upper set contains our test results also cast in similar format on the log-log plot. The lower curve (appeared as straight line on log-log graph) represents one single layer with 1.75 gsm of PVDF nanofibers, while the upper curve represents also 1.75 gsm but in form of two stack-up layers with each layer having 0.87 gsm of PVDF nanofibers. Two observations have been made with the nanofiber test results.

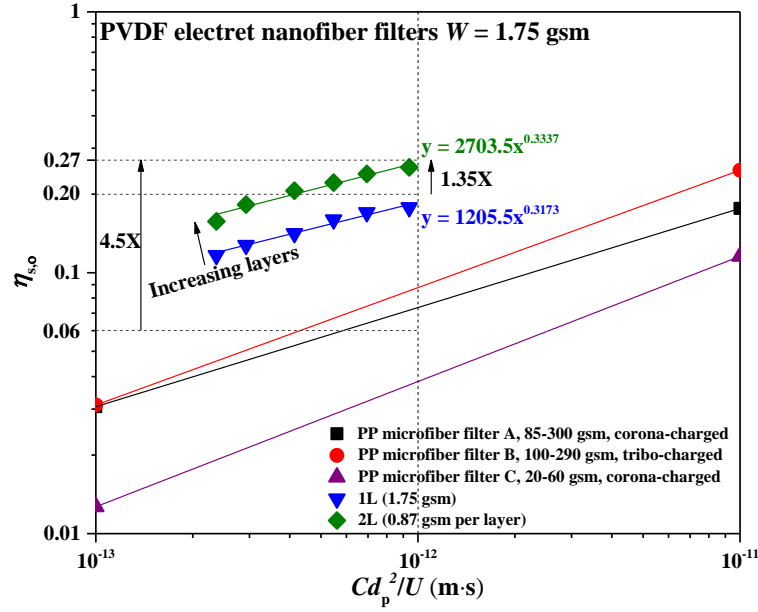


**Fig. 3.23.** Single fiber efficiency of different electret filters due to dielectrophoretic filtration effect ( $\eta_{s,o}$ ) versus reduced parameter ( $Cd_p^2/U$ ).

First,  $\eta_{s,o}$  for both the 1-layer and 2-layer filters test data are well correlated with  $Cd_p^2/U$  through a power law despite the power index of 0.325 is slightly lower than the theoretical value of 0.4 (Eq. 3.16). Therefore, we can conclude the aerosol capture phenomenon was still attributed to the dielectrophoretic filtration effect, i.e. inducing dipole on a neutrally charged aerosol by the charged fibers, and subsequent capture by the electrostatic interaction of the charged dipole of the aerosol with the charged fibers. Note the behaviour of the coulombic interaction between a charged aerosol and a charged fiber is quite different from Eq. 3.16. Therefore, the dielectrophoretic filtration is indeed the mechanism of capture in our tests.

Second, despite both curves have the same total amount of 1.75 gsm of nanofibers, when this amount of fibers is distributed into two layers, the resultant filter has 35% higher single fiber efficiency across all particle sizes than that with all the fibers contained in a single layer.

Another interesting observation is that when  $Cd_p^2/U$  is  $1 \times 10^{-12}$  m·s, taking the average  $\eta_{s,o}$  of the microfiber filters being 0.06 and  $\eta_{s,o}$  of the nanofiber filter (2-layer) being 0.27, their ratio is 4.5. Given the single fiber efficiency for dielectrophoretic filtration effect, Eqs. 3.12-3.13, varies inversely as fiber diameter to the power of 0.4, therefore

$$\frac{(\eta_{s,o})_{\text{nano}}}{(\eta_{s,o})_{\text{micro}}} = \left[ \frac{(d_f)_{\text{micro}}}{(d_f)_{\text{nano}}} \right]^{0.4} = \left[ \frac{20,000}{450} \right]^{0.4} = 4.5$$

This indeed is in accord with the experimental ratio of 4.5 determined.

Next, we compare the single fiber dielectrophoretic filtration efficiency between the 6L (6-layer electret filter, similarly hereinafter, with 0.87 gsm per layer) with the 1L (5.10 gsm) in Fig. 3.24. As clearly seen, the multilayer electret filter is better by a factor of 2.7 compared to the 1-layer one.

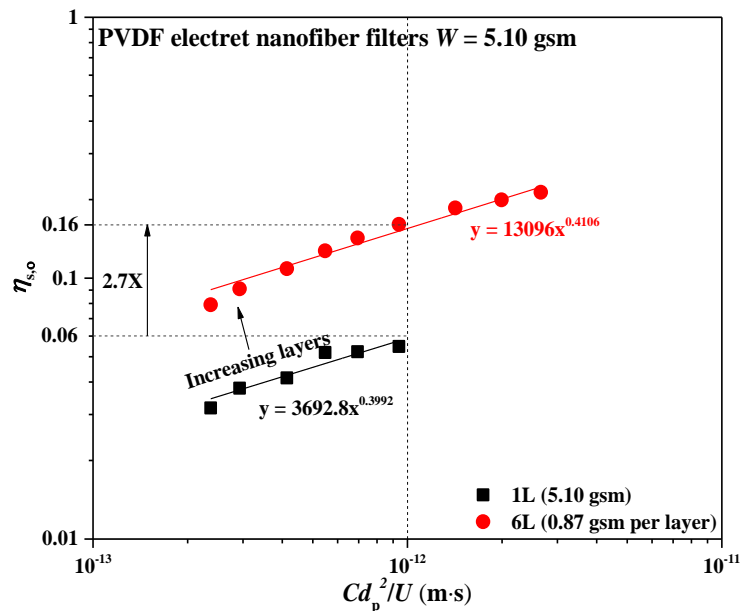


**Fig. 3.24.** Comparison of single fiber efficiency due to dielectrophoretic filtration effect ( $\eta_{s,o}$ ) versus reduced parameter ( $Cd_p^2/U$ ) between 1-layer and 6-layer electret filters both at 5.10 gsm and  $5.3 \text{ cm s}^{-1}$ .

Fig. 3.25 again further illustrates the effect of aerosol diameter (50-400 nm) and velocity effect (2.5, 5.3, and 7.5 cm s<sup>-1</sup>). All the results are well correlated on a single trend in agreement with Eq. 3.16,

$$\eta_{s,o} \propto \left[ \frac{C(d_p)^2}{U} \right]^n$$

with  $n$  varying between 0.327 to 0.405, which is comparable to the theoretical power index of 0.4 (Eq. 3.16). The effect due to increasing velocity (shorter retention time) with resulting lower single fiber capture efficiency from dielectrophoretic filtration effect is clearly evident; vice versa for lower challenging velocity or longer retention time.

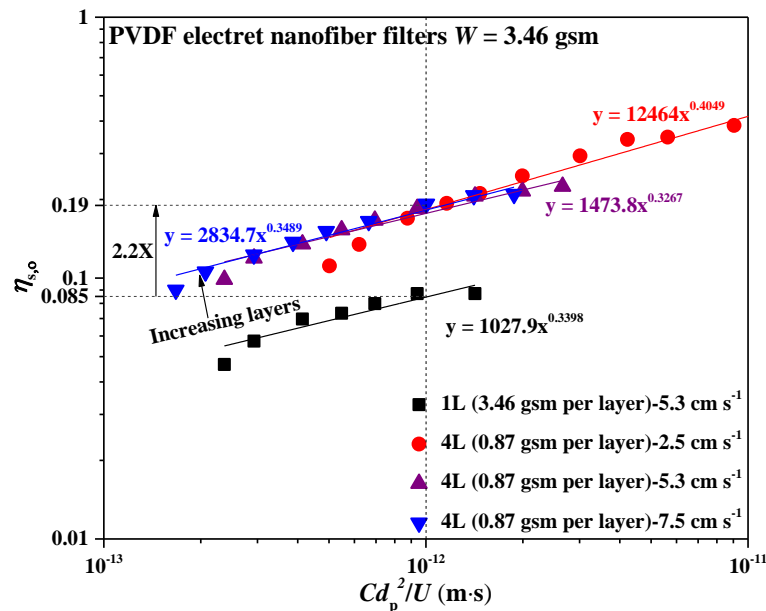


**Fig. 3.25.** Comparison of single fiber efficiency due to dielectrophoretic filtration effect ( $\eta_{s,o}$ ) versus reduced parameter ( $Cd_p^2/U$ ) between 1-layer and 4-layer (0.87 gsm per layer) electret filters both at 3.46 gsm and 5.3 cm s<sup>-1</sup>, and also 4-layer (0.87 gsm per layer) electret filters at 2.5 and 7.5 cm s<sup>-1</sup>, respectively.

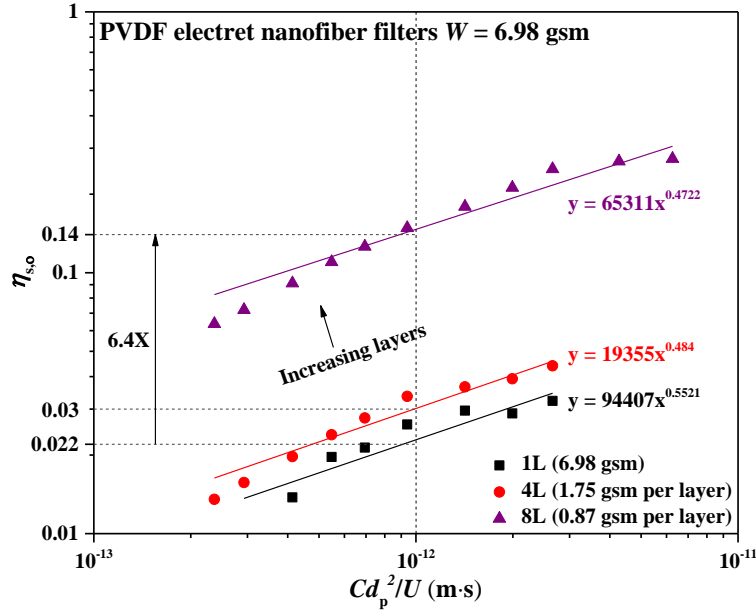


**Fig. 3.26.** Comparison of single fiber efficiency due to dielectrophoretic filtration effect ( $\eta_{s,o}$ ) versus reduced parameter ( $Cd_p^2/U$ ) between 1-layer and 8-layer (0.87 gsm per layer) electret filters both at 6.98 gsm and  $5.3 \text{ cm s}^{-1}$ .

Another interesting aspect is with a single nanofiber layer with 3.46 gsm, the 4-layer filter (0.87 gsm per layer) has much higher single fiber efficiency. Given the lines are parallel, we can take a given value of the abscissa  $Cd_p^2/U = 1 \times 10^{-12} \text{ m}\cdot\text{s}$ , the  $\eta_{s,o}$  for the 4L is 0.19 while the 1L is 0.085, with the ratio being 2.2. This ratio is the same across all sizes. This can also be seen by rewriting Eq. 3.16 with power being  $n$  instead of 0.4.

$$\eta_{s,o} = G \left[ \frac{C(d_p)^2}{U} \right]^n \quad (3.16)$$

where  $\eta_{s,o}$  is the single fiber filtration efficiency due to dielectrophoretic force,  $G$  is a constant,  $C$  is the Cunningham slip correction factor,  $d_p$  is the particle diameter, and  $U$  is the face velocity.

At  $d_{p1}$ , for 4L (0.87 gsm),

$$\eta_{s,o2} = G_2 \left[ \frac{c(d_{p1})^2}{U} \right]^n \quad (3.17a)$$

And for 1L (3.5 gsm),

$$\eta_{s,o1} = G_1 \left[ \frac{c(d_{p1})^2}{U} \right]^n \quad (3.17b)$$

Taking the ratio of Eq. 3.17b and Eq. 3.17a,

$$\frac{\eta_{s,o2}}{\eta_{s,o1}} = \frac{G_2}{G_1}$$

This ratio does not depend on the aerosol size,  $d_p$ ! In other words, the slopes of the two lines or  $n$  for the two curves are nearly the same. Then it does not matter where the efficiencies of the two are compared so long as they have the same abscissa value  $Cd_p^2/U$ . In our case, for convenience we take  $Cd_p^2/U = 1 \times 10^{-12} \text{ m}\cdot\text{s}$ . In any case, the 4-layer filter is better than the 1-layer filter by 2.2 times. This multilayering benefit is quite evident.

In reviewing Figs. 3.23-3.26. It can be seen that as  $W$  increases, the multilayer benefit seems to be much greater. We believe that as the amount of charged fibers increase, there is electrical interference on aerosol capture from different fibers in a thick single layer [48, 49]. By isolating the fibers into thinner layers using substrate material, we can reduce the interference effect, thus harvesting more electrostatic induction and attraction from the dielectrophoretic filtration effect. Also, it can be seen that the power index (i.e. slope of the linear trend in the log-log plot) increases with increasing  $W$  – 0.33 (1.75 gsm), 0.35 (3.46 gsm), 0.40 (5.10 gsm) and finally 0.51 (6.98 gsm) with the mean value being 0.4, which is identical to the theoretical value [7]. Fig. 3.27 plots the ratio of the single fiber efficiency based on dielectrophoretic capture of the  $n$ -layer electret filter to the corresponding 1-layer electret filter,  $\eta_{s,o,n}/\eta_{s,o,1}$ . It can

be seen that this ratio increases exponentially with increasing  $W$  from multilayering of the filter. This points out importantly that as more fibers are deployed in a filter to enhance the capture efficiency, multilayering should be used to reduce the electrostatic interference among fibers to realize the enhanced capture efficiency [48, 49]. Of course, multilayering can also reduce the pressure drop, which is another key advantage.

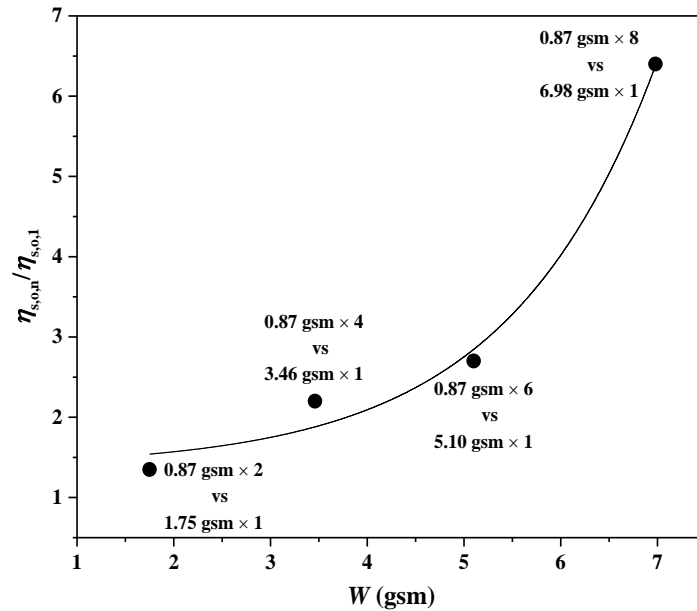


**Fig. 3.27.** Ratios of single fiber efficiency ( $\eta_{s,o,n}/\eta_{s,o,1}$ ) due to dielectrophoretic force of multilayer electret filters to that of corresponding 1-layer electret filters.

### 3.4.7. Stability test

One key factor that is used for the performance evaluation of an electret filter is its durability. Charges on or within filter medium will dissipate with time, whose decay is greatly affected by the polymeric material and is detrimental to electret filters [19]. Since electret filters are generally designed to have a more open structure than mechanical filters, once electrostatic effect is lost and only mechanical capture mechanisms can operate, there will be a drastic drop in filtration performance [13, 97]. To investigate the performance stability of our multilayer electret filters, filtration

efficiency tests were carried out at different time after the preparation of 450-M4-1.75-P. To avoid the influence of differences in filter structure and charge distribution, the same electret filter was used throughout the stability test. And the filter was always stored in a desiccator when it was not being used. As shown in Fig. 3.28, 1 day after charging, the filter performance was quite satisfactory, and filtration efficiency was almost unchanged after storing in the desiccator for 15 days. Even when the storage time was prolonged to 90 days, there was only an insignificant decrease of about 1%. The decay of filtration efficiency was in conformity to the  $SP$  change with time. As can be seen in Fig. 3.29,  $SP_{Avg}$  decreased dramatically in the first 12 h after charging (due to the rapid loss of charges with low release energy) followed by an increasingly slower decay rate and nearly kept identical after 24 h. The long-time effectiveness of our multilayer electret filter should be attributed to the highly hydrophobic and the excellent electrical resistant properties of PVDF, leading to superior electrostatic charge stability and thus durable filtration performance [30, 38, 39]. The test results show that the multilayer PVDF electret filters are suitable for long-term storage and filtration use.

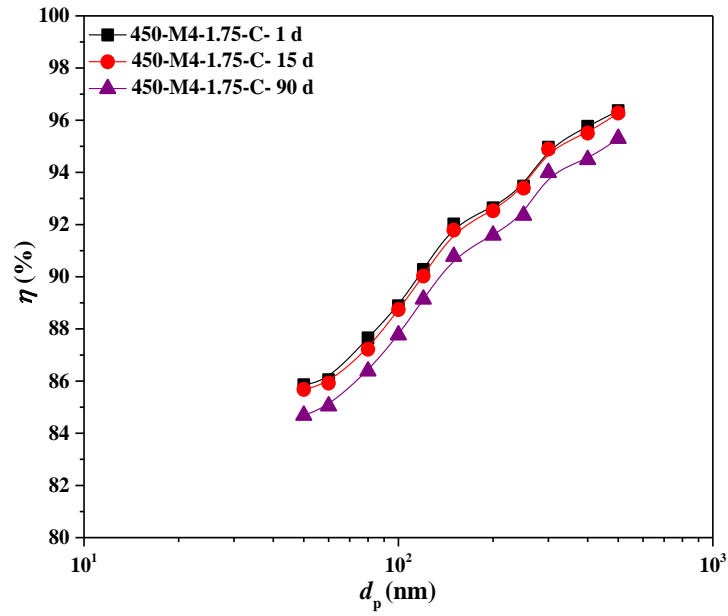


**Fig. 3.28.** Filtration efficiency of M4-1.75-C with storage time.

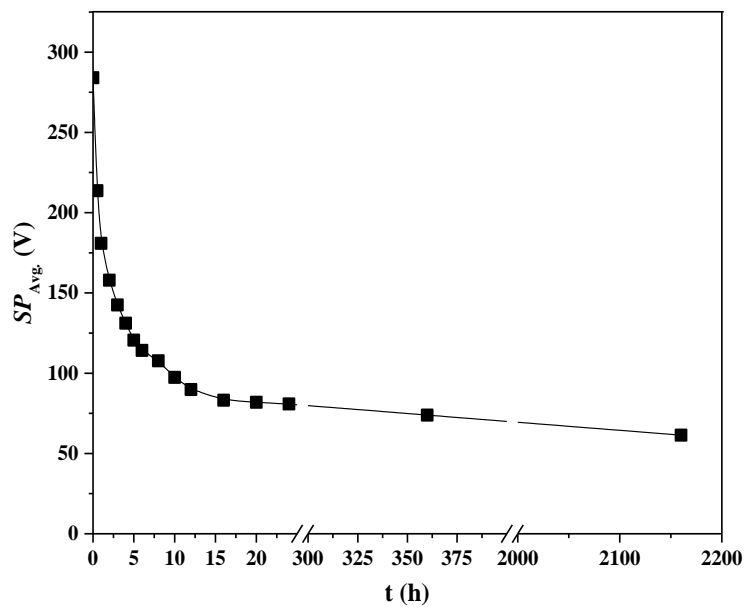


**Fig. 3.29.** Surface potential decay of S-1.75-C with time.

### 3.5. Summary

A novel approach based on the concept “multilayering” was applied for the first time to develop multilayer PVDF electret filters with high filtration efficiency and low

pressure drop. Also as a first, we have been successful in charging PVDF nanofibers using corona discharge. Several points were confirmed and summarized as follows:

1) High charging voltages and short charging distances favored high filtration efficiency due to high charge densities on filters and thus stronger electrostatic mechanism.

2) Purely introducing more fibers (i.e., higher filter basis weight) to filters could not significantly enhance their filtration performance as well as electric field within filters. Instead, by using the configuration of multiple layers with fewer fibers in each layer, augmented electrical attraction was reached due to reduction in electrical interference with lower air flow resistance benefitting from much lower fiber packing density, resulting in much better filtration property.

3) Using single fiber efficiency analysis, the capture enhancement above-and-beyond mechanical means (diffusion and interception) was confirmed to be due to dielectrophoretic filtration effect as the single fiber efficiency depends on the Cunningham slip factor and the square of the aerosol size raised to the power of 0.4.

4) By multilayering, the single fiber efficiency can be maintained at a high level which is important for the filter to harvest the benefit of dielectrophoretic filtration effect.

5) Larger aerosols benefit most as the dipole induced is larger and the subsequent capture is also greater.

6) Filter durability test proves the multilayer PVDF electret filters could maintain high performance for a long time and are promising for long-term storage and use for submicron and nono- aerosol removal.

## **Chapter 4: Performance Optimization of Multilayer PVDF**

### **Electret Filters**

#### **4.1. Overview**

The advantages of multilayer PVDF electret nanofiber filters in enhancing efficiency and reducing pressure drop for aerosol filtration have been confirmed in Chapter 3. By multilayering of charged fibers, the antagonist effect between overly adjacent fibers can be alleviated. Also, attributed to the higher porosity, charges on the fibers deep within the filter are more accessible to aerosols, resulting in more sufficient utilization of charges and a stronger electrostatic effect. Moreover, air resistance of each layer is low because of the low fiber packing density. In addition, for there is relatively large space between each two adjacent layers, aerosol flow from the upstream layer can be straightened to a steady state before entering the downstream layer, thus further reduce the air resistance brought by air turbulence [105].

To get the best filtration performance, it is essential to optimize the physical properties of filters. Extensive researches have been carried out to investigate the influences of varied parameters, e.g. filter thickness, filter porosity, fiber diameter and fiber orientation, on the filtration performance of mechanical filters [1, 7, 8, 11]. Yet, fewer studies were conducted on the optimization of electret filters, let alone the multilayer ones. The available work to improve the performance of electret filters mainly focused on increasing the charge density on filters, including applying higher electric field strength of charging process and incorporating dielectric particles into filters during filter fabrication [40, 41, 56, 58, 60, 92]. Although some improvement in filter performance could be obtained, certain drawbacks of these two methods limit

their application. For the former method, there oftentimes existed a threshold of field strength beyond which back corona or even electrical breakdown was initiated, leading to local discharge or generation of pinholes inside the filter [58, 66, 103]. For the latter method, the potential detachment of the weakly bonded particles from filters could be hazardous to human health [106]. Apart from the above two approaches, modified charging methods have also been adopted to facilitate electrostatic effects without adding to pressure drop. Two main techniques are suggested to be effective by increasing the surface potential of electret filters during corona discharge [27, 59, 60, 62, 66, 91, 92, 107, 108]. One is placing a metallic grid between two electrodes to get a higher charge density and a more even distribution. And the other is heating the filter up to the glass transition temperature of the fiber material during charging followed by a fast freezing, which can make the charges permanent in the fibers. However, these methods either has the risk of electrical breakdown, thus damaging filters and charging devices, or needs complicated apparatus to carry out charging processes, which makes the preparation of electret filters less feasible.

Given the availability and ease of electrospinning technique, adjustment of fiber size and filter basis weight seem to be more approachable means to optimize the electret filters. They were exclusively applied to improve the filtration efficiency of mechanical fibrous filters [11, 46, 47, 104]. Nonetheless, we believe that these approaches can also be utilized for the optimization of electret filters. For one thing, mechanical filtration effect plays an intrinsic role for all filters, regardless of mechanical or electret ones. More importantly, it has been confirmed in Chapter 3 that, for the 1-layer electret filters, the most benefit from electrostatic effect could be obtained by using an optimal basis weight to both ensure sufficient deposited charges and prevent electrical interference

[49, 105]. One problem of utilizing low fiber sizes or high filter basis weights is that high pressure drop can be caused as an adverse effect, despite the high filtration efficiency. However, this problem can be easily solved by multilayering through which air flow resistance can be alleviated, as widely proved in literature [46, 105, 109].

Based on the above discussion, adjustment of fiber size and filter basis weight were chosen as the method to optimize the multilayer PVDF electret filters. In Chapter 3, it has been shown that the quality factors of the multilayer electret filters decreased with layer number. Nonetheless, quality factors higher than  $0.1 \text{ Pa}^{-1}$  were still reached after stacking up several identical 1-layer electret filters and much improved filtration efficiency was obtained. Therefore, as long as the quality factors of module single layer are high enough with moderate filtration efficiency, excellent filtration performance of multilayer electret filters can also be assured.

The study in this chapter mainly concerns finding a fiber diameter and a layer basis weight for the best filtration performance. To exclude the interference from fiber morphology difference, filters consisting of straight fibers with varied diameters and without defects (beads or neuron-like structures) were firstly fabricated by adjusting PVDF solution properties and electrospinning conditions. Then, the filtration performance of 1-layer PVDF electret filters with varied fiber diameters and basis weights were tested, where the filter with the highest quality factors was chosen as the module layer to fabricate multilayer PVDF electret filters. Finally, the optimal filter with both high quality factors and filtration efficiency was determined from the multilayer PVDF electret filters.

To a less important extent, the influences of filter basis weight and fiber diameter on the filtration performance of 1-layer PVDF electret filters were investigated. Also,

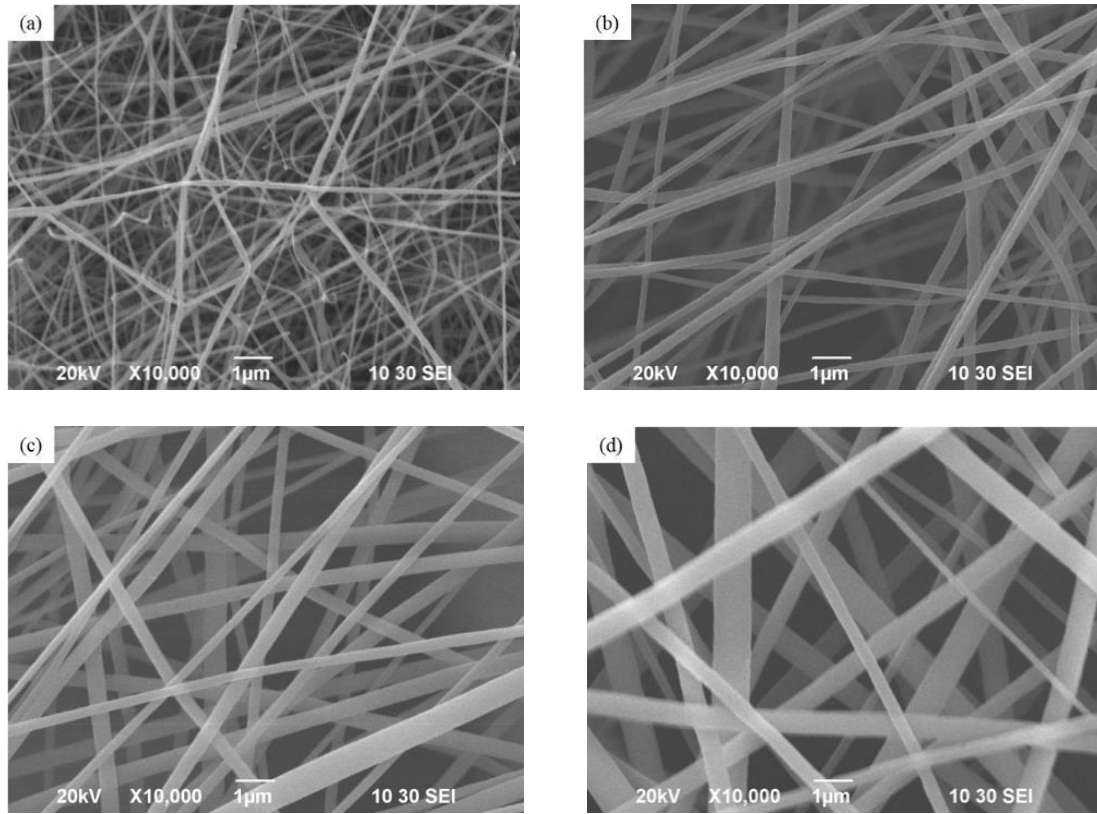
MPPS variations with charging state, layer number, filter basis weight and fiber diameter were reported and discussed.

## **4.2.Experimental**

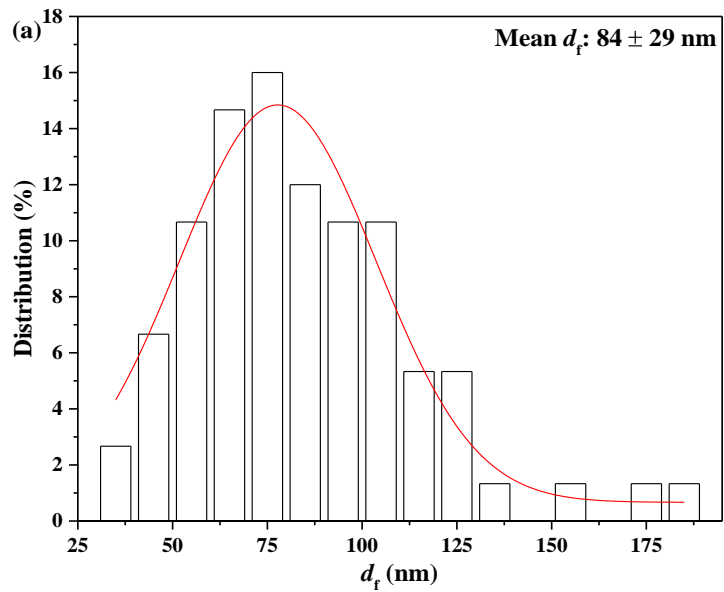
### **4.2.1. Fabrication of filters**

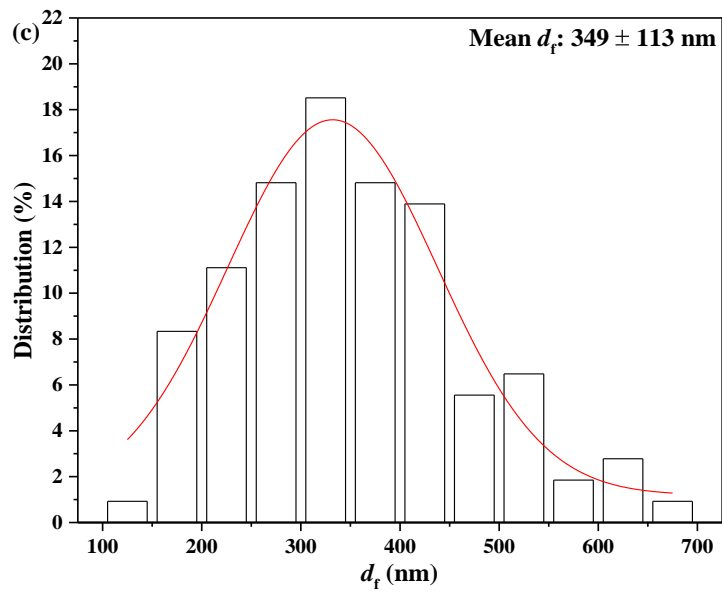
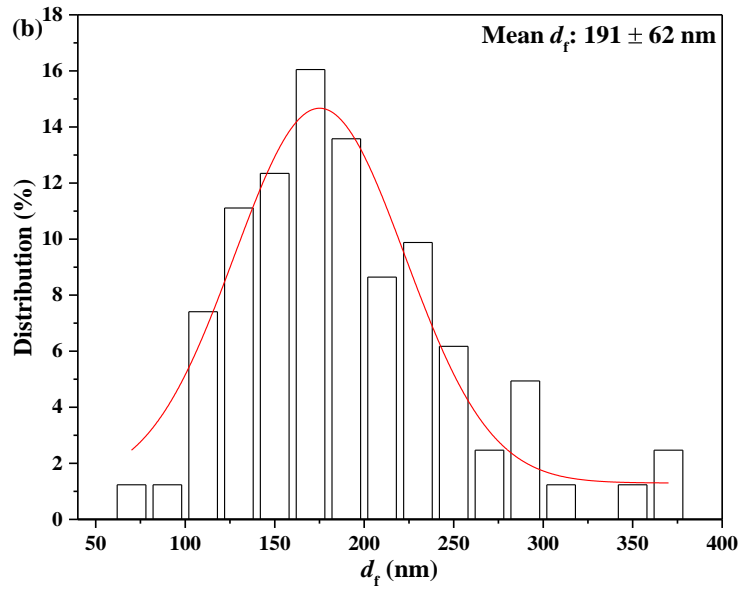
The general fabrication method of PVDF nano-fiber filters with varied fiber sizes was similar to that in last chapter [105]. To get different fiber diameters, PVDF solution properties and electrospinning conditions can be adjusted, including changing polymer molecular weight, solution concentration, solvent composition and additive agents for the former approach and spinning voltage and needle-to-collector distance for the latter one. Nevertheless, the influences of the various factors are often interrelated or overlapped so that they need to be finely tuned in certain ranges to get continuous, straight and defect-free fibers [78, 110]. With proper viscosity and conductivity of the solution, a jet can be continually initiated from the formed Taylor cone when the electrostatic force on the cone tip overcomes the surface tension. And then the jet is steadily stretched under the combined effects of the electrical force and sufficient polymer chain entanglements, during which solvent keeps evaporating before fibers randomly deposit on the collector wrapped by substrate (PP nonwoven cloth in this study). To avoid the formation of droplets or even electrospaying, the solution should be viscous enough by using a relatively high concentration or a polymer with a large molecular weight. Furthermore, to produce bead-free fibers, apart from the high solution concentration for a strong chain entanglement, solvent composition adjustment and additives (e.g. salts) should be applied to assure a high electrostatic force over low solution surface tension. However, solution concentration and electric field intensity should not be too high in case of generating lumps (e.g. the “neuron” structure in last

chapter), crooked fibers or fiber bundles due to the significant instability of jet [77, 78]. In order to meet the above requirements, several batches of parameter combination were used to determine the optimized conditions. Specifically, sodium chloride (NaCl) was chosen because of its much milder ionicity than lithium chloride (LiCl) which brought many branches and lumps [111]. Different volumes of NaCl solution diluted from a mother solution, instead of solid NaCl, were added to PVDF solutions to make sure the accuracy of salt dosages. During each batch of electrospinning, PP substrate was horizontally inverted at intervals to get more uniform fiber distribution. And because a portion of fibers were not collected on the substrate, fiber weight was closely monitored throughout the spinning process until the target value was reached. To facilitate the study on the influence of filter basis weight, the fiber amount barely covering the PP substrate surface was set to be the lower limit of the basis weight range. Based on charging state, the filters could be divided into uncharged and electret filters, with the former prepared by discharging the pristine filters using isopropanol, while the latter by charging the uncharged filters using corona discharge. The filters were named in the same way as that in last chapter. For instance, 525-M2-0.191-C denotes a 2-layer electret filter with the average diameter of 525 nm and the layer basis weight of 0.191 gsm, but the total basis weight for both 2 layers added up to 0.383 gsm. The SEM images and fiber diameter distributions of filters with different mean fiber diameters are shown in Fig. 4.1 and Fig. 4.2.



**Fig. 4.1.** SEM images of PVDF filters with mean sizes of (a) 84, (b) 191, (c) 349 and (d) 525 nm.





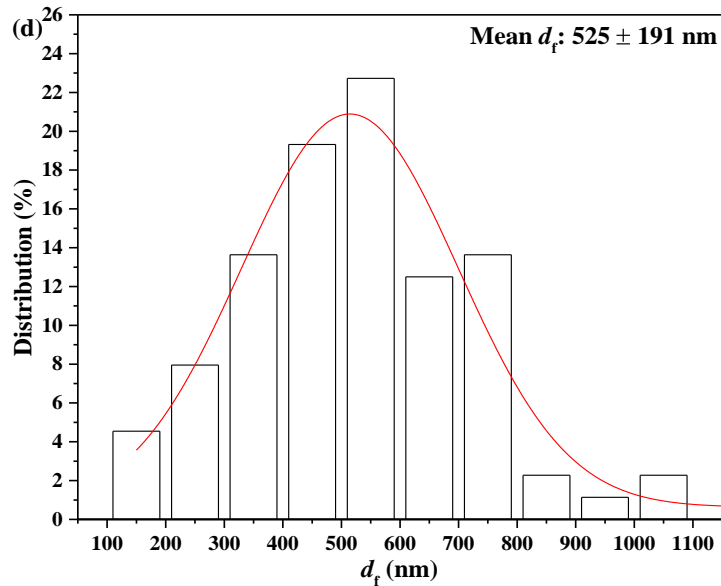


**Fig. 4.2.** Fiber size distribution of (a) 84-nm, (b) 191-nm, (c) 349-nm and (d) 525-nm PVDF filters.

#### 4.2.2. Filter performance evaluation

The same test method as that in Chapter 3 was adopted to determine filtration efficiency, pressure drop and quality factors of each filter [105]. Within the upper detection limit of CPC, concentration of each particle size was ensured to be sufficiently high to reduce errors of measurement. Specially, for filters charged by corona discharge, identical device setting (i.e. charging voltage, distance and time) and ambient condition (i.e. temperature and humidity) were applied. Afterwards, the electret filters were stored in a desiccator for a certain period to reach charge-steady state before further filtration tests.

### 4.3. Results and discussion

Based on the conclusion drawn in last chapter, for filters with a specific fiber size, it was expected the results would follow the same pattern where multilayer filters showed better filtration properties than corresponding 1-layer filters. Nevertheless, due

to the various parameters determining performance of filters, things might be complicated if more elements are considered. In this chapter, PVDF filters with varied fiber diameters, basis weights and charging states were tested for filtration performance and the results are shown in Figs. A1-A6 (Appendix 1). To make analysis clear, in most cases, only the data for aerosols of a specific size were selected to represent the filtration performance of filters. Here, 200 nm was chosen as the representative aerosol size because it was around the MPPS of the uncharged PVDF filters in this chapter.

#### **4.3.1. Influence of filter properties on filtration performance**

Fig. 4.3 depicts filtration efficiency and quality factors and Fig. 4.4 shows pressure drop of 1-layer PVDF filters used for performance optimization in this chapter. In general, for both the uncharged and electret filters, the filtration efficiency, as well as the pressure drop, increased with increasing basis weight and decreasing fiber diameter. As to quality factor, the value decreased with increasing basis weight except for both 525-S-U and 525-S-C groups and increased with increasing fiber diameter for S-C group, whereas no clear trend with fiber diameter can be observed for S-U group. The detailed influences of filter basis weight and fiber diameter are described below.

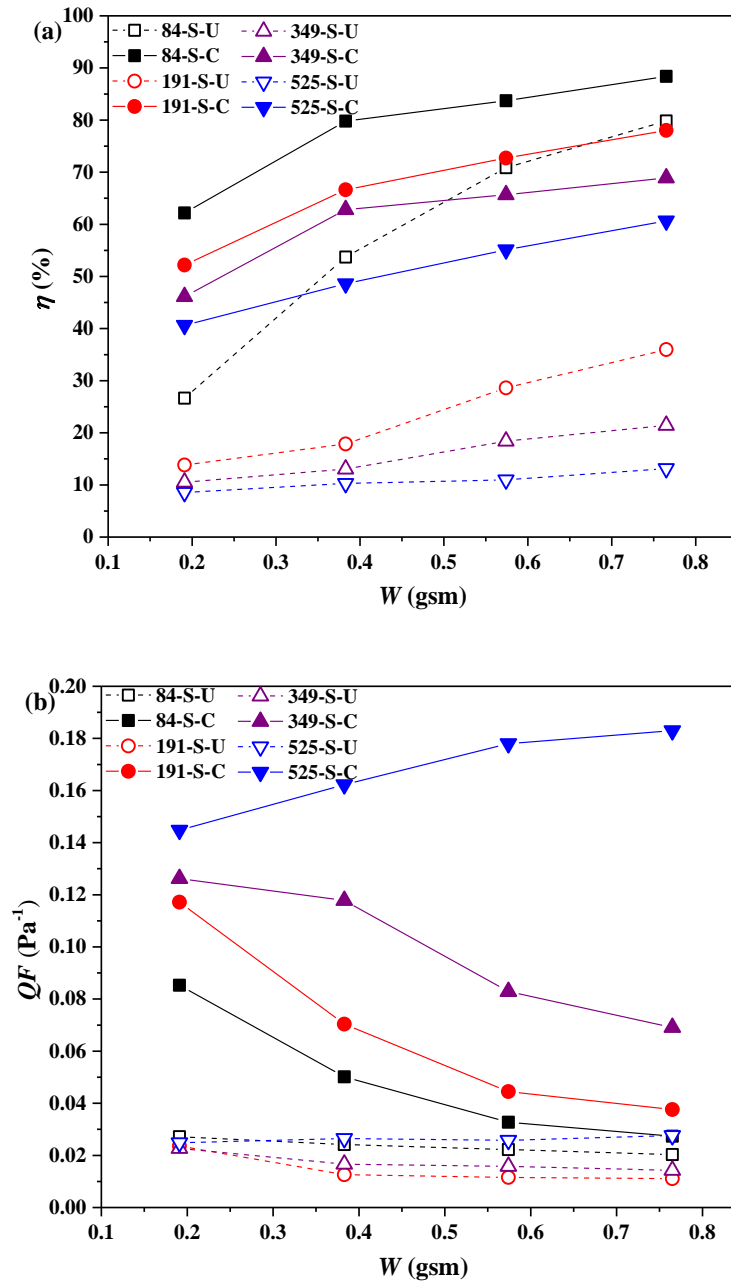


**Fig. 4.3.** (a) Filtration efficiency ( $\eta$ ) and (b) quality factors ( $QF$ ) of 1-layer PVDF filters with varied filter basis weights and fiber sizes for 200-nm aerosols. (Filters were in uncharged or charged state).

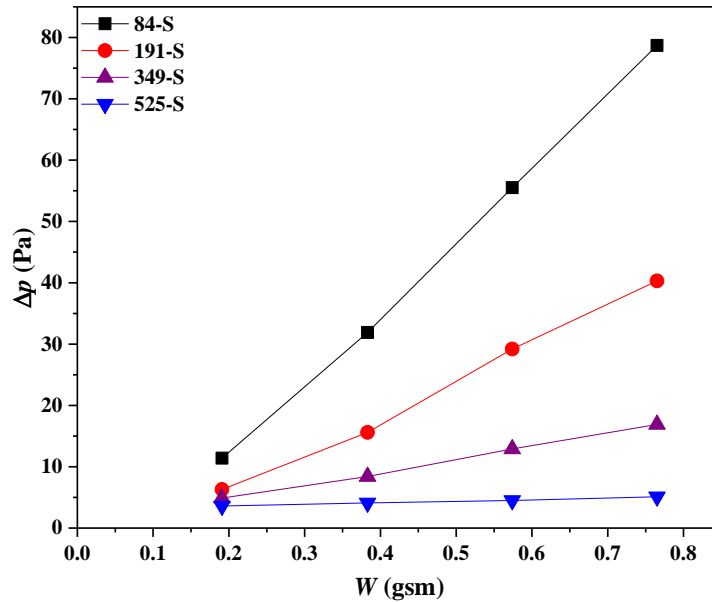


**Fig. 4.4.** Pressure drop ( $\Delta p$ ) of 1-layer PVDF filters with varied filter basis weights and fiber sizes. (Each filter had the same pressure drop in uncharged and charged states).

#### 4.3.1.1. Influence of filter basis weight

Given a specific fiber size, the amount of fiber is a main factor determining the filtration performance of a filter. By adding additional fibers to the filter, whether the filter porosity changes (for 1-layer filters) or not (for multilayer filters), the filtration efficiency and the pressure drop will accordingly increase, while the quality factor varies with different conditions [7].

In terms of filtration efficiency, for 1-layer filters with a certain fiber size in both uncharged and charged states, the values gradually increased with basis weight (Fig. 4.3a). This trend was more profound for the uncharged filters composed of thin fibers due to the more enhanced diffusion and interception effects [7, 45, 47]. For instance, with four times more fiber amount, the efficiency of 84-S-0.765-U for 250-nm particles reached 81.8% from 28.2% of 84-S-0.191-U, while there was only a minor increase of 4.6% for 525-S-0.765-U from 8.2% of 525-S-0.191-U. For the electret filters, the

insignificant improvement in filtration efficiency should result from the opposite influences of higher amount of charged fibers and interference among adjacent charges on electrostatic filtration effect [49].

As to quality factor, the values of all but 525-S groups decreased with filter basis weight (Fig. 4.3b), resulting from the different responses of pressure drop towards fiber amount (Fig. 4.4). With the same increase in basis weight, the pressure drop of filters with thinner fibers increased more rapidly than those with thicker fibers [7]. As an example, the pressure drop of 84-S-0.191-C was only 11.4 Pa, but the value drastically rose to 78.7 Pa of 84-S-0.765-C. Because of the relatively large diameter, 1-layer 525-nm filters had high porosities, so the pressure drop values were overwhelmingly low even for the one with the highest basis weight. With the same basis weights as 84-nm filters, 525-S-0.191-C and 525-S-0.765-C had pressure drops of only 3.6 Pa and 5.1 Pa respectively, indicating the increasing rate with fiber amount was exceedingly low. Thus, the increase in filtration efficiency was more significant than that in pressure drop for 525-S-C with higher filter basis weight, leading to increasing quality factor which was opposite to the others with smaller fiber diameters.

#### **4.3.1.2. Influence of fiber diameter**

Fiber size is an important parameter for a fibrous filter for aerosol capture, which affects filtration efficiency mainly through the mechanical filtration mechanisms of Brownian diffusion and interception. Also, it has a profound influence on the pressure drop of the filter. Combining the two effects leads to the variations in benefit-to-cost ratio, i.e. quality factor [7].

For the 1-layer filters with the same basis weight, the filtration efficiency (Fig. 4.3a) decreased with fiber diameter in both uncharged and charged states due to the

increasingly weakening effects of Brownian diffusion and interception [7, 45, 47]. Compared with the uncharged filters, the reduction in filtration efficiency of the electret filters was less prominent. For example, the efficiency of 525-S-0.574-U was 58.0% lower than that of 84-S-0.574-U, while the difference was 28.8% for the electret filter pair. This was owing to the much-enhanced electrostatic effect after charging the filters even with a large fiber diameter of 525 nm.

In respect of quality factor (Fig. 4.3b), things can be complicated as a result of the different responses of filtration efficiency and pressure drop to the change of fiber diameter. For the 1-layer uncharged filters with the same basis weight, the quality factor first decreased and then increased with fiber diameter. The initial decrease in quality factor was due to the more pronounced drop in filtration efficiency than pressure drop. For instance, the filtration efficiency decreased from 70.9% of 191-S-0.574-U to 28.6% of 84-S-0.574-U, while the pressure drop from 55.5 Pa to 29.2 Pa. With higher fiber diameters, however, the decrease in filtration efficiency was much less significant but the pressure drop kept high decreasing rates (for pressure drop is inversely proportional to the fiber diameter squared as shown in Davies' equation [1, 7]), thus leading to the higher quality factor with the higher fiber diameter. For the electret filters with the same basis weight, the filter with larger fibers had higher quality factor on account of the larger relative increment in filtration efficiency after charging and the much reduced pressure drop. As an example, after charging, the relative increase of efficiency of 84-S-0.574-C was only 14.4%, while that of 525-S-0.574-C was 259.5%. Meanwhile, 84-S-0.574-C had a pressure drop of 55.5 Pa, more than 12 times higher than that of 525-S-0.574-C (4.5 Pa).

#### **4.3.2. MPPS variations with filter basis weight and fiber size**

As stated before, several mechanisms, including mechanical filtration ones and electrostatic filtration ones, are involved in particle capture using an electret fibrous filter. Because each mechanism has its preference towards particles of a certain size range, there normally exists a most penetrating particle size (MPPS) during filtration. The physical properties of the filter are of great importance in determining its MPPS by affecting the contributory proportions of different filtration mechanisms [1, 7, 13]. Figs. 4.5a-b show the MPPS variations of uncharged and electret 1-layer PVDF filters with varied basis weights and fiber sizes, where the MPPS of the filters decreased after charging due to the more remarkable dielectrophoretic filtration effect on larger neutral particles [1, 7]. Nevertheless, when individually studying the uncharged or electret filters, all the MPPS values were not the same depending on filter basis weight and fiber diameter. The main reason for the variations was the different parts played by varied mechanical and electrostatic filtration effects [7]. In this section, the influences of filter basis weights and fiber sizes were briefly described and discussed. Note that the particle sizes in this study (50-500 nm) was relatively small so the negligible effect of inertia impaction in aerosol filtration was excluded.

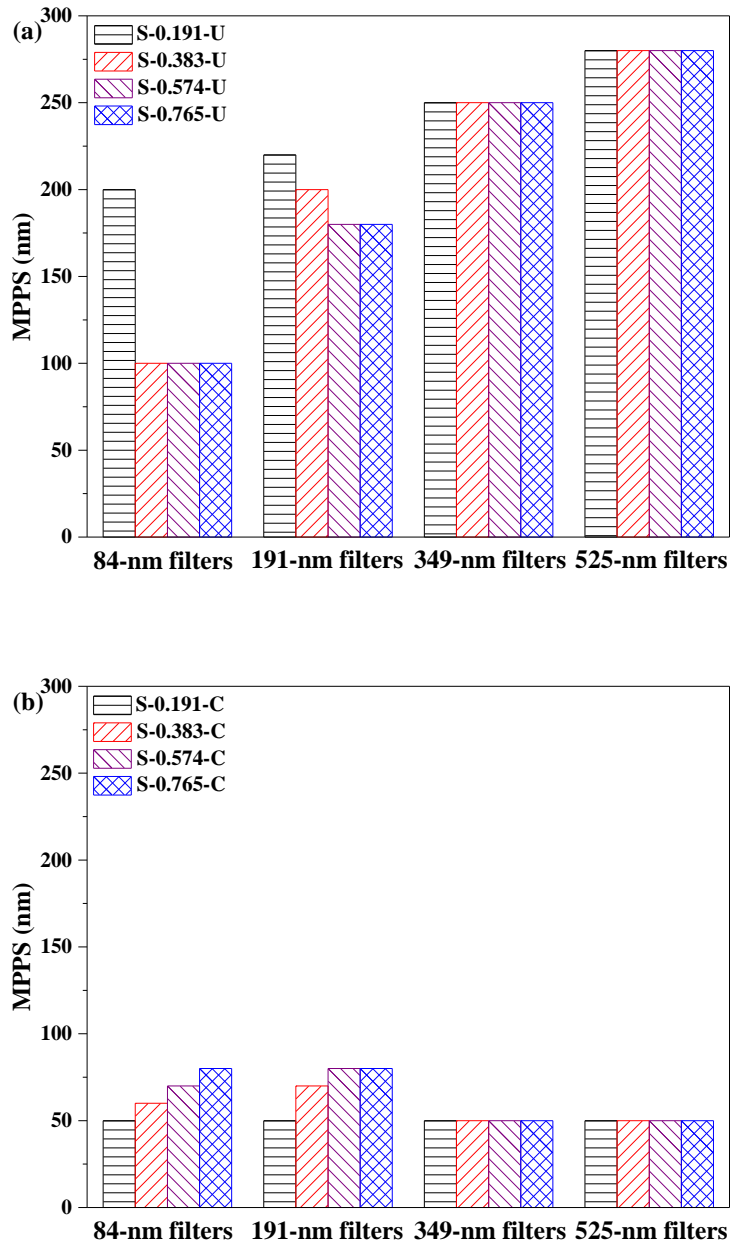


**Fig. 4.5.** MPPS of (a) uncharged and (b) electret 1-layer PVDF filters with varied filter basis weights and fiber sizes.

#### 4.3.2.1. MPPS variations with filter basis weight

For a filter, its basis weight mainly affects the MPPS through changes in porosity and interaction among charges [7].

For the uncharged 1-layer filters, as can be seen in Fig. 4.5a, the MPPS of 349-S-

U and 525-S-U groups remained unchanged with increasing filter basis weight at 250 nm and 280 nm, respectively. This was because the fiber packing densities of these filters did not vary much with the small range of basis weight and the large fibers [12]. With low fiber diameters, the MPPS of 191-S-U group decreased from 220 nm to 180 nm and that of 84-S-U group from 200 nm to 100 nm before reaching constant values with basis weight. For these two groups of uncharged filters, the fiber packing densities increased with more fibers, leading to both the improvements in Brownian diffusion and interception effects. The enhancement of interception effect was greater than that of Brownian diffusion effect with the initial increase of fiber amount and the two effects enhanced at similar paces afterwards, thus causing the above trend [45, 47].

For the electret filters (Fig. 4.5b), the MPPS were more determined by the relative strength of mechanical and electrostatic effects [81, 86]. The 349-S-C and the 525-S-C groups had the same MPPS of 50 nm because of the dominance of electrostatic mechanism in aerosol filtration. The two groups of filters with lower fiber diameters (191 and 84 nm) showed ascending trends of MPPS with basis weight due to the increasingly strong mechanical effect, as well as the diminishing electrostatic effect from the competition of charges on nearby fibers [7, 105].

#### **4.3.2.2. MPPS variations with fiber diameter**

For a filter with a certain basis weight, changes in fiber diameter alter the porosity and the fiber specific surface area, thus bringing variation of MPPS via affecting the roles played by mechanical and electrostatic effects.

For the uncharged filters, as shown in Fig. 4.5a, the MPPS of the 1-layer filters increased with fiber diameter. With the increasing fiber size, Brownian diffusion and interception effects both weakened [7]. The increasing MPPS with fiber diameter

should be caused by a more declining interception effect than the Brownian diffusion effect [45, 47].

For the electret filters, there was no definite trend of MPPS variation with fiber size (Fig. 4.5b). The 84-S-C and the 191-S-C groups with the lowest filter basis weight (0.191 gsm), the 349-S-C and the 525-S-C groups all had a MPPS of 50 nm, thanks to the major role of electrostatic effect in aerosol collection. At higher filter basis weights of 0.383 gsm and 0.574 gsm, both the MPPS of the 84-S-C and the 191-S-C groups increased due to higher proportions of mechanical effect. The 84-S-C group had slightly lower MPPS than the 191-S-C group, which was probably because the interceptional effect of the former ones was stronger due to the lower fiber diameter. At 0.765 gsm, 84-S-0.765-C and 191-S-0.765-C had the same MPPS of 80 nm, partly due to the weakened electrostatic effect of the former filter from stronger charge interference [49, 103, 105].

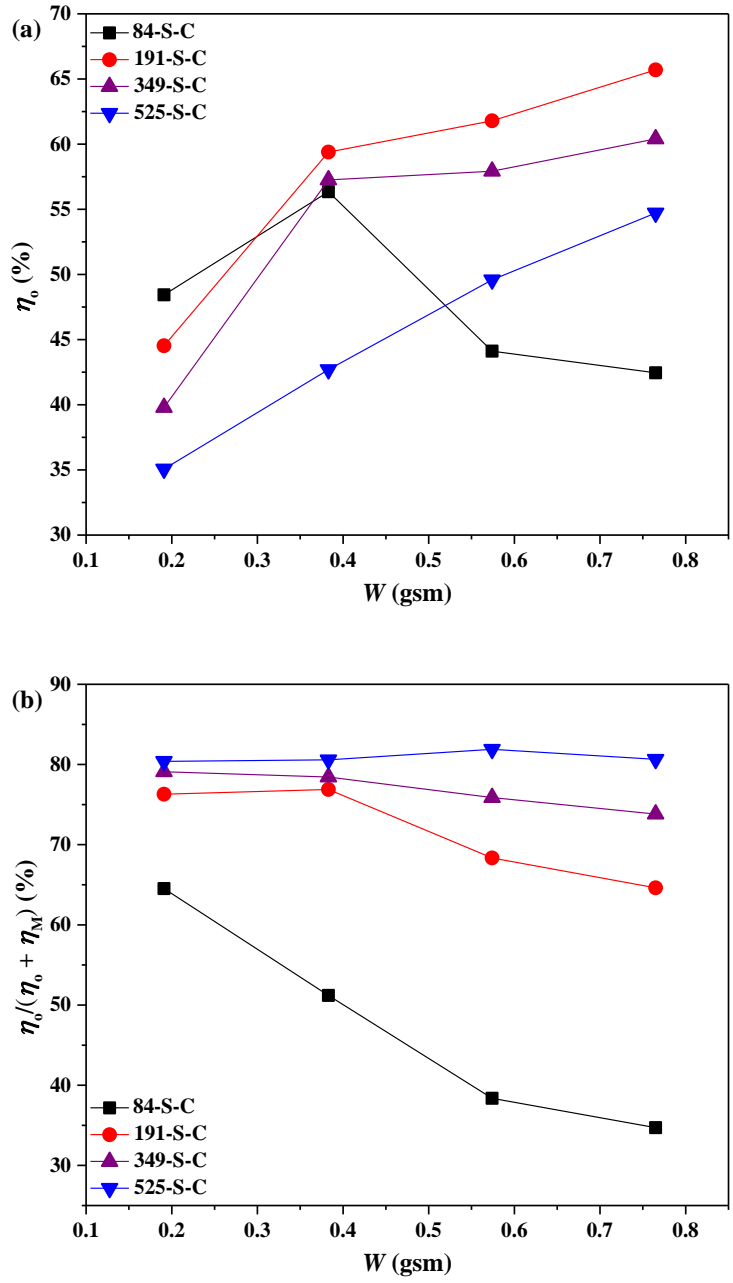
#### **4.3.3. Determination of optimized module single PVDF layer**

It has been shown in Section 4.3.1 that high filter basis weight and low fiber diameter facilitated high filtration efficiency, which however also caused low quality factor due to the high pressure drop. Since both mechanical and dielectrophoretic filtration effects played roles in aerosol filtration, what matters more for the improvement of filter quality factor is the extent of the latter effect which only promotes aerosol capture but does not incur additional air resistance.

The dielectrophoretic filtration efficiency ( $\eta_o$ ) of PVDF electret filters for 200-nm aerosols was calculated from Eq. 3.4 and the result is shown in Fig. 4.6a. Except for the 84-S-C group, all the other 1-layer electret filters had higher dielectrophoretic filtration efficiency with higher filter basis weight and lower fiber diameter. This could be

explained by the more deposited charges during corona charging due to the larger filter specific surface area. Though high amount of charges may also bring electrical interference, the enhancement of dielectrophoretic filtration effect from more charges was clearly more prominent. For the 84-S-C group, the decrease in dielectrophoretic filtration efficiency after the initial increase with filter basis weight was attributed to the increasingly stronger electrical interference among adjacent charges on the less and less porous filters [7, 49]. This was also consistent with the result of 1-layer 450-nm electret filters shown in Fig. 3.20 (Chapter 3), where high fiber amounts and low filter porosities were detrimental to dielectrophoretic filtration effect.

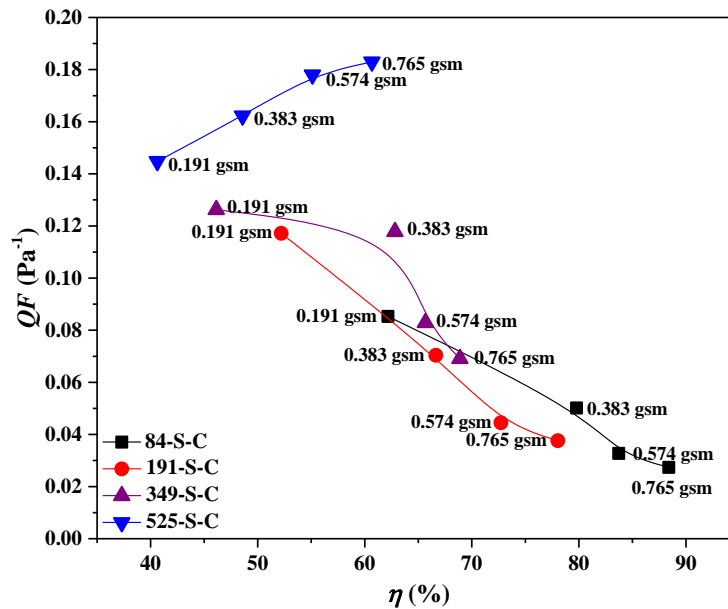
Increasing fiber amount or decreasing fiber diameter could not only affect dielectrophoretic but also increase mechanical filtration efficiency. A better way to show the extent of dielectrophoretic filtration effect is the ratio of dielectrophoretic filtration efficiency ( $\eta_o$ ) in the combined dielectrophoretic and mechanical filtration efficiency ( $\eta_o + \eta_M$ ), which is depicted in Fig. 4.6b for 200-nm aerosols. For most of the filters, the ratio decreases with filter basis weight due to the increasingly important mechanical filtration effect, especially for filters with thin fibers where mechanical efficiency was significant. The only exception is the 525-S-C group which keeps a relatively constant ratio around 80%. This means the dielectrophoretic and mechanical filtration effects of these filters improved at similar paces with filter basis weight and the 525-S-C group had better capability to sustain a substantial contribution of dielectrophoretic effect to aerosol filtration.



**Fig. 4.6.** (a) Dielectrophoretic filtration efficiency ( $\eta_0$ ) of PVDF electret filters with varied filter basis weights and fiber sizes for 200-nm aerosols; (b) Proportions of dielectrophoretic filtration efficiency ( $\eta_0$ ) in combined dielectrophoretic and mechanical filtration efficiency ( $\eta_0 + \eta_M$ ) for 200-nm aerosols.

The merits of the 525-S-C group compared to the filters with lower fiber diameters can also be seen in Fig. 4.7, which illustrates the filtration efficiency versus the quality

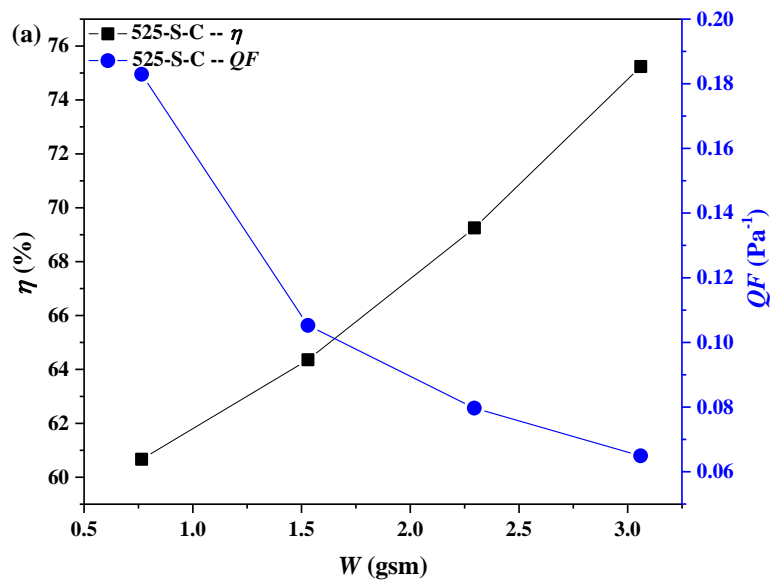
factors of 1-layer PVDF electret filters for 200-nm aerosols. The quality factors of 84-S-C, 191-S-C and 349-S-C groups all remarkably decreased with their corresponding higher filtration efficiency in accordance to the larger fiber amount. On the contrary, both the quality factor and the filtration efficiency of the 525-S-C group improved with increasing filter basis weight, and the highest quality factor of 0.183 Pa<sup>-1</sup> was achieved for 525-S-0.765-C.



**Fig. 4.7.** Filtration efficiency ( $\eta$ ) versus quality factors ( $QF$ ) of 1-layer PVDF electret filters with varied filter basis weights and fiber sizes for 200-nm aerosols.

From the above analysis, it was concluded the filters in the 525-S-C group were eligible to be the module layer for the multilayer electret filters. Nonetheless, as shown in Fig. 4.7, the question remained whether further adding more fibers could lead to higher quality factor for 525-S-C filters. To solve this question, 525-S-C filters with higher basis weights were fabricated and tested for filtration performance. As shown in Fig. 4.8a, the increase in filtration efficiency was insignificant with the increasing fiber amount, where only 14.5% of increment was achieved from 0.765 to 3.06 gsm. This

disproportionate increase was due to the increasing electrical interference among charges of higher densities [49]. Meanwhile, with the filter basis weight increasing to 3.06 gm, the pressure drop of 525-S-3.060-C rapidly rose to 21.5 Pa, 4.2 times higher than that of 525-S-0.765-C (Fig. 4.8b). As a result of the unremarkable efficiency improvement and the notable pressure drop increase, the quality factor of 525-S-C filters evidently decreased with filter basis weight (Fig. 4.8a). It is worth mentioning that if the applied range of filter basis weight started at a much lower value, instead of 0.191 gm, there could probably also be an initial increasing trend in the  $QF$  vs  $\eta$  figure for each of the three filters with larger diameters due to the potential much lower pressure drop. This means filters with thinner fibers can also be applied as the module layer, as long as a proper fiber amount is found. Nevertheless, for the convenience of spinning, 0.191 gm was set as the lowest single-layer filter basis weight.



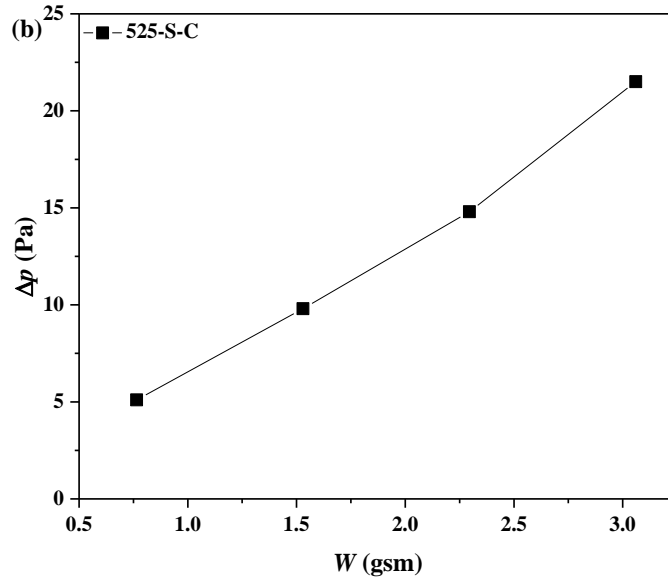


**Fig. 4.8.** (a) Filtration efficiency ( $\eta$ ) and quality factors ( $QF$ ) for 200-nm aerosols and (b) pressure drop ( $\Delta p$ ) of 1-layer 525-nm PVDF electret filters with the lowest filter basis weight being 0.765 gsm.

Combining with the filters with basis weights of 0.191, 0.383 and 0.574 gsm, Fig. 4.9 depicts the filtration efficiency versus the quality factors of 1-layer 525-nm PVDF electret filters for 200-nm aerosols. It is shown that 525-S-0.765-C had the highest quality factor, thus it was chosen as the module layer for fabricating multilayer electret filters. Although the filtration efficiency of 525-S-0.765-C was only 60.7%, the efficiency was hopeful to reach a high level while keeping decent quality factors if stacking up several identical filters.

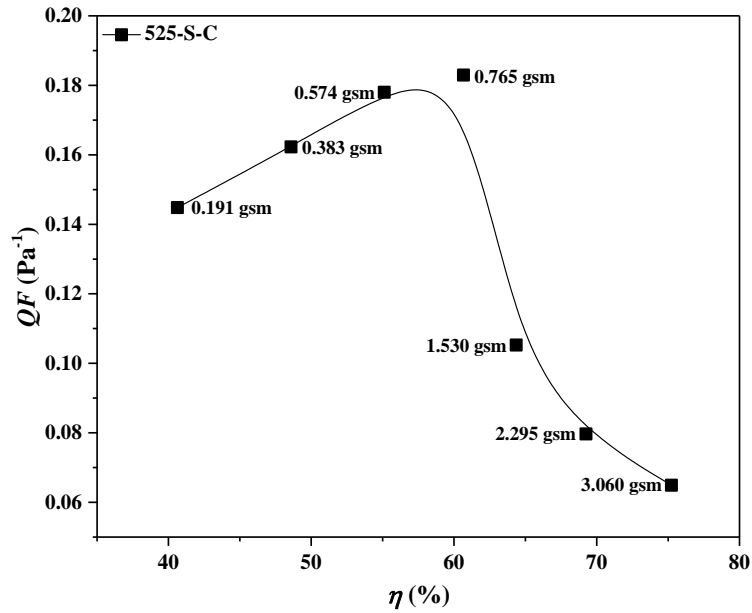
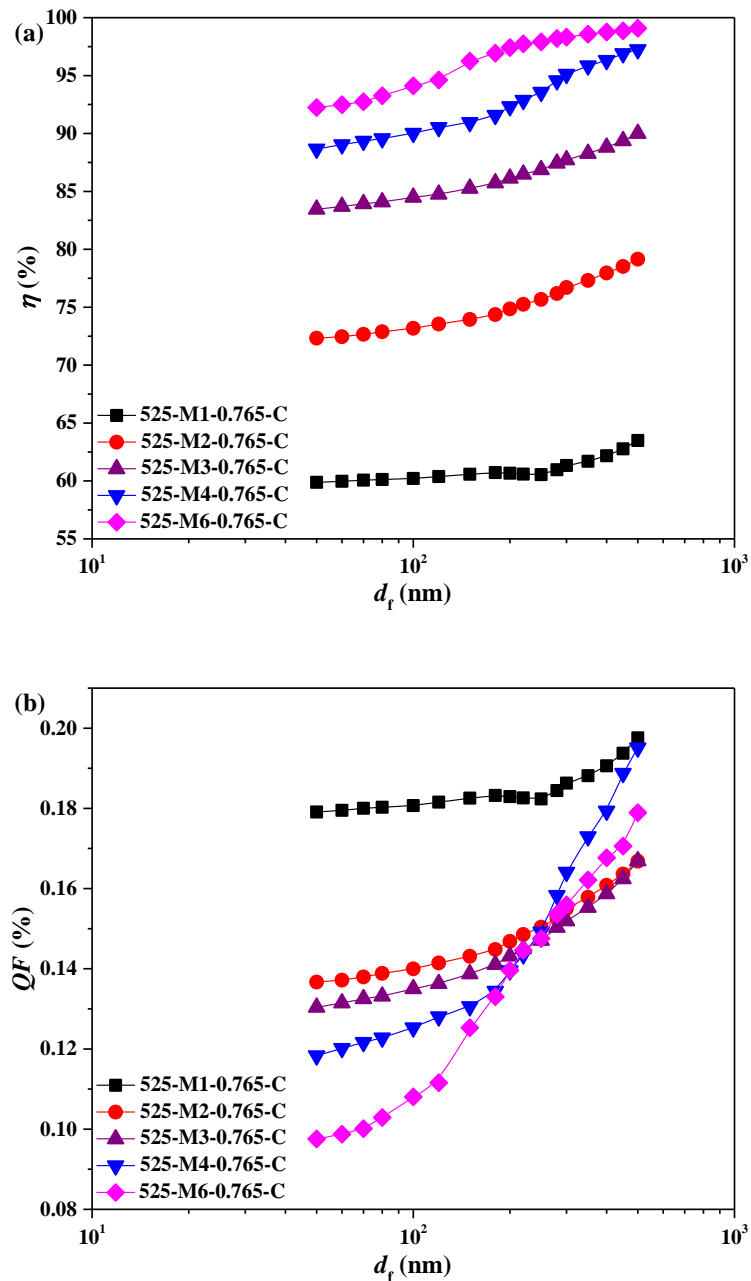


**Fig. 4.9.** Filtration efficiency ( $\eta$ ) versus quality factors ( $QF$ ) of 1-layer 525-nm PVDF electret filters with varied filter basis weights for 200-nm aerosols.

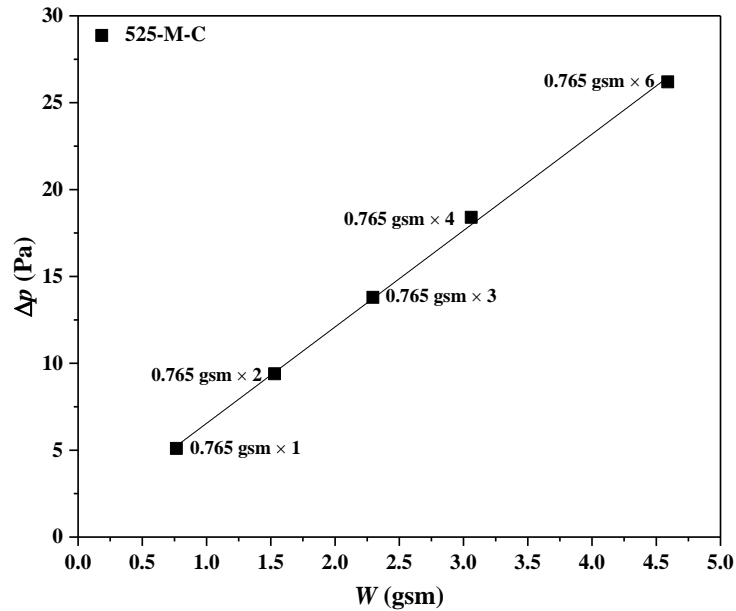
#### 4.3.4. Filtration performance of multilayer electret PVDF filters composed of optimized single layers

Based on the result in Section 4.3.3, multilayer electret filters taking 525-S-0.765-C as the module layer were prepared and tested for filtration performance as shown in Fig. 4.10 and Fig. 4.11. Conforming to the previous tests, the filtration efficiency was greatly improved by stacking up several electret layers (Fig. 4.10a). For 525-M6-0.765-C, the removal efficiency for 300-nm NaCl aerosols reached 98.3%, while its air resistance was only 26.2 Pa as shown in Fig. 4.11. The low pressure drop resulted from the relatively thick fibers which made the filter remain intensely porous and the air resistance rise mildly with fiber amount. As to quality factor (Fig. 4.10b), though for aerosols of 50-180 nm the values decreased with layer number, high values from 0.098 Pa<sup>-1</sup> to 0.133 Pa<sup>-1</sup> were still obtained by 525-M6-0.765-C and the values (0.154-0.179) were the second highest for 280-500-nm aerosols among the multilayer filters.

Moreover, the low pressure drop of 525-M6-0.765-C (Fig. 4.11) means that there is room for further improvement in filtration efficiency while maintaining acceptable air resistance.

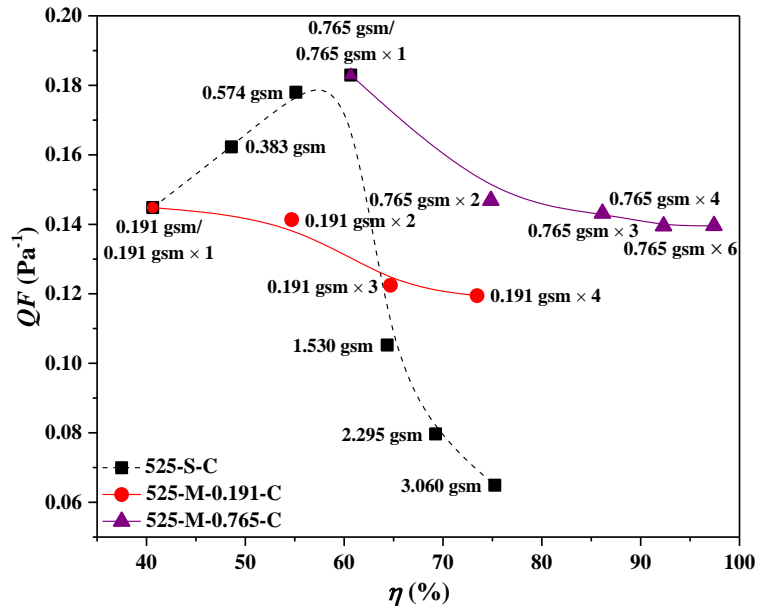


**Fig. 4.10.** (a) Filtration efficiency ( $\eta$ ) and (b) quality factors ( $QF$ ) of multilayer 525-nm PVDF electret filters with the layer basis weight being 0.765 gsm.



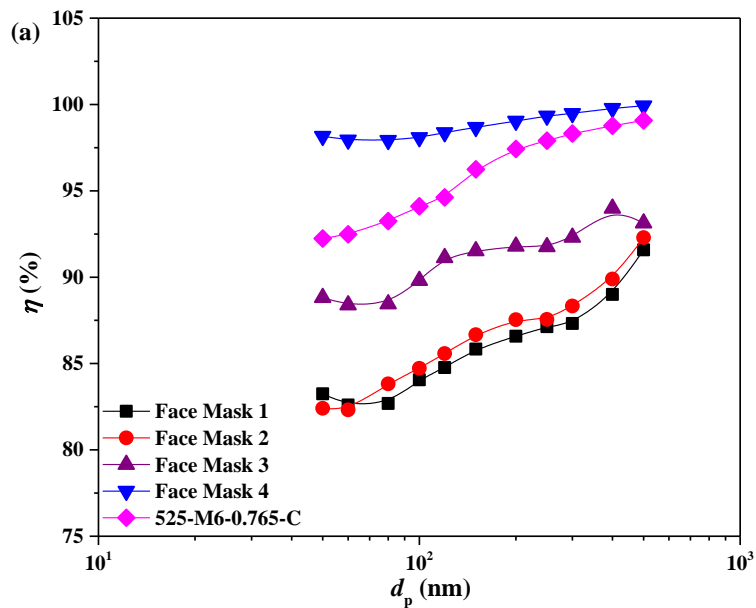
**Fig. 4.11.** Pressure drop ( $\Delta p$ ) of multilayer 525-nm electret filters with the layer basis weight being 0.765 gsm.

The filtration efficiency versus quality factors for 200-nm aerosols of 525-S-C, 525-M-0.191-C and 525-M-0.765-C groups with varied filter basis weights is compared in Fig. 4.12. Each filter in the 525-M-0.765-C group showed far better filtration properties, both in filtration efficiency and quality factor, compared to those in the 525-S-C group with the same basis weight. Though the quality factor of 525-M-0.765-C also decreased with the increasing fiber amount, multilayering prominently mitigated the decrease rate of quality factor per filtration efficiency. In addition, by comparing 525-M-0.191-C and 525-M-0.765-C groups, it is shown that the quality factors of the filters in the latter group were higher than those in the former one, which indicates that a proper amount of fibers in each layer of a multilayer electret filter is of great importance for optimizing the filtration performance.



**Fig. 4.12.** Comparison of filtration efficiency ( $\eta$ ) versus quality factors ( $QF$ ) for 200-nm aerosols between 525-S-C, 525-M-0.191-C and 525-M-0.765-C with varied filter basis weights.

#### 4.3.5. Comparison of filtration performance of optimized multilayer PVDF electret filter with commercial face masks



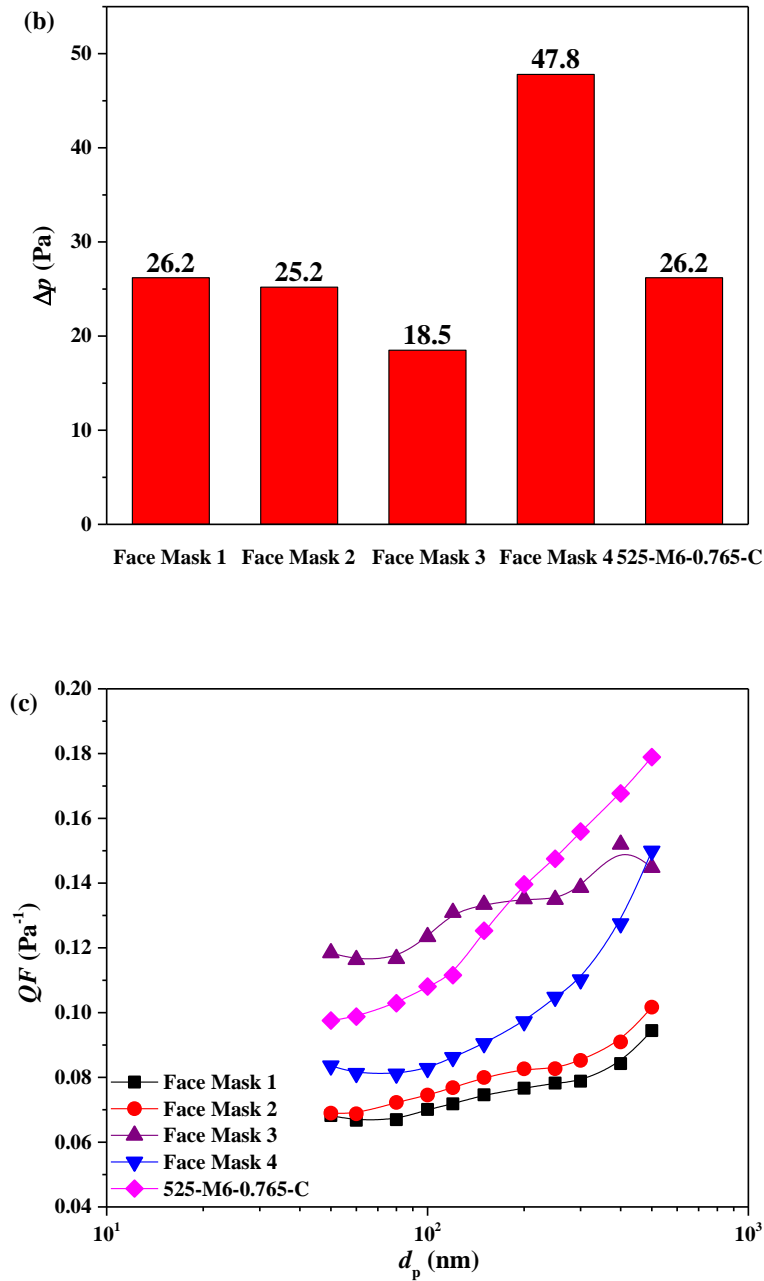


**Fig. 4.13.** Comparisons of (a) filtration efficiency ( $\eta$ ), (b) pressure drop ( $\Delta p$ ) and (c) quality factors ( $QF$ ) between 450-M8-0.87-C and commercial face masks.

To further validate the commercialization potential of multilayer PVDF electret filters, the filtration performance of 525-M6-0.765-C was compared with that of several commercial face masks. These face masks were all made of electret fibrous materials and widely available on the market in Hong Kong. The identical test method to that of

525-M6-0.765-C was used for the face masks and the results were shown in Figs. 4.13a-c.

As can be seen in Fig. 4.13a, similar to 525-M6-0.765-C, all the four face masks generally show increasing filtration efficiency with increasing particle size, indicating that dielectrophoretic effect played a major role in aerosol capture for these commercial masks. Face Mask 1 and Face Mask 2 had comparable pressure drop (26.2 and 25.2 Pa, respectively) to 525-M6-0.765-C (26.2 Pa) as shown in Fig. 4.13b, which is fairly good in terms of breathing resistance. However, the filtration efficiency was in the range of 82.3-92.3% which was about 9.7% lower than that of 525-M6-0.765-C for each particle size. As a result, the quality factors of these two face masks were not sufficiently high (Fig. 4.13c), with 0.067-0.094 Pa<sup>-1</sup> for Face Mask 1 and 0.069-0.102 Pa<sup>-1</sup> for Face Mask 2. Face Mask 3 had the lowest pressure drop of 18.5 Pa among the four commercial masks and captured more aerosols than Face Mask 1 and Face Mask 2 (Fig. 4.13b), therefore performing much better in quality factors (Fig. 4.13c). For particles smaller than 200 nm, Face Mask 3 had higher quality factors than 525-M6-0.765-C (Fig. 4.13c). Yet, the capture efficiency of 525-M6-0.765-C was higher than that of Face Mask 3, especially for larger particles (Fig. 4.13a). This contributed to the much higher quality factors of 525-M6-0.765-C than Face Mask 3 for particles larger than 200 nm. Considering only efficiency, Face Mask 4 had the best performance in aerosol removal, filtering out 97.9-99.9% of particles ranging from 50 to 500 nm (Fig. 4.13a). Nevertheless, as depicted in Fig. 4.13b, the air resistance of Face Mask 4 (47.8 Pa) was nearly double that of 525-M6-0.765-C, making it less desirable in view of breathing convenience. The high pressure drop of Face Mask 4 also led to much lower quality factors, i.e. benefit-to-cost ratios, than that of 525-M6-0.765-C (Fig. 4.13c).

Overall, by comparing the filtration performance of 525-M6-0.765-C with that of the commercial face masks, the merits of multilayer PVDF electret filters were shown in both high filtration efficiency and low breathing resistance. Although the capture efficiency was not as good as Face Mask 4, multilayer PVDF electret filters have a high potential to perform better after adjusting filter physical and charging parameters.

#### **4.4. Summary**

Multilayer PVDF electret filters were optimized through the approach of modifying the module single layer. And the outstanding filtration performance of the resultant filter was verified via both lab tests and field tests. Besides, it was concluded that the physical properties of filters, including basis weight and fiber diameter, were of great importance in optimizing multilayer PVDF electret filters. The conclusions drawn from the study were listed as follows:

1) Higher filter basis weights and lower fiber diameters favored higher filtration efficiency of the 1-layer PVDF electret filters. However, the quality factors of the filters responded differently to filter basis weight and fiber diameter, which was affected by the variation in the contribution of mechanical filtration effect. With increasing filter basis weight, the values of all filters except for 525-nm filters decreased resulting from the rapidly increasing pressure drop. The quality factor of 525-nm filters increased with filter basis weight because of the low increasing rates of pressure drop caused by the relatively large fiber diameter. With increasing fiber diameter, the filters had higher quality factor on account of the larger relative increment in filtration efficiency after charging and the much reduced pressure drop.

2) The MPPS of the 1-layer PVDF filters all decreased after charging due to the more remarkable dielectrophoretic filtration effect on larger neutral particles.

Nevertheless, the MPPS of individual filters varied according to their filter basis weight and fiber diameter based on the relative importance of mechanical and electrostatic filtration effects.

3) High dielectrophoretic filtration efficiency did not guarantee high filtration performance of the 1-layer PVDF electret filters. The contribution of dielectrophoretic filtration effect compared to that of mechanical filtration effect was found to be the key factor for filter performance improvement. Therefore, a proper filter basis weight was needed to not only ensure enough electrostatic effect but also to avoid excessive mechanical effect.

4) The filter 525-S-0.765-C with the highest quality factor was chosen as the module layer to compose multilayer PVDF electret filters. The optimized filter 525-M6-0.765-C showed both high filtration efficiency and quality factors (98.3% and  $0.156 \text{ Pa}^{-1}$  for 300-nm NaCl aerosols). Moreover, the pressure drop of 525-M6-0.765-C was only 26.2 Pa, showing the high potential for further improvement in filtration performance.

5) Performance comparison with commercial face masks indicates that multilayer PVDF electret filters have a high potential for application of personal health protection.

## **Chapter 5: Filtration Performance of Multilayer PVDF**

### **Electret Filters in Real Aerosol-Laden Environment**

#### **5.1. Overview**

The advantages of electret multilayer filters, i.e., redistributing charged fibers from a densely packed 1-layer filter to a filter with multiple layers, have been verified from both the improved filtration efficiency and the reduced pressure drop in our laboratory experiments. Yet, it is the effectiveness of the filters in real applications that is of greater importance considering their potential use for personal health care and environmental protection. In most of the research on nano-aerosol filtration, experiments were carried out in labs, where aerosols with a single component, e.g. sodium chloride (NaCl), Dioctyl Phthalate (DOP) or test dust, was generated and applied. Besides, to abide by test standards, oftentimes only monodisperse aerosols were used to challenge filters. Also, to simplify test procedures and avoid difficulties for data analysis, aerosols were always pre-treated to reach a specific charge state, i.e. discharged, single charged or neutralized (Boltzmann distribution) [13, 112, 113]. In our lab tests, neutralized monodisperse NaCl nano-aerosols were used to conduct the filtration experiments. Although the aerosol concentrations used in this study, like many other researches, presented an extremely harsh condition and far exceeded the concentrations in real environments, the test results were too preliminary to directly equate with filter performance in real applications due to the complex nature of environmental nano-aerosols. Airborne nano-aerosols consist of varied components, including inorganic and organic matters and exist in solid or liquid forms. Different from our standardized tests using dry NaCl aerosol flow, the oily particles and moisture in the air to some extent

may degrade filters and impair their filtration performance, especially for electret filters. Furthermore, airborne nanoparticles with a wide range of sizes co-exists and may interact with each other during filter tests. To make things more complicated, nanoparticles normally do not have a stable pattern of charge distribution, thus the performance of a same filter may vary from case to case. Also note that atmospheric aerosols have various and usually irregular shapes from different sources and transformation routes, which differs from the lab-generated ones [1, 2]. All the particularities of airborne nano-aerosols mentioned above render filter tests under real environments necessary. One major source of airborne nano-aerosols is road transportation, where aerosols, nitrogen oxides (NO<sub>x</sub>) and volatile organic compound (VOC) are emitted from fossil fuel combustion in vehicles and transform in the atmosphere [1, 2]. Given the importance and availability of vehicles, traffic environment seems an ideal condition for filter tests. Several researchers used the exhaust from a gasoline car for testing the performance of their filters [99, 114]. Nevertheless, it was still quite different from the real traffic environment. Moreover, in their work the filters used were comprised of fibers with micro-sizes with a high basis weight.

To the best of our knowledge, little work has been done on filtration using nanofiber filters for aerosol removal in real conditions. In the study of this chapter, a test site was carefully selected in order to have a stable aerosol source so that reliable filtration results could be obtained. The site is located near a road with busy traffic where there is a relatively constant concentration of aerosols generated from passing vehicles using different kinds of fuels. A portable filter test system was specially developed to conduct the real-time measurements instead of the sophisticated but bulky

SMAG system used in the lab tests [115]. The multilayer PVDF electret filters were tested in the real traffic environment for filtration performance to investigate whether they could still retain the merits shown in the last two chapters, i.e. having high aerosol capture efficiency while keeping low air resistance.

## **5.2.Experimental**

### **5.2.1. Fabrication of filters**

To have a fair comparison of filter performance between tests using lab- and traffic-generated aerosols, filters, including four 1-layer and four multilayer filters with similar structures to the optimized ones used in the last chapter from the same spinning batch, were adopted in the field tests. Fibers in each filter had a mean diameter of 525 nm measured from 100 fibers in SEM images. The four 1-layer filters had basis weights of 0.765, 1.530, 2.295 and 3.060 gsm, respectively. Different numbers of the 1-layer filters of 0.765 gsm were stacked up to form the four multilayer filters, with basis weights of  $0.765 \times 2$ ,  $0.765 \times 3$ ,  $0.765 \times 4$  and  $0.765 \times 6$  gsm. All the filters were first discharged and tested for their mechanical filtration efficiency, and then were charged to investigate the improvement in filter performance. Each filter is denoted by its fiber diameter, layer number, layer basis weight and charging state. For instance, 525-S-1.530-C represents a 1-layer 525-nm electret filter with the basis weight of 1.530 gsm, while 525-M4-0.765-U means an uncharged 4-layer 525-nm filter with the basis weight of 0.765 gsm for each layer, but the total basis weight for all 4 layers added up to 3.060 gsm.

### **5.2.2. Description of micro-environment for field tests**

The experimental site was located by a heavy traffic road which connects to the entrance of the Hung Hom Cross-Harbor tunnel about 220 m away. Vehicles powered

by varied fossil fuels, including liquid petroleum gas, gasoline and diesel, continuously passed by the site and the driveway was frequently obstructed because of traffic light or traffic jam. Therefore, particulate matters, which were directly exhausted from the vehicles or formed from interactions between different vehicular pollutants, were significantly present in the surrounding air. To some extent, the generated nano-aerosols were trapped by buildings along the road due to the “Street canyon effect”, which formed a micro-environment and provided a constant aerosol source [1, 2, 116]. To avoid the turbulent airflow caused by the passing vehicles, the sampling site was intentionally chosen to be 30 m away from the main road, where the airflow was relatively steady and aerosol size distribution was less affected. The credibility of sampled data was further assured by conducting the tests during rush hour on sunny and windless days when there were relatively high and stable aerosol concentrations.

### **5.2.3. Filtration performance evaluation of filters**

Filter tests were carried out using the homemade portable filter test system (PFTS), as shown in Fig. 5.1. The pressure drop values ( $\Delta p$ ) of filters were measured beforehand by the SMAG system. The PFTS mainly consists of two identical holders, a vacuum pump and a Portable Aerosol Mobility Spectrometer (PAMS). Each holder was made up by two stainless steel cones and the two holders were parallelly installed. Ambient air was sucked into the system by the vacuum pump. A three-way valve was installed downstream of the two holders to control the flow to only pass through either one of them. The flow rate through the holder in use was measured by a flow meter (Model 4100, TSI, USA) and controlled precisely to the required value by a needle valve right before the vacuum pump. A small amount of aerosol flow was introduced into the PAMS where large particles were removed by a cyclone at the inlet of the PAMS and

the aerosol size distribution with the size range of 10-433.7 nm (count median diameter (CMD)) was obtained under “Scan Mode”. For a typical run, the three-way valve was first set to link to the “blank holder” side where no filters were installed to acquire the aerosol size distribution of the ambient air by the PMAS. This set of data was taken as the aerosol concentrations upstream of the tested filter. Subsequently, by adjusting the three-way valve, the air flow was switched into the “filter holder” side where a filter was mounted and the size spectrum of aerosols downstream of the filter was obtained. Note that before the switch, the air flow rate through the “filter holder” side was adjusted to the same value with that of the “blank holder” side in compensation for the pressure drop across the filter. For every filter, the test was repeated and the average values for the upstream ( $c_{up}$ ) and the downstream ( $c_{down}$ ) aerosol concentrations were obtained, respectively. From the measurements above, the filtration efficiency ( $\eta$ ) and quality factor ( $QF$ ) of the filter for aerosols with any known sizes were calculated by Eq. 3.2 and Eq. 3.3.

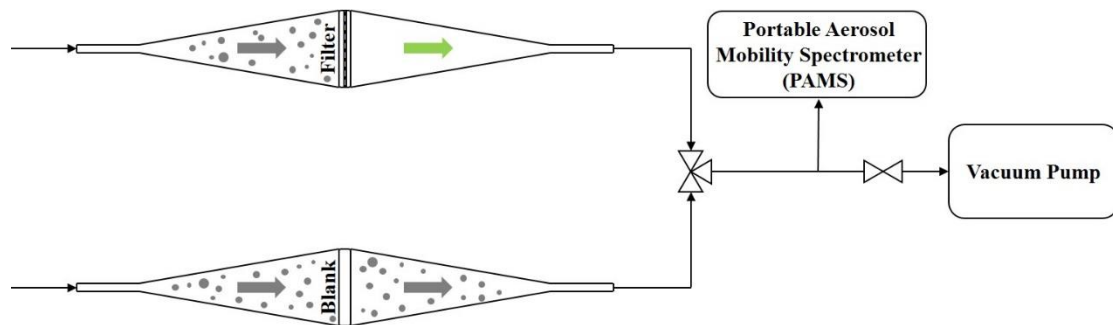


**Fig. 5.1.** Schematic diagram of set-up for aerosol filtration field tests of filters.

### 5.3. Results and discussions

For filter tests using real aerosols, it is important to maintain a steady aerosol feed to get convincing conclusions. In this study, the aerosol size distribution at the experimental site was log-normal and the most frequent aerosol size was centered

around 95 nm with a variation of approximately  $\pm 17$  nm, which conformed to the results in the literature [115]. The aerosol concentrations peaked at  $77.23 \pm 9.54 \text{ cm}^{-3}$  which was apparently much lower than the values adopted in lab experiments. A typical air aerosol concentration variation with size is shown in Fig. 5.2, with a peak value of  $85.86 \text{ cm}^{-3}$  at  $83.81 \text{ nm}$  and about 80% of the total particle concentration within the range of 30-200 nm.

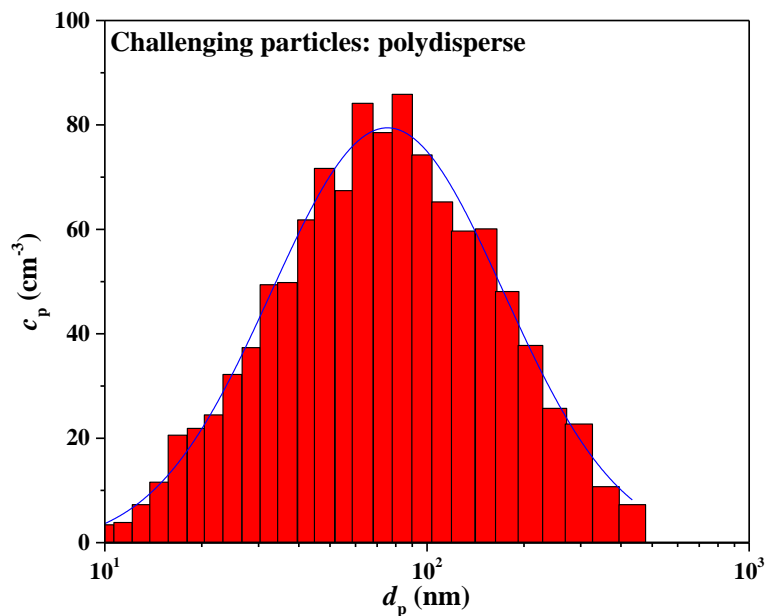


**Fig. 5.2.** Typical diameter distribution of aerosols detected by inner CPC of PAMS at the field test site.

Compared with the optimized filters tested using the SMAG system in the last chapter, the filters here had similar pressure drop and also showed reduced air resistance for the multilayer filters than the corresponding 1-layer ones with identical basis weights, as can be seen in Fig. 5.3. On the other hand, as shown in Fig. 5.4, most of the filters had lower filtration efficiency for the vehicular aerosols than their counterparts evaluated by the lab-generated NaCl particles. This was partly because aerosols formed from vehicle emission were often oily and could be quite damaging to the nanofiber

filters, especially to the electret ones [1, 2]. Janssen and Bidwell tested the filtration performance of N95 electret filters against diesel particulate matter. They found that after only 2-h exposure to the oily particles, the penetration through one of their N95 electret filters increased from the initial 0.61% to 12.1% [99]. Also, the high humidity (higher than 80% most of the time) of the air in the subtropical city of Hong Kong was detrimental to the electret filters, while in the lab the aerosol flow was dried before challenging filters [19, 57, 117]. Yang et al. studied the influence of relative humidity (RH) on the particle penetration properties of a PP electret filter. They found the penetration of 0.3  $\mu\text{m}$  aerosol through the electret filter increased from approximately 17% to 27% as the RH increases from 30% to 70%, due to the higher dissipation rate of surface charge under higher RH [118]. Besides, different from the lab tests where monodisperse aerosols were applied one size at a time, the tests in the real environment employed polydisperse aerosols. Despite aerosols are always assumed to be independent in filtration theories, particles with different sizes might interact with each other along the aerosol flow path in the PAMS system and interfered with the filtration process, though it was unclear whether the interaction brought a positive or negative effect [1].

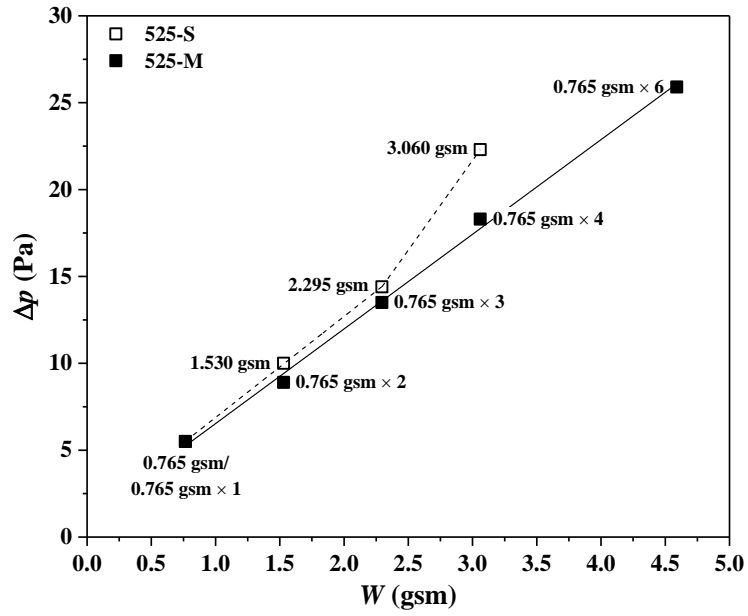


**Fig. 5.3.** Pressure drop of 525-nm 1-layer and multilayer filters with varied filter basis weights at the outdoor experimental site. (Each filter had the same pressure drop in uncharged and charged states).

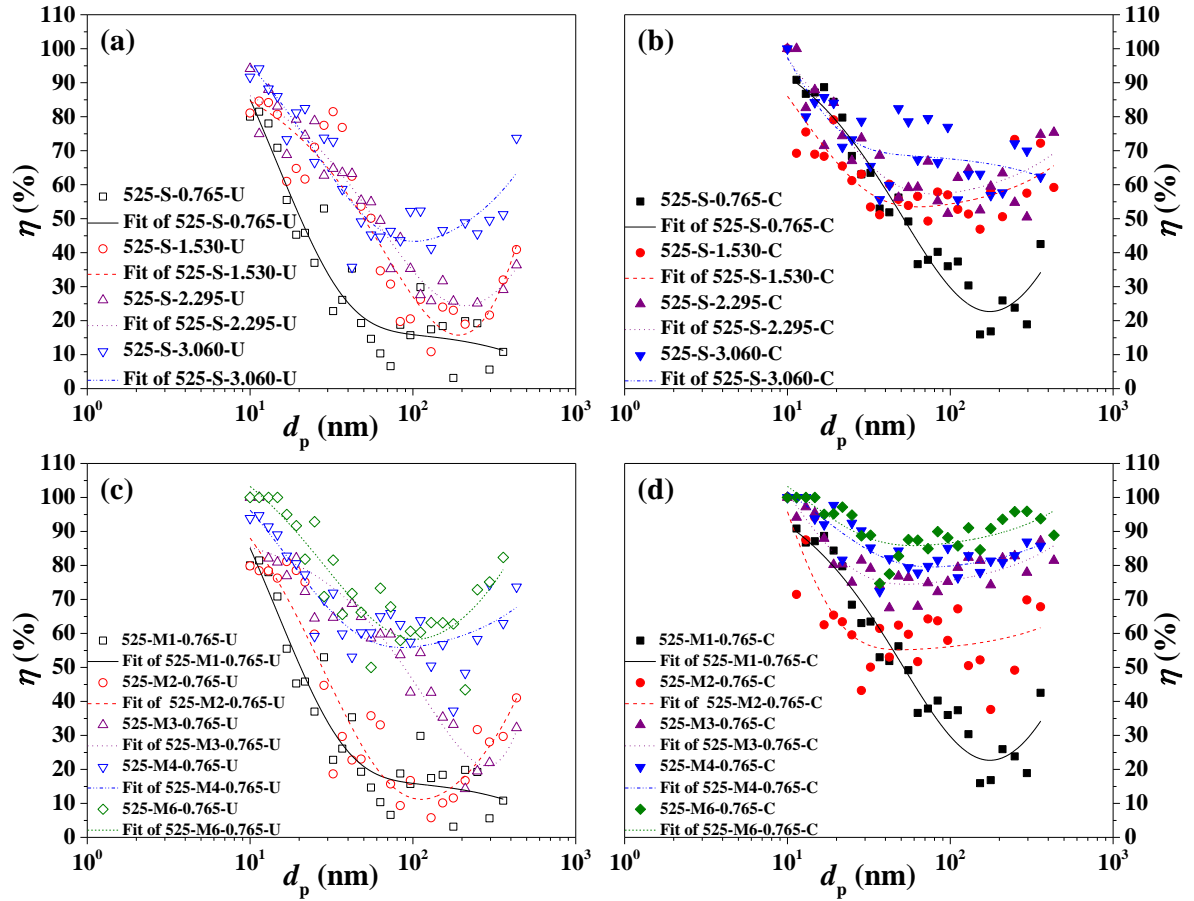


**Fig. 5.4.** Filtration efficiency ( $\eta$ ) and fit curves of 525-nm (a) 1-layer uncharged, (b) 1-layer electret, (c) multilayer uncharged and (d) multilayer electret PVDF filters with varied filter basis weights in field tests. (Note 525-S-0.765 and 525-M1-0.765 denote the same filter.)

In contrast to the lab tests, the efficiency data points here are far more scattered, especially for the filters with lower basis weights. This is mainly due to the low aerosol concentrations around the experimental site. The peak concentrations were only about  $77 \text{ cm}^{-3}$  in average, let alone the particles smaller than 30 nm or larger than 200 nm, for which less than  $30 \text{ cm}^{-3}$  were detected by the PAMS. A small variation in concentration could lead to a big change in filtration efficiency, which was more problematic for low-efficiency filters. In addition, the aerosol-aerosol interaction and the irregular charge

distribution on aerosols could also contribute to the scattering of the efficiency points [1, 2].

Regardless of the data scattering, certain patterns can be found among the filtration curves. All the multilayer filters, whatever the charging state was, had higher efficiency than the corresponding 1-layer filters. And the better performance was more significant when quality factors were taken into account, as can be seen in Fig. 5.5. Lower penetration rates of most particles larger than 40 nm were observed for electret filters than uncharged ones. And in spite of the fluctuations of the efficiency with aerosol size, most filtration curves of electret filters in general show a flat or an ascending trend, particularly for those of the multilayer filters. These trends accord with the results seen in the lab tests, where to some extent filtration efficiency increased with aerosol size due to the enhanced electrostatic effect [105]. The abnormal filtration curves of 525-S-0.765-C and 525-S-1.530-C might result from the large data point variations due to the low efficiency and the complex aerosol charge distribution. For aerosols smaller than 40 nm, diffusion filtration played the major role and electrostatic effect barely influenced their capture [1, 7]. Thus, together with the low particle concentrations in the range of 10-40 nm, the efficiency values of electret filters were not necessarily higher than that of uncharged ones.

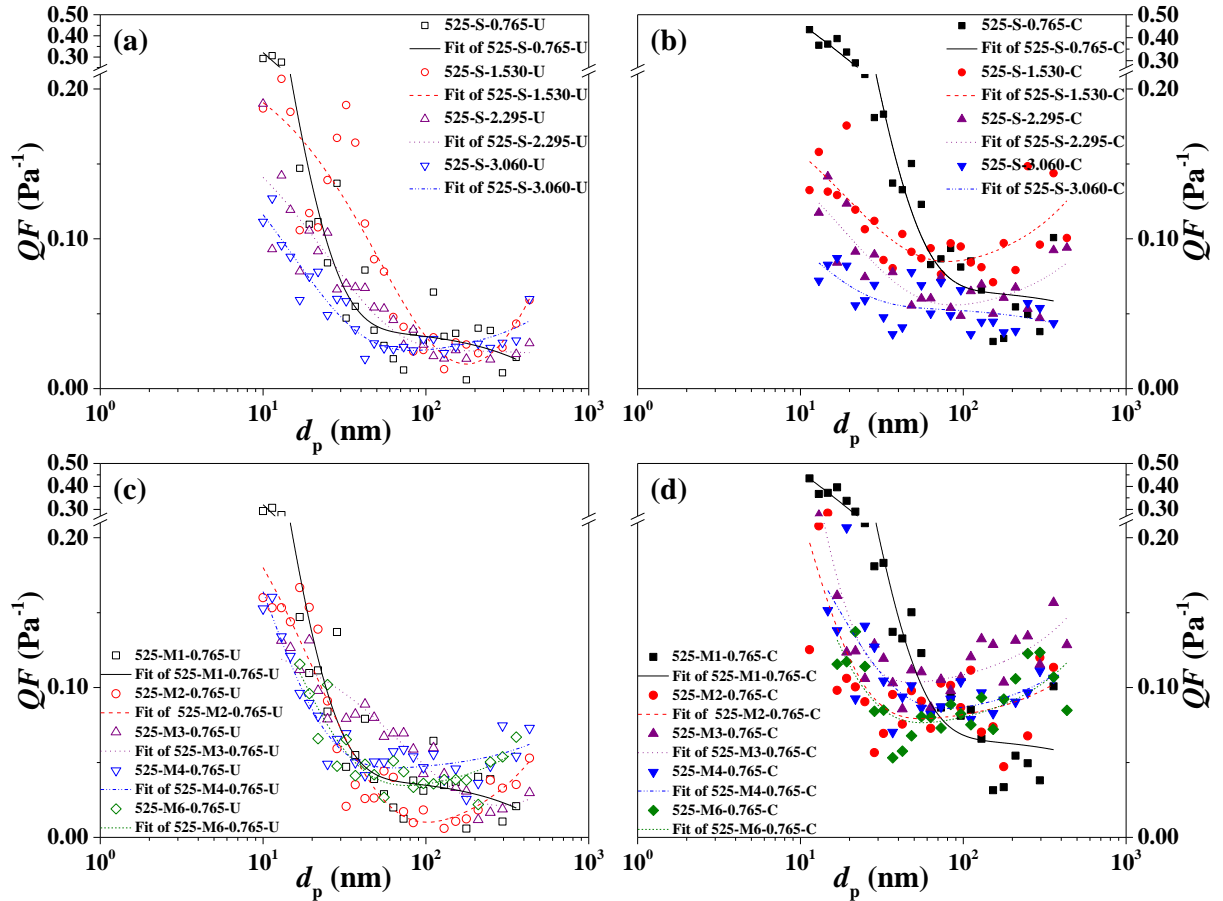


**Fig. 5.5.** Quality factors ( $QF$ ) and fit curves of 525-nm (a) uncharged 1-layer, (b) electret 1-layer, (c) uncharged multilayer and (d) electret multilayer PVDF filters with varied filter basis weights in field tests. (Note 525-S-0.765 and 525-M1-0.765 denote the same filter.)

For the filter with the highest filtration efficiency, 525-M6-0.765-C could remove at least 87% of vehicular aerosols of most sizes, and it had similar filtration curve for field test to that for lab test, as shown in Fig. 5.6. Moreover, its pressure drop was only 25.9 Pa which was much lower than commercially available microfiber filters and the quality factors were mostly higher than  $0.08 \text{ Pa}^{-1}$ . The results indicate that the multilayer PVDF electret filters show a promising prospect for real applications.

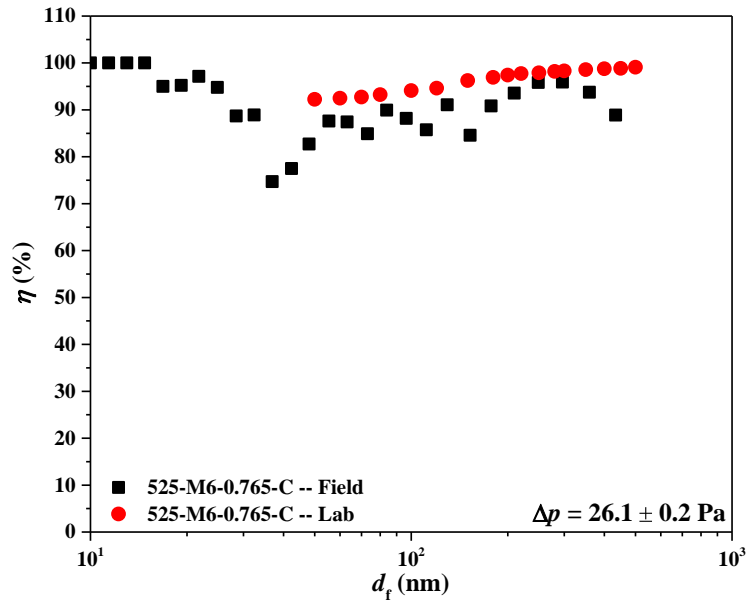


**Fig. 5.6.** Comparison of filtration efficiency ( $\eta$ ) of 525-M6-0.765-C in field test (polydisperse ambient aerosols) and lab test (monodisperse NaCl aerosols).

## 5.4. Summary

The filtration performance of filters was examined using vehicular aerosols in the real traffic environment. Though certain differences existed from the lab experiments, some comparable results were obtained. The main outcomes were summarized below:

1) Similar merits of the multilayer electret filters than the 1-layer counterparts, i.e. improved filtration efficiency and reduced pressure drop, were shown in treating traffic-generated aerosols to lab-generated aerosols.

2) Compared to the lab experiments, the tests using real vehicular aerosols usually showed lower filtration efficiency values, mainly due to the oiliness of the aerosols and the high humidity of air which were detrimental to the electret filters.

3) The data points for the filed tests were intensely scattered because of the low concentration of aerosols, as well as the interaction among aerosols with different sizes

and the irregular charge distribution on aerosols.

4) The multilayer PVDF electret filters have great potential for real application in aerosol removal, which was proved by the high filtration efficiency and the low pressure drop in a traffic environment.

## **Chapter 6: Aerosol Loading Behaviors of Multilayer PVDF**

### **Electret Filters**

#### **6.1. Overview**

In the last three chapters, the merits of multilayer PVDF electret filters have been well-proven by their great filtration properties, both in efficiency improvement and pressure drop reduction, compared with their 1-layer counterpart. Nevertheless, as a filter is continually challenged with aerosols, both the aerosol penetration (i.e. inverse of filtration efficiency) and the filter resistance (i.e. pressure drop) gradually change while the filter becomes increasingly loaded [1, 7]. Regardless of the usage in real applications, it is the long-term performance that is more valued when health impact, financial cost or energy consumption is considered. For face masks (which are the targeted application of filters in this study), especially during the COVID-19 pandemic worldwide, the long-term performance is of greater significance because people may repeatedly wear a same mask due to the shortage of supply.

In terms of filtration efficiency, as a departure from conventional uncharged filters which show increasing values throughout the loading process, the efficiency of electret filters initially decreases to a certain point before increasing with loading. This phenomenon is due to the shielding of electrostatic effect and the enhanced mechanical capture due to deposit that can be considered as artificial fibers and ultimately forming an aerosol “cake” on the filter surface that becomes the effective filter media [7, 16, 17, 50-52]. In the early stage of filtration using an electrically active fibrous filter, electrostatic mechanism, including Coulombic force collection for charged particles and induction charging collection for uncharged particles, plays the dominant role in

aerosol capture. With filtration proceeding, the initially captured particles may act as collection sites for the latter particles and gradually form dendritic structures. The adjacent dendrites gradually join together, which initiates the formation of a “cake” on the front side of the filter. During the dendrites/cake growth stage, the electrostatic effect diminishes because of the “shielding effect” on the fiber charges by deposited particles, while the mechanical collection enhances contributed by the dendrites/cake. The filtration efficiency keeps decreasing until the reduction in electrostatic efficiency is equally compensated by the improvement in mechanical efficiency, at which point the filtration efficiency falls to its minimum values before increasing thereafter. On forming a complete cake layer (cake filtration stage), particle penetration falls to zero or filter efficiency reaches 100%, where electrostatic effect is fully shielded and the future incoming particles are solely collected via the mechanical effect of the cake layer, i.e., the aerosol capture has totally transferred from depth filtration to surface filtration.

As for pressure drop, electret filters have generally similar increasing trend to conventional filters [16, 17, 50-52]. In the early stage, particles deposit on the surface of individual fibers across the porous filter depth. Due to the exceedingly limited space occupied by the captured particles, the fluid flow is only slightly being affected and the pressure drop increases at fairly low rates. With dendrites/cake forming and the filter more and more clogged, the pressure drop keeps rising with the rate of increase accelerating. When the cake is completely formed, the increase rate of pressure drop reaches its peak value, after which the pressure drop increases linearly at this rate with the loading mass, indicting a constant cake resistance with additional aerosol deposit.

From the description above, it seems that an electret filter only has a minor advantage of initially higher filtration efficiency over a conventional filter regarding

aerosol loading process because it basically works as a surface filter once being fully clogged. However, due to the big role played by electrostatic mechanism in the early stage of loading, it is naturally expected that for an electret filter, the deposition properties of particles, including the capture position, dendrite/cake formation rates and cake structures, are different from a purely mechanical filter. Therefore, the electret filter may show a different pressure drop increase trend in the subsequent cake filtration. In fact, the lower clogging rates of some electrically active fibrous filters have already been reported in the literature and the authors attributed the improved holding capacities to more uniform distribution of deposited particles. Nonetheless, without investigating the real morphology of particle deposition, such as use of SEM images on deposition pattern in the filter, previous research merely qualitatively drew conclusions based on the difference in pressure drop evolutions between electret and mechanical filters [16, 17, 51]. Moreover, the electret filters in these researches usually had large thicknesses within just one single layer. It has been well proved that “skin effect” exists in aerosol filtration using a fibrous filter, where much more particles deposit at the face region than at the back side [45, 47]. For an electret filter, that means when a complete cake is already formed on the surface of the filter, the charged fibers downstream of the surface fibers are far from being fully used and therefore wasted.

Filtration efficiency has been confirmed to improve by redistributing charged fibers from a single layer to multiple thinner layers of nanofibers stacking one on top of each other in the last three chapters [105]. The aim of work in this chapter is to study the aerosol loading behaviors of the multilayer PVDF filters, especially of the electret ones. In fact, loading of multilayer nanofiber filter, uncharged or electret, have never been done. Even loading of a 1-layer electret nanofiber filter has not been reported,

which in our study serves as a basis of comparison as well. It was hypothesized that compared to a 1-layer filter, a multilayer filter with an identical total fiber basis weight but a much lower packing fraction has a higher resistance to clogging and a larger aerosol holding capacity. Due to the higher porosity and smaller thickness of each layer in the multilayer filter, it will take a longer time for the dendrites to grow to a significant size that blocks the aerosol flow, thus slowing down the pace of skin layer formation and leading to more uniform aerosol capture across the filter layers. Specifically, for the multilayer PVDF electret filters, the charges on the fibers of downstream layers are hopeful to be more effectively utilized. Further, on the level of individual fiber, the distribution of captured particles is expected to be more uniform surrounding and along the fiber.

In this chapter, the filtration efficiency evolution of uncharged/electret, single-/multi-layer filters with aerosol loading time were compared for the first time. Moreover, the pressure drop increase of different filters were analyzed in accordance to their physical properties. Besides, the deposition of captured aerosols on the filters, both in amount and distribution, was illustrated using SEM images. Ultimately, the efficiency, pressure drop and aerosol capacity were addressed for the 4 types of test filters (uncharged/electret, single-/multi-layer filters) under loading starting with a clean filter, moving to depth filtration, and subsequent cake filtration.

## **6.2.Experimental**

### **6.2.1. Fabrication of filters**

The same methods as the other chapters were applied to prepare the filters used in this chapter. Based on the results of filter optimization obtained from Chapter 4, filters with same fiber diameter of 525 nm and same total basis weight of 3.060 gsm were

used. To investigate the differences in loading behaviors between uncharged and electret filters, and 1-layer and multilayer filters, 525-S-3.060-U, 525-S-3.060-C, 525-M4-0.765-U and 525-M4-0.765-C were fabricated. In case that parallel groups of filters were used to repeat the test run, different numbers are added at the end of each filter tag to differentiate them. Filters of 4-layer were used in this study because they were expected to show more distinct behaviors from 1-layer filters having the same basis weight of nanofibers.

### **6.2.2. Filtration performance evaluation of filters**

Before loading up a filter, it is essential to test the filtration performance in a clean (i.e. unloaded) state. The experimental set-up for clean filter tests is shown in Fig. 3.3. A clean and dry compressed air flow from a filtered air supply system was fed to a sub-micrometer atomizer containing a certain concentration of sodium chloride (NaCl) solution, where liquid droplets containing salt aerosol were generated. The stream was then passed through a Nafion membrane air dryer for moisture removal, resulting in dry aerosol particles ranging between 10-1000 nm (CMD). The compressed air flow rate and the salt solution concentration were finely tuned to get a proper aerosol size distribution. For the former parameter, an overwhelmingly high rate could cause stream instability and leakage at the atomizer, thus leading to unstable aerosol output. For the latter one, intensely high solution concentrations were avoided in case of clogging along or corrosion to the flow route due to salt accumulation. Besides, the two parameters were set to generate aerosol concentrations which did not exceed the upper detection limit ( $1 \times 10^4 \text{ cm}^{-3}$ ) of the condensation particle counter (CPC, Model 3010, TSI Inc., Shoreview, MN) used in this study and high enough to prevent inaccurate measurements. After drying, the aerosol stream flowed through an impactor where

particles larger than the cut size were removed. The cut size was determined by the flow rate through and the nozzle size of the impactor, which in this study was 550 nm. The particles left were then introduced to a neutralizer where they were brought to a Boltzmann charge distribution (i.e. neutralized). Subsequently, the neutralized particles were directed to a differential mobility analyzer (DMA) which classified particles in the size range from 10 to 1000 nm by adjusting voltage accordingly using the “Generation” function of SMAG system. Only particles with specific electrical mobility diameter (EMD) could penetrate the DMA while others were removed, therefore producing particles with a relatively monodisperse size. After exiting the DMA, the aerosol stream passed a second neutralizer to be neutralized, leaving most of the particles zero-charged. The neutralized monodisperse aerosol stream, mixed with a clean and dry make-up air flow to reach a face velocity of  $5.3 \text{ cm s}^{-1}$  when challenging the filter, was then sent to a test column where the filter was mounted with its surface perpendicular to the incoming flow. At the beginning of the filtration test, the pressure drop ( $\Delta p$ ) across the clean filter was measured by a digital pressure manometer (Model 2080P, Digitron, Elektron Technology, UK). The aerosol flows upstream and downstream of the filter respectively were sampled in an isokinetic way in case of disturbing the aerosol stream, and the concentrations of particles with a known size were determined by the aforementioned CPC. Eq. 3.2 was applied to calculate filtration efficiency ( $\eta$ ).

### **6.2.3. Aerosol loading behavior evaluation of filters**

When the behavior of a filter during aerosol loading was to be studied, as shown in Fig. 6.1, a similar set-up to that of clean filter tests was applied except for the position of the differential mobility analyzer (DMA). After the first neutralizer, the polydisperse

aerosols (40-500 nm, CMD) were directly fed to the test column to challenge the filter. The reason for the modification was that it would take impractical long time to load up the filter. Every ten minutes, the aerosol flow upstream of the filter was sampled to the DMA under the “Scanning Mode” of “Measurement” function to get the size distribution of the particles used for filter loading, coupled with the CPC to measure particle concentrations channel by channel. Note that in the set-up for filter loading, the real concentrations shown in aerosol size distribution were obtained by automatically calculating the corresponding values measured by the CPC which only counted the fairly low fractional particles exiting the DMA. At prescribed intervals, the set-up was switched back to that of Fig. 3.3 for testing the filtration efficiency with loading mass until the values all rose close to 100% after which a complete cake was formed and surface filtration was the only mechanism for aerosol capture. The set-up for aerosol loading was not used to determine filtration efficiency because of the difficulty in tuning the equipment response time for polydisperse aerosols, which could bring inaccurate and misleading results. Constantly switching the two modes may interrupt the loading process, which was a major limitation of the loading set-up. Nevertheless, because the aerosol concentration used for loading was far higher than that for efficiency tests (which are shown later), the interruption was actually negligible. Throughout the loading process, the pressure drop was monitored at regular intervals, which was expected to show a linear trend after the formation of the full cake. The loading was terminated until the pressure drop reached an arbitrary limit which had been far past the starting point of complete surface filtration. In this study, this limit was set at about 800 Pa.

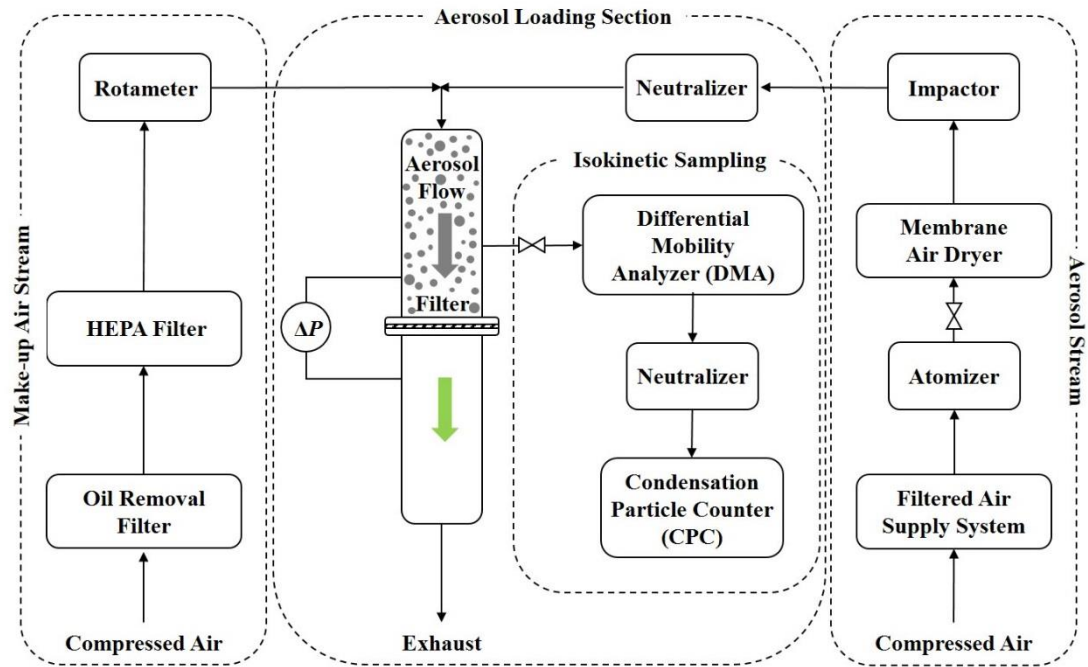


**Fig. 6.1.** Schematic diagram of set-up for aerosol loading of filters.

Fig. 6.2a and Fig. 6.2b show the typical aerosol size distributions of set-ups for filtration efficiency tests and filter loading, respectively. The maximum concentration for the former set-up is around  $0.6 \times 10^4 \text{ cm}^{-3}$ , while for the latter one above  $3.9 \times 10^5 \text{ cm}^{-3}$  which is almost 62 times higher than the former case. Therefore, the occasional efficiency tests had little interference in the loading behaviors of filters. The loading period could be further shortened by using NaCl solution with a higher concentration. Nevertheless, apart from the risks of clogging and corrosion, higher concentrations were not chosen with concern that the filtration efficiency would change too quickly during the efficiency test.

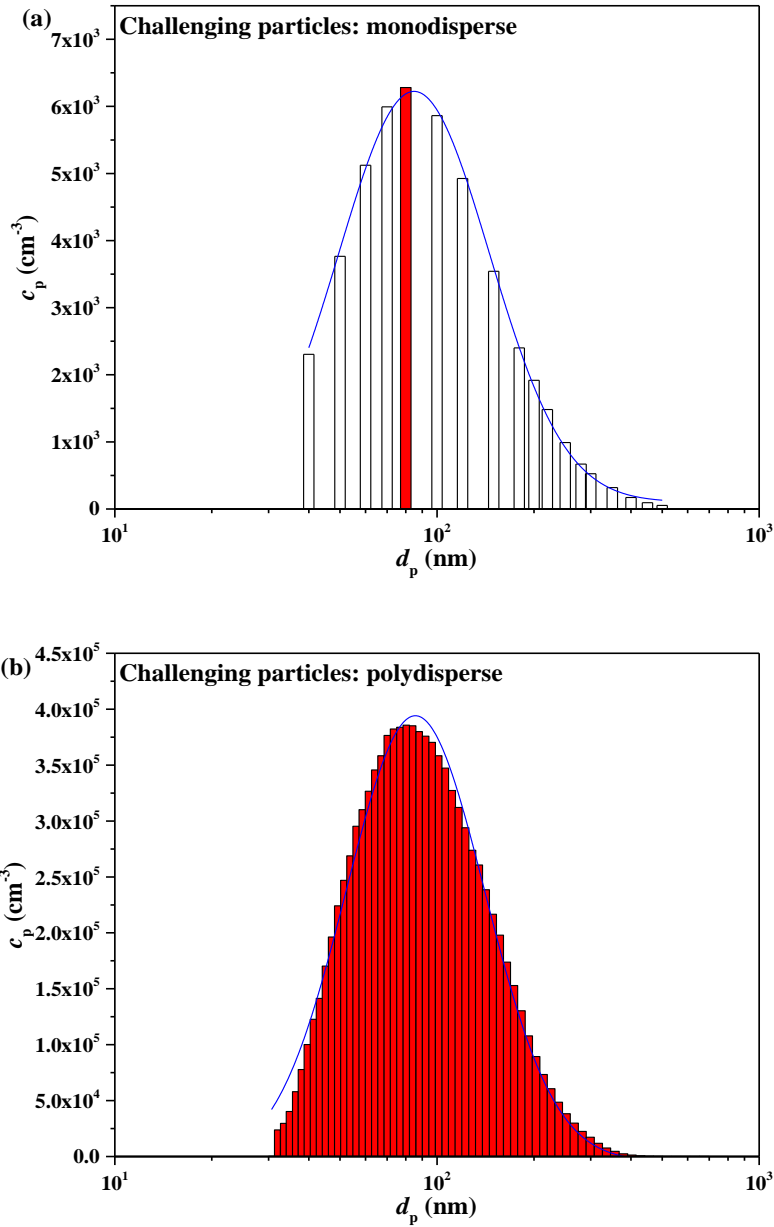


**Fig. 6.2.** Typical diameter distribution of particles for (a) filtration efficiency tests and (b) aerosol loading.

Combining the particle size distribution, filtration efficiency with loading time, face velocity of the aerosol stream and the filter surface area, the specific captured aerosol mass ( $M_{\text{dep}}$ ) during any time period and the cumulative mass at any time point could be calculated. In the literature some people weighed the filters before and after aerosol loading and took the weight differences as the loaded aerosol masses [119]. This

method was not used in this study mainly due to two reasons. For one thing, removing the filter can easily break the structures formed by captured aerosols, e.g. dendrites and cake, and cause loss in deposited aerosols. For another, the weight of deposited aerosols is often too light to be distinguished, which can bring significant errors to the calculations.

Similar to our previous study, the algorithm for  $M_{\text{dep}}$  is described as follows [120].

Under continuous aerosol loading, the real-time  $M_{\text{dep}}$  is given by:

$$M_{\text{dep}} = \int_{\tau=0}^{\tau=t} \int_{d_p=40 \text{ nm}}^{d_p=500 \text{ nm}} c(d_p, \tau) \eta(d_p, \tau) U \frac{\pi d_p^3}{6} \rho_p d(d_p) d\tau \quad (6.1)$$

where  $c(d_p, \tau)$  is the number concentration of upstream particles in the size bin with a geometric mean diameter  $d_p$  at loading time  $\tau$ ,  $\eta(d_p, \tau)$  is the filtration efficiency of particles with a diameter  $d_p$  at loading time  $\tau$ ,  $U$  is the face velocity,  $\pi d_p^3/6$  is the volume of an aerosol particle with a diameter  $d_p$ , and  $\rho_p$  is the particle material weight density. Because  $\eta(d_p, \tau)$  was sampled sparsely, over each time interval  $\eta(d_p, \tau)$  was assumed to be constant. Though this assumption may make the calculation of  $M_{\text{dep}}$  less accurate, from a qualitative point, it was sufficient to differentiate the loading properties of the four studied filters with significant difference in filtration efficiency. The loading data of 525-M4-0.765-C-1 and the conversion of loading time to specific loaded mass are presented in Table A2 (Appendix 2) and Appendix 3, respectively.

The loaded filters were sampled for SEM characterization to study the aerosol deposition properties of uncharged/electret, single-/multi-layer filters. Specially, the back side (i.e. downstream side) of the loaded filters were also observed under SEM to investigate whether the fibers and fibrous layers were more fully utilized after charging or distributing into multiple layers.

### 6.3. Results and discussions

To investigate the differences in loading behaviors between uncharged and electret filters, and 1-layer and multilayer filters, filters with same average fiber diameter of 525 nm and same total basis weight of 3.060 gsm were used, including uncharged and electret 1-layer filters, and uncharged and electret 4-layer filters. The filters were hereafter denoted 525-S-3.060-U, 525-S-3.060-C, 525-M4-0.765-U and 525-M4-0.765-C. In case that parallel groups of filters were used to repeat the test run, different numbers are added at the end of each filter tag to differentiate them. Filters of 4-layer were used in this study because they were expected to have evidently different behavior as compared to that of the 1-layer filters. The SEM images of S-3.060 and a typical layer of M4-0.765 are shown in Fig. 6.3a and Fig. 6.3b, respectively. It is clearly shown that the fibers in S-3.060 are much more densely packed than that in a single layer of M4-0.765.

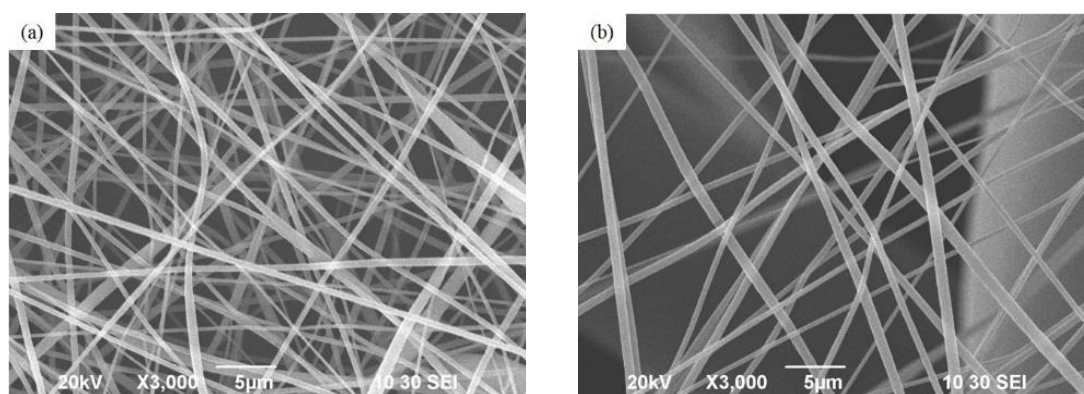


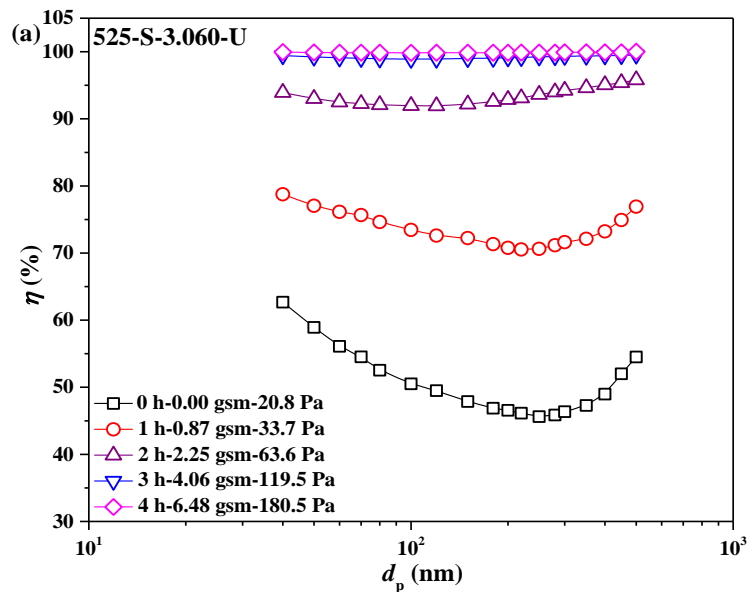
**Fig. 6.3.** SEM images of (a) S-3.060 and (b) one layer of M4-0.765 in clean state.

### **6.3.1. Comparison of loading behaviors between 1-layer and multilayer uncharged PVDF filters—merits of multilayering**

#### **6.3.1.1. Variation of filtration efficiency and pressure drop of uncharged PVDF filters with loaded mass**

The filtration efficiency curves of 525-S-3.060-U and 525-M4-0.765-U with loading time/loaded mass are shown in Fig. 6.4a and Fig. 6.4b, respectively. Generally, the two uncharged filters show similar trend with the efficiency increasing with loading time/loaded mass, which has been widely confirmed in the literature [45, 47, 121]. The deposited aerosols, including individual particles, dendrites and cake, could all act as new aerosol collection sites or as additional “artificial fibers”, thus improving the filtration efficiency of, as well as increasing the pressure drop across the filter [11, 18, 122]. It is also interesting to note that the most penetrating particle sizes (MPPS) of both filters gradually decreased with loading mass—250 nm to 80 nm for 525-S-3.060-U and 280 nm to 80 nm for 525-M4-0.765-U as shown in Fig. 5, a phenomenon of which was also observed by Leung et al. [45, 47]. This was due to the more prominent interception effect than the diffusion effect of the deposited aerosol agglomeration, with the two effects being the main mechanisms for filtration efficiency improvement before pure surface filtration took place. However, regardless of the similarities, the efficiency of 525-S-3.060-U apparently increased at a much higher rate than that of 525-M4-0.765-U. In clean state, the two filters had similar efficiency curves. After 2-h loading, the efficiency of 525-S-3.060-U at the MPPS (120 nm) drastically increased to 91.9% from the clean filter efficiency of 45.6%, while that of 525-M4-0.765-U at 280 nm increased only from 40.1% to 43.8%. It merely took 4 h for 525-S-3.060-U to closely reach the efficiency of 100% in contrast to 14 h for 525-M4-0.765-U. Due to the

constantly higher filtration efficiency, more aerosols deposited on 525-S-3.060-U than 525-M4-0.765-U at the same loading time. For example, after 2-h loading, 525-S-3.060-U had a loaded mass of 2.25 gsm, which was 0.67 gsm higher than 525-M4-0.765-U (1.58 gsm). Corresponding to filtration efficiency, the pressure drop of 525-S-3.060-U rose much faster than that of 525-M4-0.765-U. Before loading, the pressure drop values were 20.8 Pa and 17.1 Pa for 525-S-3.060-U and 525-M4-0.765-U, respectively. At 2 h, the pressure drop for 525-S-3.060-U increased by 42.8 Pa while only 1.5 Pa for 525-M4-0.765-U. Barely 4 h was needed for 525-S-3.060-U to reach 180.5 Pa whereas 12 h for 525-M4-0.765-U to rise to 189.3 Pa by contrast.



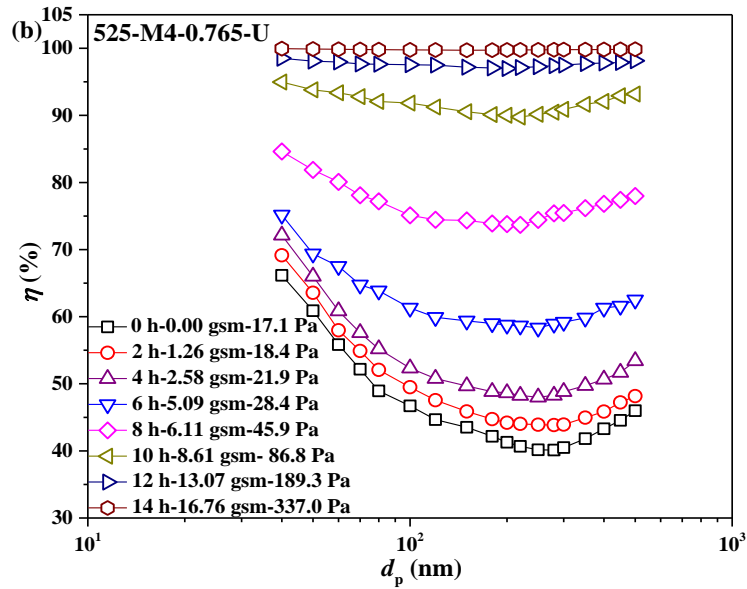


**Fig. 6.4.** Evolution of filtration efficiency ( $\eta$ ) of (a) 525-S-3.060-U and (b) 525-M4-0.765-U with loading time.

Contributed by the slower growth of dendrites/cake, the filtration efficiency of 525-M4-0.765-U increased at lower rates than that of 525-S-3.060-U with loading time. Moreover, benefitting from the higher uniformity of aerosol deposition across the filter, 525-M4-0.765-U had much lower increase in pressure drop per loaded aerosol mass than 525-S-3.060-U. In other words, multilayer filters could mitigate the clogging by aerosol accumulation and enhance the aerosol holding capacity. As can be seen in Fig. 6.4, when the filtration efficiency approached near 100%, 525-M4-0.765-U had an aerosol loaded mass of 16.76 gsm (at 14 h) while 525-S-3.060-U only 6.48 gsm (at 4 h). The only drawback for M4-0.765-U was that the efficiency before approaching the deposit of 6.1 gsm (8h) was less than 80% whereas S-3.060-U with about 1 gsm deposit (1-2 h) could achieve 80% efficiency reducing loss of uncaptured aerosols.

The pressure drop variations of 525-S-3.060-U and 525-M4-0.765-U with the aerosol deposition mass throughout the loading processes can be seen in Fig. 6.5. Both

curves show the typical trend where pressure drop increased slowly in the early stage of loading, followed by an accelerating increase until the cakes were formed and the curves become linear lines with the deposition mass [45, 47, 121]. Nonetheless, for 525-S-3.060-U, the early stage was much shorter than that of 525-M4-0.765-U. 525-M4-0.765-U had a clogging point of 16.76 gsm, which was 2.59 times higher than that of 525-S-3.060-U (6.48 gsm). This further indicates that the multilayer filter had a higher aerosol holding capacity and was less prone to clogging due to the high filter porosity of each layer. As a result, even the downstream layers such as second, third and fourth layer in M4-0.765-U could effectively capture aerosols, unlike the case of a 1-layer filter. We shall see this in the SEM images to be presented in latter section.

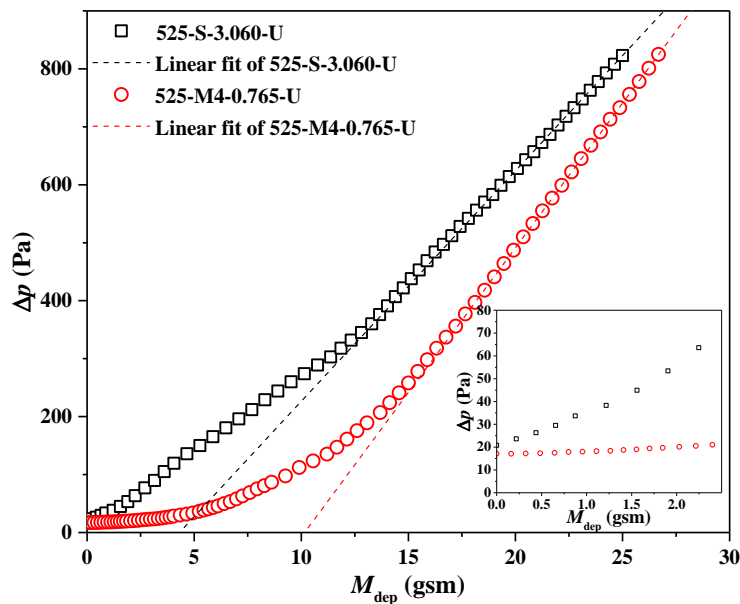


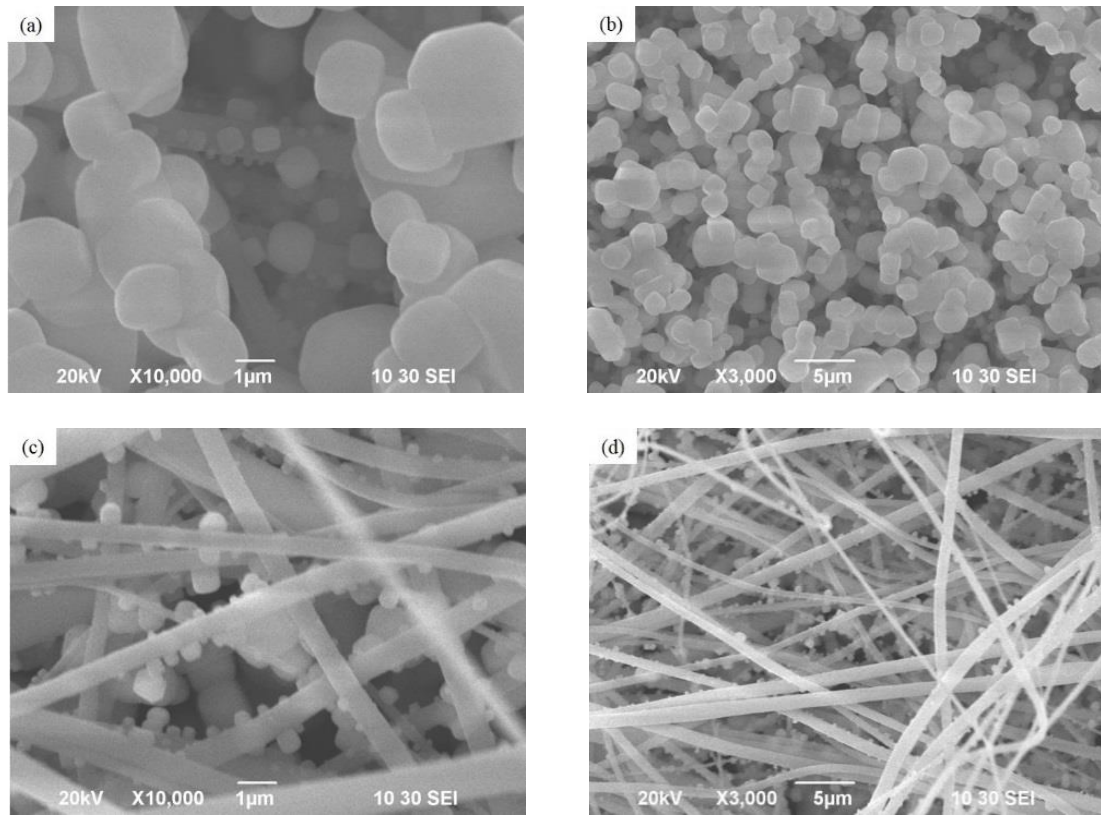
**Fig. 6.5.** Evolution of pressure drop ( $\Delta p$ ) of 525-S-3.060-U and 525-M4-0.765-U with loaded aerosol mass.

### 6.3.1.2. Deposition of aerosols on uncharged PVDF filters

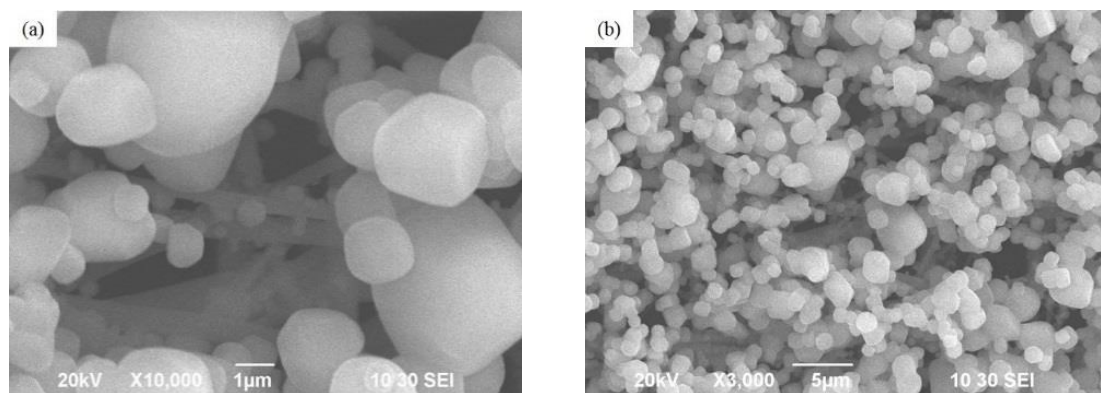
The significant difference in the variation of filtration efficiency and pressure drop with loading time between the two filters resulted from the different filter structures

and aerosol deposition properties. 525-S-3.060-U, with only one layer, had a high fiber packing fraction and a low porosity. The space between individual fibers was so small that dendrites formed and grew considerably fast into a cake on the filter surface with the high concentration of incoming aerosols, leading to the rapid increase in both filtration efficiency and pressure drop and leaving the nanofibers downstream of the filter surface insufficiently utilized [45, 47]. By redistributing the same amounts of fibers in a single layer to 4 layers, each layer of 525-M4-0.765-U consisted of much loosely packed fibers. The aerosols could penetrate to the downstream layers of the filter before dendrites and cake grew to an extent to seriously block the incoming aerosol stream. This hypothesis was confirmed by SEM images of the loaded filters. Figs. 6.6-6.8 are SEM images which depict the aerosol deposition on the front or back side of loaded 525-S-3.060-U and each layer of 525-M4-0.765-U, respectively. The surface of the loaded 525-S-3.060-U is covered by a cake, so it is hard to infer the aerosol profile within the filter. Yet, from Figs. 6.6c-d which shows the back side of the loaded 525-S-3.060-U, not many particles are present within the filter depth near the back side. On the contrary, aerosol deposits more uniformly across the four layers of 525-M4-0.765-U (Fig. 6.7), though the loaded amount decreases with the layer depth. When a multilayer filter is used for aerosol filtration, a portion of the aerosols are filtered out by the first layer directly facing the whole incoming mass, leaving the rest of the aerosols challenging the downstream layers. The result is that fewer aerosol particles are available for the layer further back. If all layers have similar structures and thus similar filtration efficiency in clean state, more aerosols will deposit on the more upstream layer at any given time, making its filtration efficiency and pressure drop always higher and increase at faster rates than the immediately downstream layer. This is actually the very reason for “skin layer” effect which was also observed by Leung et

al. [45, 47]. In this study, nevertheless, there are still a lot of particles on the bottom layer of 525-M4-0.765-U, benefiting from the high permeability of each layer.



**Fig. 6.6.** SEM images of (a) and (b) the front side, and (c) and (d) the back side of loaded 525-S-3.060-U.



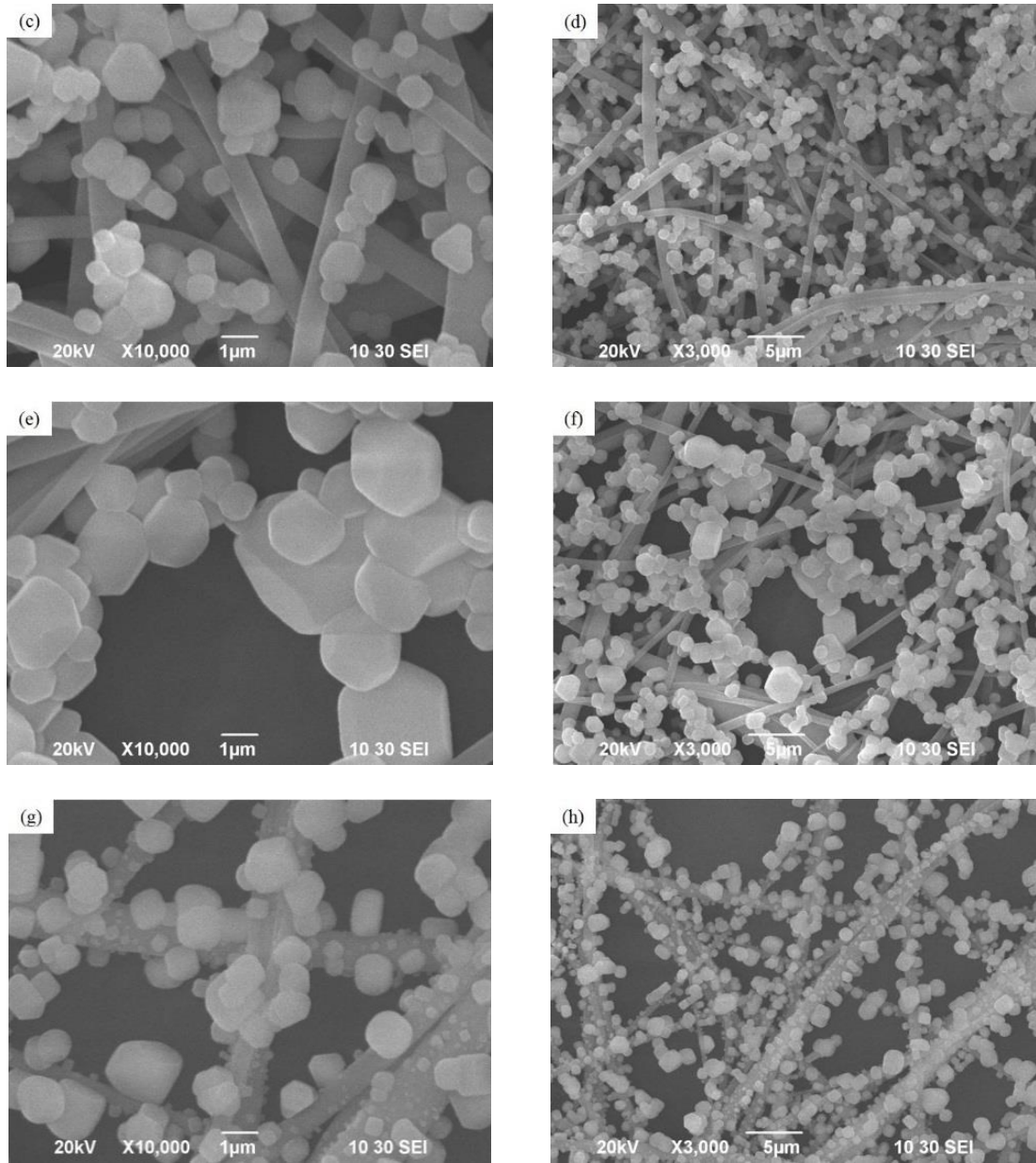


**Fig. 6.7.** SEM images of (a) and (b) the first, (c) and (d) the second, (e) and (f) the third and (g) and (h) the fourth layers of loaded 525-M4-0.765-U seen from the front side.

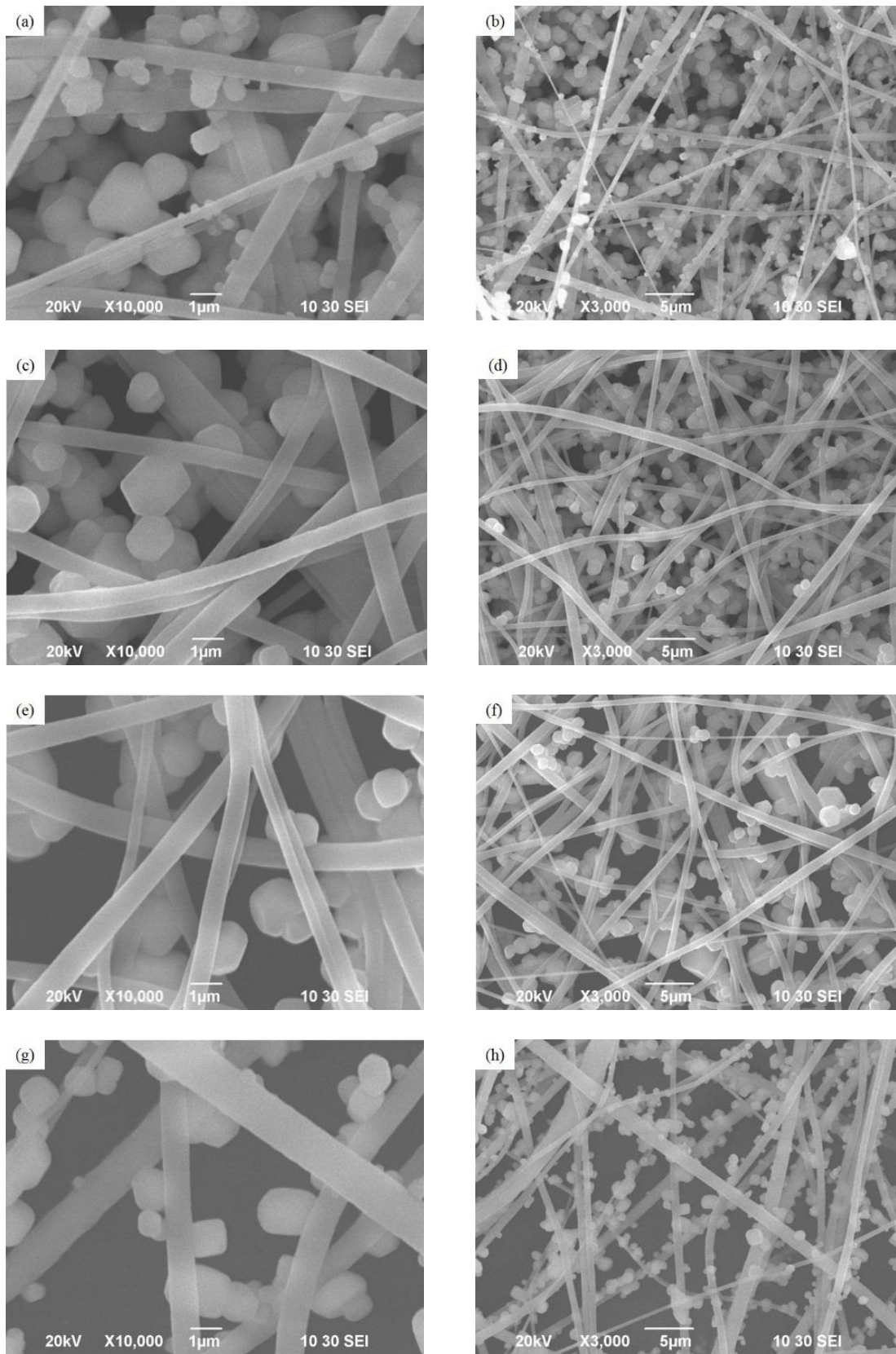


**Fig. 6.8.** SEM images of (a) and (b) the first, (c) and (d) the second, (e) and (f) the third

and (g) and (h) the fourth layers of loaded 525-M4-0.765-U seen from the back side.

It is also worth noting that few particles can be seen on the back of individual fibers in both 525-S-3.060-U (Figs. 6.6c-d) and 525-M4-0.765-U (Fig. 6.8). Theoretically, particles can deposit on the back of a fiber through Brownian diffusion. However, due to the large fiber diameter of the filters (525 nm) used in this study, Brownian diffusion was just a minor mechanism whereas interception played the major role for the uncharged filters, leaving aerosols mainly depositing on the front or side surfaces of uncharged fibers [7].

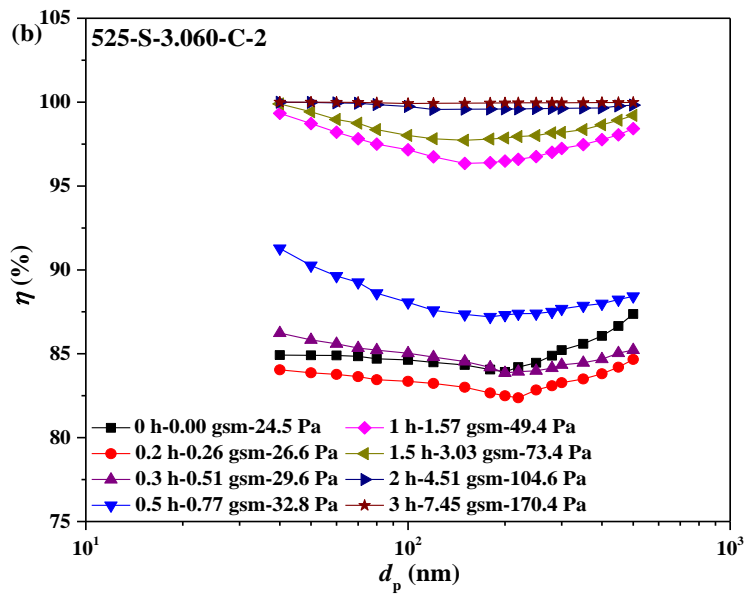
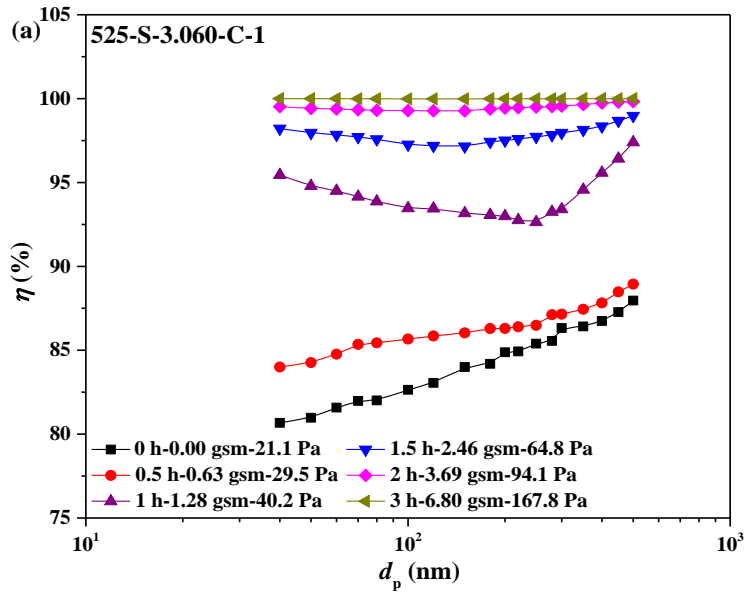
### **6.3.2. Loading behaviors of 1-layer PVDF electret filters—effects of charging**

#### **6.3.2.1. Variation of filtration efficiency and pressure drop of 1-layer PVDF electret filters with loaded mass**

For electret filters, filtration efficiency has been observed by many researchers to first decrease to some extent before gradually increasing to 100% when a cake completely formed. This was attributed to the variations of two opposing effects—the reduction in electrostatic filtration due to charge shielding by the deposited aerosols and the increase in mechanical filtration from the continuous growth of dendrites and cake [16, 17, 51, 52]. Fig. 6.9a shows the filtration efficiency evolution of 525-S-3.060-C-1. Contrary to the expectation, the efficiency increased at all times till pure surface filtration was reached, despite that the clean filter exhibits a typical efficiency pattern of PVDF electret nanofiber filters, with the value increasing from 80.7% at 50 nm to 88.0% at 500 nm. After 1-h loading, mechanical filtration was the dominant mechanism indicated from the efficiency curve, and the efficiency was 92.6% at MPPS of 250 nm. Gradually, the efficiency approached approximately 100% and the MPPS dropped to 80 nm (Fig. A6.1, Appendix 1). Correspondingly, the pressure drop of 525-S-3.060-C-

1 markedly increased by 146.7 Pa from the initial 21.1 Pa after 3-h loading with a deposited mass of 6.80 gsm.

Given that the efficiency tests were only carried out intermittently with loading time, there is a possibility that the efficiency initially dropped during the first half hour. To prove this point, another electret filter (525-S-3.060-C-2) with similar physical properties was used to repeat the test under the identical experimental condition except that two more efficiency tests were done at 10 min and 20 min. As can be seen from Fig. 6.9b, like 525-S-3.060-C-1, the pressure drop of 525-S-3.060-C-2 rose from 24.5 to 170.4 Pa with 7.45 gsm of deposited mass after 3 h. However, the filtration efficiency did decrease in the first 10 min and increased in the next 10 min. Subsequent loading time followed similar trend as that of S-3.060-C-1. Nonetheless, the largest reduction in efficiency of particles was only 2.7% which was too small to make a convincing conclusion from. It is also worth mentioning that 525-S-3.060-C-1 and 525-S-3.060-C-2 behaved a little differently concerning the variation of filtration efficiency, pressure drop and loaded mass, which was because of the randomness and inhomogeneity of fibers and charge distributions on the filters [123].



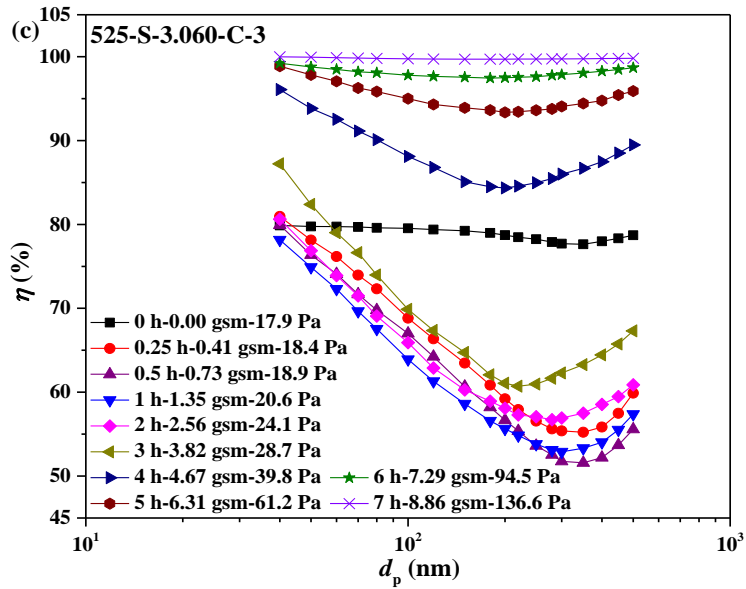


**Fig. 6.9.** Evolution of filtration efficiency ( $\eta$ ) of (a) 525-S-3.060-C-1, (b) 525-S-3.060-C-2 and (c) 525-S-3.060-C-3 with loading time.

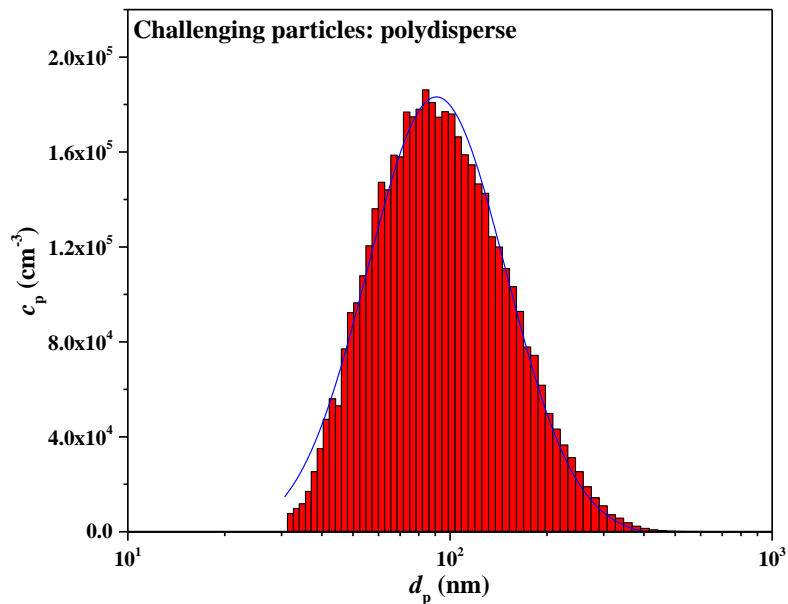


**Fig. 6.10.** Typical diameter distribution of particles for aerosol loading of 525-S-3.060-C-3.

Considering the high concentration of aerosol flow for loading up the filter, it was hypothesized that, once the loading began, the mechanical effect strengthened so fast

that the mechanical efficiency improvement trumped the electrostatic efficiency loss. Therefore, an aerosol flow with much lower concentrations (shown in Fig. 6.10) was applied for 3 h to load up a third similar electret filter (525-S-3.060-C-3). After the first 3 h, the aerosol concentrations were raised to the values used for loading up 525-S-3.060-C-1 and 525-S-3.060-C-2, which was aimed to further confirm the influence of loading aerosol concentration qualitatively. As shown in Fig. 6.9c, after 0.25-h loading, there were remarkable decreases in filtration efficiency for all particles, especially for those with larger sizes. Particles of 350 nm (MPPS at 0.25 h as shown in Fig. A6.1, Appendix 1) experienced a reduction of 22.4% from 77.6% to 55.2%. After further reductions ranging from 0.8% to 4.3% at 0.5 h, slowly the efficiency values increased and the MPPS decreased, with 60.7% of filtration efficiency at an MPPS of 220 nm. Note that for extremely small particles, the variations in filtration were insignificant. For instance, the efficiency for 50-nm particles slightly varied between 74.9% and 82.4%. This should result from the different mechanisms dominating filtration by electret filters for neutralized aerosols with different sizes [1, 7]. In this study, particles were brought to a Boltzmann charge distribution before challenging a filter, with most of them being zero-charged so induction charging was the main approach followed by Columbic attraction for electrostatic filtration. Compared with larger particles, small particles were less prone to induction effect, therefore they were less affected when the charges on filters were shielded by aerosol deposition. It should be aware that from 0.5 h to 1 h, the filtration efficiency of particles with sizes between 40 nm to 220 nm decreased, while that of the rest increased. The reason might be that during this period, the decrease in electrostatic efficiency was not fully compensated by the increase in mechanical efficiency, leading to the further efficiency reduction for smaller particles. While for larger particles, they might be trapped due to the increasingly strong surface

filtration effect. During 1-3 h, the filtration efficiency increased with slow paces and the average value remained low, corresponding to the gradual increase of loaded aerosol mass from 1.35 to 3.82 gsm.

Compared with the former two counterparts, with similar loaded mass, 525-S-3.060-C-3 always had much lower pressure drop. For instance, the pressure drop of 525-S-3.060-C-3 with 3.82 gsm of deposited aerosols was only 28.7 Pa, while that of 525-S-3.060-C-1 and 525-S-3.060-C-2 with fewer loaded aerosols (2.46 and 3.03 gsm, respectively) reached 64.8 and 73.4 Pa, respectively. The much alleviated air resistance of 525-S-3.060-C-3 was attributed to the low aerosol loading concentration, which prevented the fast formation of dendrites and cake on the filter surface and made the downstream fibers more accessible. Similar conclusion was obtained by Tang et al., where higher particle concentrations led to higher increase rate of pressure drop and lower clogging point from the faster formation of dendrites and cake [50]. This point was further proved by the characterization of the deposited particles. As shown in SEM images in Fig. 6.11, more particles exist on the inner fibers of 525-S-3.060-C-3 than 525-S-3.060-C-1 observed from the back side of loaded filters. In contrast to 1-3 h, from 3 to 4 h, there was a great surge in filtration efficiency, which is in accordance with the big increase in the concentration of loading aerosols. Afterwards, the filtration efficiency of 525-S-3.060-C-3 increased with a trend similar to the aerosol loading during 1-3 h of 525-S-3.060-C-1 and 525-S-3.060-C-2. Corresponding to the filtration efficiency, the pressure drop during 3-7 h increased with significantly higher rates than that during 0-3 h, indicating the much faster growth of dendrites. Because more aerosols deposited within the filter, when no aerosol penetration was detected, 525-S-3.060-C-3 had 8.86 gsm of loaded aerosols (at 136.6 Pa), higher than 525-S-3.060-C-1 (6.80 gsm

at 167.8 Pa) and 525-S-3.060-C-2 (7.45 gsm at 170.4 Pa). Through the loading tests for 525-S-3.060-C, aerosol concentrations for loading were shown to affect the loading behaviors of a filter. Nevertheless, the major aim of this study was to investigate the differences in aerosol holding capacities among various test filters. Therefore, aerosols with similar size distribution were used for most loading tests and no further experiments using varied aerosol concentrations were conducted.

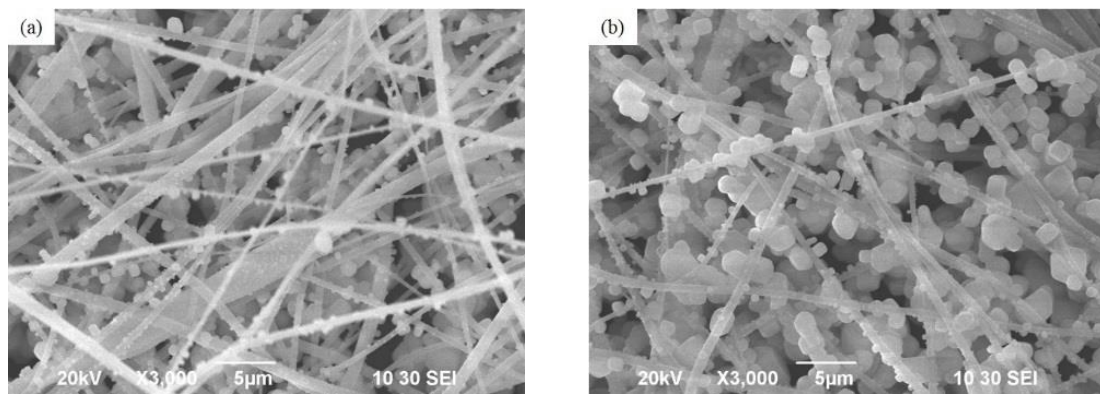


**Fig. 6.11.** SEM images of the back side of loaded (a) 525-S-3.060-C-1 and (b) 525-S-3.060-C-3.

Comparing 525-S-3.060-C-1 (Fig. 6.9a) with 525-S-3.060-U (Fig. 6.4a), the electret filter always had higher filtration efficiency than the uncharged filter with loading time, benefiting from the pronounced electrostatic effect. With same loading time and aerosol concentrations, the aerosol deposition amount was higher for the electret filter owing to the constantly higher filtration efficiency. For instance, at 2 h, 3.69 gsm of aerosols were loaded on 525-S-3.060-C-1 while 2.25 gsm on 525-S-3.060-U. Moreover, the pressure drop of 525-S-3.060-C-1 increased at slightly lower rates than the uncharged filter with loaded mass before zero penetration (i.e. 100% efficiency) was reached. For example, 525-S-3.060-C-1 and 525-S-3.060-U had pressure drop of 64.8 and 63.6 Pa with loaded masses of 2.46 and 2.25 gsm, respectively. This was

attributed by the more uniform distribution of captured aerosols on individual electret fibers than uncharged fibers [7, 16, 18]. That is to say, more aerosols could be captured on the back side of the charged fibers due to dielectrophoretic filtration effect, resulting in slower dendrites formation within 525-S-3.060-C-1. In fact, if we examine the slope of the linear portion that indicates the pressure drop from the cake formed on the nanofiber filter, the S-3.060-C-1 has a lower slope ( $34.0 \text{ Pa gsm}^{-1}$ ), thus a lower pressure drop than that of S-3.060-U ( $39.8 \text{ Pa gsm}^{-1}$ ). The electret filter represents a 17% reduction as compared to the uncharged one. This may have to do with the more porous cake formed on the electret nanofiber media as captured aerosols were distributed on both front and back faces of the fibers. As charged fibers more favored aerosols with large sizes in induction effect, a higher number of large particles were estimated to be trapped on the front side surface of the filter, leaving the cake more porous and permeable [124]. In other words, the skin effect was somewhat reduced, but this advantage can be much fully utilized when the multilayer electret filter was subsequently investigated.

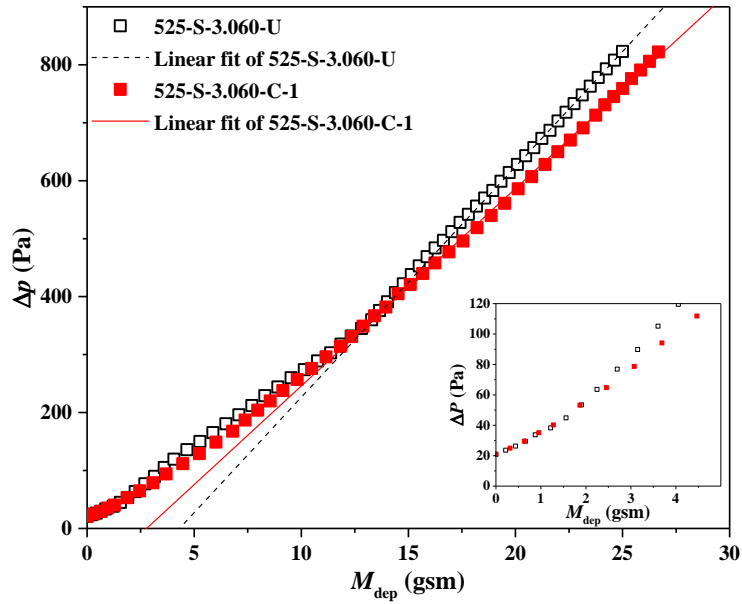


**Fig. 6.12.** Evolution of pressure drop ( $\Delta p$ ) of 525-S-3.060-U and 525-S-3.060-C-1 with loaded aerosol mass.

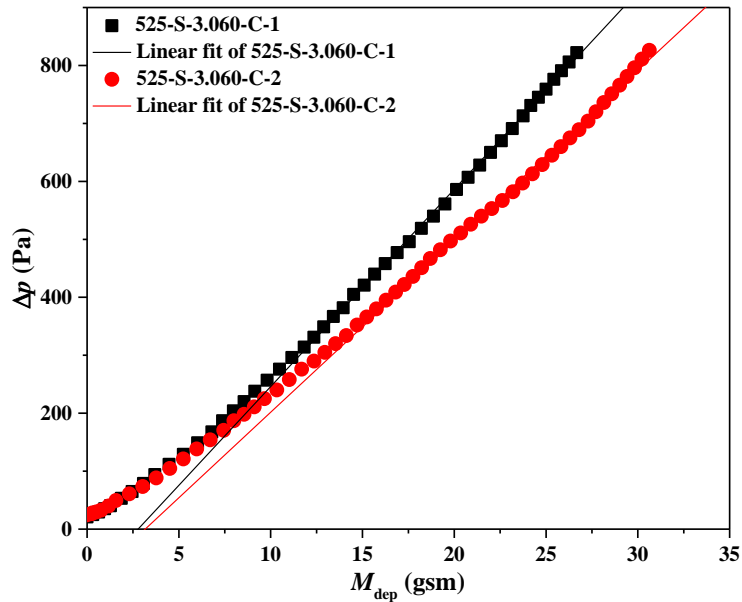


**Fig. 6.13.** Evolution of pressure drop ( $\Delta p$ ) of 525-S-3.060-C-1 and 525-S-3.060-C-2 with loaded aerosol mass.

The pressure drop evolution of 525-S-3.060-C-2 with aerosol loaded mass is also shown in Fig. 6.13. The two filters had similar behavior suggesting the repeatability of

the filter performance. The slope for S-3.060-C-2 is even lower at  $29.5 \text{ Pa gsm}^{-1}$ . As compared to  $39.8 \text{ Pa gsm}^{-1}$ , the reduction in pressure drop of 28% is even more substantial.

### 6.3.2.2. Deposition of aerosols on 1-layer PVDF electret filters

As described in the above section, dielectrophoretic filtration effect facilitated the deposition of aerosols on the back side of individual fibers. This can be proved by the SEM images of loaded filters in Figs. 6.14c-d and Figs. 6.6c-d, where aerosols are present on the back side of fibers of S-3.060-C-1 but almost no aerosols for S-3.060-U were observed from the downstream loading flow.

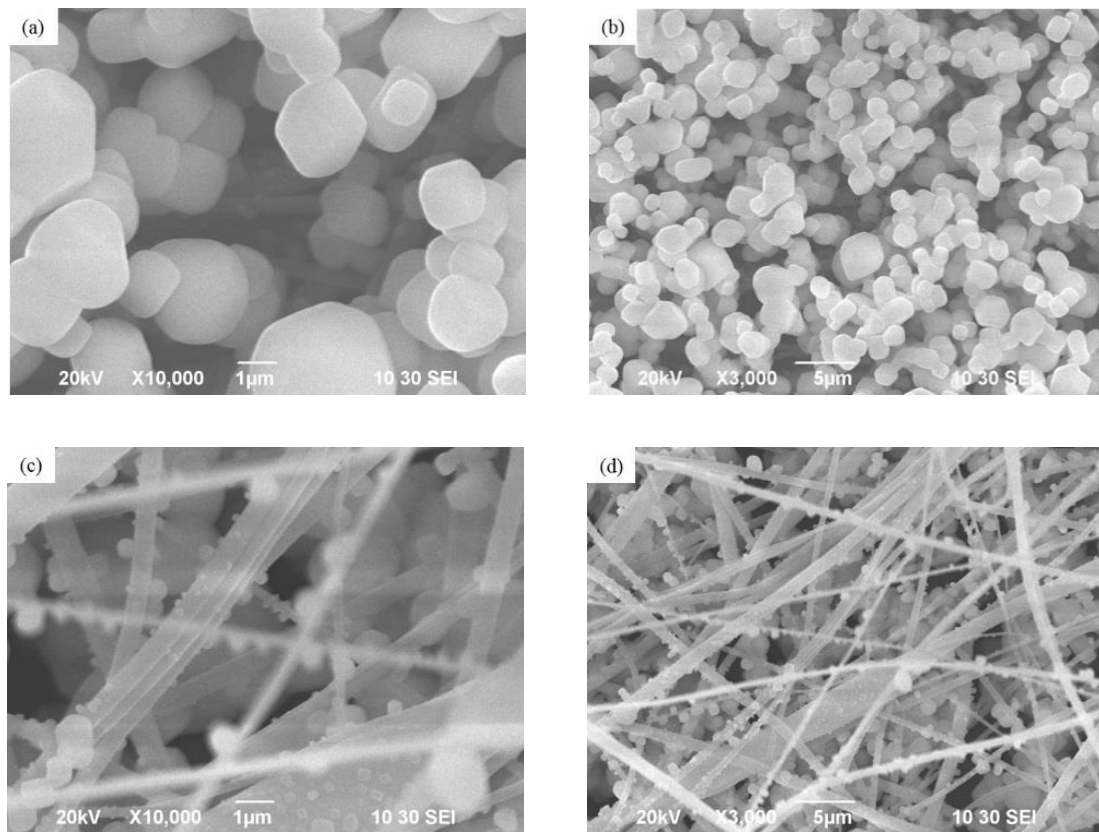


**Fig. 6.14.** SEM images of (a) and (b) the front side and (c) and (d) the back side of loaded 525-S-3.060-C-1.

Given the lower pressure drop during surface filtration for a 1-layer electret

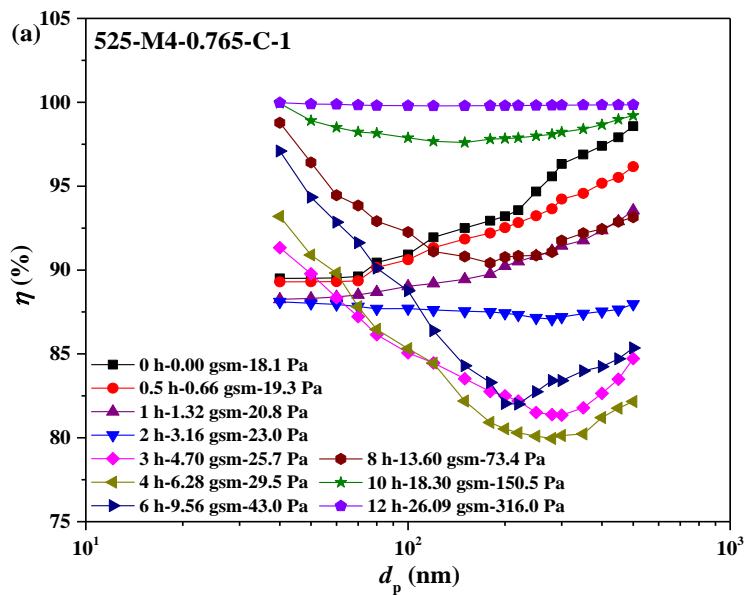
nanofiber filter, than the uncharged 1-layer filter, the issue is whether a different arrangement of the fibers can further facilitate more uniform capture of initial aerosols upstream of the filter that provides a more permeable cake to be formed. As we have seen, if the fiber packing density is not sufficiently low, a cake can form after a short loading period, leaving the charged fibers downstream of the “skin layer” insufficiently used. As shown in Figs. 6.14c-d, not many aerosols can be seen within the loaded 525-S-3.060-C-1 looking through the filter surface facing downstream. Owing to the electrostatic effect, a fraction of the particles penetrating 525-S-3.060-C-1 were attracted by the charged fibers on the backside surface. Nonetheless, most particles had already been trapped in the “skin layer” due to the low porosity and the high initial filtration efficiency, thus only a small number of particles can be observed on the back side of S-3.060-C-1. Based on this, we will explore the multilayer electret filter to investigate if the filter can be fully utilized across the entire filter thickness from upstream to downstream layers by redistributing the charged fibers.

### **6.3.3. Enhanced loading performance of multilayer PVDF electret filters due to both multilayering and charging**

#### **6.3.3.1. Variation of filtration efficiency and pressure drop of multilayer PVDF electret filters with loaded mass**

Since the advantages of multilayering have been shown for the uncharged 4-layer filter in easing the pace of clogging and improving the capability of aerosol holding, compared to the uncharged 1-layer filter with the same basis weight, it is intuitive that the multilayer electret filter would show similar properties. Fig. 6.15a shows the filtration efficiency variation of 525-M4-0.765-C-1 with loading time, where the filter exhibits a clear trend of an initial decrease and a latter continuous increase till near

100%. From 0 h to 2 h, the efficiency values gradually dropped, with more reduction for large particles while insignificant changes for very small ones, which was due to the more prominent electrostatic induction effect towards aerosols with larger diameters [1, 7]. At 3 h, the filtration efficiency curve transferred to a typical shape of a mechanical filter from the curve at 2 h depicting a strong electrostatic mechanism. This means mechanical filtration, mainly by the growing dendrites and cake, began to play a remarkable role in trapping aerosols, especially for the smaller ones (40-60 nm) for which the efficiency increased while that of others were still decreasing during 3-4 h. From 4 h on, after which the enhancement of mechanical filtration exceeded the decline of electrostatic filtration, the filtration efficiency increased at high rates with the slowly decreasing MPPS (Fig. A6.1, Appendix 1), from 80.0% at 280 nm to 99.1% at 150 nm.



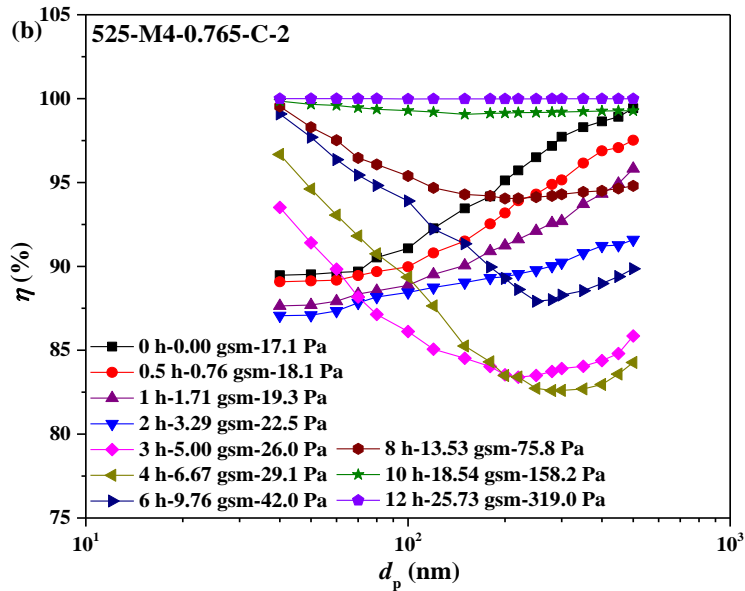


**Fig. 6.15.** Evolution of filtration efficiency ( $\eta$ ) of (a) 525-M4-0.765-C-1 and (b) 525-M4-0.765-C-2 with loading time.

Similar to 525-S-3.060-C-1, benefitting from the electrostatic effect, 525-M4-0.765-C-1 had continuously higher filtration efficiency and aerosol deposited mass than its uncharged counterpart 525-M4-0.765-U before 100% of filtration efficiency. However, the pressure drop of 525-M4-0.765-C-1 was significantly lower than that of 525-M4-0.765-U with similar loaded mass, especially at higher deposition amount. 525-M4-0.765-U and 525-M4-0.765-C-1 had pressure drop of 45.9 and 25.7 Pa with 6.11 and 6.28 gsm of loaded masses, whereas 337.0 and 150.5 Pa with 16.76 and 18.30 gsm, respectively. The prominently alleviated air flow resistance shows that the advantage of charged fibers in uniform aerosol deposition was greatly enhanced through redistributing nanofibers in 525-S-3.060-C-1 into each layer of 525-M4-0.765-C-1. Though 525-M4-0.765-C-1 filtered out more aerosols than 525-S-3.060-C-1 in the initial 1 h due to higher initial filtration efficiency, the captured aerosols accumulated so fast on the surface of the 1-layer electret filter that it progressed to cake filtration in

an extremely short time during which the efficiency of the 4-layer electret filter kept decreasing, leading to higher mass of captured aerosols for 525-S-3.060-C-1 after 1 h until the complete formation of the cake. 525-M4-0.765-C-1 and 525-S-3.060-C-1 had pressure drop values of 18.1 Pa and 21.1 Pa in clean state, respectively. After 1-h loading with similar aerosol loaded masses (1.32 and 1.28 gsm, respectively), the pressure drop of the former filter increased to 20.8 Pa, about half that of the latter (40.2 Pa). With additional 1-h loading, 525-M4-0.765-C-1 had an increase of only 2.2 Pa in air flow resistance with 1.84 gsm added deposit, in contrast to the huge increase of 50.9 Pa for 525-S-3.060-C-1 with an additional 2.41 gsm. When complete filtration was reached on each filter, it took 12 h for the 4-layer filter with 26.09 gsm of loaded aerosols, 9 h longer and 19.29 gsm more than its 1-layer counterpart. The much slower saturation rate demonstrated the merits of multilayering for electret filters. During the loading process of 525-S-3.060-C-1, which had a high fiber packing density, dendrites and cake shielded the filter surface in such a short period that charges as well as fibers within the filter were far from being sufficiently used [50]. In contrast, by separating fibers to different layers, as the surface of the upstream layers was porous enough, the charges on both sides of the fibers in the downstream layers were more accessible to aerosols, thus trapping more aerosols while maintaining a significantly lower increase rate of pressure drop. Besides, different from 525-M4-0.765-U, each layer of 525-M4-0.765-C-1 experienced an initial drop of filtration efficiency, hence facilitating the penetration of more aerosols through the upstream to downstream layers, and consequently more uniform aerosol distribution across the thickness of the electret filter. It is also worth noting that the filtration efficiency kept at relatively high values for particles of all sizes, indicating that aerosol penetration in the initial loading stage was not significant and the filter has a potential for real application.

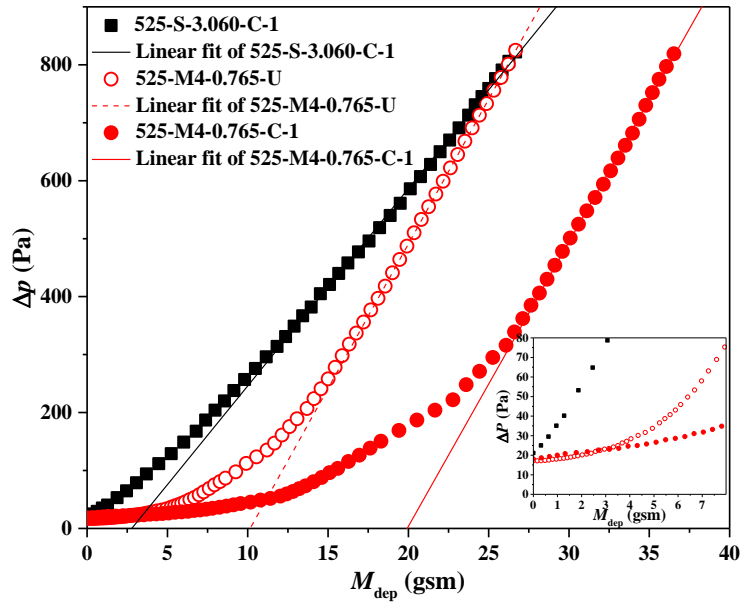


**Fig. 6.16.** Evolution of pressure drop ( $\Delta p$ ) of 525-S-3.060-C-1, 525-M4-0.765-U and 525-M4-0.765-C-1 with loaded aerosol mass.

The pressure drop variation of 525-M4-0.765-C-1 with aerosol deposition mass is depicted in Fig. 6.16. The 4-layer electret filter had a much lower pressure drop than that of the 4-layer uncharged filter and 1-layer electret filter, respectively. This can be explained by the more efficient use of electrostatic effect of the electret filter downstream of the filter surface after multilayering, by which aerosols could not only deposit on the back of fibers but also distributed more uniformly across the filter, therefore reducing the formation and growth rates of dendrites and cake at the upstream layer that catalyze the formation of skin layer.

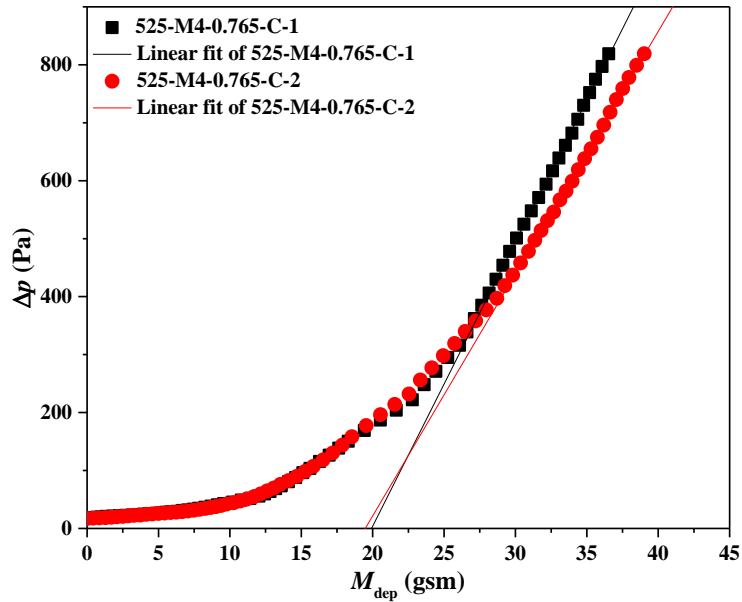


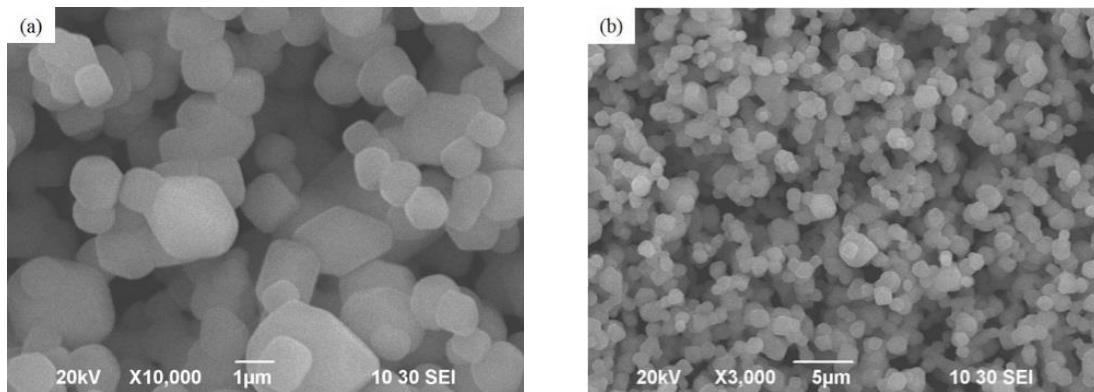
**Fig. 6.17.** Evolution of pressure drop ( $\Delta p$ ) of 525-M4-0.765-C-1 and 525-M4-0.765-C-2 with loaded aerosol mass.

To make a convincing conclusion, another 4-layer electret filter prepared from the same batch was used to repeat the loading process. As shown in Fig. 6.15b and Fig. 6.17, similar result to 525-M4-0.765-C-1 was obtained, indicating the merits of multilayering and charging were reliable instead of being random.

### 6.3.3.2. Deposition of aerosols on multilayer PVDF electret filters

The hypothesis of more sufficient use of charged fibers in the multilayer PVDF electret filter was further proved by SEM images of loaded filters. Fig. 6.18 and Fig. 6.19 respectively show different layers of the loaded 525-M4-0.765-C-1 seen from the front and the back sides. By comparison, more aerosols can be seen depositing on both sides of the fibers of the two middle layers of 525-M4-0.765-C-1 than the fibers deep in 525-S-3.060-C-1 (Figs. 6.14c-d), showing more effective use of charged fibers. Compared with 525-M4-0.765-U (Fig. 6.7), the aerosol deposition across the four layers of 525-M4-0.765-C-1 was more uniform, which was attributed to the role of

electrostatic mechanism in aerosol capture [7, 16, 18, 124]. Moreover, many particles can be seen adhering to the back side of individual fibers in all layers of 525-M4-0.765-C-1 (Fig. 6.19) resulting from the charges distributed there, while nearly no particles can be observed at the similar positions of 525-M4-0.765-U (Fig. 6.8). Besides, it seems that the main size of particles decreases with layer depth for 525-M4-0.765-C-1, while this phenomenon was not found for 525-M4-0.765-U. This can be explained by the relation between the size of uncharged particles and the strength of induction effect by charged fibers. As well known, large particles are prone to charge induction than small particles, so electrostatic mechanism is more pronounced for the capture of aerosols with bigger size [1, 7]. During the loading process of 525-M4-0.765-C-1, larger aerosols were removed more by the first layer and smaller aerosols were more penetrating, resulting in relatively high fractions of smaller-sized aerosols in more downstream layers. In other words, there was a prominent classification effect on particle size with the multilayer electret nanofiber filter.



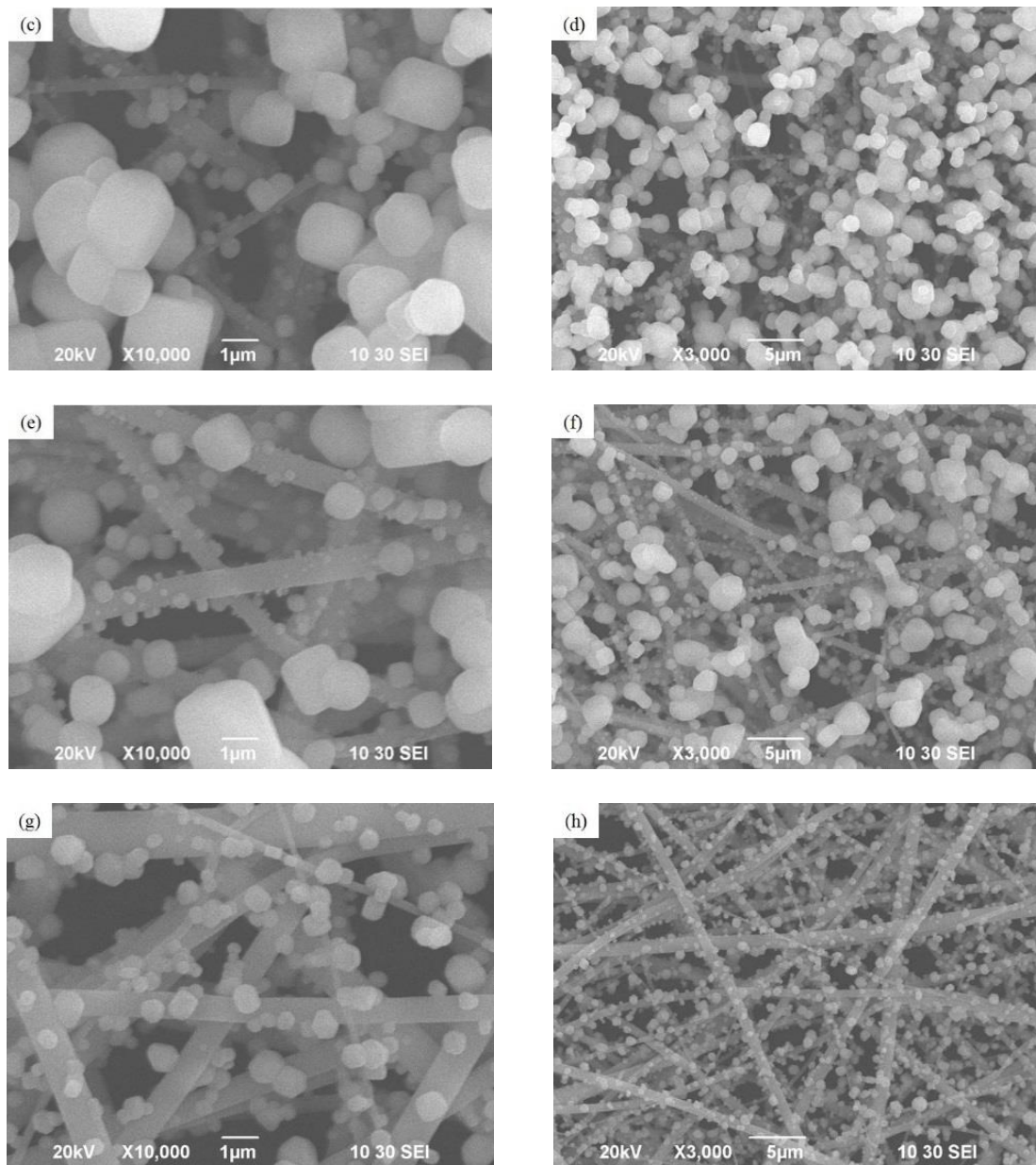


**Fig. 6.18.** SEM images of (a) and (b) the first, (c) and (d) the second, (e) and (f) the third and (g) and (h) the fourth layers of loaded 525-M4-0.765-C-1 seen from the front side.

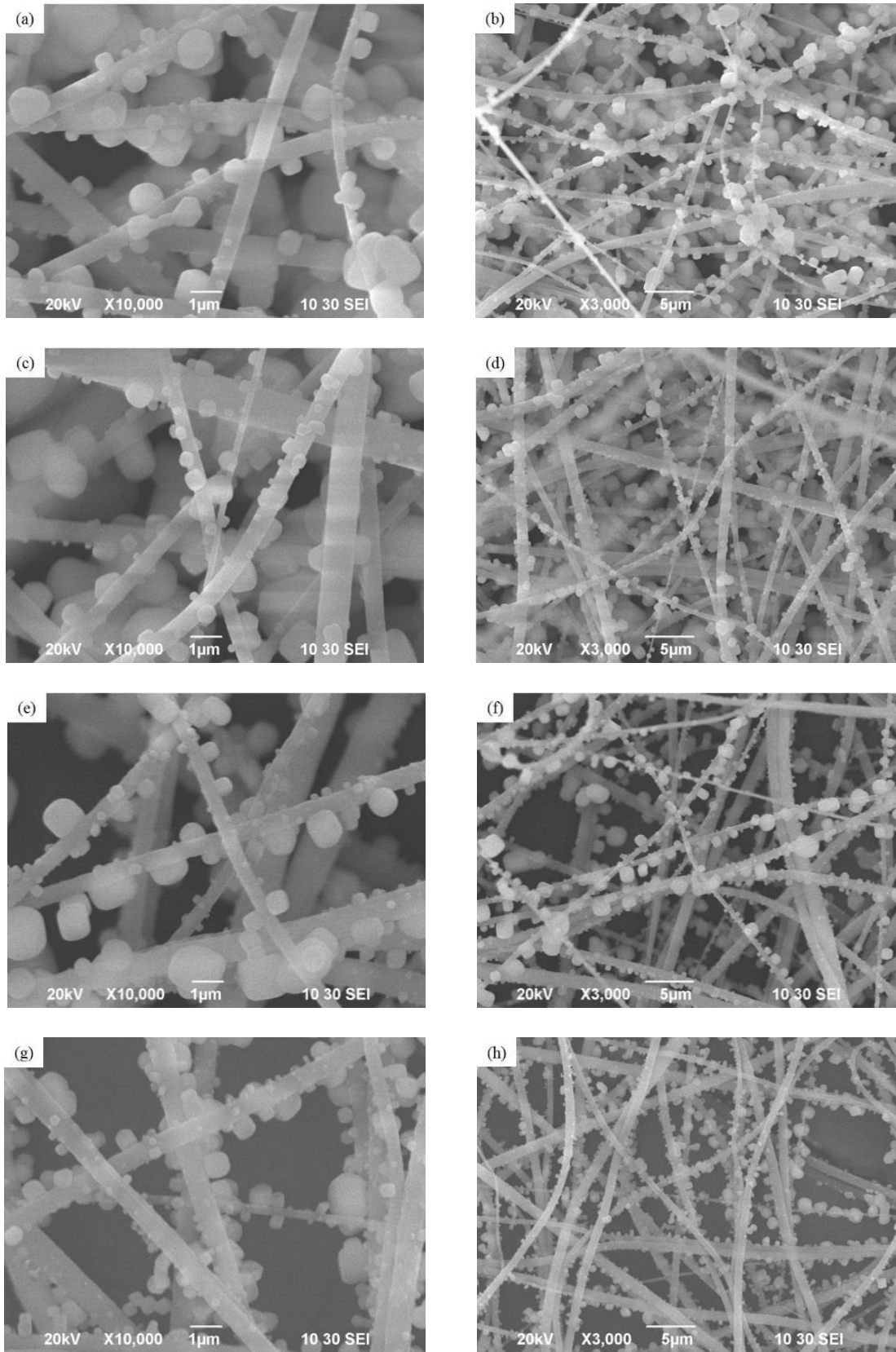


**Fig. 6.19.** SEM images of (a) and (b) the first, (c) and (d) the second, (e) and (f) the

third and (g) and (h) the fourth layers of loaded 525-M4-0.765-C-1 seen from the back side.

#### **6.3.4. Theoretical analyses of filter efficiency, loading capacity and pressure drop**

There are three merits for a loaded filter – high efficiency, low pressure drop, and high aerosol storage capacity per unit filter area. Here, we denote 1-layer uncharged nanofiber filter as SU, 1-layer electret nanofiber filter as SC, 4-layer/multilayer uncharged nanofiber filter as MU, 4-layer/multilayer electret nanofiber filter as MC, and all 4 filters have a total fiber basis weight of 3.060 gsm.

##### **6.3.4.1. Efficiency**

The clean filter efficiency of the SU and MU filters were 45.6-62.7% and 40.1-66.2%, respectively. With longer loading time, the efficiency of the two filters kept increasing until a cake was formed at which the efficiency reached 100%. The SU could attain 80+% efficiency after 1 h of aerosol loading while the MU needed 8 h of loading to attain 80+%. On the other hand, SC had 80.7-88.0% of initial filtration efficiency and achieved 100% after 3 h. Different from the other three filters, MC started at much higher efficiency of 89.5-98.6% and dropped shortly to 80+% due to shielding of the charges but quickly restored back to 100% efficiency when a cake formed on the filter surface.

##### **6.3.4.2. Loading capacity and pressure drop**

It is desirable for a filter to have large aerosol storage capacity but with low incurred pressure drop. The typical pressure drop versus loading for a filter is depicted in Fig. 6.20.

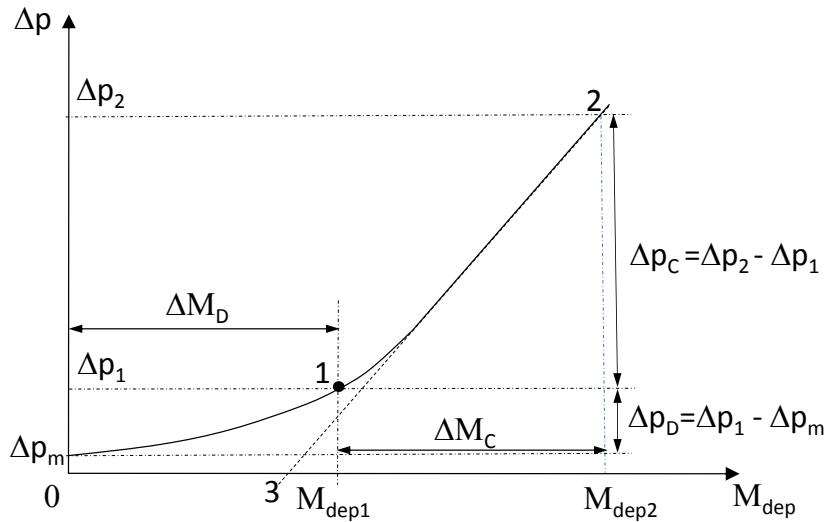


**Fig. 6.20.** Schematic of pressure drop versus aerosol deposit.

With reference to the schematic Fig. 6.20, starting from a clean filter with initial pressure drop  $\Delta p_m$ , there are two regimes of operation: depth filtration followed by cake or surface filtration. During depth filtration, aerosols are trapped and deposited in the filter until it reaches Point 1, where the filter efficiency of all challenging aerosols (i.e. all sizes) reaches 100%, the total deposited mass reaches  $M_{dep1}$ , and the pressure drop has escalated to  $\Delta p_1$ . This point marks the ending of depth filtration and the beginning of surface filtration, where the challenging aerosols are captured and form a cake on the filter surface. The cake becomes the effective filter media and its thickness keeps growing with more aerosol deposition. The pressure drop,  $\Delta p$ , continues to build up and eventually a “structured cake” forms on the filter surface with approximately constant permeability or resistivity, which can be determined from the slope of the linear portion of the  $\Delta p$  escalation curve. Once the pressure drop of the entire filter reaches Point 2 in Fig. 6.20, with an arbitrary set maximum pressure drop,  $\Delta p_2$ , the filtration operation stops and the loaded filter needs to be replaced or regenerated. The following interesting issues arise:

1) Which filter among the four filters has the maximum aerosol deposit at the end of the filtration as imposed/set by the maximum pressure drop  $\Delta p_2$ ?

2) For each filter, how much aerosol is deposited during depth and cake filtration, respectively?

3) What is the pressure drop in depth and cake filtration, respectively?

4) What is rate of change of pressure drop with additional mass deposit during cake buildup [125]?

Table 6.1 summarizes the essential values for the four filters – SU, MU, SC and MC that address the above questions. Obviously, given the total pressure drop increase is set as  $\Delta p_2 - \Delta p_m$ , it is desired to have a small pressure rise gradient in the depth filtration  $(\Delta p_1 - \Delta p_m)/\Delta M_D (= \Delta p_D/\Delta M_D)$  and in cake filtration  $(\Delta p_2 - \Delta p_1)/\Delta M_C (= \Delta p_C/\Delta M_C)$ . Both are determined for the four filters in Table 6.1. Unfortunately, we typically have a small slope in one regime (e.g. depth filtration) but a much larger slope in another regime (e.g. cake filtration) and vice versa, but not in both regimes. The goal is to maximize the total aerosol deposit in the filter in both depth filtration  $\Delta M_D$  as well as cake filtration  $\Delta M_C$ . This will be apparent in the following parts.

**Table 6.1.** Pressure drop and deposit mass during depth and cake filtration

Filter media		Depth filtration (1) End of depth filtration (100% efficiency)					Cake or surface filtration (2) End of cake filtration (reach $\Delta p_2 = 800$ Pa)							Clogging point (gsm)
Name	$\Delta p_m$ (Pa)	$\Delta M_D$ (gsm)	$\Delta p_1$ (Pa)	$\Delta p_D =$ $(\Delta p_1 - \Delta p_m)$ (Pa)	$\Delta p_D/\Delta M_D$ (Pa gsm <sup>-1</sup> )	$\Delta t$ (h)	$\Delta M_D + \Delta M_C$ (gsm)	$\Delta M_C$ (gsm)	$\Delta p_C =$ $(\Delta p_2 - \Delta p_1)$ (Pa)	$\Delta p_C/\Delta M_C$ (Pa gsm <sup>-1</sup> )	Slope (Pa gsm <sup>-1</sup> )	$\Delta M_C$ $/(\Delta M_D + \Delta M_C)$	$\Delta p_C$ $/(\Delta p_2 - \Delta p_m)$	
SU	20.8	6.5	180.5	159.7	24.6	4	24.4	17.9	619.5	34.6	39.8	73.4%	79.5%	4.3
SC	21.1	6.8	167.8	146.7	21.6	3	26.4	19.6	632.2	32.3	34.0	74.2%	81.2%	2.8
MU	17.1	16.8	337.0	319.9	19.1	14	26.4	9.6	463.0	48.2	49.9	36.4%	59.1%	10.2
MC	18.1	26.1	316.0	297.9	11.4	12	36.5	10.4	484.0	46.5	49.0	28.5%	61.9%	19.9

#### 6.3.4.2.1. SU and SC

Both SU and SC had a short (3-4 h) depth filtration as a skin formed quickly upstream of the filter layer, leaving the downstream layers of the filter not fully utilized for aerosol capture. This has been discussed and confirmed previously by the SEM images. Interestingly, the total mass deposit in depth filtration from the electret filter SC was actually 6.8 gsm, 0.3 gsm more than the uncharged filter SU with deposit of 6.5 gsm; yet  $\Delta p_1$  was slightly lower at 167.8 Pa for SC versus 180.5 Pa for SU. This was all courtesy of the electrostatic mechanism in assisting capture of the aerosols forming a more porous aerosol deposit structure inside the filter, with perhaps lowered skin effect. In subsequent cake filtration, 17.9-19.6 gsm of aerosols were deposited in form of a cake, the higher deposit was attributed to SC despite there was no added electrostatic force due to complete shielding of the charged fibers in the filter by the cake, but the cake formed from the electret filter was found to have a more porous structure. The pressure drop for cake filtration was higher for SC versus SU, 632.2 Pa versus 619.5 Pa, but the rate of increase of pressure drop per additional deposit,  $\Delta p_C/\Delta M_C$ , is actually lower at 32.3 Pa gsm<sup>-1</sup> for SC versus 34.6 Pa gsm<sup>-1</sup> for SU. This indeed supports the assumption that the formed SC cake was more porous and permeable. A more direct measure on the pressure drop per deposit mass is obtained from the slope of the graph in Fig. 6.12. As seen in Table 6.1, SC gives a slope of 34.0 Pa gsm<sup>-1</sup> while SU gives 39.8 Pa gsm<sup>-1</sup>. Based on these considerations in both depth and cake filtration, the SC filter is better than the SU filter. Interestingly, the clogging point (Point 3 in Fig. 6.20) has been suggested for evaluating the filter clogging during cake formation. The clogging point is a hypothetical point wherein the aerosol loading in the filter during depth filtration is replaced by a hypothetical clogging point

corresponding to an initial deposition in the filter at equivalent zero pressure drop. Simply put, it is an extrapolation of the “cake line” extending to zero  $\Delta p$ . Based on this, the clogging points for the 4 filters are determined in Table 6.1 for SC as 2.8 gsm and SU as 4.3 gsm. From the clogging point consideration, it appears that the SC filter was more clogged during depth filtration than SU which is incorrect! As can be seen in Table 6.1, the average  $\Delta p_D/\Delta M_D$  is 21.6 Pa gsm<sup>-1</sup> for SC which is lower than 24.6 Pa gsm<sup>-1</sup> for SU. This casts a shadow of doubt on the use of the clogging point as an index for comparison between filters. In fact, what is important is the rate of increase, i.e.  $\Delta p_D/\Delta M_D$ , between the two filters as demonstrated herein.

#### **6.3.4.2.2. MU and MC**

The MU allows a better utilization of the filter trapping more aerosols not only in the upstream layers but also in the downstream layers as compared to SU. This is even more so when the nanofiber filter is charged. As a result, from Table 6.1, 16.8 gsm of aerosols had been captured in depth filtration for MU during depth filtration. On the other hand, MC had 55.4% more trapped aerosols reaching 26.1 gsm. This is courtesy of the charged fibers that trapped aerosols on all faces of the fiber in addition to interception mechanism. Further, all the layers across the entire filter depth from upstream to downstream layers were fully utilized for capturing aerosols. This provides a good combat against the skin effect which affects greatly the 1-layer electret/uncharged filters and also the multilayer uncharged filter to some extent. Given the aerosols are uniformly distributed across the filter, the pressure drop,  $\Delta p_1$ , is 6.2% lower at 316.0 Pa for MC as compared to 337.0 Pa for MU despite it had more aerosols trapped. In fact, the average  $\Delta p_D/\Delta M_D$  for MC is indeed very low at 11.4 Pa gsm<sup>-1</sup> while that of MU is 19.1 Pa gsm<sup>-1</sup>. In subsequent cake filtration, the pressure drop rose very

steeply with increasing deposit. Such steep rise was attributed to the fact that a cake was formed on a filter with both PVDF fibers as well as deposit trapped in the filter that acts also like artificial fibers [120]. This is equivalent to a filter with higher fiber packing density which results in an impervious cake with high pressure drop to fluid flow. Indeed, in surface filtration the MU filter had a further increase in  $\Delta p$  of 463.0 Pa for a 9.6-gsm cake, while MC had an increase in  $\Delta p$  of 484.0 Pa for a 10.4-gsm cake. In fact,  $\Delta p_C/\Delta M_C$  is 48.2 Pa gsm<sup>-1</sup> for MU and is greater than 46.5 Pa gsm<sup>-1</sup> for MC, given the skin effect for the latter was being reduced. Despite both pressure-drop increase is much higher than their counterparts – the 1-layer filters, cake filtration duration for the multilayer filters was shorter. From Table 6.1, only 28.5% of aerosol deposit was attributed to cake filtration for MC and 36.4% for MU. This demonstrates cake filtration was indeed short for the multilayer filters. This is actually favorable, otherwise the pressure escalation could be extremely high in cake filtration taking away the earlier benefit of depth filtration where most aerosols were deposited.

In contrary, it is the reverse for 1-layer uncharged and electret filter. From Table 6.1, 74.2% of aerosol deposit is attributed to cake filtration for SC and 73.4% for SU. Majority of the deposit were made during cake filtration for the 1-layer uncharged and electret filters, as a skin formed very fast upstream of the filters that quickly changed over to cake filtration. The multilayer filters (MC and MU) had a long depth filtration period with short steep pressure gradient in cake filtration, whereas the 1-layer filters (SC and SU) had short depth filtration (not fully utilizing the downstream fibers) with milder pressure rise in cake filtration. The behavior of these 4 filters are rather “polarized” but the ultimate question is which filter have the highest capacity for trapping and storing aerosols when a pressure limit is imposed on the filtration cycle.

In the present study, the pressure limit was set at 800 Pa, which was similar to our early investigation [22]. Overall, with a maximum pressure drop of 800 Pa for the filter operation, MC had a total capacity of 36.5 gsm, both MU and SC had equal capacity of 26.4 gsm, and SU had 24.4 gsm. (Note the media resistance for all 4 filters in their clean state was within a narrow range between 17.1 and 21.1 Pa, see Table 6.1.) We summarize both efficiency and capacity results for the 4 filters in Table 6.2 based on a maximum pressure drop of 800 Pa. In order of descending performance based on efficiency and capacity, MC is the best followed by SC, then MU, and finally SU. The two electret filters are better than their uncharged counterparts. MC has 49.6% more storage capacity than SU, and it has also 38.3% more capacity than both SC and MU. Note, the clogging point that is used for assessing loading of filters does not provide meaningful interpretation on the capacity nor pressure drop in our present filter study despite we also include their values in Table 6.1 for reference.

**Table 6.2.** Ranking of 4 filters based on maximum pressure, efficiency and capacity

<b>Ranking</b>	<b>Filter</b>	<b>Efficiency (%)</b>	<b>Capacity (gsm)</b>	<b>Capacity ratio</b>	<b>Capacity ratio</b>
1	MC	80-100%	36.5	1.50	1.38
2	SC	80-100%	26.4	/	1
3	MU	40-100%	24.4	1	/
4	SU	40-100%	24.4	1	/

## 6.4. Summary

Comparative experiments were conducted to investigate the differences of aerosol loading behaviors between 1-layer and multilayer filters and uncharged and electret filters. Distinctive results were acquired and analyzed, which led to several points listed

below:

1) With loaded aerosol mass, the filtration efficiency of uncharged filters increased, while that of electret filters initially decreased and then increased until reaching 100%. Nonetheless, the electret filters always had higher efficiency than the uncharged counterparts before a complete cake was formed on the filters.

2) For the electret filters during the initial stage of aerosol loading, the deposited aerosol influenced the capture efficiency of particles by the shielding of electrostatic and the growing mechanical filtration effects, with larger particles more affected by the variation of the former effect.

3) In uncharged state, the 1-layer filter had a lower aerosol holding capacity than the multilayer filter with the same basis weights, due to the quick formation of “skin layer” from the low filter porosity and the initial high filtration efficiency.

4) For the 1-layer filter, though the pressure drop was reduced after charging before the complete cake formation, the holding capacity of the electret filters was lower than that of the uncharged counterparts due to the short initial loading stage from the low filter porosity and the high initial filtration efficiency, thus forming the “skin aerosol layer” faster and leaving most downstream charged fibers insufficiently utilized. However, once a cake layer was formed, the cake had a lower pressure drop for the 1-layer electret filter than the 1-layer uncharged filter. The cake on the surface of the electret filter appears more permeable.

5) Combining the advantages of multilayering and charging, the multilayer electret filter had the best aerosol holding capacity and the highest aerosol distribution uniformity, which was further enhanced by the more sufficient use of charges on individual fiber across the entire filter depth/thickness. Under the same loading

conditions with a maximum pressure drop of 800 Pa, filter performance based on efficiency and capacity is in the descending order of:

- a) multilayer electret filter
- b) 1-layer electret filter
- c) multilayer uncharged filter
- d) 1-layer uncharged filter

6) The multilayer filters had ~70% aerosols trapped in the filter and ~30% trapped in the cake, while the 1-layer filters had ~30% aerosols trapped in the filter and ~70% trapped in the cake.

7) The 4-layer electret nanofiber filter with 3.060-gsm basis weight had 52% more aerosol holding capacity than the 1-layer uncharged nanofiber filter. It had also 38% more aerosol holding capacity than the 1-layer electret nanofiber filter as well as the 4-layer uncharged nanofiber filter.

## Chapter 7: Conclusions and Suggestions for Future

### Research

#### 7.1. Conclusions

In this study, the properties of multilayer PVDF electret filters for the removal of micron- and nano-aerosols were systematically and thoroughly investigated. Defect-free fibrous PVDF filters were fabricated successfully by the great effort of trial and error before use. Their excellent filtration performances were then verified through the batches of comparative tests and data analyses. After confirming the superiority of these filters, their potential for real environment application was also proved. Based on the merits of multilayer PVDF electret filters in short-term filtration, their outstanding long-term filtration quality was further demonstrated from the results of heavy aerosol loading. Overall, the main findings of this study are summarized as follows:

##### 1) Fabrication of PVDF filters

To spin all PVDF filters with good morphology, the PVDF solution properties (e.g. polymer molecular weight, solution concentration, solvent composition and additive agents) and the electrospinning conditions (e.g. spinning voltage, needle-to-collector distance, temperature and humidity) should be finely tuned. Usually, the targeted filter characteristics can not be obtained by simply changing one single parameter due to the complexity of electrospinning. Instead, several parameters should be coordinately adjusted to get the desired filters.

For the fabrication of PVDF electret filters, a higher charging voltage or a shorter charging distance is not necessarily better for improving filtration performance, because of the limited charge traps, the unevenness of charge distribution or the

potential of electrical breakdown. The two parameters should be set at values within proper ranges.

## 2) Filtration properties of PVDF filters

PVDF filters have superior chargeability and their filtration performance can be greatly enhanced after charging. However, purely increasing charged fiber amount can only lead to diminishing increases in filtration efficiency owing to the electrical interference between adjacent fibers. What is worse, because of the high fiber packing density, impractically high pressure drop is incurred, which makes the benefit-to-cost ratios much lower. On the contrary, without changing the filter basis weight, redistributing the fibers from a 1-layer filter into a multilayer filter can not only weaken the electrical interference and make individual charged fibers more efficiently used, but also alleviate the air flow resistance by increasing filter porosity. The result of multilayering is the significantly improved quality factors, which can be as high as  $0.18 \text{ Pa}^{-1}$ , while the highest value of the 1-layer electret filter does not reach  $0.1 \text{ Pa}^{-1}$ .

Dielectrophoretic filtration effect plays the main role in aerosol capture enhancement using PVDF electret filters confirmed through single fiber efficiency analysis, which especially benefits large particle attributed to larger induced dipole. The single fiber efficiency is proportional to the Cunningham slip factor and the square of the aerosol size raised to the power of 0.4. Multilayering can help maintain the single fiber efficiency of electret filters at high levels, while 1-layer electret filters tend to have low values.

The PVDF electret filters have superior charge stability. After initial fast decay, the surface potential can remain relatively unchanged in 90 days and there is only

insignificant drop in filtration efficiency of the multilayer filters, which proves the high potential for long-term storage.

### 3) Optimization of multilayer PVDF electret filters

When the aim is to find optimized PVDF electret filters, filtration efficiency and quality factor should both be considered as effectiveness and efficientness are equally important for filters. Like mechanical filters, electret filters can have high filtration efficiency when fiber diameter is overwhelmingly low or filter basis weight is intensely high, where the costs are inefficiently high pressure drop and low quality factors. On the other hand, quality factors of an electret filter can be much higher than  $0.1 \text{ Pa}^{-1}$  when filter basis weight is markedly low due to low pressure drop, but the result is ineffective removal of aerosols.

High dielectrophoretic filtration efficiency does not guarantee high filtration performance of the 1-layer PVDF electret filters. The relative importance of dielectrophoretic filtration effect over mechanical filtration effect is found to be the key factor for filter performance improvement. Therefore, a proper filter basis weight is needed to not only ensure enough electrostatic effect but also to avoid excessive mechanical effect. In this study, the filter 525-S-0.765-C with the highest quality factor is chosen as the module layer to compose multilayer PVDF electret filters. The 6-layer PVDF electret filter with a mean fiber diameter of 525 nm and a basis weight of 4.590 gsm is determined as the optimized filter. It has a filtration efficiency value of 98.3% and a quality factor of  $0.156 \text{ Pa}^{-1}$  for aerosols of 300 nm. Moreover, the pressure drop of the optimized filter is only 26.2 Pa, indicating the high potential for further improvement in filtration performance.

### 4) Performance of multilayer PVDF electret filters in real environment

Multilayer PVDF electret filters can work well in real aerosol-laden environment and have promising prospect for real applications. Although the oily aerosols and the humid air are detrimental to the electret filters, high filtration efficiency and quality factors can still be achieved. The efficiency of aerosols of 36.87-433.7 nm follows the same trend as that of the tests using lab-generated aerosols, where the efficiency increases with aerosol diameter attributed to the stronger dielectrophoretic filtration effect on large particles. Aerosols with lower sizes are largely removed thanks to the dominant diffusion effect which is independent of electrostatic effects.

#### 5) Loading behaviors of PVDF filters

Similar to literature, with aerosol loading, pure mechanical PVDF filters have continuously increasing filtration efficiency, while PVDF electret filters have initially decreasing and subsequently increasing filtration efficiency until reaching 100%. Nevertheless, the filtration efficiency of PVDF electret filters is higher than that of the uncharged counterparts before the complete formation of aerosol cake. The efficiency variation of the electret filters in the first stage of loading is caused by the shielding of electrostatic effect and the growing mechanical filtration effect from the deposited aerosols.

Multilayer PVDF filters can significantly slow down the pace of filter clogging and elevate the aerosol holding capacity through more sufficient utilization of downstream fibers. The multilayer filters have most of the captured aerosols trapped in the filter, while the 1-layer filters in the cake. Moreover, by charging fibers, the aerosols deposit on both sides of charged fibers and distribute more uniformly, leading to slower growth of dendrites. However, simply charging a 1-layer filter with a relatively high basis weight and thus high initial filtration efficiency can only insignificantly improve its

aerosol loading performance because an aerosol cake will quickly form on the filter surface, leaving most downstream fibers insufficiently used. Multilayering, on the contrary, for both mechanical and electret filters, can delay dendrites linkage and surface cake formation and make the downstream fibers more accessible. Summarily speaking, charging and multilayering improve the aerosol distribution on the individual fibers and across the filter, respectively. Under the same loading conditions with a maximum pressure drop of 800 Pa, filter performance based on efficiency and capacity is in the descending order of multilayer electret filter, 1-layer electret filter, multilayer uncharged filter and 1-layer uncharged filter.

To conclude, multilayer PVDF electret filters possess excellent filtration performance for both short-term and long-term aerosol filtration, as well as high stability during storage. They have a great potential for commercial use in the fields of personal health care and environmental protection.

## **7.2.Suggestions for future research**

In this study, the application potential of multilayer PVDF electret filters was investigated and some positive results were obtained. Nevertheless, more work can be done to investigate filter behaviors in depth. The suggestions for future work are listed as below:

- 1) Improve surface potential of electret filters by modifying the charging device

Although the filtration performance of PVDF filters was improved after charging using the home-made corona discharge device, the filter surface potentials were relatively low even with the optimized charging condition. This drawback seriously limits further improvement in filtration efficiency. The charging device should be

modified, maybe through inserting a metal grid between the two electrodes or adding a heating/freezing unit for filters, to achieve higher surface potentials. By doing this, the efficiency of PVDF electret filters can be greatly enhanced with fewer fibers and lower pressure drop.

2) Find a model to show the interference between charged fibers

The improved filtration efficiency after redistributing charged fibers into multiple layers was suggested to be caused by the reduced electrical interference between adjacent fibers. Nevertheless, this was only indirectly proved by the higher single fiber efficiency. It would be best if a model is created to simulate the electric field in an electret filter and the electrostatic force a neutral particle experiences when approaching the filter. By doing this, the mechanism proposed in this study will be further confirmed.

3) Test filter efficiency in real time instead of at intervals

During aerosol loading in this study, filtration efficiency of filters for aerosols with a wide size range were acquired at long intervals, because it would take impractical long time if the measurement was taken constantly. The aim of testing the efficiency for aerosols of a range was to study the variation of MPPS. However, the detailed variation of filtration efficiency with loaded aerosol mass was not obtained. To get a clearer efficiency evolution, aerosols with a certain size can be selected for efficiency test at intensely short intervals to have more data points.

4) Establish the relationship between filter properties and aerosol holding capacity

This study found that filter porosity and charging state could affect the aerosol holding capacities of filters. But the exact relationship between filter physical properties and aerosol holding ability was not established. More work needs to be done to

investigate the change of clogging point with varied parameters, including fiber diameter, filter porosity, filter thickness, aerosol size and filter charge density. Hopefully, an empirical equation can be derived, which helps to predict the aerosol holding capacities of other electret filters.

#### 5) Real-time monitoring of the processes of dendrites and cake formation

In this study, as well as in literature, the images of loaded aerosols were always taken after the loading processes finished in case of filter destruction brought by sampling. These images only showed dendrites or cake at a certain stage of loading, instead of the whole formation process. Besides, preparing samples of loaded filters will inevitably damage the structures of aerosol aggregates to some extent, however carefully the preparation is done. This means the images obtained may not reflect the real properties. Although some efforts have been made to simulate the trajectories of aerosol deposition and the formation of dendrites on filters, the reliability of the simulations still needs to be verified. Therefore, new technologies should be developed to monitor aerosol movement and deposition in real time, which will also facilitate the interpretation of filtration efficiency variation during aerosol loading.

#### 6) Influences of pre-treatment and post-treatment on filtration performance

Since filters are exposed to real environment when applied as face masks, performance of filters tends to be affected by various conditions. It is of necessity that filtration tests are carried out after treatment using physical methods (e.g. heating or UV radiation) and chemical methods (e.g. immersion in water or organic solvents) to test the resistance of filters.

Alternatively, these treatment methods can be investigated to disinfect filters or restore filter performance after the filters are used for a relatively long time, especially when personal protective equipment is in short supply in many countries during a pandemic.

# Appendices

## Appendix 1. - Figures



**Fig. A3.1.**Electrospinning apparatus used for spinning PVDF fibrous filters in this study.

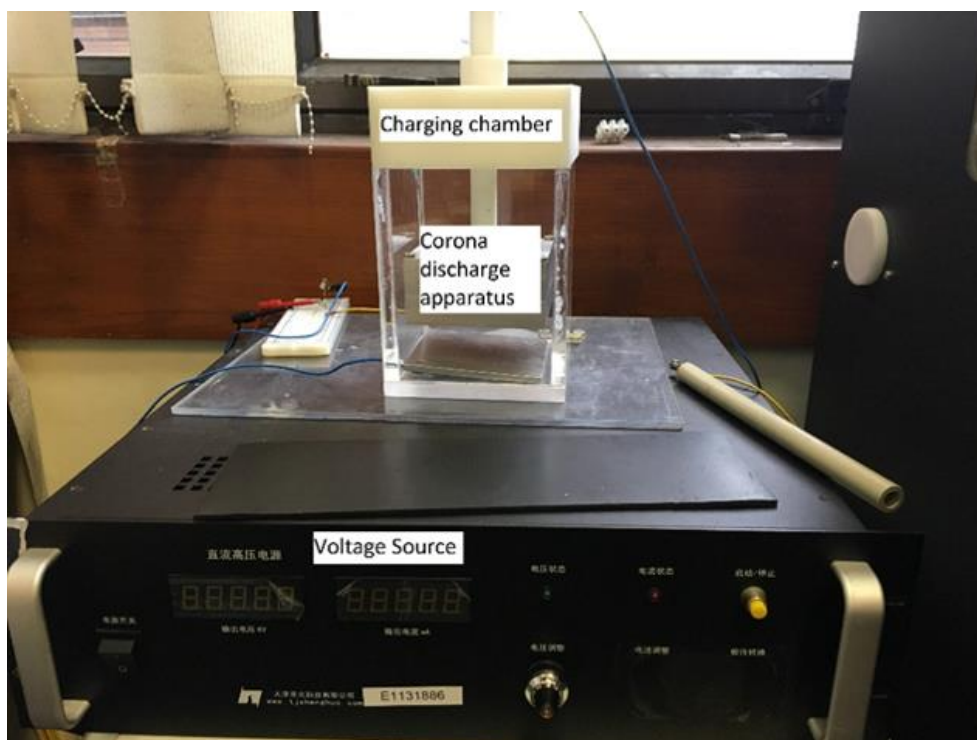


**Fig. A3.2.** Corona discharge set-up used for charging PVDF filters in this study.



**Fig. A3.3.** Apparatus for surface potential (SP) tests in this study.

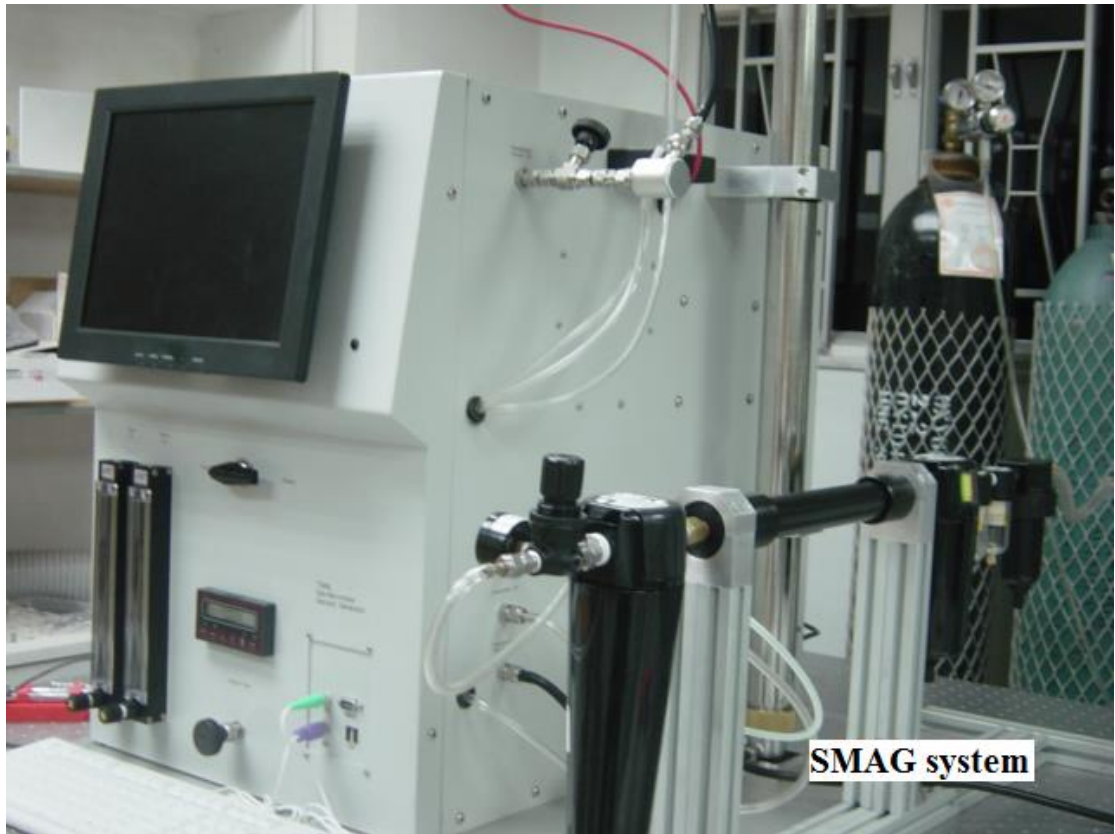


**Fig. A3.4.** SMAG system used for aerosol filtration tests and loading of filters in this study.

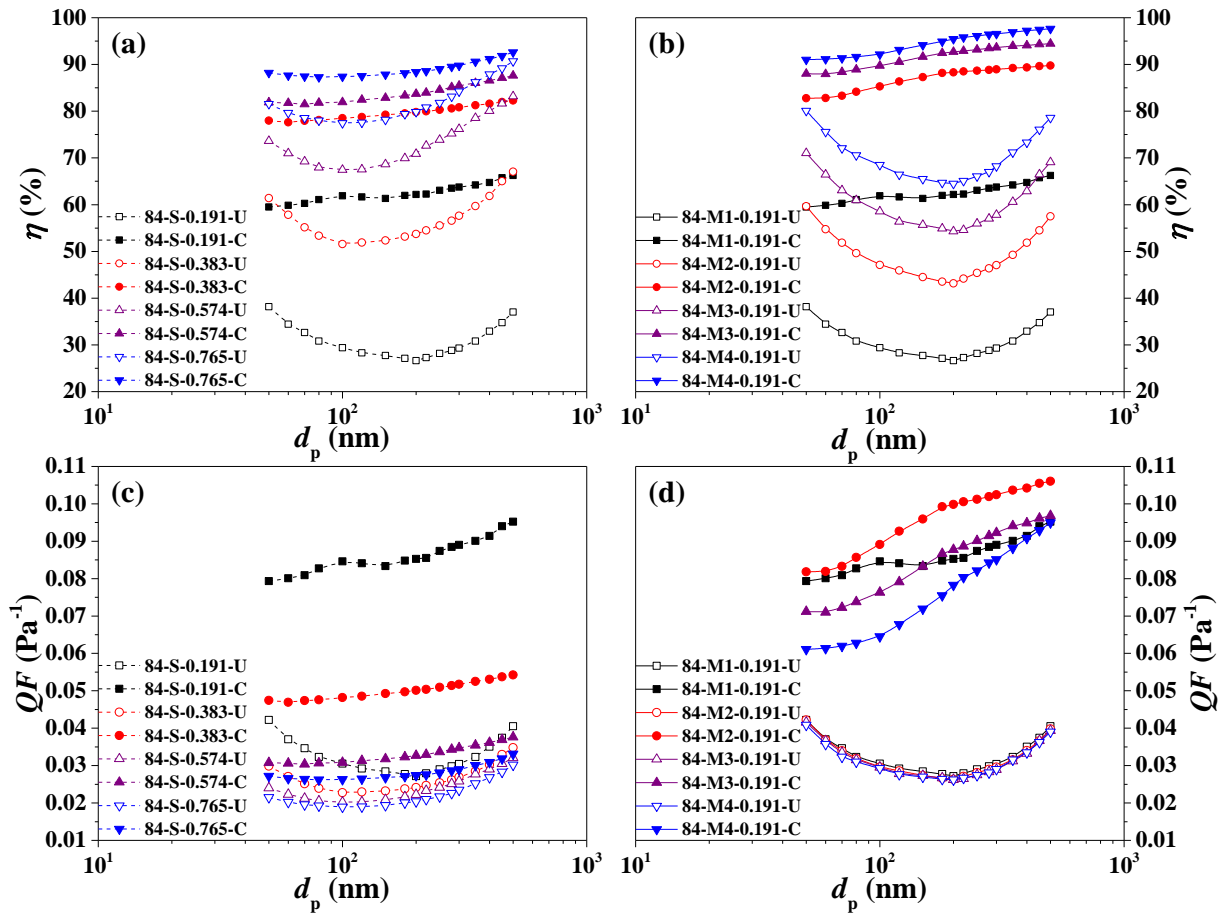


**Fig. A4.1.** Filtration efficiency ( $\eta$ ) of 84-nm (a) 1-layer and (b) multilayer PVDF filters; quality factors ( $QF$ ) of 84-nm (c) 1-layer and (d) multilayer PVDF filters. (Filters were in uncharged or charged state with varied layer filter weights. Note 84-S-0.191 and 84-M1-0.191 denote the same filter.)

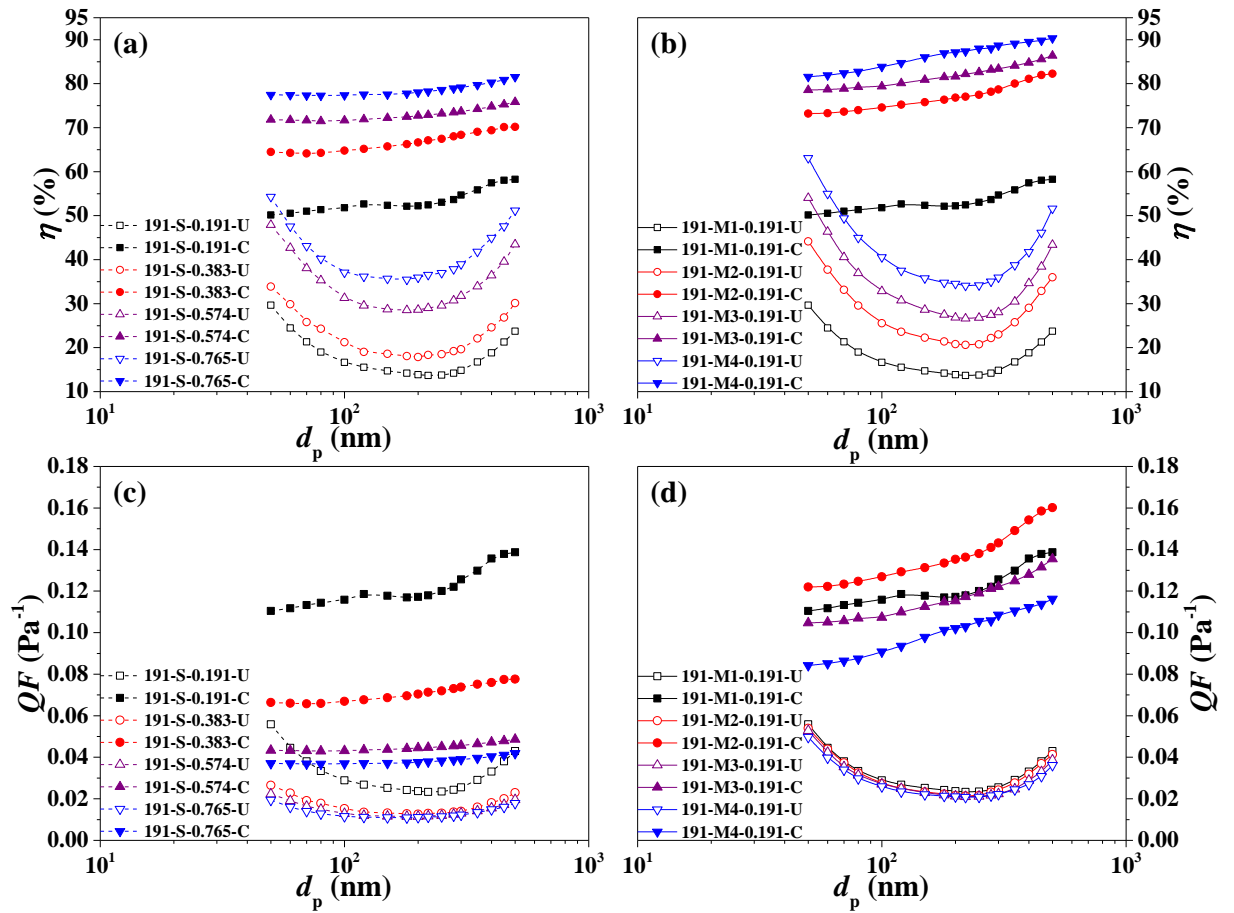


**Fig. A4.2.** Filtration efficiency ( $\eta$ ) of 191-nm (a) 1-layer and (b) multilayer PVDF filters; quality factors ( $QF$ ) of 191-nm (c) 1-layer and (d) multilayer PVDF filters. (Filters were in uncharged or charged state with varied filter basis weights. Note 191-S-0.191 and 191-M1-0.191 denote the same filter.)

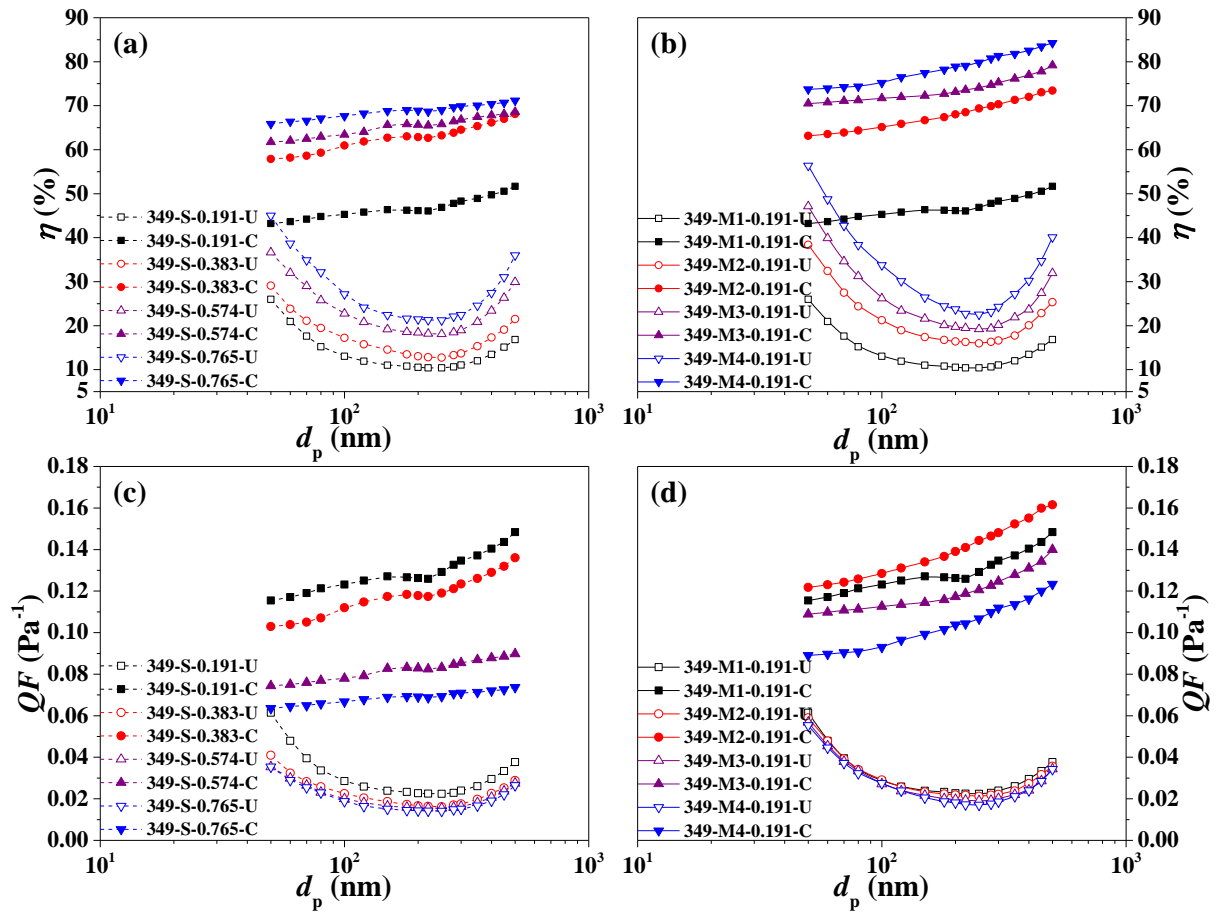


**Fig. A4.3.** Filtration efficiency ( $\eta$ ) of 349-nm (a) 1-layer and (b) multilayer PVDF filters; quality factors ( $QF$ ) of 349-nm (c) 1-layer and (d) multilayer PVDF filters. (Filters were in uncharged or charged state with varied filter basis weights. Note 349-S-0.191 and 349-M1-0.191 denote the same filter.)

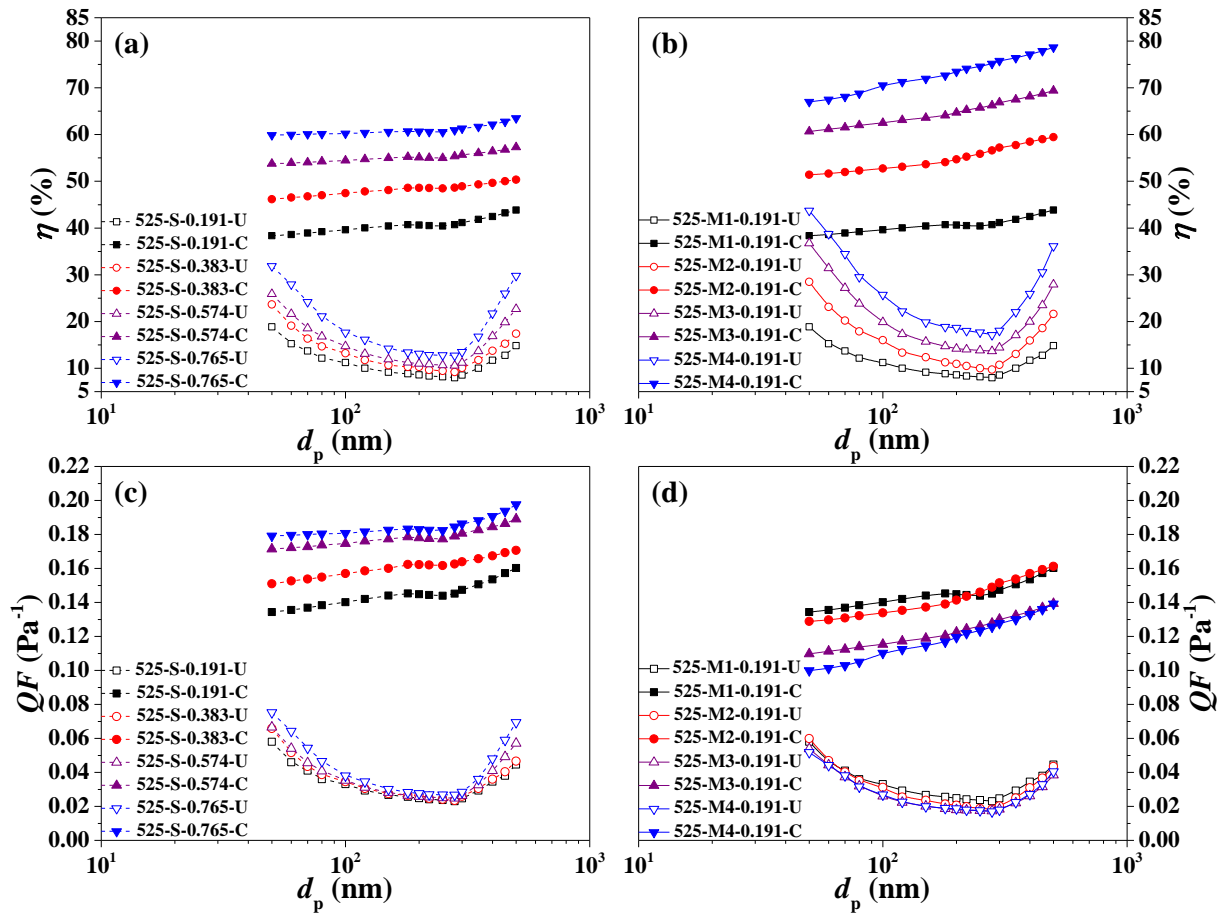


**Fig. A4.4.** Filtration efficiency ( $\eta$ ) of 525-nm (a) 1-layer and (b) multilayer PVDF filters; quality factors ( $QF$ ) of 525-nm (c) 1-layer and (d) multilayer PVDF filters. (Filters were in uncharged or charged state with varied filter basis weights. Note 525-S-0.191 and 525-M1-0.191 denote the same filter.)

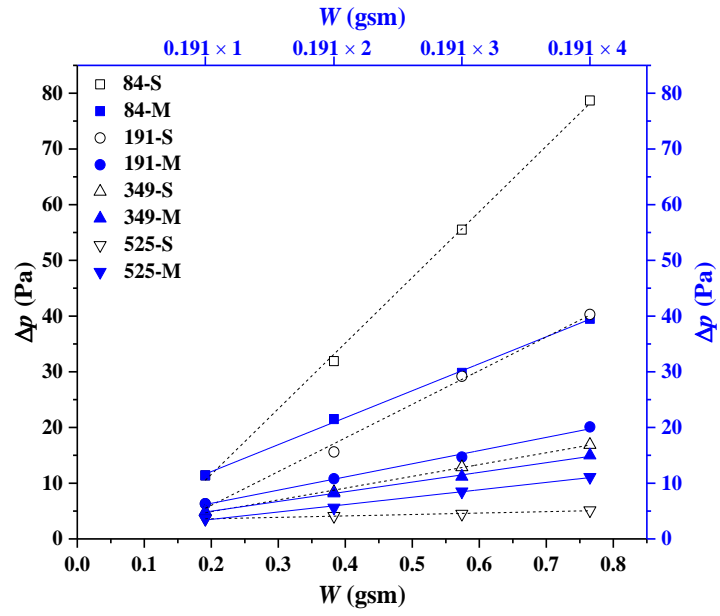


**Fig. A4.5.** Pressure drop ( $\Delta p$ ) of 1-layer and multilayer PVDF filters with varied filter basis weights and fiber sizes. (Each filter had the same pressure drop in uncharged and charged states.)

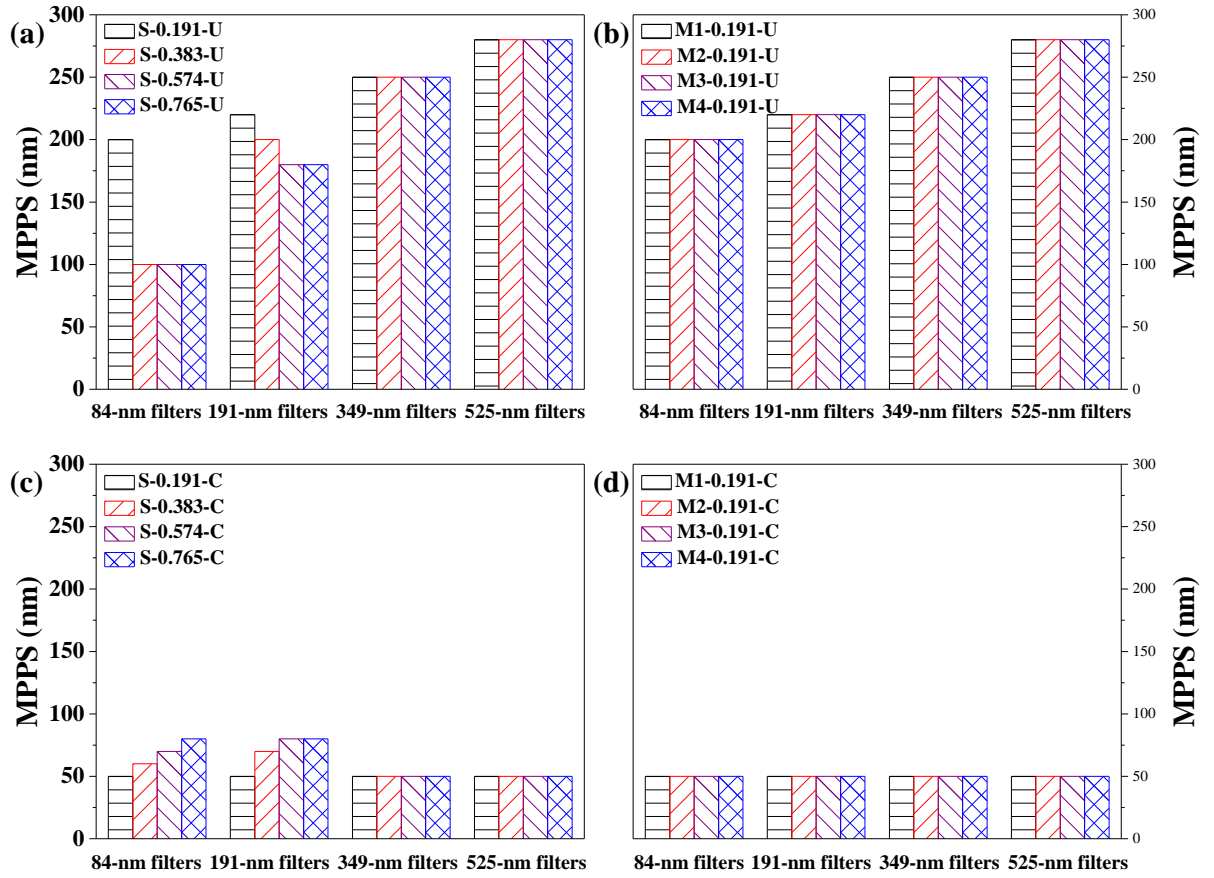


**Fig. A4.6.** MPPS of (a) 1-layer uncharged, (b) multilayer uncharged, (c) 1-layer electret and (d) multilayer electret PVDF filters with varied fiber sizes and filter basis weights.

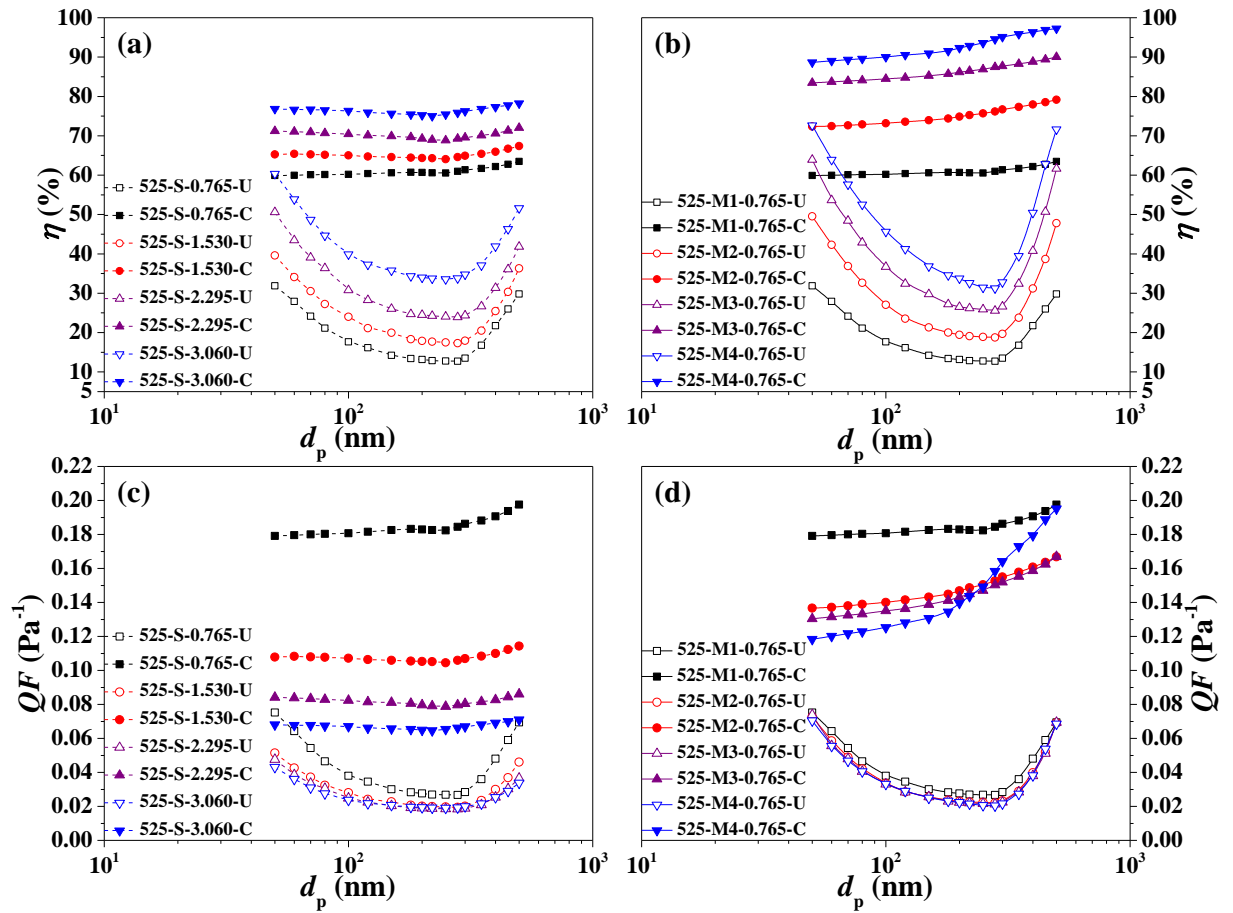


**Fig. A4.7.** Filtration efficiency ( $\eta$ ) of the optimized 525-nm (a) 1-layer and (b) multilayer PVDF filters; quality factors ( $QF$ ) of the optimized 525-nm (c) 1-layer and (d) multilayer PVDF filters. (Filters were in uncharged or charged state with varied layer basis weights. Note 525-S-0.765 and 525-M1-0.765 denote the same filter.)

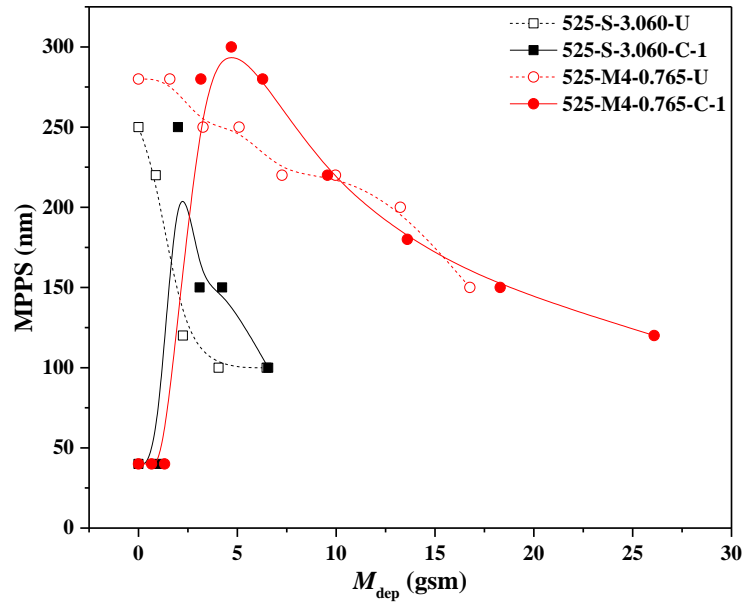


**Fig. A6.1.** Variation of most penetrating particle size (MPPS) of different filters with loaded aerosol mass ( $M_{dep}$ ).

## Appendix 2. – Tables

**Table A1.** Physical properties of 450-nm PVDF filters and PP substrate

Chapter	Filter	$d_f$ (nm)	$W$ (gsm)	$\eta$ of 300-nm	$QF$ of 300-nm	$\Delta p$ at 5.3 cm s <sup>-1</sup> (Pa)
				NaCl aerosol (%)	NaCl aerosol (Pa <sup>-1</sup> )	
3	450-S-0.87-P	450	0.87	13.9	0.034	4.4
3	450-S-0.87-C	450	0.87	44.5	0.137	4.3
3	450-S-1.75-P	450	1.75	17.2	0.031	6.1
3	450-S-1.75-C	450	1.75	50.4	0.125	5.6
3	450-S-1.75-U	450	1.75	14.8	0.029	5.6
3	450-S-3.46-P	450	3.46	28.1	0.024	13.8
3	450-S-3.46-C	450	3.46	53.7	0.058	13.2
3	450-S-5.10-P	450	5.10	36.3	0.023	20
3	450-S-5.10-C	450	5.10	58.4	0.045	19.3
3	450-S-6.98-P	450	6.98	52.7	0.020	37.7
3	450-S-6.98-C	450	6.98	67.0	0.031	35.9
3	450-M2-1.75-P	450	3.46	36.9	0.037	12.4
3	450-M2-1.75-C	450	3.46	80.3	0.138	11.8
3	450-M3-1.75-P	450	5.10	46.3	0.035	17.8
3	450-M3-1.75-C	450	5.10	90.1	0.135	17.2
3	450-M4-1.75-P	450	6.98	56.9	0.035	24.1
3	450-M4-1.75-C	450	6.98	95.0	0.128	23.3
3	450-M2-0.87-P	450	1.75	29.9	0.050	7.1

3	450-M2-0.87-C	450	1.75	67.7	0.161	7.0
3	450-M4-0.87-P	450	3.46	52.2	0.049	14.9
3	450-M4-0.87-C	450	3.46	87.1	0.145	14.1
3	450-M6-0.87-P	450	5.10	62.4	0.046	21.3
3	450-M6-0.87-C	450	5.10	93.6	0.139	19.8
3	450-M8-0.87-P	450	6.98	68.2	0.044	26.2
3	450-M8-0.87-C	450	6.98	98.0	0.154	25.2
4	84-S-0.191-U	84	0.191	29.3	0.030	11.4
4	84-S-0.191-C	84	0.191	63.7	0.089	11.4
4	84-S-0.383-U	84	0.383	57.6	0.027	31.9
4	84-S-0.383-C	84	0.383	80.8	0.052	31.9
4	84-S-0.574-U	84	0.574	76.2	0.026	55.5
4	84-S-0.574-C	84	0.574	85.5	0.035	55.5
4	84-S-0.765-U	84	0.765	84.2	0.023	78.7
4	84-S-0.765-C	84	0.765	89.7	0.029	78.7
4	84-M2-0.191-U	84	0.383	47.1	0.030	21.5
4	84-M2-0.191-C	84	0.383	88.9	0.102	21.5
4	84-M3-0.191-U	84	0.574	57.8	0.029	29.8
4	84-M3-0.191-C	84	0.574	93.6	0.092	29.8
4	84-M4-0.191-U	84	0.765	68.2	0.029	39.5
4	84-M4-0.191-C	84	0.765	96.5	0.085	39.5
4	191-S-0.191-U	191	0.191	14.9	0.026	6.3
4	191-S-0.191-C	191	0.191	54.7	0.126	6.3
4	191-S-0.383-U	191	0.383	19.6	0.014	15.6

4	191-S-0.383-C	191	0.383	68.4	0.074	15.6
4	191-S-0.574-U	191	0.574	31.8	0.013	29.2
4	191-S-0.574-C	191	0.574	73.7	0.046	29.2
4	191-S-0.765-U	191	0.765	38.9	0.012	40.3
4	191-S-0.765-C	191	0.765	79.2	0.039	40.3
4	191-M2-0.191-U	191	0.383	23.0	0.024	10.8
4	191-M2-0.191-C	191	0.383	78.7	0.143	10.8
4	191-M3-0.191-U	191	0.574	28.1	0.022	14.7
4	191-M3-0.191-C	191	0.574	83.4	0.122	14.7
4	191-M4-0.191-U	191	0.765	35.9	0.022	20.1
4	191-M4-0.191-C	191	0.765	88.7	0.109	20.1
4	349-S-0.191-U	349	0.191	11.1	0.024	4.9
4	349-S-0.191-C	349	0.191	48.3	0.135	4.9
4	349-S-0.383-U	349	0.383	13.7	0.018	8.4
4	349-S-0.383-C	349	0.383	64.5	0.123	8.4
4	349-S-0.574-U	349	0.574	18.9	0.016	12.9
4	349-S-0.574-C	349	0.574	66.8	0.085	12.9
4	349-S-0.765-U	349	0.765	22.5	0.015	16.9
4	349-S-0.765-C	349	0.765	69.9	0.071	16.9
4	349-M2-0.191-U	349	0.383	16.6	0.022	8.2
4	349-M2-0.191-C	349	0.383	70.3	0.148	8.2
4	349-M3-0.191-U	349	0.574	20.1	0.020	11.2
4	349-M3-0.191-C	349	0.574	75.3	0.125	11.2
4	349-M4-0.191-U	349	0.765	24.3	0.019	15

4	349-M4-0.191-C	349	0.765	81.3	0.112	15
4	525-S-0.191-U	525	0.191	8.5	0.025	3.6
4	525-S-0.191-C	525	0.191	41.2	0.147	3.6
4	525-S-0.383-U	525	0.383	10.1	0.026	4.1
4	525-S-0.383-C	525	0.383	48.9	0.164	4.1
4	525-S-0.574-U	525	0.574	11.2	0.026	4.5
4	525-S-0.574-C	525	0.574	55.6	0.181	4.5
4	525-S-0.765-U	525	0.765	13.5	0.028	5.1
4	525-S-0.765-C	525	0.765	61.3	0.186	5.1
4	525-M2-0.191-U	525	0.383	10.7	0.020	5.6
4	525-M2-0.191-C	525	0.383	57.2	0.152	5.6
4	525-M3-0.191-U	525	0.574	14.4	0.018	8.5
4	525-M3-0.191-C	525	0.574	66.9	0.130	8.5
4	525-M4-0.191-U	525	0.765	18.0	0.018	11.1
4	525-M4-0.191-C	525	0.765	75.8	0.128	11.1
4	525-S-1.530-U	525	1.530	17.9	0.020	9.8
4	525-S-1.530-C	525	1.530	64.9	0.107	9.8
4	525-S-2.295-U	525	2.295	24.3	0.019	14.8
4	525-S-2.295-C	525	2.295	69.6	0.080	14.8
4	525-S-3.060-U	525	3.060	34.8	0.020	21.5
4	525-S-3.060-C	525	3.060	76.3	0.067	21.5
4	525-M2-0.765-U	525	1.530	19.6	0.023	9.4
4	525-M2-0.765-C	525	1.530	76.7	0.155	9.4
4	525-M3-0.765-U	525	2.295	26.6	0.022	13.8

4	525-M3-0.765-C	525	2.295	87.7	0.152	13.8
4	525-M4-0.765-U	525	3.060	32.8	0.022	18.4
4	525-M4-0.765-C	525	3.060	95.1	0.164	18.4
4	525-M6-0.765-C	525	4.590	98.3	0.156	26.2
5	525-S-0.765-U	525	0.765	5.6	0.010	5.5
5	525-S-0.765-C	525	0.765	18.9	0.038	5.5
5	525-S-1.530-U	525	1.530	21.6	0.024	10.0
5	525-S-1.530-C	525	1.530	57.5	0.086	10.0
5	525-S-2.295-U	525	2.295	n/a	n/a	14.4
5	525-S-2.295-C	525	2.295	50.4	0.049	14.4
5	525-S-3.060-U	525	3.060	49.5	0.031	22.3
5	525-S-3.060-C	525	3.060	69.9	0.054	22.3
5	525-M2-0.765-U	525	1.530	28.0	0.037	8.9
5	525-M2-0.765-C	525	1.530	69.8	0.135	8.9
5	525-M3-0.765-U	525	2.295	22.0	0.018	13.5
5	525-M3-0.765-C	525	2.295	77.9	0.112	13.5
5	525-M4-0.765-U	525	3.060	74.4	0.074	18.3
5	525-M4-0.765-C	525	3.060	86.9	0.111	18.3
5	525-M6-0.765-U	525	4.590	75.1	0.054	25.9
5	525-M6-0.765-C	525	4.590	95.9	0.124	25.9
6	525-S-3.060-U	525	3.060	46.4	0.030	20.8
6	525-S-3.060-C-1	525	3.060	86.3	0.094	21.1
6	525-S-3.060-C-2	525	3.060	85.2	0.078	24.5
6	525-S-3.060-C-3	525	3.060	77.7	0.084	17.9

6	525-M4-0.765-U	525	3.060	40.5	0.030	17.1
6	525-M4-0.765- C-1	525	3.060	96.3	0.183	18.1
6	525-M4-0.765- C-2	525	3.060	97.7	0.221	17.1

---

**Table A2.** Loading data of 525-M4-0.765-C-1

Channel	Size bin geometric mean d <sub>p</sub> (nm)	0-0.5 h			0.5-1 h			1-2 h			2-3 h			3-4 h		
		c(d <sub>p</sub> , τ) (cm <sup>-3</sup> )	η(d <sub>p</sub> , τ) (%)	M <sub>dep</sub> (d <sub>p</sub> , Δτ) (g m <sup>-2</sup> )	c(d <sub>p</sub> , τ) (cm <sup>-3</sup> )	η(d <sub>p</sub> , τ) (%)	M <sub>dep</sub> (d <sub>p</sub> , Δτ) (g m <sup>-2</sup> )	c(d <sub>p</sub> , τ) (cm <sup>-3</sup> )	η(d <sub>p</sub> , τ) (%)	M <sub>dep</sub> (d <sub>p</sub> , Δτ) (g m <sup>-2</sup> )	c(d <sub>p</sub> , τ) (cm <sup>-3</sup> )	η(d <sub>p</sub> , τ) (%)	M <sub>dep</sub> (d <sub>p</sub> , Δτ) (g m <sup>-2</sup> )	c(d <sub>p</sub> , τ) (cm <sup>-3</sup> )	η(d <sub>p</sub> , τ) (%)	M <sub>dep</sub> (d <sub>p</sub> , Δτ) (g m <sup>-2</sup> )
1	39.6	155572	89.5	0.0009	155572	89.3	0.0009	136958	88.3	0.0016	97856	88.1	0.0012	142231	91.3	0.0017
2	41.34	183583	89.5	0.0013	183583	89.3	0.0013	150669	88.3	0.0020	114581	88.1	0.0015	166158	91.0	0.0023
3	43.17	199889	89.5	0.0016	199889	89.3	0.0016	177406	88.3	0.0027	130394	88.1	0.0020	196031	90.8	0.0031
4	45.08	223000	89.5	0.0020	223000	89.3	0.0020	201139	88.3	0.0035	147561	88.1	0.0026	216806	90.4	0.0039
5	47.08	252250	89.5	0.0025	252250	89.3	0.0025	216139	88.3	0.0043	164531	88.0	0.0033	237972	90.2	0.0048
6	49.18	270250	89.5	0.0031	270250	89.3	0.0031	238222	88.3	0.0054	183386	88.0	0.0042	260972	89.8	0.0060
7	51.38	280111	89.5	0.0037	280111	89.3	0.0037	255194	88.3	0.0066	190814	88.0	0.0049	278167	89.5	0.0073
8	53.69	297694	89.5	0.0045	297694	89.3	0.0044	270722	88.3	0.0080	198603	88.0	0.0058	294500	89.1	0.0088
9	56.1	304778	89.5	0.0052	304778	89.3	0.0052	277000	88.4	0.0093	209158	88.0	0.0070	307028	88.8	0.0104
10	58.63	306722	89.5	0.0060	306722	89.3	0.0060	286556	88.4	0.0110	212811	87.9	0.0082	320722	88.5	0.0124
11	61.3	307389	89.5	0.0069	307389	89.3	0.0068	289194	88.4	0.0127	222253	87.9	0.0097	324250	88.2	0.0142
12	64.08	312278	89.6	0.0080	312278	89.4	0.0079	291194	88.5	0.0147	229139	87.9	0.0115	320444	87.8	0.0160
13	67.01	310694	89.7	0.0091	310694	89.4	0.0090	295111	88.5	0.0170	230333	87.8	0.0132	318528	87.4	0.0181
14	70.09	303306	89.8	0.0101	303306	89.5	0.0101	292306	88.5	0.0193	233083	87.8	0.0152	312611	87.1	0.0203
15	73.33	289028	90.0	0.0111	289028	89.7	0.0111	285000	88.6	0.0215	231389	87.8	0.0173	303972	86.8	0.0225
16	76.73	280667	90.2	0.0124	280667	89.9	0.0123	274694	88.6	0.0238	228528	87.7	0.0196	298639	86.5	0.0252
17	80.3	272222	90.4	0.0138	272222	90.1	0.0137	267194	88.7	0.0265	227306	87.7	0.0223	285028	86.2	0.0275
18	84.06	259028	90.5	0.0151	259028	90.2	0.0150	260667	88.8	0.0297	220917	87.7	0.0249	274444	85.9	0.0303
19	88.02	246306	90.7	0.0165	246306	90.3	0.0164	252889	88.8	0.0331	214611	87.7	0.0278	266167	85.7	0.0336
20	92.2	231778	90.8	0.0178	231778	90.5	0.0178	241750	88.9	0.0364	203669	87.7	0.0303	251278	85.4	0.0364
21	96.59	217139	90.9	0.0192	217139	90.6	0.0192	232333	89.0	0.0403	199478	87.7	0.0341	240278	85.2	0.0399
22	101.2	200111	91.1	0.0204	200111	90.7	0.0204	216139	89.0	0.0431	194897	87.7	0.0383	224778	85.0	0.0428
23	106.1	182361	91.3	0.0215	182361	90.9	0.0214	202917	89.1	0.0467	174572	87.7	0.0395	212833	84.8	0.0466
24	111.3	168017	91.5	0.0229	168017	91.0	0.0228	189917	89.1	0.0505	164683	87.7	0.0430	196778	84.7	0.0497
25	116.7	149164	91.7	0.0235	149164	91.2	0.0234	175808	89.2	0.0539	155889	87.6	0.0470	178861	84.5	0.0520
26	122.5	136739	91.9	0.0250	136739	91.3	0.0248	159244	89.2	0.0565	144333	87.6	0.0503	162519	84.3	0.0545
27	128.6	118778	92.1	0.0252	118778	91.5	0.0250	147900	89.3	0.0607	132153	87.6	0.0533	148061	84.1	0.0573
28	135	103756	92.2	0.0255	103756	91.6	0.0253	132725	89.3	0.0631	121092	87.6	0.0564	132689	83.9	0.0593
29	141.9	90811	92.4	0.0259	90811	91.7	0.0257	116644	89.4	0.0644	106614	87.6	0.0577	115014	83.7	0.0595
30	149.1	78842	92.5	0.0261	78842	91.8	0.0260	106656	89.5	0.0684	92264	87.5	0.0579	101294	83.5	0.0607
31	156.8	66078	92.6	0.0255	66078	92.0	0.0253	91628	89.5	0.0684	84037	87.5	0.0613	87808	83.3	0.0610
32	164.9	57322	92.7	0.0258	57322	92.1	0.0256	83958	89.6	0.0730	73887	87.5	0.0627	75925	83.1	0.0612
33	173.6	48803	92.9	0.0256	48803	92.1	0.0254	70658	89.7	0.0718	63359	87.5	0.0627	65647	82.9	0.0616
34	182.8	39814	93.0	0.0245	39814	92.3	0.0243	60956	89.9	0.0724	54688	87.5	0.0632	54897	82.7	0.0600
35	192.6	32063	93.2	0.0231	32063	92.4	0.0229	52467	90.1	0.0731	44269	87.4	0.0598	46608	82.6	0.0595
36	203	26317	93.3	0.0222	26317	92.6	0.0220	44133	90.3	0.0721	36344	87.4	0.0575	40069	82.4	0.0598
37	214.1	19893	93.6	0.0198	19893	92.7	0.0196	36958	90.4	0.0709	31215	87.3	0.0579	32156	82.2	0.0561
38	226	14999	94.0	0.0176	14999	92.9	0.0174	30194	90.6	0.0683	26206	87.3	0.0571	26308	82.0	0.0539
39	238.7	12034	94.4	0.0167	12034	93.1	0.0165	25550	90.7	0.0682	21441	87.2	0.0550	20787	81.7	0.0500
40	252.2	9091	94.9	0.0150	9091	93.3	0.0147	19377	90.9	0.0611	16292	87.2	0.0493	16130	81.5	0.0456
41	266.7	6728	95.3	0.0132	6728	93.5	0.0129	15418	91.0	0.0576	12966	87.1	0.0463	12468	81.4	0.0417
42	282.3	4974	95.9	0.0116	4974	93.8	0.0114	12023	91.2	0.0534	9815	87.1	0.0416	9371	81.4	0.0371
43	298.9	3481	96.3	0.0097	3481	94.1	0.0095	9306	91.4	0.0491	7289	87.2	0.0367	6838	81.4	0.0322
44	316.8	2306	96.6	0.0077	2306	94.4	0.0075	6583	91.6	0.0415	5528	87.3	0.0332	4792	81.5	0.0269
45	335.9	1543	96.8	0.0061	1543	94.5	0.0060	4445	91.7	0.0334	3745	87.4	0.0268	3016	81.7	0.0202
46	356.5	849	97.0	0.0040	849	94.7	0.0039	2790	91.9	0.0251	2413	87.4	0.0207	1805	82.0	0.0145
47	378.7	463	97.3	0.0026	463	95.0	0.0026	1690	92.2	0.0183	1405	87.5	0.0144	919	82.4	0.0089
48	402.5	250	97.5	0.0017	250	95.2	0.0017	903	92.4	0.0118	738	87.5	0.0091	446	82.7	0.0052
49	428.2	190	97.8	0.0016	190	95.4	0.0015	436	92.7	0.0069	357	87.6	0.0053	181	83.3	0.0026
50	455.8	92	98.1	0.0009	92	95.7	0.0009	174	93.0	0.0033	155	87.7	0.0028	71	83.8	0.0012
51	485.7	118	98.5	0.0014	118	96.0	0.0014	92	93.4	0.0021	101	87.9	0.0022	59	84.4	0.0012
M <sub>dep</sub> (Δτ) (g m <sup>-2</sup> )		0.66			0.66			1.84			1.54			1.59		
M <sub>dep</sub> (τ) (g m <sup>-2</sup> )		0.7			1.3			3.2			4.7			6.3		

Annotation:  $U = 5.3 \text{ cm s}^{-1}$ , aerosol material: NaCl,  $\rho_p = 2165 \text{ kg m}^{-3}$ .

Channel	Size bin geometric mean d <sub>p</sub> (nm)	4-5 h			5-6 h			6-7 h			7-8 h			8-9 h		
		$c(d_p, \tau)$ (cm <sup>-3</sup> )	$\eta(d_p, \tau)$ (%)	$M_{\text{dep}}(d_p, \Delta\tau)$ (g m <sup>-2</sup> )	$c(d_p, \tau)$ (cm <sup>-3</sup> )	$\eta(d_p, \tau)$ (%)	$M_{\text{dep}}(d_p, \Delta\tau)$ (g m <sup>-2</sup> )	$c(d_p, \tau)$ (cm <sup>-3</sup> )	$\eta(d_p, \tau)$ (%)	$M_{\text{dep}}(d_p, \Delta\tau)$ (g m <sup>-2</sup> )	$c(d_p, \tau)$ (cm <sup>-3</sup> )	$\eta(d_p, \tau)$ (%)	$M_{\text{dep}}(d_p, \Delta\tau)$ (g m <sup>-2</sup> )	$c(d_p, \tau)$ (cm <sup>-3</sup> )	$\eta(d_p, \tau)$ (%)	$M_{\text{dep}}(d_p, \Delta\tau)$ (g m <sup>-2</sup> )
1	39.6	129083	93.1	0.0016	91019	93.1	0.0011	99672	97.0	0.0013	108817	97.0	0.0014	107044	98.7	0.0014
2	41.34	151142	92.8	0.0021	108400	92.8	0.0015	116750	96.6	0.0017	126375	96.6	0.0019	128125	98.4	0.0019
3	43.17	170022	92.4	0.0027	129942	92.4	0.0021	137497	96.1	0.0023	151197	96.1	0.0025	157389	97.9	0.0027
4	45.08	197522	91.9	0.0036	144286	91.9	0.0026	153231	95.5	0.0029	176131	95.5	0.0033	173953	97.4	0.0034
5	47.08	220778	91.5	0.0046	167006	91.5	0.0035	170875	95.1	0.0037	198925	95.1	0.0043	192300	97.0	0.0042
6	49.18	226694	91.1	0.0053	184103	91.1	0.0043	185672	94.5	0.0045	214050	94.5	0.0052	211833	96.5	0.0053
7	51.38	248722	90.8	0.0066	195078	90.8	0.0052	207889	94.1	0.0057	231806	94.1	0.0064	225686	96.1	0.0064
8	53.69	269944	90.4	0.0082	198150	90.4	0.0060	226639	93.7	0.0071	246417	93.7	0.0077	237528	95.6	0.0076
9	56.1	279083	90.1	0.0096	213625	90.1	0.0074	233778	93.4	0.0083	256083	93.4	0.0091	258806	95.2	0.0094
10	58.63	286528	89.7	0.0112	221944	89.7	0.0087	246806	93.0	0.0100	273778	93.0	0.0111	270028	94.8	0.0112
11	61.3	302056	89.4	0.0134	238917	89.4	0.0106	254083	92.7	0.0117	275917	92.7	0.0127	281528	94.5	0.0132
12	64.08	299583	88.8	0.0151	242500	88.8	0.0123	266500	92.3	0.0140	270889	92.3	0.0142	298139	94.2	0.0160
13	67.01	295028	88.2	0.0169	246472	88.2	0.0142	267361	91.8	0.0160	274889	91.8	0.0164	297194	93.9	0.0182
14	70.09	292722	87.8	0.0191	246556	87.8	0.0161	280000	91.4	0.0191	283000	91.4	0.0193	303139	93.7	0.0212
15	73.33	289528	87.3	0.0215	249139	87.3	0.0185	279444	91.0	0.0217	283000	91.0	0.0220	303028	93.4	0.0241
16	76.73	288917	86.9	0.0245	247694	86.9	0.0210	278778	90.6	0.0247	275389	90.6	0.0244	309806	93.2	0.0282
17	80.3	278556	86.5	0.0270	242917	86.5	0.0235	274611	90.2	0.0277	273111	90.2	0.0276	303917	93.0	0.0316
18	84.06	274611	86.2	0.0304	240389	86.2	0.0266	272083	89.8	0.0314	269306	89.8	0.0311	294694	92.8	0.0351
19	88.02	258389	86.0	0.0328	229667	86.0	0.0291	268806	89.5	0.0355	259917	89.5	0.0343	286667	92.6	0.0392
20	92.2	245583	85.7	0.0357	230778	85.7	0.0335	267806	89.2	0.0405	244722	89.2	0.0370	279556	92.4	0.0438
21	96.59	236889	85.5	0.0395	224139	85.5	0.0373	254861	88.8	0.0441	233972	88.8	0.0405	273944	92.3	0.0493
22	101.2	224139	85.2	0.0428	214167	85.2	0.0409	246944	88.3	0.0489	220444	88.3	0.0436	261722	92.0	0.0540
23	106.1	213333	85.0	0.0468	207389	85.0	0.0455	241889	87.8	0.0548	211083	87.8	0.0479	246083	91.8	0.0584
24	111.3	192164	84.7	0.0486	195556	84.7	0.0494	233389	87.3	0.0608	197194	87.3	0.0514	232722	91.6	0.0636
25	116.7	179708	84.4	0.0522	190069	84.4	0.0552	225944	86.8	0.0674	184783	86.8	0.0551	220622	91.4	0.0693
26	122.5	165189	84.1	0.0552	177233	84.1	0.0592	208806	86.2	0.0716	172669	86.2	0.0592	204278	91.2	0.0741
27	128.6	145803	83.7	0.0561	161450	83.7	0.0621	197197	85.7	0.0778	154694	85.7	0.0610	181294	91.1	0.0759
28	135	132817	83.2	0.0588	147550	83.2	0.0653	188381	85.3	0.0855	136728	85.3	0.0620	162181	90.9	0.0785
29	141.9	118439	82.8	0.0606	132981	82.8	0.0680	169819	84.8	0.0890	122992	84.8	0.0645	141581	90.9	0.0795
30	149.1	103522	82.3	0.0611	117914	82.3	0.0696	155667	84.4	0.0942	106678	84.4	0.0646	123742	90.8	0.0805
31	156.8	92844	81.8	0.0634	104161	81.8	0.0711	139911	84.0	0.0980	91006	84.0	0.0638	115222	90.7	0.0871
32	164.9	80025	81.5	0.0632	92058	81.5	0.0727	120575	83.7	0.0979	78936	83.7	0.0641	95869	90.6	0.0842
33	173.6	65897	81.2	0.0605	79419	81.2	0.0729	108542	83.4	0.1024	66983	83.4	0.0632	84042	90.6	0.0861
34	182.8	56358	80.9	0.0602	68289	80.9	0.0730	94592	83.0	0.1037	55953	83.0	0.0614	70431	90.6	0.0843
35	192.6	48689	80.7	0.0607	58200	80.7	0.0725	79850	82.5	0.1017	46598	82.5	0.0594	58701	90.7	0.0822
36	203	38041	80.5	0.0554	48572	80.5	0.0707	68683	82.1	0.1021	38181	82.1	0.0567	47303	90.8	0.0777
37	214.1	31558	80.3	0.0538	39719	80.3	0.0677	59250	82.1	0.1032	31169	82.1	0.0543	39142	90.8	0.0755
38	226	25017	80.3	0.0501	32441	80.3	0.0650	49983	82.3	0.1026	25086	82.3	0.0515	30866	90.8	0.0700
39	238.7	18716	80.1	0.0441	27603	80.1	0.0651	41664	82.5	0.1011	19223	82.5	0.0467	24682	90.9	0.0660
40	252.2	15066	80.1	0.0419	21659	80.1	0.0602	33889	82.8	0.0974	14875	82.8	0.0427	19857	90.9	0.0626
41	266.7	11739	80.0	0.0385	16545	80.0	0.0543	26872	83.1	0.0917	10851	83.1	0.0370	12979	91.0	0.0485
42	282.3	8437	80.0	0.0329	12340	80.0	0.0481	20209	83.4	0.0820	7817	83.4	0.0317	9719	91.3	0.0432
43	298.9	5687	80.1	0.0263	8993	80.1	0.0416	15485	83.5	0.0746	5419	83.5	0.0261	6926	91.7	0.0367
44	316.8	4073	80.2	0.0225	6537	80.2	0.0360	11568	83.6	0.0665	3667	83.6	0.0211	4477	91.9	0.0283
45	335.9	2584	80.3	0.0170	4022	80.3	0.0265	7911	83.9	0.0544	2312	83.9	0.0159	2956	92.1	0.0223
46	356.5	1345	80.5	0.0106	2512	80.5	0.0198	5069	84.0	0.0417	1381	84.0	0.0114	1712	92.2	0.0155
47	378.7	759	80.9	0.0072	1425	80.9	0.0135	3093	84.2	0.0306	720	84.2	0.0071	891	92.4	0.0097
48	402.5	320	81.2	0.0037	670	81.2	0.0077	1657	84.3	0.0197	339	84.3	0.0040	540	92.5	0.0070
49	428.2	116	81.6	0.0016	301	81.6	0.0042	898	84.6	0.0129	159	84.6	0.0023	297	92.8	0.0047
50	455.8	43	81.8	0.0007	123	81.8	0.0021	393	84.8	0.0068	80	84.8	0.0014	124	92.9	0.0024
51	485.7	54	82.0	0.0011	88	82.0	0.0018	233	85.2	0.0049	75	85.2	0.0016	147	93.1	0.0034
$M_{\text{dep}}(\Delta\tau)$ (g m <sup>-2</sup> )			1.53			1.75			2.48			1.56			2.00	
$M_{\text{dep}}(\tau)$ (g m <sup>-2</sup> )			7.8			9.6			12.0			13.6			15.6	

Annotation:  $U = 5.3 \text{ cm s}^{-1}$ , aerosol material: NaCl,  $\rho_p = 2165 \text{ kg m}^{-3}$ .

Channel	Size bin geometric mean d <sub>p</sub> (nm)	9-10 h			10-11 h			11-12 h			12-13 h			13-14 h		
		c(d <sub>p</sub> , τ) (cm <sup>-3</sup> )	η(d <sub>p</sub> , τ) (%)	M <sub>dep</sub> (d <sub>p</sub> , Δτ) (g m <sup>-2</sup> )	c(d <sub>p</sub> , τ) (cm <sup>-3</sup> )	η(d <sub>p</sub> , τ) (%)	M <sub>dep</sub> (d <sub>p</sub> , Δτ) (g m <sup>-2</sup> )	c(d <sub>p</sub> , τ) (cm <sup>-3</sup> )	η(d <sub>p</sub> , τ) (%)	M <sub>dep</sub> (d <sub>p</sub> , Δτ) (g m <sup>-2</sup> )	c(d <sub>p</sub> , τ) (cm <sup>-3</sup> )	η(d <sub>p</sub> , τ) (%)	M <sub>dep</sub> (d <sub>p</sub> , Δτ) (g m <sup>-2</sup> )	c(d <sub>p</sub> , τ) (cm <sup>-3</sup> )	η(d <sub>p</sub> , τ) (%)	M <sub>dep</sub> (d <sub>p</sub> , Δτ) (g m <sup>-2</sup> )
1	39.6	99931	98.7	0.0013	121736	99.9	0.0016	86242	99.9	0.0012	104353	100.0	0.0014	126328	100.0	0.0017
2	41.34	132569	98.4	0.0020	133964	99.7	0.0020	108056	99.7	0.0016	131328	100.0	0.0020	150411	100.0	0.0023
3	43.17	148381	97.9	0.0025	160586	99.6	0.0028	141169	99.6	0.0024	150606	100.0	0.0026	173267	100.0	0.0030
4	45.08	177942	97.4	0.0034	189717	99.4	0.0037	159742	99.4	0.0031	191625	99.9	0.0038	196889	100.0	0.0039
5	47.08	202861	97.0	0.0044	215639	99.2	0.0048	185736	99.2	0.0042	220769	99.9	0.0050	218750	100.0	0.0049
6	49.18	213167	96.5	0.0053	252111	99.0	0.0064	201319	99.0	0.0051	244556	99.9	0.0063	231667	100.0	0.0060
7	51.38	243167	96.1	0.0069	273389	98.9	0.0079	212611	98.9	0.0062	266944	99.9	0.0078	253889	100.0	0.0074
8	53.69	252139	95.6	0.0081	290444	98.7	0.0096	233833	98.7	0.0077	285417	99.9	0.0095	269417	100.0	0.0090
9	56.1	277639	95.2	0.0101	310917	98.6	0.0117	260833	98.6	0.0098	296306	99.9	0.0113	277750	100.0	0.0106
10	58.63	295694	94.8	0.0122	324917	98.5	0.0140	267444	98.5	0.0115	314222	99.9	0.0137	286389	100.0	0.0125
11	61.3	300556	94.5	0.0141	338167	98.5	0.0166	281389	98.5	0.0138	335806	99.9	0.0167	289528	100.0	0.0144
12	64.08	302722	94.2	0.0162	350000	98.4	0.0196	292722	98.4	0.0164	344722	99.9	0.0196	298028	100.0	0.0170
13	67.01	310944	93.9	0.0190	363722	98.3	0.0233	299472	98.3	0.0192	345806	99.8	0.0225	297861	100.0	0.0194
14	70.09	319806	93.7	0.0223	380444	98.2	0.0278	305528	98.2	0.0224	350889	99.8	0.0261	293472	100.0	0.0219
15	73.33	324583	93.4	0.0259	385083	98.2	0.0323	313694	98.2	0.0263	345889	99.8	0.0294	288694	100.0	0.0246
16	76.73	325167	93.2	0.0296	384250	98.2	0.0369	308972	98.2	0.0296	342556	99.8	0.0334	282778	100.0	0.0276
17	80.3	319667	93.0	0.0333	389750	98.1	0.0428	321139	98.1	0.0353	339167	99.8	0.0379	275167	100.0	0.0308
18	84.06	318361	92.8	0.0379	377167	98.1	0.0475	308528	98.1	0.0389	332833	99.8	0.0427	264028	100.0	0.0339
19	88.02	312417	92.6	0.0427	379333	98.0	0.0548	302639	98.0	0.0438	322722	99.8	0.0475	253083	100.0	0.0373
20	92.2	305361	92.4	0.0479	372944	98.0	0.0619	304639	98.0	0.0506	307222	99.8	0.0520	241778	100.0	0.0410
21	96.59	289222	92.3	0.0520	368694	97.9	0.0704	304750	97.9	0.0582	293556	99.8	0.0571	231750	100.0	0.0452
22	101.2	296417	92.0	0.0612	350417	97.9	0.0769	295639	97.9	0.0649	273528	99.8	0.0612	215306	100.0	0.0483
23	106.1	268889	91.8	0.0638	338750	97.8	0.0856	280889	97.8	0.0710	264389	99.8	0.0682	201694	100.0	0.0521
24	111.3	258694	91.6	0.0707	317861	97.8	0.0927	269972	97.8	0.0787	249167	99.8	0.0741	187500	100.0	0.0559
25	116.7	248056	91.4	0.0779	315389	97.7	0.1059	259917	97.7	0.0873	220431	99.8	0.0756	173328	100.0	0.0596
26	122.5	228194	91.2	0.0827	298694	97.7	0.1160	245861	97.7	0.0955	203431	99.8	0.0807	159953	100.0	0.0636
27	128.6	217667	91.1	0.0912	284278	97.7	0.1277	227544	97.7	0.1022	183792	99.8	0.0844	145083	100.0	0.0667
28	135	195556	90.9	0.0946	268667	97.6	0.1396	213214	97.6	0.1108	158369	99.8	0.0841	130350	100.0	0.0694
29	141.9	189972	90.9	0.1067	250194	97.6	0.1510	196028	97.6	0.1183	142808	99.8	0.0881	115742	100.0	0.0715
30	149.1	164697	90.8	0.1072	232083	97.6	0.1625	180467	97.6	0.1263	122017	99.8	0.0873	102428	100.0	0.0734
31	156.8	149431	90.7	0.1130	214250	97.7	0.1745	161589	97.7	0.1316	106678	99.8	0.0888	89275	100.0	0.0744
32	164.9	131058	90.6	0.1152	194919	97.7	0.1847	142647	97.7	0.1352	88525	99.8	0.0857	77878	100.0	0.0755
33	173.6	116033	90.6	0.1189	168711	97.8	0.1866	128889	97.8	0.1426	73303	99.8	0.0828	66525	100.0	0.0753
34	182.8	100556	90.6	0.1203	152600	97.8	0.1972	108625	97.8	0.1404	61264	99.8	0.0808	57039	100.0	0.0754
35	192.6	85372	90.7	0.1196	135236	97.8	0.2044	98908	97.8	0.1495	49851	99.8	0.0769	48206	100.0	0.0745
36	203	72411	90.8	0.1189	117072	97.9	0.2073	83139	97.9	0.1472	40296	99.8	0.0728	40081	100.0	0.0725
37	214.1	58819	90.8	0.1134	99478	97.9	0.2067	70530	97.9	0.1465	32164	99.8	0.0681	33817	100.0	0.0718
38	226	46394	90.8	0.1052	80731	97.9	0.1974	59008	97.9	0.1443	26585	99.8	0.0662	26841	100.0	0.0670
39	238.7	40244	90.9	0.1076	68662	98.0	0.1979	47024	98.0	0.1355	19044	99.8	0.0559	21541	100.0	0.0634
40	252.2	31070	90.9	0.0980	57314	98.0	0.1949	36658	98.0	0.1247	14292	99.8	0.0495	17755	100.0	0.0616
41	266.7	22118	91.0	0.0826	44205	98.1	0.1779	30386	98.1	0.1223	11043	99.8	0.0452	13141	100.0	0.0539
42	282.3	17945	91.3	0.0797	33973	98.2	0.1623	23277	98.2	0.1112	7519	99.8	0.0365	9809	100.0	0.0477
43	298.9	12552	91.7	0.0665	24818	98.2	0.1408	17115	98.2	0.0971	5242	99.8	0.0302	7429	100.0	0.0429
44	316.8	8625	91.9	0.0545	18188	98.3	0.1230	12234	98.3	0.0827	3739	99.8	0.0257	5463	100.0	0.0376
45	335.9	5521	92.1	0.0417	13287	98.4	0.1072	8572	98.4	0.0691	2227	99.8	0.0182	3571	100.0	0.0293
46	356.5	3299	92.2	0.0298	8675	98.5	0.0837	5866	98.5	0.0566	1320	99.8	0.0129	2353	100.0	0.0231
47	378.7	1984	92.4	0.0215	5562	98.6	0.0644	3541	98.6	0.0410	779	99.8	0.0091	1396	100.0	0.0164
48	402.5	916	92.5	0.0120	3453	98.8	0.0481	2091	98.8	0.0291	433	99.8	0.0061	753	100.0	0.0106
49	428.2	452	92.8	0.0071	1926	98.9	0.0324	1085	98.9	0.0182	257	99.8	0.0044	416	100.0	0.0071
50	455.8	244	92.9	0.0046	1022	99.1	0.0207	586	99.1	0.0119	144	99.8	0.0030	231	100.0	0.0047
51	485.7	225	93.1	0.0052	603	99.2	0.0148	336	99.2	0.0083	89	99.9	0.0022	130	100.0	0.0032
M <sub>dep</sub> (Δτ) (g m <sup>-2</sup> )			2.69			4.48			3.31			2.07			1.92	
M <sub>dep</sub> (τ) (g m <sup>-2</sup> )			18.3			22.8			26.1			28.2			30.1	

Annotation:  $U = 5.3 \text{ cm s}^{-1}$ , aerosol material: NaCl,  $\rho_p = 2165 \text{ kg m}^{-3}$ .

Channel	Size bin geometric mean diameter $d_p$ (nm)	14-15 h			15-16 h			16-17 h			17-17.5 h		
		$c(d_p, \tau)$ ( $\text{cm}^{-3}$ )	$\eta(d_p, \tau)$ (%)	$M_{\text{dep}}(d_p, \Delta\tau)$ ( $\text{g m}^{-2}$ )	$c(d_p, \tau)$ ( $\text{cm}^{-3}$ )	$\eta(d_p, \tau)$ (%)	$M_{\text{dep}}(d_p, \Delta\tau)$ ( $\text{g m}^{-2}$ )	$c(d_p, \tau)$ ( $\text{cm}^{-3}$ )	$\eta(d_p, \tau)$ (%)	$M_{\text{dep}}(d_p, \Delta\tau)$ ( $\text{g m}^{-2}$ )	$c(d_p, \tau)$ ( $\text{cm}^{-3}$ )	$\eta(d_p, \tau)$ (%)	$M_{\text{dep}}(d_p, \Delta\tau)$ ( $\text{g m}^{-2}$ )
1	39.6	109756	100.0	0.0015	115772	100.0	0.0016	122344	100.0	0.0016	32442	100.0	0.0002
2	41.34	131631	100.0	0.0020	139169	100.0	0.0021	139425	100.0	0.0021	42939	100.0	0.0003
3	43.17	154472	100.0	0.0027	164586	100.0	0.0029	157569	100.0	0.0027	53256	100.0	0.0005
4	45.08	174572	100.0	0.0035	188200	100.0	0.0037	186150	100.0	0.0037	65267	100.0	0.0006
5	47.08	195522	100.0	0.0044	210833	100.0	0.0048	198706	100.0	0.0045	79981	100.0	0.0009
6	49.18	215750	100.0	0.0056	233056	100.0	0.0060	226750	100.0	0.0058	90872	100.0	0.0012
7	51.38	233028	100.0	0.0068	251000	100.0	0.0074	254778	100.0	0.0075	103067	100.0	0.0015
8	53.69	250389	100.0	0.0084	266222	100.0	0.0089	255111	100.0	0.0085	119050	100.0	0.0020
9	56.1	264361	100.0	0.0101	280750	100.0	0.0107	280250	100.0	0.0107	126672	100.0	0.0024
10	58.63	273722	100.0	0.0119	288972	100.0	0.0126	279222	100.0	0.0122	136761	100.0	0.0030
11	61.3	281250	100.0	0.0140	292611	100.0	0.0146	286972	100.0	0.0143	150717	100.0	0.0038
12	64.08	285694	100.0	0.0163	302917	100.0	0.0172	294611	100.0	0.0168	157447	100.0	0.0045
13	67.01	286556	100.0	0.0186	308194	100.0	0.0201	294083	100.0	0.0191	167536	100.0	0.0055
14	70.09	285000	100.0	0.0212	309806	100.0	0.0231	292972	100.0	0.0218	173183	100.0	0.0064
15	73.33	286361	100.0	0.0244	299444	100.0	0.0255	284556	100.0	0.0243	179431	100.0	0.0077
16	76.73	280722	100.0	0.0274	298000	100.0	0.0291	277472	100.0	0.0271	182269	100.0	0.0089
17	80.3	275861	100.0	0.0309	294806	100.0	0.0330	271278	100.0	0.0304	190528	100.0	0.0107
18	84.06	268111	100.0	0.0344	289556	100.0	0.0372	260167	100.0	0.0334	190639	100.0	0.0122
19	88.02	259083	100.0	0.0382	270306	100.0	0.0399	256250	100.0	0.0378	185564	100.0	0.0137
20	92.2	250056	100.0	0.0424	257278	100.0	0.0436	254556	100.0	0.0432	188233	100.0	0.0160
21	96.59	238278	100.0	0.0464	246694	100.0	0.0481	231833	100.0	0.0452	183833	100.0	0.0179
22	101.2	225444	100.0	0.0505	232639	100.0	0.0522	224972	100.0	0.0504	184917	100.0	0.0207
23	106.1	212722	100.0	0.0550	220694	100.0	0.0570	209033	100.0	0.0540	175622	100.0	0.0227
24	111.3	199439	100.0	0.0595	196208	100.0	0.0585	196339	100.0	0.0585	169750	100.0	0.0253
25	116.7	186911	100.0	0.0643	182575	100.0	0.0628	176886	100.0	0.0608	162381	100.0	0.0279
26	122.5	173261	100.0	0.0689	168719	100.0	0.0671	170156	100.0	0.0677	150061	100.0	0.0298
27	128.6	157764	100.0	0.0726	152111	100.0	0.0700	150344	100.0	0.0692	144028	100.0	0.0331
28	135	143389	100.0	0.0763	134217	100.0	0.0714	128528	100.0	0.0684	133517	100.0	0.0355
29	141.9	127656	100.0	0.0789	118803	100.0	0.0734	117867	100.0	0.0728	123308	100.0	0.0381
30	149.1	113497	100.0	0.0814	104750	100.0	0.0751	104542	100.0	0.0749	109833	100.0	0.0394
31	156.8	99497	100.0	0.0830	91797	100.0	0.0765	92814	100.0	0.0774	99133	100.0	0.0413
32	164.9	86503	100.0	0.0839	75442	100.0	0.0732	76708	100.0	0.0744	85914	100.0	0.0417
33	173.6	74836	100.0	0.0847	63914	100.0	0.0723	62869	100.0	0.0711	77778	100.0	0.0440
34	182.8	63861	100.0	0.0844	53883	100.0	0.0712	50825	100.0	0.0671	66517	100.0	0.0439
35	192.6	53669	100.0	0.0829	43900	100.0	0.0678	40950	100.0	0.0633	53817	100.0	0.0416
36	203	45736	100.0	0.0828	35468	100.0	0.0642	34619	100.0	0.0626	44325	100.0	0.0401
37	214.1	36221	100.0	0.0769	29279	100.0	0.0622	24614	100.0	0.0522	37789	100.0	0.0401
38	226	28560	100.0	0.0713	23068	100.0	0.0576	18357	100.0	0.0458	31814	100.0	0.0397
39	238.7	23246	100.0	0.0684	18791	100.0	0.0553	14483	100.0	0.0426	24108	100.0	0.0355
40	252.2	18204	100.0	0.0632	13751	100.0	0.0477	9627	100.0	0.0334	18842	100.0	0.0327
41	266.7	14102	100.0	0.0579	10018	100.0	0.0411	7021	100.0	0.0288	14173	100.0	0.0291
42	282.3	10966	100.0	0.0534	7789	100.0	0.0379	4573	100.0	0.0222	10299	100.0	0.0251
43	298.9	8109	100.0	0.0468	5237	100.0	0.0302	3134	100.0	0.0181	7756	100.0	0.0224
44	316.8	5957	100.0	0.0410	3457	100.0	0.0238	2127	100.0	0.0146	5112	100.0	0.0176
45	335.9	4005	100.0	0.0328	2238	100.0	0.0183	1173	100.0	0.0096	3402	100.0	0.0139
46	356.5	2650	100.0	0.0260	1318	100.0	0.0129	754	100.0	0.0074	2116	100.0	0.0104
47	378.7	1640	100.0	0.0193	748	100.0	0.0088	394	100.0	0.0046	1232	100.0	0.0072
48	402.5	905	100.0	0.0128	403	100.0	0.0057	238	100.0	0.0034	696	100.0	0.0049
49	428.2	542	100.0	0.0092	218	100.0	0.0037	134	100.0	0.0023	385	100.0	0.0033
50	455.8	319	100.0	0.0065	126	100.0	0.0026	62	100.0	0.0013	191	100.0	0.0020
51	485.7	187	100.0	0.0046	75	100.0	0.0019	58	100.0	0.0014	124	100.0	0.0015
$M_{\text{dep}}(\Delta\tau)$ ( $\text{g m}^{-2}$ )		2.07			1.81			1.65			0.93		
$M_{\text{dep}}(\tau)$ ( $\text{g m}^{-2}$ )		32.2			34.0			35.6			36.5		

Annotation:  $U = 5.3 \text{ cm s}^{-1}$ , aerosol material: NaCl,  $\rho_p = 2165 \text{ kg m}^{-3}$ .

### Appendix 3. – Calculation method of $M_{\text{dep}}$

As described in Section 6.23, the real-time  $M_{\text{dep}}$  under continuous aerosol loading can be expressed as:

$$M_{\text{dep}} = \int_{\tau=0}^{\tau=t} \int_{d_p=40 \text{ nm}}^{d_p=500 \text{ nm}} c(d_p, \tau) \eta(d_p, \tau) U \frac{\pi d_p^3}{6} \rho_p d(d_p) d\tau \quad (6.1)$$

where  $c(d_p, \tau)$  is the number concentration of upstream particles in the size bin with a geometric mean diameter  $d_p$  at loading time  $\tau$ ,  $\eta(d_p, \tau)$  is the filtration efficiency of particles with a diameter  $d_p$  at loading time  $\tau$ ,  $U$  is the face velocity,  $\pi d_p^3/6$  is the volume of an aerosol particle with a diameter  $d_p$ , and  $\rho_p$  is the particle material weight density.

The detailed calculation of  $M_{\text{dep}}(101.2)$ , i.e. the specific deposited mass of aerosols in the aerosol size bin with the geometric mean diameter being 101.2 nm (Channel 22), by 525-M4-0.765-C-1 in 17.5 h is shown below. This serves as an example to obtain  $M_{\text{dep}}$  of aerosols in a specific channel ( $M_{\text{dep}}(d_p)$ ). From Eq. 6.1 and Table A2,  $M_{\text{dep}}(101.2)$  is calculated as follows:

$$\begin{aligned} M_{\text{dep}}(101.2) &= \int_{\tau=0}^{\tau=17.5} c(101.2, \tau) \eta(101.2, \tau) U \frac{\pi(101.2 \text{ nm})^3}{6} \rho_p d\tau \\ &= \sum_{i=1}^m M_{\text{dep}}(101.2, \Delta\tau_i) \\ &= \sum_{i=1}^m c(101.2, \tau) \eta(101.2, \tau) U \frac{\pi(101.2 \text{ nm})^3}{6} \rho_p \Delta\tau_i \\ &= c(101.2, 0) \eta(101.2, 0) U \frac{\pi(101.2 \text{ nm})^3}{6} \rho_p (0.5 \text{ h}) \\ &\quad + c(101.2, 0.5) \eta(101.2, 0.5) U \frac{\pi(101.2 \text{ nm})^3}{6} \rho_p (0.5 \text{ h}) \\ &\quad + \dots \\ &\quad + c(101.2, 17.5) \eta(101.2, 17.5) U \frac{\pi(101.2 \text{ nm})^3}{6} \rho_p (0.5 \text{ h}) \end{aligned}$$

$$\begin{aligned}
&= 200111 \text{ cm}^{-3} \times 91.1\% \times 5.3 \text{ cm s}^{-1} \times \frac{\pi(101.2 \text{ nm})^3}{6} \times 2165 \text{ kg m}^{-3} \times 0.5 \text{ h} \\
&\quad + 200111 \text{ cm}^{-3} \times 90.7\% \times 5.3 \text{ cm s}^{-1} \times \frac{\pi(101.2 \text{ nm})^3}{6} \times 2165 \text{ kg m}^{-3} \times 0.5 \text{ h} \\
&\quad + \dots \\
&\quad + 184917 \text{ cm}^{-3} \times 100.0\% \times 5.3 \text{ cm s}^{-1} \times \frac{\pi(101.2 \text{ nm})^3}{6} \times 2165 \text{ kg m}^{-3} \times 0.5 \text{ h} \\
&= 0.02044 \text{ g m}^{-2} + 0.02035 \text{ g m}^{-2} + \dots + 0.02073 \text{ g m}^{-2} \\
&= 0.8815 \text{ g m}^{-2}
\end{aligned}$$

where  $\Delta\tau_i$  is the segmented loading time periods during each of which  $c(d_p, \tau)$  and  $\eta(d_p, \tau)$  are deemed constant.

Using the same calculation method,  $M_{\text{dep}}(d_p)$  of all channels by 525-M4-0.765-C-1 in 17.5 h can be achieved, which gives  $M_{\text{dep}}$  by:

$$\begin{aligned}
M_{\text{dep}} &= \sum_{k=1}^n M_{\text{dep}}(d_{p,k}) \\
&= M_{\text{dep}}(39.6) + M_{\text{dep}}(41.34) + \dots + M_{\text{dep}}(485.7) \\
&= 0.0254 \text{ g m}^{-2} + 0.0342 \text{ g m}^{-2} + \dots + 0.0643 \text{ g m}^{-2} \\
&= 36.5 \text{ g m}^{-2}
\end{aligned}$$

where  $d_{p,k}$  is the geometric mean diameter of the aerosols in the  $k$ th channel size bin.

## References

- [1] W.C. Hinds, *Aerosol technology: Properties, behavior, and measurement of airborne particles*, 2nd ed., John Wiley & Sons, New York, 1999.
- [2] D. Vallero, *Fundamentals of air pollution*, 5th ed., Academic Press, Oxford, UK, 2014.
- [3] C.-S. Liang, F.-K. Duan, K.-B. He, Y.-L. Ma, Review on recent progress in observations, source identifications and countermeasures of PM<sub>2.5</sub>, *Environ. Int.* 86 (2016) 150-170.
- [4] J. Lelieveld, J.S. Evans, M. Fnais, D. Giannadaki, A. Pozzer, The contribution of outdoor air pollution sources to premature mortality on a global scale, *Nature* 525 (2015) 367.
- [5] J.O. Anderson, J.G. Thundiyil, A. Stolbach, Clearing the air: A review of the effects of particulate matter air pollution on human health, *J. Med. Toxicol.* 8 (2012) 166-175.
- [6] D.Y.H. Pui, S.-C. Chen, Z. Zuo, PM<sub>2.5</sub> in China: Measurements, sources, visibility and health effects, and mitigation, *Particuology* 13 (2014) 1-26.
- [7] R.C. Brown, *Air filtration: An integrated approach to the theory and applications of fibrous filters*, Pergamon, New York, 1993.
- [8] R. Barhate, S. Ramakrishna, Nanofibrous filtering media: Filtration problems and solutions from tiny materials, *J. Membr. Sci.* 296 (2007) 1-8.
- [9] V. Thavasi, G. Singh, S. Ramakrishna, Electrospun nanofibers in energy and environmental applications, *Energy Environ. Sci.* 1 (2008) 205.

- [10] A. Brochocka, K. Makowski, K. Majchrzycka, P. Grzybowski, Efficiency of filtering materials used in respiratory protective devices against nanoparticles, *Int. J. Occup. Saf. Ergon.* 19 (2013) 285-295.
- [11] C.-s. Wang, Y. Otani, Removal of nanoparticles from gas streams by fibrous filters: A review, *Ind. Eng. Chem. Res.* 52 (2012) 5-17.
- [12] A. Podgórski, A. Bałazy, L. Gradoń, Application of nanofibers to improve the filtration efficiency of the most penetrating aerosol particles in fibrous filters, *Chem. Eng. Sci.* 61 (2006) 6804-6815.
- [13] R. Thakur, D. Das, A. Das, Electret air filters, *Sep. Purif. Rev.* 42 (2013) 87-129.
- [14] R.C. Brown, *Effect of electric charge in filter materials*, London, UK, 1989.
- [15] D.C. Walsh, *The behaviour of electrically active and prefilter fibrous filters under solid aerosol load*, Loughborough University, 1995.
- [16] D.C. Walsh, J.I.T. Stenhouse, Clogging of an electrically active fibrous filter material: Experimental results and two-dimensional simulations, *Powder Technol.* 93 (1997) 63-75.
- [17] D.C. Walsh, J.I.T. Stenhouse, Parameters affecting the loading behavior and degradation of electrically active filter materials, *Aerosol Sci. Technol.* 29 (1998) 419-432.
- [18] C. Kanaoka, S. Hiragi, W. Tanthapanichakoon, Stochastic simulation of the agglomerative deposition process of aerosol particles on an electret fiber, *Powder Technol.* 118 (2001) 97-106.
- [19] A. Kilic, S. Russell, E. Shim, B. Pourdeyhimi, *The charging and stability of electret filters*, 2017.

- [20] E. Tian, J. Mo, Z. Long, H. Luo, Y. Zhang, Experimental study of a compact electrostatically assisted air coarse filter for efficient particle removal: Synergistic particle charging and filter polarizing, *Build. Environ.* 135 (2018) 153-161.
- [21] Z.Z. Yang, J.H. Lin, I.S. Tsai, T.Y. Kuo, Particle filtration with an electret of nonwoven polypropylene fabric, *Text. Res. J.* 72 (2002) 1099-1104.
- [22] R.-R. Cai, L.-Z. Zhang, A.-B. Bao, PM collection performance of electret filters electrospun with different dielectric materials – A numerical modeling and experimental study, *Build. Environ.* 131 (2018) 210-219.
- [23] K.M. Sim, H.S. Park, G.N. Bae, J.H. Jung, Antimicrobial nanoparticle-coated electrostatic air filter with high filtration efficiency and low pressure drop, *Sci. Total Environ.* 533 (2015) 266-274.
- [24] B.Y. Yeom, E. Shim, B. Pourdeyhimi, Boehmite nanoparticles incorporated electrospun Nylon-6 nanofiber web for new electret filter media, *Macromol. Res.* 18 (2010) 884-890.
- [25] L.L. Janssen, J.O. Bidwell, H.E. Mullins, T.J. Nelson, Efficiency of degraded electret filters: Part I – Laboratory testing against NaCl and dop before and after exposure to workplace aerosols, *J. Int. Soc. Respir. Prot.* (2003).
- [26] L.L. Janssen, J.O. Bidwell, H.E. Mullins, T.J. Nelson, Efficiency of degraded electret filters: Part II – Field testing against workplace aerosols, *J. Int. Soc. Respir. Prot.* (2003).
- [27] B. Tabti, M.R. Mekideche, M.-C. Plopeanu, L.M. Dumitran, L. Herous, L. Dascalescu, Corona-charging and charge-decay characteristics of nonwoven filter media, *IEEE Trans. Ind. Appl.* 46 (2010) 634-640.

- [28] H.R. Gallantree, Review of transducer applications of polyvinylidene fluoride, IEE Proc. I – Solid-State Electron. Devices 130 (1983) 219-224.
- [29] R. Gregorio, E.M. Ueno, Effect of crystalline phase, orientation and temperature on the dielectric properties of poly (vinylidene fluoride) (PVDF), J. Mater. Sci. 34 (1999) 4489-4500.
- [30] G.-d. Kang, Y.-m. Cao, Application and modification of poly(vinylidene fluoride) (PVDF) membranes – A review, J. Membr. Sci. 463 (2014) 145-165.
- [31] Z. Zhao, J. Li, X. Yuan, X. Li, Y. Zhang, J. Sheng, Preparation and properties of electrospun poly(vinylidene fluoride) membranes, J. Appl. Polym. Sci. 97 (2005) 466-474.
- [32] K.P. Matabola, R.M. Moutloali, The influence of electrospinning parameters on the morphology and diameter of poly(vinylidene fluoride) nanofibers – Effect of sodium chloride, J. Mater. Sci. 48 (2013) 5475-5482.
- [33] M. Baqeri, M.M. Abolhasani, M.R. Mozdianfard, Q. Guo, A. Oroumei, M. Naebe, Influence of processing conditions on polymorphic behavior, crystallinity, and morphology of electrospun poly(Vinylidene fluoride) nanofibers, J. Appl. Polym. Sci. 132 (2015).
- [34] H. Asai, M. Kikuchi, N. Shimada, K. Nakane, Effect of melt and solution electrospinning on the formation and structure of poly(vinylidene fluoride) fibres, RSC Adv. 7 (2017) 17593-17598.
- [35] M.M. Abolhasani, S. Azimi, H. Fashandi, Enhanced ferroelectric properties of electrospun poly(vinylidene fluoride) nanofibers by adjusting processing parameters, RSC Adv. 5 (2015) 61277-61283.

- [36] Z.-X. Huang, X. Liu, J. Wu, S.-C. Wong, G.G. Chase, J.-P. Qu, Electrospun poly(vinylidene fluoride) membranes functioning as static charge storage device with controlled crystalline phase by inclusions of nanoscale graphite platelets, *J. Mater. Sci.* 53 (2017) 3038-3048.
- [37] Z. Li, W. Kang, H. Zhao, M. Hu, J. Ju, N. Deng, B. Cheng, Fabrication of a polyvinylidene fluoride tree-like nanofiber web for ultra high performance air filtration, *RSC Adv.* 6 (2016) 91243-91249.
- [38] A. Vanangamudi, S. Hamzah, G. Singh, Synthesis of hybrid hydrophobic composite air filtration membranes for antibacterial activity and chemical detoxification with high particulate filtration efficiency (PFE), *Chem. Eng. J.* 260 (2015) 801-808.
- [39] F. Yang, Y. Li, X. Yu, G. Wu, X. Yin, J. Yu, B. Ding, Hydrophobic polyvinylidene fluoride fibrous membranes with simultaneously water/windproof and breathable performance, *RSC Adv.* 6 (2016) 87820-87827.
- [40] S. Wang, X. Zhao, X. Yin, J. Yu, B. Ding, Electret polyvinylidene fluoride nanofibers hybridized by polytetrafluoroethylene nanoparticles for high-efficiency air filtration, *ACS Appl. Mater. Interfaces* 8 (2016) 23985-23994.
- [41] Z.-X. Huang, X. Liu, X. Zhang, S.-C. Wong, G.G. Chase, J.-P. Qu, A. Baji, Electrospun polyvinylidene fluoride containing nanoscale graphite platelets as electret membrane and its application in air filtration under extreme environment, *Polymer* 131 (2017) 143-150.
- [42] X. Ding, Y. Li, Y. Si, X. Yin, J. Yu, B. Ding, Electrospun polyvinylidene fluoride/SiO<sub>2</sub> nanofibrous membranes with enhanced electret property for

- efficient air filtration, *Compos. Commun.* 13 (2019) 57-62.
- [43] A.G. Kravtsov, H. Brunig, S.F. Zhandarov, Analysis of the polarization state of melt-spun polypropylene fibers, *J Mater Process Tech* 124 (2002) 160-165.
- [44] D.P. Erhard, R. Florian, C.B.A. Bartz, S. Hans-Werner, Fluorinated aromatic polyimides as high-performance electret materials, *Macromol. Rapid Commun.* 36 (2015) 520-527.
- [45] W.W.-F. Leung, C.-H. Hung, P.-T. Yuen, Experimental investigation on continuous filtration of sub-micron aerosol by filter composed of dual-layers including a nanofiber layer, *Aerosol Sci. Technol.* 43 (2009) 1174-1183.
- [46] W.W.-F. Leung, C.-H. Hung, P.-T. Yuen, Effect of face velocity, nanofiber packing density and thickness on filtration performance of filters with nanofibers coated on a substrate, *Sep. Purif. Technol.* 71 (2010) 30-37.
- [47] W.W.-F. Leung, C.-H. Hung, Skin effect in nanofiber filtration of submicron aerosols, *Sep. Purif. Technol.* 92 (2012) 174-180.
- [48] F. Henry, T. Ariman, The effect of neighboring fibers on the electric field in a fibrous filter, *J. Aerosol Sci.* 12 (1981) 137-149.
- [49] D.Y. Choi, E.J. An, S.H. Jung, D.K. Song, Y.S. Oh, H.W. Lee, H.M. Lee, Al-Coated Conductive Fiber Filters for High-Efficiency Electrostatic Filtration: Effects of Electrical and Fiber Structural Properties, *Sci. Rep.* 8 (2018) 5747.
- [50] M. Tang, D. Thompson, D.-Q. Chang, S.-C. Chen, D.Y.H. Pui, Filtration efficiency and loading characteristics of PM<sub>2.5</sub> through commercial electret filter media, *Sep. Purif. Technol.* 195 (2018) 101-109.
- [51] D. Walsh, I. Stenhouse, Experimental studies of electrically active fibrous filter

- loading, Part. Part. Syst. Charact. 13 (1996) 47-53.
- [52] J.A. Schutz, J.S. Church, Respiratory protection for physiologically straining environments, Text. Res. J. 81 (2011) 1367-1380.
- [53] M. Meunier, N. Quirke, Molecular modeling of electron trapping in polymer insulators, J. Chem. Phys. 113 (2000) 369-376.
- [54] M. Meunier, N. Quirke, A. Aslanides, Molecular modeling of electron traps in polymer insulators: Chemical defects and impurities, J. Chem. Phys. 115 (2001) 2876-2881.
- [55] P.P. Tsai, H. Schreuder-Gibson, P. Gibson, Different electrostatic methods for making electret filters, J. Electrostat. 54 (2002) 333-341.
- [56] B. Tabti, L. Dascalescu, M. Plopeanu, A. Antoniu, M. Mekideche, Factors that influence the corona charging of fibrous dielectric materials, J. Electrostat. 67 (2009) 193-197.
- [57] M.C. Plopeanu, P.V. Notingher, L.M. Dumitran, Surface potential decay characterization of non-woven electret filter media, IEEE Transactions on Dielectrics and Electrical Insulation (2011).
- [58] D. Das, R. Thakur, A.K. Pradhan, Optimization of corona discharge process using Box-Behnken design of experiments, J. Electrostat. 70 (2012) 469-473.
- [59] B. Yahiaoui, M. Megherbi, A. Smaili, A. Antoniu, B. Tabti, L. Dascalescu, Distribution of electric potential at the surface of corona-charged polypropylene nonwoven fabrics after neutralization, IEEE Trans. Ind. Appl. 49 (2013) 1758-1766.
- [60] R. Thakur, D. Das, A. Das, Optimization study to improve filtration behaviour of

- electret filter media, *J. Text. Inst.* 107 (2016) 1456-1462.
- [61] Y. Matsuda, Y. Saito, S. Tasaka, Dipole polarization formed on surface of polypropylene electrets, *IEEE Transactions on Dielectrics and Electrical Insulation* 17 (2010) 1015-1020.
- [62] A. Kilic, E. Shim, B. Pourdeyhimi, Effect of annealing on charging properties of electret fibers, *J. Text. Inst.* 108 (2016) 987-991.
- [63] T.J. Lewis, Charge Transport, Charge injection and breakdown in polymeric insulators, *J. Phys. D: Appl. Phys.* 23 (1990) 1469-1478.
- [64] T.A. Yovcheva, I.A. Avramova, G.A. Mekishev, T.S. Marinova, Corona-charged polypropylene electrets analyzed by XPS, *J. Electrostat.* 65 (2007) 667-671.
- [65] M.C. Plopeanu, L. Dascalescu, B. Yahiaoui, A. Antoniu, M. Hulea, P.V. Notingher, Distribution of electric potential at the surface of corona-charged non-woven fabrics, *IEEE. Ind. Applic. Soc. Annu. Meeting Orlando, FL, USA, 2011.*
- [66] R. Kacprzyk, W. Mista, The surface potential of perforated dielectric layers, *IEEE Transactions on Dielectrics and Electrical Insulation* 13 (2006) 986-991.
- [67] Y. Zhang, T. Shao, Contact electrification between polymers and steel, *J. Electrostat.* 71 (2013) 862-866.
- [68] I. Krucinska, S. Zakrzewski, I. Kowalczyk, J. Wisniewska-Konecka, Investigation of blended fibre filtering materials, *Int. J. Occup. Saf. Ergon.* 3 (1997) 141-149.
- [69] L.W. Barrett, A.D. Rousseau, Aerosol loading performance of electret filter media, *Am. Ind. Hyg. Assoc. J.* 59 (2010) 532-539.
- [70] V. Albrecht, A. Janke, E. Németh, S. Spange, G. Schubert, F. Simon, Some aspects

- of the polymers' electrostatic charging effects, *J. Electrostat.* 67 (2009) 7-11.
- [71] M. Sakaguchi, M. Makino, T. Ohura, T. Iwata, Contact electrification of polymers due to electron transfer among mechano anions, mechano cations and mechano radicals, *J. Electrostat.* 72 (2014) 412-416.
- [72] A.F. Diaz, R.M. Felix-Navarro, A semi-quantitative tribo-electric series for polymeric materials: The influence of chemical structure and properties, *J. Electrostat.* 62 (2004) 277-290.
- [73] C.H. Park, J.K. Park, H.S. Jeon, B.C. Chun, Triboelectric series and charging properties of plastics using the designed vertical-reciprocation charger, *J. Electrostat.* 66 (2008) 578-583.
- [74] L.S. McCarty, G.M. Whitesides, Electrostatic charging due to separation of ions at interfaces: Contact electrification of ionic electrets, *Angew. Chem. Int. Ed.* 47 (2008) 2188-2207.
- [75] S. Pence, V.J. Novotny, A.F. Diaz, Effect of surface moisture on contact charge of polymers containing ions, *Langmuir* 10 (1994) 592-596.
- [76] G.C. Rutledge, S.V. Fridrikh, Formation of fibers by electrospinning, *Adv. Drug Deliv. Rev.* 59 (2007) 1384-1391.
- [77] D.H. Reneker, A.L. Yarin, Electrospinning jets and polymer nanofibers, *Polymer* 49 (2008) 2387-2425.
- [78] N. Bhardwaj, S.C. Kundu, Electrospinning: A fascinating fiber fabrication technique, *Biotechnol. Adv.* 28 (2010) 325-347.
- [79] F.E. Ahmed, B.S. Lalia, R. Hashaikeh, A review on electrospinning for membrane fabrication: Challenges and applications, *Desalination* 356 (2015) 15-30.

- [80] G. Collins, J. Federici, Y. Imura, L.H. Catalani, Charge generation, charge transport, and residual charge in the electrospinning of polymers: A review of issues and complications, *J. Appl. Phys.* 111 (2012) 044701.
- [81] F.J. Romay, B.Y.H. Liu, S.-J. Chae, Experimental study of electrostatic capture mechanisms in commercial electret filters, *Aerosol Sci. Technol.* 28 (1998) 224-234.
- [82] H. Emi, C. Kanaoka, Y. Otani, T. Ishiguro, Collection mechanisms of electret filter, *Part. Sci. Technol.* 5 (1987) 161-171.
- [83] C. Kanaoka, H. Emi, Y. Otani, T. Iiyama, Effect of charging state of particles on electret filtration, *Aerosol Sci. Technol.* 7 (1987) 1-13.
- [84] R.A. Fjeld, T.M. Owens, The effect of particle charge on penetration in an electret filter, *IEEE Trans. Ind. Appl.* 24 (1988) 725-731.
- [85] D.C. Walsh, J.I.T. Stenhouse, The effect of particle size, charge, and composition on the loading characteristics of an electrically active fibrous filter material, *J. Aerosol Sci.* 28 (1997) 307-321.
- [86] A.L. Sanchez, J.A. Hubbard, J.G. Dellinger, B.L. Servantes, Experimental study of electrostatic aerosol filtration at moderate filter face velocity, *Aerosol Sci. Technol.* 47 (2013) 606-615.
- [87] C.C. Chen, S.H. Huang, The effects of particle charge on the performance of a filtering facepiece, *Am. Ind. Hyg. Assoc. J.* 59 (1998) 227-233.
- [88] K. Makowski, Deposition and resuspension of selected aerosols particles on electrically charged filter materials for respiratory protective devices, *Int. J. Occup. Saf. Ergon.* 11 (2005) 363-376.

- [89] M. Nifuku, Y. Zhou, A. Kisiel, T. Kobayashi, H. Katoh, Charging characteristics for electret filter materials, *J. Electrostat.* 51 (2001) 200-205.
- [90] D. Lolla, M. Lolla, A. Abutaleb, H.U. Shin, D.H. Reneker, G.G. Chase, Fabrication, polarization of electrospun polyvinylidene fluoride electret fibers and effect on capturing nanoscale solid aerosols, *Materials* 9 (2016).
- [91] A. Kilic, E. Shim, B. Pourdeyhimi, B.-Y. Yeom, Aerosol filtration properties of nucleating agent containing electret filters, *Polym. Eng. Sci.* 54 (2014) 1533-1539.
- [92] A. Kilic, E. Shim, B. Pourdeyhimi, Electrostatic capture efficiency enhancement of polypropylene electret filters with barium titanate, *Aerosol Sci. Technol.* 49 (2015) 666-673.
- [93] Q. Zhang, F. Liu, T.-Y. Yang, X.L. Si, G.R. Hu, C.-T. Chang, Deciphering effects of surface charge on particle removal by TiO<sub>2</sub> polyacrylonitrile nanofibers, *Aerosol Air Qual. Res.* 17 (2017) 1909-1916.
- [94] D. Lovera, C. Bilbao, P. Schreier, L. Kador, H.-W. Schmidt, V. Altstädt, Charge storage of electrospun fiber mats of poly(phenylene ether)/polystyrene blends, *Polym. Eng. Sci.* 49 (2009) 2430-2439.
- [95] Y. Bai, C.B. Han, C. He, G.Q. Gu, J.H. Nie, J.J. Shao, T.X. Xiao, C.R. Deng, Z.L. Wang, Washable multilayer triboelectric air filter for efficient particulate matter PM<sub>2.5</sub> removal, *Adv. Funct. Mater.* 28 (2018) 1706680.
- [96] X. Li, C. Yao, F. Sun, T. Song, Y. Li, Y. Pu, Conjugate electrospinning of continuous nanofiber yarn of poly(L-lactide)/nanotricalcium phosphate nanocomposite, *J. Appl. Polym. Sci.* 107 (2008) 3756-3764.
- [97] S.B. Martin, Jr., E.S. Moyer, Electrostatic respirator filter media: Filter efficiency

- and most penetrating particle size effects, *Appl. Occup. Environ. Hyg.* 15 (2000) 609-617.
- [98] L.L. Janssen, Efficiency and pressure drop effects of high concentrations of cement dust on N95 electret filters, *J. Int. Soc. Respir. Prot.* (2004).
- [99] L. Janssen, J. Bidwell, Performance of four Class 95 electret filters against diesel particulate matter, *J. Int. Soc. Respir. Prot.* (2006).
- [100] H. Chen, Z. Zhang, Z. Zhang, F. Jiang, R. Du, Enhancement of filtration efficiency by electrical charges on nebulized particles, *Particuology* 37 (2018) 81-90.
- [101] T. Ohmi, S. Sudoh, H. Mishima, Static charge removal with IPA solution, *IEEE Trans. Semicond. Manuf.* 7 (1994) 440-446.
- [102] M. Kerner, K. Schmidt, A. Hellmann, S. Schumacher, M. Pitz, C. Asbach, S. Ripperger, S. Antonyuk, Numerical and experimental study of submicron aerosol deposition in electret microfiber nonwovens, *J. Aerosol Sci.* 122 (2018) 32-44.
- [103] R. Kacprzyk, W. Mista, Back corona in fabrics, *Fibres Text. East. Eur.* 14 (2006) 35-38.
- [104] S.-H. Huang, Factors affecting filter penetration and quality factor of particulate respirators, *Aerosol Air Qual. Res.* (2013).
- [105] Q. Sun, W.W.-F. Leung, Charged PVDF multi-layer filters with enhanced filtration performance for filtering nano-aerosols, *Sep. Purif. Technol.* 212 (2019) 854-876.
- [106] P.H. Hoet, I. Brüskehohlfeld, O.V. Salata, Nanoparticles – known and unknown health risks, *J. Nanobiotechnol.* 2 (2004) 1-15.

- [107] M. Ignatova, T. Yovcheva, A. Viraneva, G. Mekishev, N. Manolova, I. Rashkov, Study of charge storage in the nanofibrous poly(ethylene terephthalate) electrets prepared by electrospinning or by corona discharge method, *Eur. Polym. J.* 44 (2008) 1962-1967.
- [108] A. Kilic, E. Shim, B.Y. Yeom, B. Pourdeyhimi, Improving electret properties of PP filaments with barium titanate, *J. Electrostat.* 71 (2013) 41-47.
- [109] Q. Zhang, J. Welch, H. Park, C.-Y. Wu, W. Sigmund, J.C.M. Marijnissen, Improvement in nanofiber filtration by multiple thin layers of nanofiber mats, *J. Aerosol Sci.* 41 (2010) 230-236.
- [110] H. Shao, J. Fang, H. Wang, T. Lin, Effect of electrospinning parameters and polymer concentrations on mechanical-to-electrical energy conversion of randomly-oriented electrospun poly(vinylidene fluoride) nanofiber mats, *RSC Adv.* 5 (2015) 14345-14350.
- [111] K. Narttamrongsutt, G.G. Chase, The influence of salt and solvent concentrations on electrospun polyvinylpyrrolidone fiber diameters and bead formation, *Polymer* 54 (2013) 2166-2173.
- [112] R.E. Shaffer, S. Rengasamy, Respiratory protection against airborne nanoparticles: A review, *J. Nanopart. Res.* 11 (2009) 1661-1672.
- [113] P. Li, C. Wang, Y. Zhang, F. Wei, Air filtration in the free molecular flow regime: A review of high-efficiency particulate air filters based on carbon nanotubes, *Small* 10 (2014) 4543-4561.
- [114] A. Bredin, R.A. O'Leary, B.J. Mullins, Filtration of soot-in-oil aerosols: Why do field and laboratory experiments differ?, *Sep. Purif. Technol.* 96 (2012) 107-116.

- [115] W.W.-F. Leung, Y.T. Chau, Experiments on filtering nano-aerosols from vehicular and atmospheric pollutants under dominant diffusion using nanofiber filter, *Sep. Purif. Technol.* 213 (2019) 186-198.
- [116] S. Janhäll, Review on urban vegetation and particle air pollution – Deposition and dispersion, *Atmos. Environ.* 105 (2015) 130-137.
- [117] B. Tabti, M.R. Mekideche, M.-C. Plopeanu, L.M. Dumitran, A. Antoniu, L. Dascalescu, Factors that influence the decay rate of the potential at the surface of nonwoven fabrics after negative corona discharge deposition, *IEEE Trans. Ind. Appl.* 46 (2010) 1586-1592.
- [118] S. Yang, W.M. Lee, H.L. Huang, Y.C. Huang, C.H. Luo, C.C. Wu, K.P. Yu, Aerosol penetration properties of an electret filter with submicron aerosols with various operating factors, *J. Environ. Sci. Health. Part A Toxic/Hazard. Subst. Environ. Eng.* 42 (2007) 51-57.
- [119] R.C. Brown, D. Wake, R. Gray, D.B. Blackford, G.J. Bostock, Effect of industrial aerosols on the performance of electrically charged filter material, *Ann. Occup. Hyg.* 32 (1988) 271-294.
- [120] W.W.-F. Leung, C.-H. Hung, Investigation on pressure drop evolution of fibrous filter operating in aerodynamic slip regime under continuous loading of sub-micron aerosols, *Sep. Purif. Technol.* 63 (2008) 691-700.
- [121] M.V. Rodrigues, M.A.S. Barrozo, J.A.S. Gonçalves, J.R. Coury, Effect of particle electrostatic charge on aerosol filtration by a fibrous filter, *Powder Technol.* 313 (2017) 323-331.
- [122] B. Huang, Q. Yao, S.-Q. Li, H.-L. Zhao, Q. Song, C.-F. You, Experimental

investigation on the particle capture by a single fiber using microscopic image technique, *Powder Technol.* 163 (2006) 125-133.

[123] S. Dhaniyala, B.Y.H. Liu, Experimental investigation of local efficiency variation in fibrous filters, *Aerosol Sci. Technol.* 34 (2010) 161-169.

[124] W. Bergman, A. Biermann, W. Kuhl, B. Lum, A. Bogdanoff, H. Hebard, M. Hall, D. Banks, M. Mazumder, J. Johnson, Electric air filtration: Theory, laboratory studies, hardware development, and field evaluations, *Aerosols* (1983).

[125] W.W.-F. Leung, C.W.-Y. Hau, H.-F. Choy, Microfiber-nanofiber composite filter for high-efficiency and low pressure drop under nano-aerosol loading, *Sep. Purif. Technol.* 206 (2018) 26-38.